

A Novel Backup Protection Scheme for Hybrid AC/DC Power Systems

Lewis Callum Hunter

Centre for Doctoral Training in
Future Power Networks and Smart Grids

A thesis submitted for the degree of Doctor of Philosophy to the
Department of Electronic and Electrical Engineering
University of Strathclyde

June 2020

This thesis is the result of the author's original research. It has been composed by the author and has not been previously submitted for examination which has led to the award of a degree.

The copyright of this thesis belongs to the author under the terms of the United Kingdom Copyright Acts as qualified by University of Strathclyde Regulation 3.50. Due acknowledgement must always be made of the use of any material contained in, or derived from, this thesis.

Abstract

This thesis presents and demonstrates (both via simulation and hardware-based tests) a new protection scheme designed to safeguard hybrid AC/DC distribution networks against DC faults that are not cleared by the main MVDC (Medium Voltage DC) link protection. The protection scheme relies on the apparent impedance measured at the AC “side” of the MVDC link to detect faults on the DC system. It can be readily implemented on existing distance protection relays with no changes to existing measuring equipment.

An overview of the literature in this area is presented and it is shown that the protection of MVDC links is only considered at a converter station level. There appears to be no consideration of protecting the MVDC system from the wider AC power system via backup – as would be the case for standard AC distribution network assets, where the failure of main protection would require a (usually remote) backup protection system to operate to clear the fault. Very little literature considers remote backup protection of MVDC links.

To address this issue, the research presented in this thesis characterises the apparent impedance as measured in the neighbouring AC system under various DC fault conditions on an adjacent MVDC link. Initial studies, based on simulations, show that a highly inductive characteristic, in terms of the calculations from the measured AC voltages and currents, is apparent on all three phases in the neighbouring AC system during DC-side pole-to-pole and pole-pole-ground faults. This response is confirmed via a series of experiments conducted at low voltage in a laboratory environment using scaled down electrical components. From this classification, a fast-acting backup protection methodology, which can detect pole-to-pole and pole-pole-ground faults within 40 ms, is proposed and trialled through simulation. The solution can be deployed on distance protection relays using a typically unused zone (e.g. zone 4). New relays could, of course, incorporate this functionality as standard in the future.

To maximise confidence and demonstrate the compatibility of the solution, the protection scheme is deployed under a real-time hardware-in-the-loop environment using a commercially available distance protection relay. Suggestions to improve the stability of the proposed solution are discussed and demonstrated. Future areas of work are identified and described.

As an appendix, early stage work pertaining to the potential application and benefits of MVDC is presented for two Scottish distribution networks. The findings from this are presented as supplementary material at the end of the thesis.

Acknowledgements

I would like to offer my sincere thanks to my supervisor Prof. Campbell Booth for his encouragement, support and guidance throughout the PhD and previously during my undergraduate degree. I'd also like to acknowledge Prof. Stephen Finney, Dr. Adrià Junyent-Ferré, Dr. Adam Dyśko and Dr. Agustí Egea-Àlvarez for their advice and technical support with the research. Thanks must also be extended to Dr. Qiteng Hong and Richard Munro for their assistance with laboratory investigations.

I'd like to express my thanks to all of my colleagues within the Future Power Networks and Smart Grids CDT and the wider Institute for Energy and Environment. Importantly, I must not forget to thank Shirley Kirk for the supply of homemade tablet and endless encouragement throughout the CDT programme.

My gratitude also extends to the Engineering and Physical Sciences Research Council (EPSRC) for financial support of the research (EP/L015471/1).

Finally, I'd like to especially thank my friends and family for their support and encouragement over the years.

Contents

Abstract	1
Acknowledgements	2
List of Figures	8
List of Tables	12
Glossary of Abbreviations	14
Chapter 1 — Introduction	17
1.1 Introduction to the Research	17
1.2 Justification for Research	19
1.3 Principal Contributions	22
1.4 Thesis Organisation	23
1.5 Publications and Achievements	24
1.5.1 Journal Articles	24
1.5.2 Conference Papers	24
1.5.3 Achievements	25
Chapter 2 — Review of AC, DC and Power Conversion Technologies	27
2.1 Introduction	27
2.2 AC Systems	27
2.2.1 Structure of AC Electricity Supply Networks.....	28
2.2.2 Limitations of AC	32
2.3 DC Conversion Systems	33
2.3.1 Summary of Power Electronic Devices	34
2.3.2 Line Commutated Conversion (LCC).....	36
2.3.3 Voltage Source Conversion (VSC).....	40
2.3.4 Comparison of HVDC Technologies.....	44
2.3.5 Modular Multilevel Converter (MMC).....	45

2.4	HVDC	47
2.5	Summary	51
 Chapter 3 — Review of Power System Protection Fundamentals		52
3.1	Introduction	52
3.2	Electrical Faults	52
3.3	The Protection System	58
3.3.1	Protection System Performance Requirements	59
3.3.2	Instrumentation for Protection Systems	59
3.3.3	Protection Relays	59
3.4	Protection Schemes	60
3.4.1	Overcurrent Protection.....	62
3.4.2	Differential Protection	66
3.4.3	Distance Protection	67
3.4.3.1	Distance Protection Principles	67
3.4.3.2	Overview of Fault Impedance Calculations and Tripping Characteristics	69
3.4.3.3	Advanced (Communication Assisted) Distance Protection Schemes	75
3.5	Protection of AC Distribution Networks	78
3.6	Protection of HVDC Systems	82
3.7	Summary	87
 Chapter 4 — Medium Voltage Direct Current Applications in Distribution Networks		88
4.1	Introduction	88
4.2	MVDC Characteristics	89
4.3	Review of Academic/Industrial MVDC Research	91
4.4	Review of Deployed MVDC Technologies in Distribution Systems	96
4.4.1	Angle-DC – SP Energy Networks	96
4.4.2	Flexible Power Link – Western Power Distribution	101
4.4.3	DC Campus – FEN Campus RWTH Aachen	104

4.5	Summary.....	107
Chapter 5 — A Fast-Acting Backup Protection System for Embedded MVDC Links.....		109
5.1	Introduction.....	109
5.2	Study Methodology	110
5.2.1	Converter Topology.....	110
5.2.2	Control Structure	111
5.2.3	Behaviour of Converters During Fault Conditions	113
5.2.3.1	AC Faults	113
5.2.3.2	DC Faults	113
5.2.4	Modelling Procedure	116
5.3	Case Study	117
5.3.1	Test Network	117
5.3.2	Relay Setting Parameters.....	118
5.3.3	Fault Impedance Analysis.....	119
5.3.3.1	Analysis of Distance Relay Settings and Fault Performance	119
5.3.3.2	DC Side Fault Analysis.....	120
5.4	Fast-Acting Backup Protection Function.....	125
5.4.1	Proposed Solution.....	125
5.4.2	Relay Setting Parameters.....	127
5.4.3	DC Fault Simulation Studies	129
5.5	Discussion.....	134
5.6	Conclusion	136
Chapter 6 — Physical Validation of DC Fault Impedance and of the Fast-Acting Protection Scheme.....		137
6.1	Introduction.....	137
6.2	Validation of AC System Response During DC Faults	138
6.2.1	Objective of Tests	138
6.2.2	Description of Test System used in Experiments	138
6.2.3	Simulated Response.....	146

6.2.4	Experimental Results	148
6.2.5	Discussion.....	152
6.3	Deployment of Protection Scheme on an Actual Distance Protection Relay.....	153
6.3.1	Introduction	153
6.3.2	Description of Experimental Setup.....	153
6.3.3	Experimental Results	159
6.3.4	Discussion.....	161
6.4	R-X Coordinate-Based Setting Approach.....	162
6.4.1	Overview of R-X Setting Approach	162
6.4.2	Description of Experimental Design.....	163
6.4.2.1	System Overview	163
6.4.2.2	Distance Relay Implementation Overview	165
6.4.2.3	Modelling.....	169
6.4.2.4	Relay Setting Parameters	170
6.4.3	Experimental Results	172
6.4.4	Discussion.....	174
6.5	Conclusions	175
Chapter 7 — Conclusions and Further Work.....		176
7.1	Conclusions	176
7.1.1	Analysis of DC Fault Impedance.....	177
7.1.2	Fast-Acting Backup Protection Scheme	177
7.1.3	Hardware Verification of AC System Performance	177
7.1.4	Commercial Relay Demonstration.....	178
7.1.5	R-X Setting Approach	178
7.2	Future Work.....	178
7.2.1	Applicability to Other Converter Types	179
7.2.2	Further Testing and Validation Activities.....	179
7.2.3	Converter Survival Time	180
7.2.4	Live Deployment	180
7.2.5	HVDC Back-Up Protection	181
7.2.6	Further Network Studies.....	181
Supplementary Material A — MVDC Simulation Case Studies.....		182

A.1	Introduction.....	182
A.2	Modelling Methodology	182
A.3	Case Study 1: Increasing Renewable Capacity	184
A.3.1	Network Overview	184
A.3.2	Benchmark Studies.....	188
A.3.2.1	Introduction of MVDC Links	188
A.3.3	Facilitating an Increase in Renewable Generation	190
A.3.4	Result Discussion	191
A.4	Case Study 2: Increasing Network Utilisation.....	192
A.4.1	Network Overview	192
A.4.2	Benchmark Studies.....	194
A.4.3	Interconnection of GSPs via MVDC	195
A.4.4	Result Analysis.....	196
A.5	Discussion of Findings	197
A.6	Conclusion	198
	References	200

List of Figures

Figure 1-1: Blinding of overcurrent protection relay.....	19
Figure 1-2: LCOE by generation type at various locations across Germany 2018 [36].....	20
Figure 1-3: 33 kV generation heat map of central and southern Scotland [42].....	21
Figure 2-1: Simplified utility-scale electricity network topology	29
Figure 2-2: Single-line distribution network topology	30
Figure 2-3: Overview of AC compensation technologies [65].....	32
Figure 2-4: 4,000 kW rotary traction converter - 1929 (≈ 400 V AC to 600 V DC) [74]	34
Figure 2-5: Electrical symbols for (a) diodes, (b) thyristors and (c) IGBTs with freewheeling diode [66]	34
Figure 2-6: Conduction characteristic for (a) diodes, (b) thyristors and (c) IGBTs [66]	36
Figure 2-7: General structure of three-phase full-bridge converter with thyristors.....	37
Figure 2-8: Conduction diagram for switches S_{1a} , S_{1b} , S_{2a} , S_{2b} , S_{3a} , S_{3b} superimposed on three-phase voltage waveform	37
Figure 2-9: Conduction envelope for LCC converter	38
Figure 2-10: Short circuit conduction path caused by commutation failure of S_{3b} [79]	40
Figure 2-11: Basic two-level converter leg	41
Figure 2-12: Voltage reference and triangular carrier with associated PWM switching output	42
Figure 2-13: Example of the series connection of IGBTs to achieve higher DC-side voltages for a conventional two-level VSC converter.....	43
Figure 2-14: Three-phase MMC topology with n submodules in each arm.....	45
Figure 2-15: MMC cell construction (a) half-bridge (HB) and (b) full-bridge (FB).....	46
Figure 2-16: Example output voltages for an MMC and a two-level VSC converter	47
Figure 2-17: Comparison of losses against transmission distance for HVDC versus HVAC for a 1.2 GW overhead line system [102].....	48
Figure 2-18: Investment cost comparison between DC and AC systems [102]	49
Figure 2-19: HVDC in the UK for mid-2018 (left) and by 2030 (right) [97]	50
Figure 3-1: Attempt to forcefully remove equipment from substation [108]	53
Figure 3-2: Tree branch spanning all conductors on an overhead line [109].....	53
Figure 3-3: Excavator cutting through an underground cable causing a short circuit [110].....	54
Figure 3-4: Main fault types in a three-phase AC system.....	57
Figure 3-5: Main fault types in two-wire DC system	58
Figure 3-6: Typical protection topology	61
Figure 3-7: Overcurrent protection system topology	62
Figure 3-8: Overcurrent protection for three serially connected feeders.....	63
Figure 3-9: Time/current characteristics for relays A-C	63
Figure 3-10: IDMT (IEC 60255) and DT relay characteristics ($I_s = 200$ A; $TMS = 1.0$)	65
Figure 3-11: Differential protection system connection topology	66

Figure 3-12: Distance protection system topology	67
Figure 3-13: Distance protection zone diagram using Mho characteristic.....	68
Figure 3-14: Standard electrical network with fault location indicated	70
Figure 3-15: Sequence component network for phase-to-phase fault [134]	70
Figure 3-16: Sequence component network for phase-to-ground faults [134].....	72
Figure 3-17: A selection of commonly used distance protection characteristics [128]	74
Figure 3-18: Flow chart summarising the operation of a distance protection relay	75
Figure 3-19: Standard distance protection tripping logic [137]	76
Figure 3-20: Simple network protected by distance protection relays [137].....	76
Figure 3-21: Distance protection tripping logic with direct transfer trip [137]	76
Figure 3-22: Distance protection tripping logic with permissive under-reach functionality [137]	77
Figure 3-23: Distance protection tripping logic with permissive over-reach functionality.....	78
Figure 3-24: Simplified diagram summarising protection of a typical distribution networks	79
Figure 3-25: NVD relay connection topology	81
Figure 3-26: VSC fault current paths during (a) capacitor discharge followed by (b) diode freewheeling and (c) grid current feeding [152].....	83
Figure 3-27: Example of DC-side voltages and current during an uncleared pole-to-pole fault at the converter terminals (0 km) for a ± 100 kV, 2,00 MVA, 75 km VSC HVDC link.....	84
Figure 3-28: DC-side voltage and current during a DC-side fault with converter fault stages identified.....	84
Figure 3-29: Simplified example topologies of (a) mechanical switch resonant circuit, (b) solid- state and (c) hybrid DC circuit breakers [153]	85
Figure 4-1: Cost of solar PV inverters for various installation scales [177] [178]	89
Figure 4-2: Losses associated with supplying a constant power 1 MW load at different DC supply voltages and circuit lengths ($0.2 \Omega/\text{km}$)	90
Figure 4-3: SIPLINK interconnection between land and ship power system via back-to-back power electronic converter (reproduced from [204])	92
Figure 4-4: Example MVDC collection network for offshore wind applications [216].....	93
Figure 4-5: Illustration of Angle-DC geographic topology [185]	97
Figure 4-6: Angle-DC two three-wire AC circuits converted to two-pole DC system.....	98
Figure 4-7: Angle-DC electrical topology.....	98
Figure 4-8: Angle-DC simplified station topology	99
Figure 4-9: Angle DC circuit reconfiguration under permanent pole-ground fault	100
Figure 4-10: FPL network topology [241].....	102
Figure 4-11: Simplified FPL electrical topology	102
Figure 4-12: Crane installation of FPL container at WPD's Exebridge substation [245]	104
Figure 4-13: Proposed RWTH Aachen MVDC topology [249].....	105
Figure 4-14: Proposed RWTH Aachen MVDC electrical topology [249].....	106

Figure 4-15: Dual active bridge conversion stages	106
Figure 5-1: Comparison of the uncontrolled fault path through IGBT diodes for a (a) HB-MMC and (b) a standard 2-level converter [150]	111
Figure 5-2: MVDC link control topology	111
Figure 5-3: Standard inner current control loop.....	112
Figure 5-4: Outer loop controllers	112
Figure 5-5: Example of the uncontrolled fault path within a VSC converter	113
Figure 5-6: Bypass thyristors installed in parallel with IGBTs.....	114
Figure 5-7: Overview of bypass thyristor controller	115
Figure 5-8: Summary of converter control actions during a fault upon the DC link.....	115
Figure 5-9: Simulation methodology	116
Figure 5-10: Test network	117
Figure 5-11: Voltage and current characteristics for AC and DC systems during PPG fault at the mid-point of the DC link	121
Figure 5-12: Voltage and current characteristics for AC and DC systems during PPG fault at the mid-point of the DC link (0.45 s to 0.6 s)	122
Figure 5-13: R-X diagram for a PPG fault at the midpoint (5km) of the DC link	124
Figure 5-14: R-X diagram showing conventional Z1-Z3 tripping zones and fast-acting Z4 quadrilateral area for detection of DC-side faults.....	126
Figure 5-15: Impedance measured by the distance protection relay during 100% real power export from Converter Station A to Converter Station B.....	127
Figure 5-16: R-X diagram for a pole-to-pole-to-ground fault at DC link midpoint.....	130
Figure 5-17: Final apparent fault impedance settling points for PPG events at Station A, mid-point and Station B.....	132
Figure 5-18: Final apparent fault impedance settling points for PP events at Station A, mid-point and Station B.....	133
Figure 5-19: AC and DC voltages and currents for PG fault at the mid-point of the DC link..	135
Figure 6-1: Single line test network diagram.....	139
Figure 6-2: Electrical schematic of test setup	142
Figure 6-3: Plan view of mechanical layout	143
Figure 6-4: 3D view of mechanical layout	143
Figure 6-5: Laboratory test setup (1)	144
Figure 6-6: Laboratory test setup (2)	144
Figure 6-7: Laboratory test setup showing hardwired remote control for fault inception and instantaneous three phase voltage and current logger	145
Figure 6-8: R-X detection subsystem.....	147
Figure 6-9: Simulated three-phase voltages and currents for a 1 Ω DC fault at Station A (fault application time = 0.5 s)	147

Figure 6-10: Experimental three-phase voltages and currents for a 1 Ω DC fault applied at Station A (fault application time \approx 1.18 s)	149
Figure 6-11: Simulated and experimental DC fault impedances	151
Figure 6-12: Test network with four fault locations indicated	153
Figure 6-13: Three-phase, secondary-referred, injection voltages and currents for fault F1 ...	155
Figure 6-14: Real time hardware-in-the-loop test setup	156
Figure 6-15: Additional tripping logic diagram	157
Figure 6-16: Hardware-in-the-loop injection amplifier	158
Figure 6-17: Anonymised commercially available relay used in HIL experiments	158
Figure 6-18: R-X diagram for fault F1	160
Figure 6-19: R-X diagram for fault F2	160
Figure 6-20: R-X diagram for fault F3	160
Figure 6-21: R-X diagram for fault F4	160
Figure 6-22: New Z4 tripping region using R-X coordinate points marked A-D	162
Figure 6-23: Experimental overview	164
Figure 6-24: Summary of distance relay processing steps	165
Figure 6-25: Distance protection relay design software flow diagram	166
Figure 6-26: R-X detection subsystem	167
Figure 6-27: Trip logic for standard (Z1-Z3) zones including time delay	167
Figure 6-28: Zone 4 trip logic including cross-check	167
Figure 6-29: Trip output	168
Figure 6-30: User interface for relay setting parameters	168
Figure 6-31: Test network with faults F1-F7	169
Figure 6-32: Fault inception and tripping times for fault scenario F6	173
Figure 6-33: Z4 tripping area of original and R-X coordinate methods	174
Figure 7-1: Proposed closed loop fault experimental setup	180
Figure A-1: Network topology for case study 1	185
Figure A-2: 33kV SNOP connecting Coylton GSP to Kilmarnock South GSP	190
Figure A-3: Simplified distribution network comprising of three GSP all of which are interconnected via normally open points	192
Figure A-4 - Network showing MVDC interconnection between GSPs.	195

List of Tables

Table 2-1: Truth table for output voltage for various switching states	41
Table 2-2: Summary of key parameters of LCC and VSC [97] [98] [99]	44
Table 3-1: Causes of grid disturbances for two Nordic countries leading to a supply interruption (2012) [111].....	55
Table 3-2: Faulted asset percentage distribution for two Nordic countries (2012) [111]	56
Table 3-3: Approximate probability distribution of AC short circuit fault types (for overhead systems) [115]	58
Table 3-4: Example of distance protection clearance times for a Scottish DNO [57].....	69
Table 4-1: IEC 60038 voltage definitions	90
Table 5-1: Summary of modelled parameters [56].....	118
Table 5-2: Summary of relay setting parameters	119
Table 5-3: Simplified relay log for Z1, Z2, Z3 AC-side faults	120
Table 5-4: Summary of relay setting parameters	129
Table 5-5: Relay Log DC-Side Faults	129
Table 6-1: Component values for experimental setup	141
Table 6-2: Circuit wiring colour codes [273]	141
Table 6-3: Description of numbered points from laboratory test setup images	146
Table 6-4: Impedance measurements during DC-side faults and pre-fault conditions.....	148
Table 6-5: Final settling impedance for fault scenarios (mean value recorded)	150
Table 6-6: Absolute impedance error between simulated and experimental faults	152
Table 6-7: Mean fault impedance across all distance elements for simulated and experimental results.....	152
Table 6-8: Distance protection relay setting parameters	156
Table 6-9: Relay log for fault simulations	159
Table 6-10: Setting coordinate calculations	163
Table 6-11: Summary of modelled parameters	170
Table 6-12: Settings for fast-acting backup protection scheme outlined in Chapter 5	171
Table 6-13 Settings for R-X coordinate-based protection solution	172
Table 6-14 Results for original and R-X tripping regions	172
Table A-1: Distributed generation connected and contracted to connect for associated GSP [42]	186
Table A-2: Winter continuous thermal rating and circuit length for conductors [42].....	186
Table A-3: Substation name, firm capacity, min/max loading and power factor for test network [56] [42].....	187
Table A-4: Key line loading for base network under maximum and minimum load.....	188
Table A-5: Introduction of an MVDC link	189
Table A-6: Loading results after the introduction of MVDC and SNOP	190

Table A-7: Results: line loading of base network and enhanced DC network under minimum system load	191
Table A-8: GSP properties	193
Table A-9: Power rating of DG	193
Table A-10: Network loading by scenario (negative indicates an exporting GSP).....	194
Table A-11: MVDC Balancing Network Studies	196

Glossary of Abbreviations

AC	Alternating Current
BS	British Standard
CB	Circuit Breaker
COMTRADE	Common Format for Transient Data Exchange for Power Systems
CSV	Comma Separated Value
CT	Current Transformer
DAB	Dual Active Bridge
DC	Direct Current
DER	Distributed Energy Resource
DG	Distributed Generation
DNO	Distribution Network Operator
DPMC	Dynamic Protection Modelling Controller
DSO	Distribution System Operator
DT	Definite Time
DTT	Direct Transfer Trip
EFR	Enhanced Frequency Response
EI	Extremely Inverse
EMC	Electromagnetic Compatibility
ER	Engineering Recommendation
ESO	Energy System Operator
EV	Electric Vehicle
FACTS	Flexible AC Transmission System
FB	Full Bridge
FFT	Fast Fourier Transform
FIT	Feed-In Tariff
FPL	Flexible Power Link
G	Ground (Earth)
GB	Great Britain
GPS	Global Positioning System
GSP	Grid Supply Point
HB	Half Bridge
HiL	Hardware-in-the-Loop
HMI	Human-Machine Interface

HV	High Voltage
HVAC	High Voltage Alternating Current
HVDC	High Voltage Direct Current
IDMT	Inverse Definite Minimum Time
IEC	International Electrotechnical Commission
IED	Intelligent Electronic Device
IEEE	Institute of Electrical and Electronics Engineers
IGBT	Insulated Gate Bipolar Transistor
LCC	Line Commutated Converter
LCOE	Levelised Cost Of Electricity
LED	Light Emitting Diode
LFDD	Low Frequency Demand Disconnect
LV	Low Voltage
LVDC	Low Voltage DC
MAV	Mercury-Arc Valve
MCB	Miniature Circuit Breaker
MCCB	Moulded-Case Circuit Breaker
MMC	Modular Multi-level Converter
MOSFET	Metal Oxide Semiconductor Field Effect Transistor
MVDC	Medium Voltage Direct Current
NCP	Normally Closed Point
NIC	Network Innovation Competition
NOP	Normally Open Point
NPC	Neutral Point Clamped
NVD	Neutral Voltage Displacement
OFGEM	Office of Gas and Electricity Markets
OHL	Overhead Line
PG	Pole-to-Ground
Ph	Phase
PhD	Doctor of Philosophy
PLC	Power Line Communication
PMAR	Pole Mounted Auto-Recloser
POTT	Permissive Over-reaching Transfer Trip
PP	Pole-to-Pole
PPG	Pole-to-Pole-to-Ground

PUTT	Permissive Under-reaching Transfer Trip
PV	(Solar) Photovoltaic
RMS	Root Mean Square
RoCoF	Rate-of-Change-of-Frequency
RTDS	Real-Time Digital Simulator
SCADA	Supervisory Control And Data Acquisition
SD	Secure Digital
SI	Standard Inverse
SNOP	Soft Normally Open Point
SOP	Soft Open Point
SPWM	Sinusoidal Pulse Width Modulation
SSEN	Scottish and Southern Energy Networks
TMS	Time Multiplier Setting
TNO	Transmission Network Operator
TPL	Technology Performance Level
TRL	Technology Readiness Level
TSO	Transmission System Operator
UDP	User Datagram Protocol
UHVDC	Ultra-High Voltage Direct Current
UK	United Kingdom
USA	United States of America
USB	Universal Serial Bus
VI	Very Inverse
VSC	Voltage Source Converter
VT	Voltage Transformer
Wi-Fi	IEEE 802.11 family of standards
WPD	Western Power Distribution
Z1	Zone 1
Z2	Zone 2
Z3	Zone 3
Z4	Zone 4
4G/5G	Fourth/fifth generation of mobile phone technology

Chapter 1

Introduction

1.1 Introduction to the Research

There is increasing interest in the use of direct current (DC) at several voltage levels within the power system. High voltage direct current (HVDC) is becoming the standard for interconnections (e.g. between countries and/or major elements of large AC systems), subsea and long-distance power transfers giving enhanced controllability and reduced losses when compared to equivalent AC (alternating current) systems [1]. Point-to-point HVDC links are well established both academically and commercially with many installations found worldwide [2]. Low voltage direct current (LVDC) is gaining attention in the building services sector [3]. Charging of electric vehicles (EVs) using DC is becoming the norm for high-powered charging technologies (e.g. 50 kW, 120 kW) [4] [5]. LED (light-emitting diode) street lighting networks powered via DC are being commercially installed in mainland Europe to improve reliability and provide secondary benefits such as the ability to host 4G/5G/Wi-Fi access points [6]. Despite the prevalence of AC in existing power systems, utilities are now trialling the supply of DC to end-users [7]. The use of DC within industrial processes [8] and datacentres [9] is also being considered increasingly in order to reduce the total number of conversion stages between AC and DC systems and so to increase efficiency and reliability [10].

Since the early 2000s, the connected capacity of renewable energy generators within Scotland, Europe and internationally has increased substantially. The uptake of low emission generation has been stimulated by the need to reduce the carbon intensity associated with the electricity sector which accounts for approximately 25% of the total energy demand in Scotland [11]. Much of this new generation is connecting to the distribution network (33 kV and below in Scotland) rather than to the transmission system as would have been the norm historically for large-capacity conventional generating stations. This is largely due to the relatively lower capacity of the renewable generation and its closer proximity to load centres.

The creation of additional network capacity is time-consuming and expensive due to design timescales, delays in planning approvals (which are often subsequently challenged), increasing

commodity and construction costs and long lead times in the supply chain. Investment maps for Scottish network operators already show relatively small (£100k - £500k) modernisation and uprating projects being worked on in 2019 which are not due for completion until 2023 [12]. These long timescales often represent a barrier to the installation and connection of further renewable generators to existing systems [13].

Medium voltage direct current (MVDC), operating between 5 kV and 50 kV, can help alleviate some of the congestion experienced by distribution system operators (DSO). This is explored and reported in this thesis via a literature review, along with several network simulation studies which are presented as supplementary material.

As the electricity network transitions towards a hybrid AC-DC grid, at various voltage levels, the protection of the system components and networks must be re-evaluated as some methods may no longer be valid [14] [15]. The appropriateness and stability of loss-of-mains (islanding) protection, for example, has been heavily investigated in recent years as more distributed and converter-based generation is being connected to the distribution system and large-scale centralised synchronous generation is being decommissioned [16] [17] [18]. The shift towards non-synchronous generation has resulted in a system which has lower inertia. Inertia is the property of the power system that resists frequency change and is primarily provided by rotating machines, and is linked to rotor mass, diameter and speed [19] [20]. Renewable generators are often mechanically and electrically decoupled from the power network, through power electronic converters, which allows variable frequency generators (e.g. wind turbines) and chemical processes (e.g. solar systems) to be interfaced to the AC grid. This decoupling means that converter-interfaced generation can only provide limited, but often no, inertia to the AC grid. Low system inertia increases the risk of rapid system changes meaning that frequency may change more quickly than was previously assumed both for normal operation and under fault conditions [19]. As a result of increased distributed generation (DG) and reducing system inertia, the tripping threshold of rate-of-change-of-frequency relays (RoCoF) in the GB power system are being adjusted from 0.125 Hz/s to 1 Hz/s [21].

Another example of a protection challenge associated with transitioning towards increased levels of DG is protection ‘blinding’ of overcurrent relays. When a distributed generator is connected between an overcurrent protection relay and a system fault, the DG will supply some of the current flowing to the fault which may cause the fault current measured by some overcurrent relays to be reduced (while at others it could be increased depending on relative locations) as in Figure 1-1 [22] [23]. This may cause slower operation of the protection relay and could, theoretically, lead to non-operation [24].

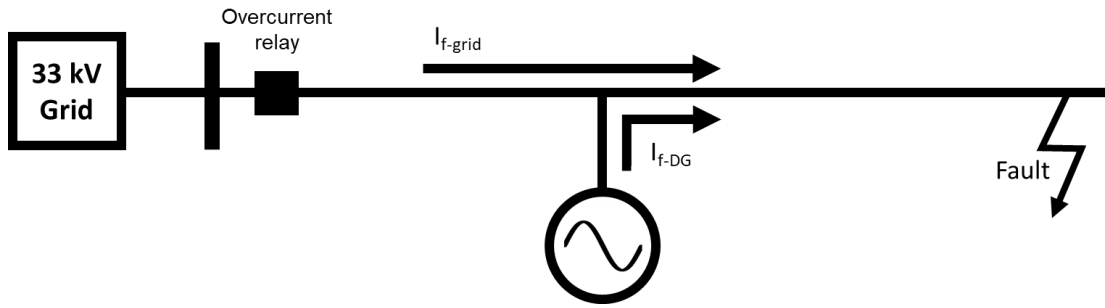


Figure 1-1: Blinding of overcurrent protection relay

It has been determined that the backup protection of MVDC links is not well considered in literature nor in practice; especially from a wider network perspective (i.e. the AC protection providing backup to the main DC protection). This thesis aims to address this shortcoming via the development and demonstration of a standalone (i.e. a system which does not require communications) fast-acting backup protection scheme for embedded MVDC links which could be realised using existing AC protection and measurement systems, albeit with modifications.

1.2 Justification for Research

Power systems of the future are being shaped by climate change policy [25], resource availability, socio-economic pressures and the increasing availability, efficiency and reducing price of power electronics devices, energy storage, communications and computing/data processing equipment. The way in which energy is consumed and produced is changing with a societal shift towards a more sustainable and lower carbon economy. The closure of large centralised electrical power generation plants [26] [27] and the increase in distributed generation, often from renewable energy sources, and more recently the uptake of battery and other forms of storage (such as compressed liquid air [28] and electrolysis to produce hydrogen [29]), is altering the everyday business of both transmission and distribution network operators. The cumulative capacity of battery storage planning applications in the UK for 2019 was 10.5 GW compared to 6.9 GW in the previous year - while in 2012 this figure was only 2 MW [30].

Support mechanisms, such as Renewable Obligation Certificates (ROCs) [31] and the Feed-In Tariff (FIT) [32], provided a financial incentive to develop renewable energy projects and have, in part, helped to reduce costs of renewable technologies. In the period 2018/2019, the mean cost of a domestic (i.e. ≤ 4 kW) solar photovoltaic (PV) installation was £1,816 per installed kW compared to £2,400 (when corrected for inflation) in 2013/2014 [33]. Renewable

generation sources often now represent the cheapest form of electrical energy [34] in terms of levelised cost of electricity (LCOE). LCOE represents the average revenue per unit of energy generated required to recover the capital and operational costs of a plant for an assumed operating life [35]. Figure 1-2 presents the ranges of LCOE of a variety of renewable and conventional generation types in Germany where it was observed that utility-scale solar and onshore wind delivered the lowest cost of electrical energy for the year 2018 [36].

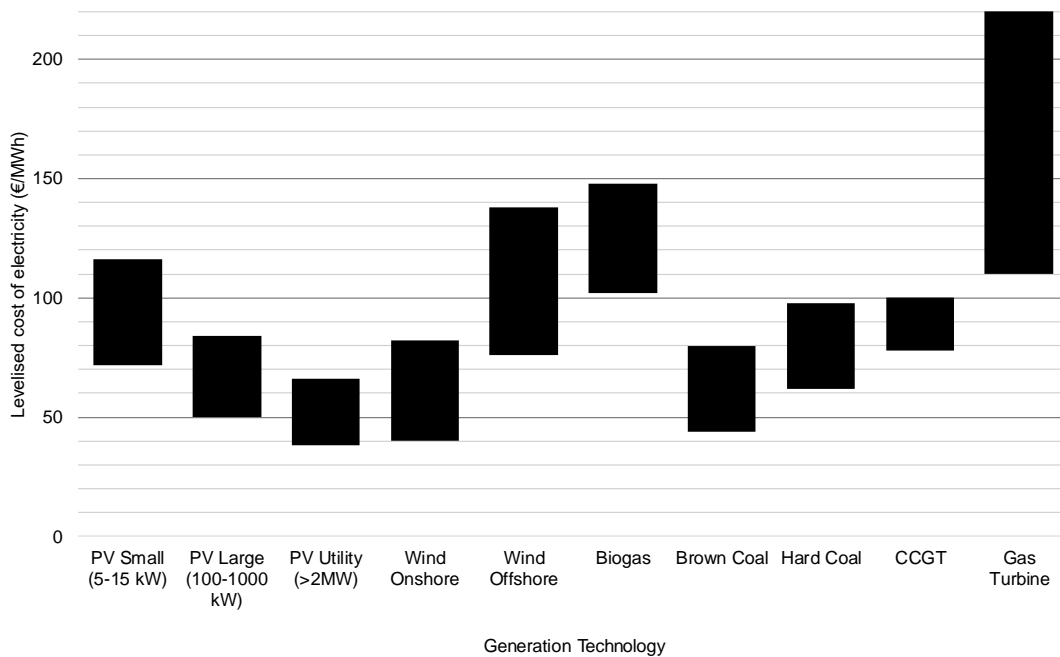


Figure 1-2: LCOE by generation type at various locations across Germany 2018 [36]

While substantial progress has been made with decarbonising the electricity system, considerably more effort and innovation will be required to make constructive emission reductions in the heat and transport sectors [37]. Ambitious climate change targets set by the Scottish Government [38] [39] have led to rapid growth in renewable energy generation over the last decade. Recently, the Scottish Government has outlined its intention to ban the sale of all petrol and diesel only vehicles by 2032 [38]. In September 2019, legislation was enacted which commits Scotland to become a “net-zero” carbon society by 2045 with a 75% reduction in carbon emissions by 2030 [40]. Various definitions for “net-zero” exist, however, the term can be broadly defined as the balancing of carbon-dioxide emissions, created through human-activity, with carbon-dioxide removal (through techniques such as carbon capture and storage, tree planting, etc.) for a specific period [41]. This will inevitably have pronounced impacts on distribution networks if the uptake of electrified transport and heat is as dramatic as the uptake in renewables. With a significant proportion of grid supply points (GSP) in southern and

central Scotland already restricting the connection of further distributed resources as outlined in Figure 1-3 (where red areas highlight regions operating close to operational limits, amber areas illustrate areas approaching limits and green regions have no constraining factors), it is apparent that new capacity needs to be made available in these networks to facilitate the connection of more low carbon generators and future low carbon demand.

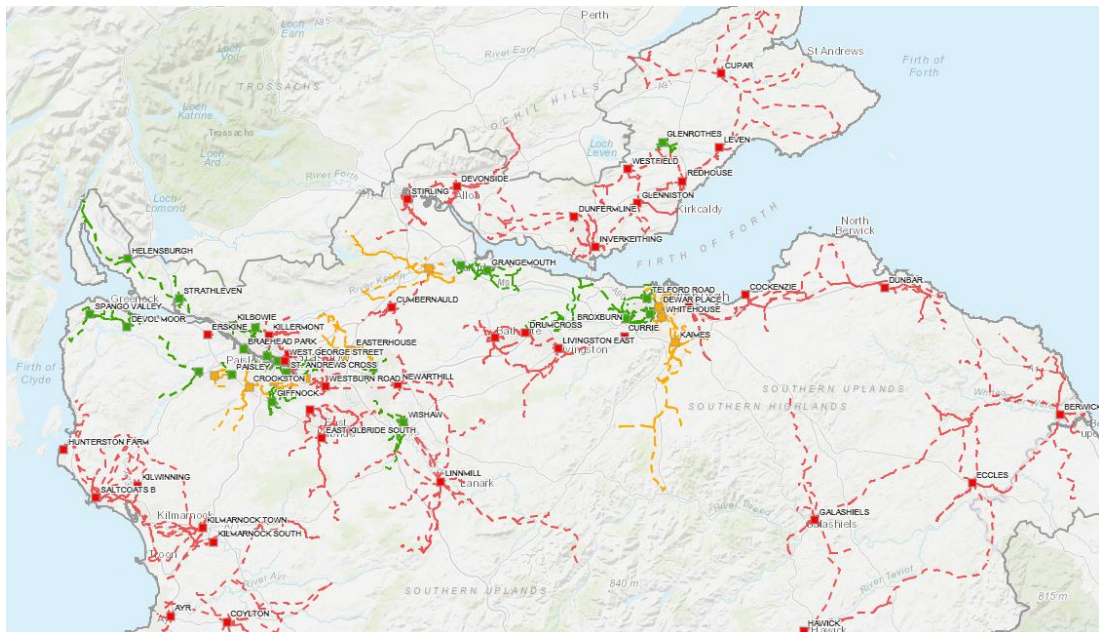


Figure 1-3: 33 kV generation heat map of central and southern Scotland [42]

While electrical power generation has witnessed a significant departure from conventional large-scale thermal power plants, the design philosophy of power transmission and distribution networks has remained largely unchanged since the 1950s [43] [44]. With further increases in distributed energy resources (DER) predicted, in conjunction with electrical load growth associated with the transition towards the electrification of heat and transportation, the way in which distribution networks are designed, operated and controlled must change to avoid expensive and invasive network reinforcement [45].

Faults are inevitable in power systems as it is impractical and prohibitively expensive (and arguably impossible) to safeguard assets against every hypothetical scenario that could lead to a fault. Protection systems, therefore, defend power networks against abnormal operating conditions by removing faulted assets from the system quickly, following the detection of a fault (the majority of faults involve an electrical short circuit where conductors come in contact with one another and/or with ground). As with HVDC, embedded MVDC links are currently treated as an individual item of plant, i.e. protection of the DC link is not considered from a wider network perspective – although it is common to have backup AC-side protection at the

converter station [46] as well as direct transfer tripping schemes [47]. Should the plant protection system fail to identify or fail to isolate a DC fault (e.g. the converter circuit breaker fails to open), the converters could remain operational in a potentially damaging situation.

No literature has been found which examines the opportunity of detecting faults on embedded MVDC links via remote measurements on the AC grid. This PhD thesis is therefore concerned with the detection of DC-side events from AC system measurements. A suitably fast, backup protection methodology is proposed and developed over the subsequent chapters and is validated through simulation studies and laboratory-based demonstrations.

1.3 Principal Contributions

In terms of the novelty of the research conducted and disseminated through this thesis, the primary contributions to knowledge can be summarised as follows:

- design, development and testing of a new fast-acting backup protection scheme for the detection of faults on MVDC links using existing AC distance protection relays without the need for any communication facilities;
- deployment of the protection scheme on a commercially available protection device in a hardware-in-the-loop simulation environment;
- implementation and verification of an improved protection algorithm, which employs an R-X coordinate based setting approach, on a low-cost computing platform within a hardware-in-the-loop environment;
- quantification of the apparent AC-side impedance associated with a DC fault through software simulation;
- validation of the apparent AC-side impedance associated with a DC fault through hardware experimentation;
- a review of MVDC projects across Europe with an emphasis on land-based power distribution applications;
- demonstration for the need for control in distribution networks to facilitate the future expansion of both load and generation; and
- the design and validation of a distance protection model suitable for use in software simulation and on dedicated hardware platforms.

1.4 Thesis Organisation

This thesis is organised into seven chapters. The remaining chapters of the thesis are briefly described below.

Chapter 2 provides an overview of both AC and DC power systems, including their key features and applications. The process of converting between AC and DC will be examined and technologies described.

Chapter 3 reviews the systems, components and methodologies employed to detect and isolate faulted components during faults on the power system. A summary of distribution protection schemes is provided along with a review of HVDC protection.

Chapter 4 introduces the concept of incorporating controlled MVDC links within distribution networks. International demonstration activity in this area will be presented alongside a critical literature review of relevant research.

The apparent AC-side impedance, as measured by a distance protection relay, is determined for faults residing on an embedded MVDC link (employing typical converters and controllers) in Chapter 5. A novel backup protection method to safeguard against DC faults is developed and verified in software. This method does not rely on communications as is the norm with existing backup methods deployed in HVDC applications. This chapter represents the main contribution to knowledge developed during the PhD.

Expanding on the proposed protection scheme outlined in the previous chapter, it is demonstrated in Chapter 6 how the solution may be implemented on a commercially available distance protection relay. Methods to improve the stability of the solution are demonstrated by deploying the protection algorithm on a low-cost hardware platform. This chapter also verifies the simulated fault impedance on a physical test network.

Chapter 7 presents a summary of the work presented in the thesis and highlights the key contributions to knowledge developed through the research. Future work opportunities are also presented.

Supplementary material is presented at the end of the thesis and consists of a series of network studies where the introduction of controlled MVDC links proves to be beneficial from several perspectives.

1.5 Publications and Achievements

The following publications and achievements have arisen during the development of this PhD:

1.5.1 Journal Articles

A new fast-acting backup protection strategy for embedded MVDC links in future distribution networks

L. Hunter, C. Booth, A. Egea-Alvarez, A. Dyško, S. J. Finney and A. Junyent-Ferré

Published in IEEE Transactions on Power Delivery (Early Access) – 18th May 2020

10.1109/TPWRD.2020.2995479

ISSN : 0885-8977

1.5.2 Conference Papers

MVDC for enhanced utility-scale distribution power delivery and control

L. Hunter, C. Booth, A. J. Ferré and S. Finney

52nd International Universities Power Engineering Conference

(UPEC)

Heraklion, Crete, 2017

10.1109/UPEC.2017.8232000

MVDC network balancing for increased penetration of low carbon technologies

L. Hunter, C. Booth, S. Finney and A. J. Ferré

IEEE Power & Energy Society (PES) Innovative Smart Grid Technologies Conference

Europe

(ISGT-Europe)

Sarajevo, Bosnia and Herzegovina, 2018

10.1109/ISGTEurope.2018.8571838

The impact of MVDC upon conventional distance protection schemes in hybrid AC-DC distribution networks

L. Hunter, C. Booth, A. Dyško, S. Finney and A.J Ferré

15th IET International Conference on AC and DC Power Transmission

(ACDC 2019)

Coventry, United Kingdom, 2019

10.1049/cp.2019.0019

Hardware in loop verification of conventional AC distance protection relays in hybrid AC-DC distribution networks

L. Hunter, Q. Hong, C. Booth, A. Dysko, S. Finney and A.J Ferré
IEEE International Conference on DC Microgrids
(ICDCM 2019)
Matsue, Japan, 2019

Integrated charging of battery electric vehicles using existing LVDC light rail infrastructure

L. Hunter, K. Smith, S. Galloway and C. Booth
IEEE International Conference on DC Microgrids
(ICDCM 2019)
Matsue, Japan, 2019

An improved fast-acting backup protection strategy for embedded MVDC links

L. Hunter, Q. Hong and C. Booth
15th International Conference on Developments in Power System Protection
(DPSP 2020)
Liverpool, UK, 2020

1.5.3 Achievements

Medium Voltage DC - Freeing up latent grid capacity quickly and affordably

B4 PS2 Young Member Showcase Presentation
2018 CIGRE Session
Paris, France, 2018

Smart Future Energy Systems (Smart FuturES 2018) conference

Main Organiser of Inaugural Conference
Technology Innovation Centre, University of Strathclyde
Glasgow, Scotland, 2018

Embedded MVDC for increased penetration of low carbon technologies

Best Poster Award
Aachen DC Grid Summit 2018
Aachen, Germany, 2018

Embedded MVDC for increased penetration of low carbon technologies

Highly Commended Poster

Hubnet Symposium

Bath, United Kingdom, 2018

A New Backup Protection Scheme for Hybrid AC/DC Power Systems

Best Presentation Award

Future Power Systems and Smart Grids – Spring 2020 Conference

Glasgow, Scotland, 2020

Chapter 2

Review of AC, DC and Power Conversion Technologies

2.1 Introduction

Over recent decades, the debate of whether AC or DC is most suited for utility-scale power delivery applications has re-emerged [48] [49] [50]. Despite the near-universal adoption of AC power systems for electricity transmission and distribution purposes, DC technologies are already very common for some applications such as the supply and charging of portable appliances e.g. laptops and mobile phones, in particular via USB standards [51]. It is also used internally in many consumer devices, with internal conversion being used to condition the AC power supply for use by the appliance. DC is particularly popular in ‘off-grid’ applications for example the use of ‘solar-home-systems’, essentially a solar panel and battery system, for developing countries. More recently, the trend towards electrification of transportation [52], via electric vehicles, represents a significant driver of DC particularly for high power charging applications [53].

In parallel with this, considerable emphasis has been put on the need to shift towards a low carbon economy [25] [38] [39]. Conventional centralised electricity generation based on coal, gas and oil are being decommissioned as distributed renewable energy resources, such as solar, onshore and offshore wind, offer a more affordable cost of energy [54].

Section 2.2 presents a discussion on the role of AC systems in modern society as the prime means of electricity delivery to customers with a particular focus on utility-scale distribution networks. The role of DC power systems and how semiconductor technology can be employed for efficient conversion between AC and DC systems will be introduced in Section 2.3. The fundamentals behind the conversion techniques will be examined for the predominant technologies on the market. The drivers behind HVDC will be investigated in Section 2.4.

2.2 AC Systems

The universal adoption of AC for utility-scale power systems is linked with the ease of changing system voltage using transformers, to allow cost-effective and efficient transmission.

A collateral advantage is that, readily engineered, highly reliable and brushless rotating machines lend themselves to AC generation of power at scale [55]. For a given power transfer, a high voltage system requires less current than a system of lower voltage, but at the expense of additional insulation. This allows economic advantage through reduction both in ohmic losses and conductor cross-sectional-area. These are the reasons that AC is widely used, and that progressively higher voltages are used to transfer progressively higher amounts of power, recognising the compromise between losses and the cost of insulation.

Accordingly, AC systems have historically been the prime candidate for transmitting power over long distances. Due to advances in power electronic conversion technologies, the dominance of AC is now open to question - as discussed in Section 2.2.2.

2.2.1 Structure of AC Electricity Supply Networks

In Scotland, there are three common utility-scale distribution and supply voltages; 33 kV, 11 kV, and 400 V with limited legacy 6.6 kV sections (all voltages expressed are the line-line rms voltages in a three-phase system). The transmission system operator (TSO) supplies the distribution network operator (DNO) at grid supply points (GSP) via transformers which convert from the transmission voltages in Scotland of 400 kV, 275 kV or 132 kV to 33 kV. In England and Wales, 132 kV is classed as a distribution voltage and the transmission/distribution interface is from 275 kV or 400 kV to 132 kV.

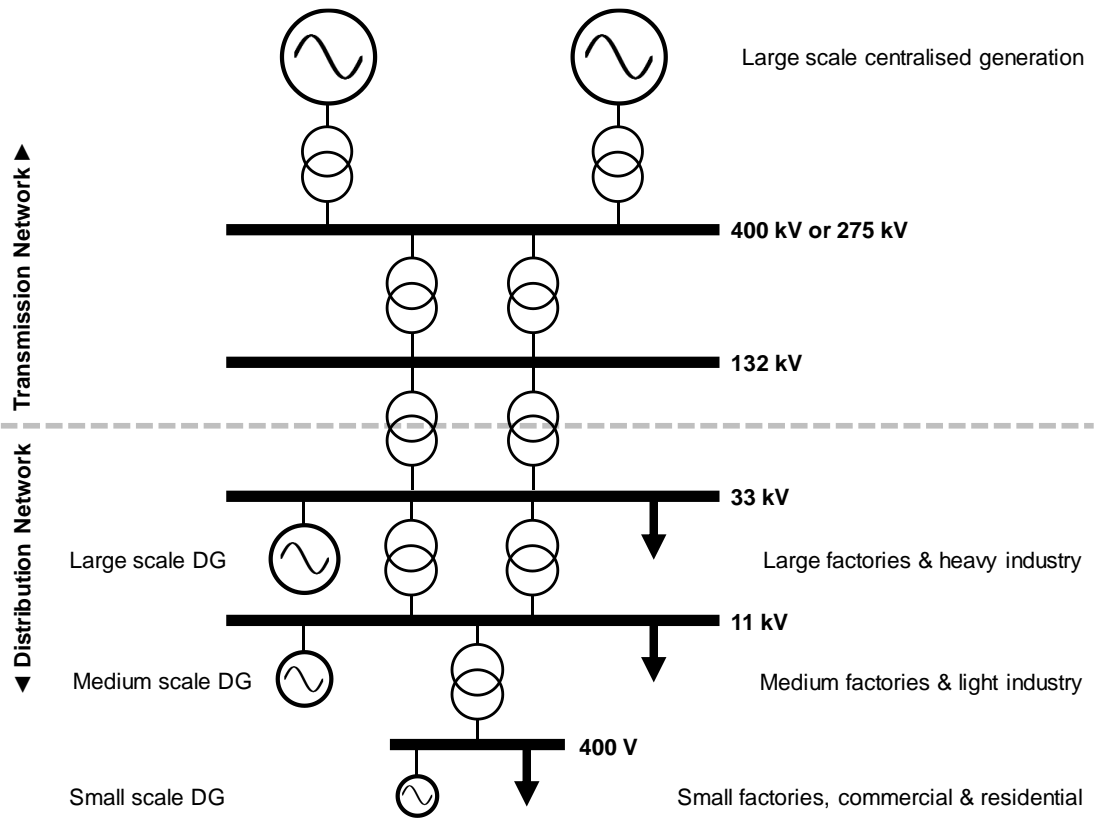


Figure 2-1: Simplified utility-scale electricity network topology

Figure 2-1 displays a diagram of a utility-scale generation, transmission, distribution and load system. Figure 2-2 presents a simplified distribution network topology. The rest of this section will make continued reference to the Long Term Development Statements produced annually by SP Energy Networks and Scottish and Southern Energy Networks (SSEN) which are the two regional electricity network operators (both at transmission and distribution) within Scotland [56] [57].

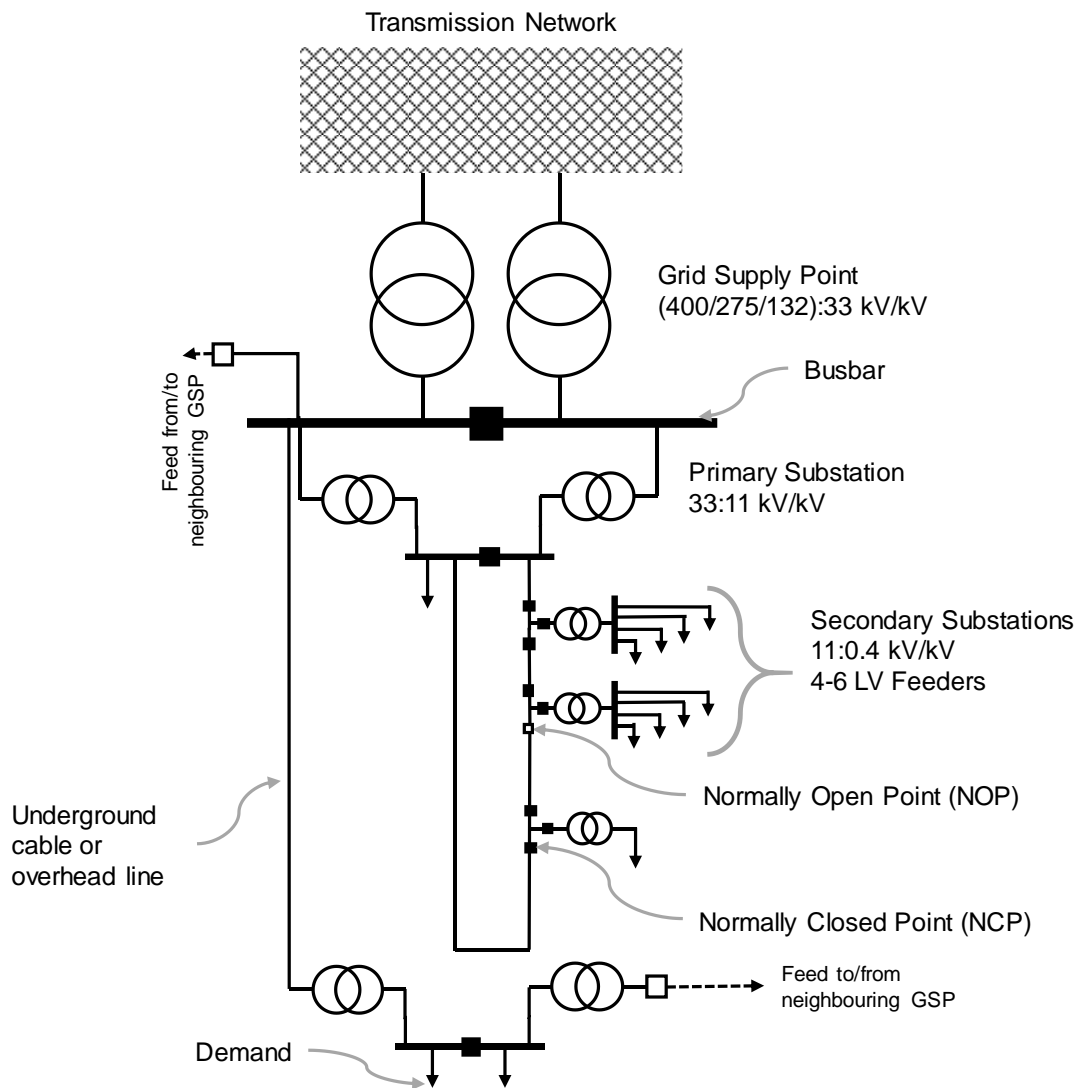


Figure 2-2: Single-line distribution network topology

From the 33 kV GSP busbar, several circuits supply primary substations located throughout the served area. A primary substation converts 33 kV to 11 kV via a transformer with a typical rating of between 5 to 20 MVA. Downstream of the 11 kV transformer there are generally between four to six feeders which are run as radial open rings. The use of normally open points (NOP) and normally closed points (NCP) allows the open rings to be reconfigured for maintenance and fault isolation and restoration purposes. This is achieved by manually opening or closing these points (although in some cases remote control and automation can be used). To reduce network downtime, switching of these points at 33 kV is generally achieved via remote telecontrol.

11 kV to 400 V transformers, commonly referred to as secondary transformers or secondary substations, are distributed along each of the 11 kV circuits. UK Power Networks (the DNO

in South-East England, East England and London) states that it typically connects 8 secondary units per 11 kV feeder in an urban environment [58]. Standard ratings of these secondary transformers are in the range of 500 kVA to 1,000 kVA for urban and suburban applications. In a rural environment, secondary transformers are often pole-mounted and of significantly lower ratings due to the lower levels of demand.

Transformers at all voltage levels, other than 11:0.4 kV units, are duplicated to ensure redundancy in the event of a transformer failure or planned outage. As alluded to previously, most substations have partial interconnection with adjacent substations to allow load to be served under a planned or forced outage.

While interconnection between separate circuits and substations is key to providing a reliable power system, too much interconnection may lead to increased fault levels as impedance between source(s) of fault current and fault locations reduces. The term fault level is used to quantify the maximum prospective current which will flow at a particular point in a network should a short circuit event occur [59]. The value is generally stated as an apparent three-phase power in MVA (with nominal voltage assumed) or as a single-phase current in kA. The maximum design fault levels in the UK for 33 kV and 11 kV distribution systems are 1,000 MVA (17.5 kA) and 250 MVA (13.12 kA) respectively [56] [60]. The rating of switchgear, such as circuit breakers (CB) and fuses, must be able to withstand and operate for the maximum fault current expected with equipment such as transformers and cables being required to withstand the maximum fault current for a period of 3 seconds [61]. Operating above switchgear rating means that current may not be interrupted successfully when devices try to open.

In addition to maintaining and operating power networks, utilities also operate communications networks or SCADA (Supervisory Control And Data Acquisition) systems which allow for remote monitoring and control of power system assets. The majority of 33 kV substations have some degree of communication and remote-control capability, while communications and control at 11 kV are considered on a case by case basis according to loading, location, communication options etc. LV (400 V) networks generally have no monitoring, however with the shift towards the distribution system operator (DSO) model¹, it is likely that utility communication networks will extend their reach into lower network voltage levels [62].

¹ DNOs traditionally adopted network designs to support maximum demand and generation. A DSO uses techniques such as automation, ancillary services, markets etc. to actively manage demand, generation and flexible customers to operate its network within regulatory and technical limits and to provide more active support to the overall system operator [51]

2.2.2 Limitations of AC

While AC systems have many benefits, they can be challenging to operate under certain conditions – particularly for underground cable circuits over long distances. Overhead circuits are more widely used for long distance transfers but are more susceptible to faults, as will be detailed in the subsequent chapter, and may not be suitable for some applications such as city centres and through areas of outstanding natural beauty etc. The reactance associated with cables and overhead lines can introduce limitations to real power transfer [63]. As AC circuits increase in length, more reactive current (known as charging current) is required to “charge” the capacitance of the system. This means that there is less “headroom” available in the conductor for the transfer of real power. Compensation technologies, such as switched compensation (e.g. capacitors and reactors) and FACTS (Flexible AC Transmission Systems) devices, enhance the controllability of AC networks and allow for the power transfer capability of a system to be increased and voltages to be managed within operational and statutory limits [64]. Figure 2-3 outlines a selection of traditional and FACTS-based compensation technologies.

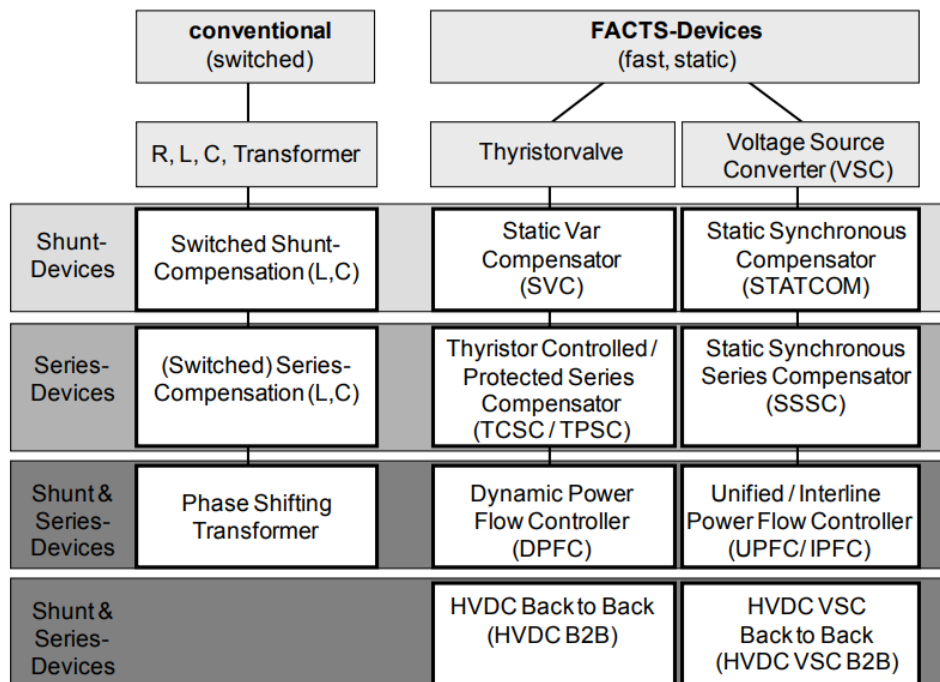


Figure 2-3: Overview of AC compensation technologies [65]

Other non-desirable properties, such as the skin effect, which is the tendency for current in an AC system to flow through the outer region of a conductor [66], start to become limiting at long distances. The skin effect effectively reduces the usable cross-sectional area of AC

conductors – although the effects of this can be reduced through the use of bundled conductors and hollow busbar sections. For the reasons outlined, the maximum length of AC conductors is typically between 50 km – 100 km for cable circuits and 600 km – 800 km for overhead lines [67].

The creation of new AC wayleaves (rights of way) is challenging and expensive. The development and delivery of the 400 kV, 220 km, Beaully-Denny transmission line in Scotland is a prime example of this [68], where electrical modelling studies were first carried out in 2001 to identify how best to reinforce the existing 132kV network between North and Central Scotland to accommodate increasing renewable generation. In 2005 the route for the circuit was proposed - a lengthy public consultation period and a public enquiry then followed. The scheme was granted planning permission in 2010 and fully energised late 2015 - 15 years after initial studies began.

With the nature of generation changing so rapidly, subsea cabling is rapidly becoming the favoured long-distance, trunk transmission reinforcement method seen in GB [69] [70]. With HVDC becoming an ever more reliable and affordable option, it is tending to displace AC since it is not subject to the issues mentioned above. Additionally, subsea cabling is not visible to the general public, unlike overhead lines, making acceptance of the approach higher and therefore potentially allowing projects to be delivered more quickly.

2.3 DC Conversion Systems

Despite the predominance of AC in power transmission and distribution applications, DC systems have long been present – notably for transportation applications. Historically, battery-electric vehicles were a common form of transportation in the USA during the early 1900s [71]. The ubiquitous (UK-centric) electric milk float also being another notable example of an electric vehicle [72]. Additionally, DC technologies have long been deployed for transport systems such as urban tramways and subway applications [73].

There are several options when converting between AC and DC systems: mechanical conversion, line commutated conversion (LCC) and voltage source conversion (VSC). The modular multi-level converter (MMC), which will be described later in this chapter, is included within the VSC category. Semiconductor-based technologies are now predominantly used due to the high losses and maintenance requirements associated with mechanical conversion.

Mechanical, or rotary, converters are effectively two machines with a shared rotating shaft; essentially, an AC motor connected to a DC generator forming a mechanical rectifier. These

were commonplace in traction applications however the improved efficiency and the reducing cost of solid-state technologies have effectively made this topology obsolete. Figure 2-4 shows a series of rotary traction converters, each of 4 MW power rating, used to supply the New York underground in the early 20th century. The last of these devices were only removed from service in the late 1990s [74] [75].

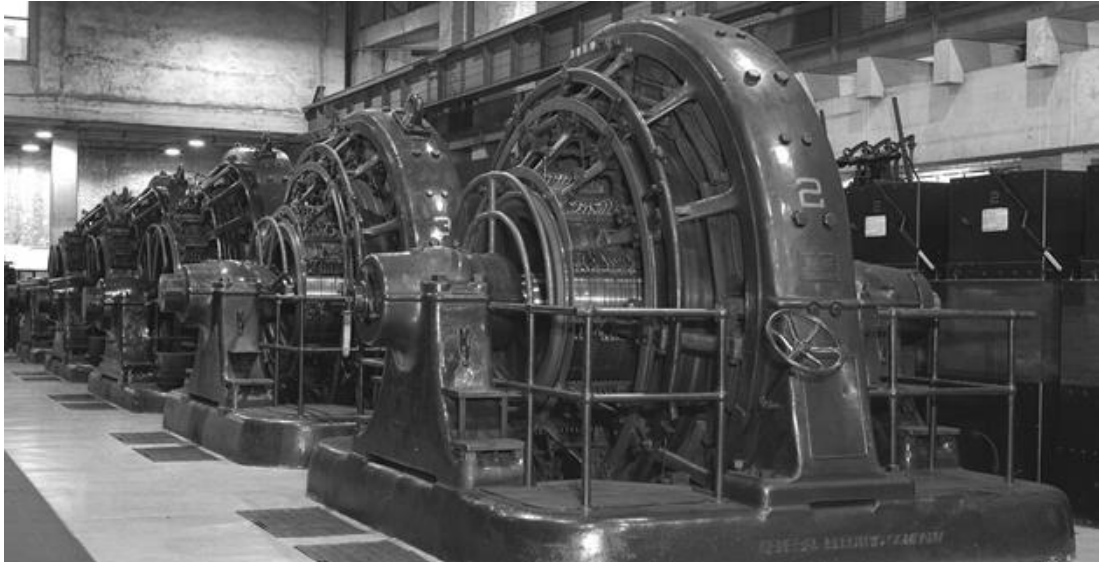


Figure 2-4: 4,000 kW rotary traction converter - 1929 (≈ 400 V AC to 600 V DC) [74]

2.3.1 Summary of Power Electronic Devices

There are three main power electronic devices which are extensively employed for the conversion between AC and DC – diodes, thyristors and IGBTs (insulated-gate bipolar transistor), with their electrical symbols depicted in Figure 2-5. The fundamental physics and detailed characteristics for these devices can be found in many power electronics textbooks [66].

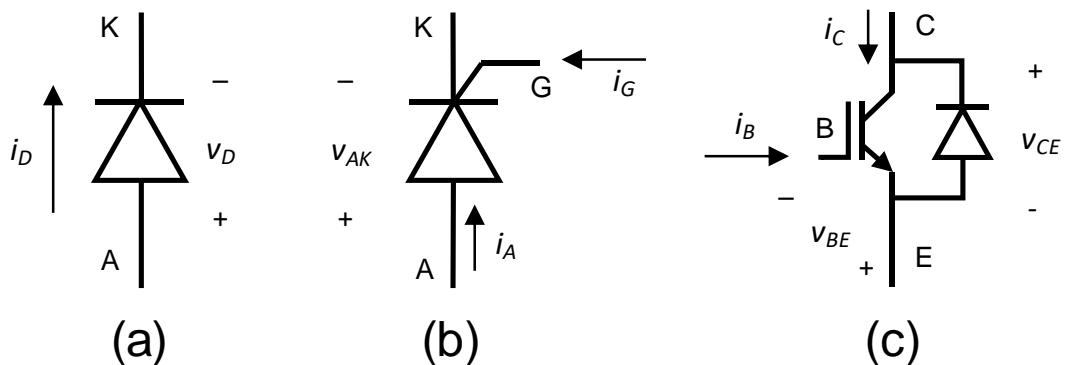


Figure 2-5: Electrical symbols for (a) diodes, (b) thyristors and (c) IGBTs with freewheeling diode [66]

Diodes are two-terminal devices and may be considered as the simplest power electronic device. A diode only permits the flow of current (i_D) in one direction from the anode (A) to the cathode (K), in the case of conventional current, and heavily resists current flow (referred to as reverse-blocking) in the opposite direction. Diodes conduct when a small positive voltage (V_D), in the order of 1 V [66], is present across the device.

Thyristors are three-terminal devices made up of an anode, cathode and a gate (G). The conduction characteristic of a thyristor is similar to that of a diode, however the gate of the device must be enabled (i_G) to put the device into an 'on-state' to allow conduction. Once enabled, the thyristor will remain in a conducting state, even if the gate signal is removed, until current flowing through the device crosses a zero (i_A). When the zero-crossing occurs, the thyristor will no longer conduct [66].

Both the diode and the thyristor are known as 'line-commutated' devices where the switching, often referred to as commutation, is influenced by the power circuit - albeit that the thyristor can be turned on independently via its gate terminal. The switching of 'self-commutated', also referred to as 'force-commutated', devices does not depend on the electrical parameters of the power circuit they are connected to with turn on and off times being fully controlled by an external control circuit.

The IGBT is an example of a force-commutated device which is extensively used in power system applications. These devices have three terminals, a collector (C), emitter (E) and gate. Like diodes and thyristors, they can only conduct in one direction however, the switching of IGBTs is independent of the power circuit to which they connect. IGBTs are enabled and disabled by applying a control signal to the gate terminal of the device. IGBTs are often packaged with a 'free-wheeling' diode connected across the device. This diode is used to protect the IGBT module against damage caused by the sudden voltage spikes protected by the discharge of energy stored in the DC-side inductors during switching of the IGBTs [66]. These diodes are also commonly referred to as clamping diodes, snubbers, anti-parallel diodes or fly-back diodes in literature.

The ideal ' $i-v$ ' (current-voltage) conduction characteristics for the three power electric devices discussed in this section are presented and annotated below in Figure 2-6.

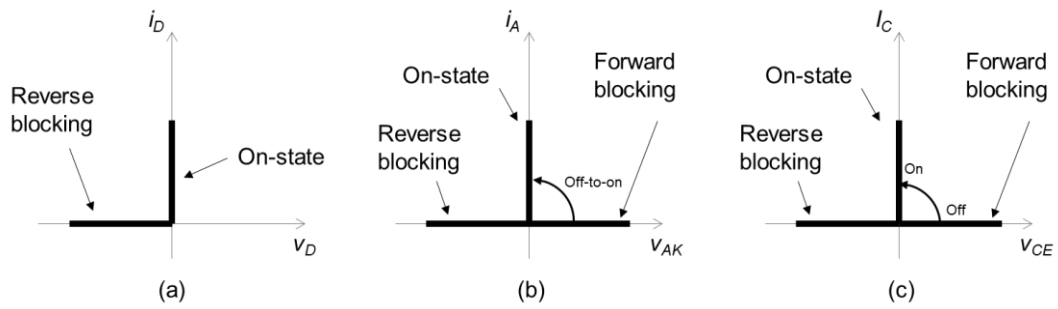


Figure 2-6: Conduction characteristic for (a) diodes, (b) thyristors and (c) IGBTs [66]

The following subsections will provide an overview of LCC and VSC conversion technologies and discuss the development of Modular Multilevel Converter (MMC).

2.3.2 Line Commutated Conversion (LCC)

Line-commutated current source converters consist of devices which are switched by the current of the AC system. As mentioned previously, these devices may include diodes, thyristors and, historically, mercury arc valves (prior to the power electronic semiconductor age).

In an HVDC environment, LCC systems are generally employed for long-distance bulk energy transfers and are often used to interface remote hydro generation plants with large cities or for energy trading between countries. There are many global examples with notable schemes in both Canada and China [76]. The 2.2 GW point-to-point Western Link which connects between Hunterston, Scotland and Flintshire Bridge, Wales is another example of an LCC HVDC scheme [77].

LCC technologies are not limited to high voltage applications with extensive use in low voltage (e.g. 750 V) traction applications primarily due to simplicity, robustness and low cost [78]. Additionally, diode rectification is commonplace within many domestic appliances such as LED luminaires, televisions, USB chargers and computers.

The physical structure of a three-phase LCC converter is outlined in Figure 2-7 where S_{1a} , S_{1b} , S_{2a} , S_{2b} , S_{3a} and S_{3b} represent power electronic switching devices (e.g. thyristors). This arrangement (also known as a six-pulse full-bridge converter) is the fundamental basis of all AC-DC and DC-AC semiconductor-based power electronic conversion techniques whether it be a twelve pulse LCC system or more complex VSC-MMC style system.

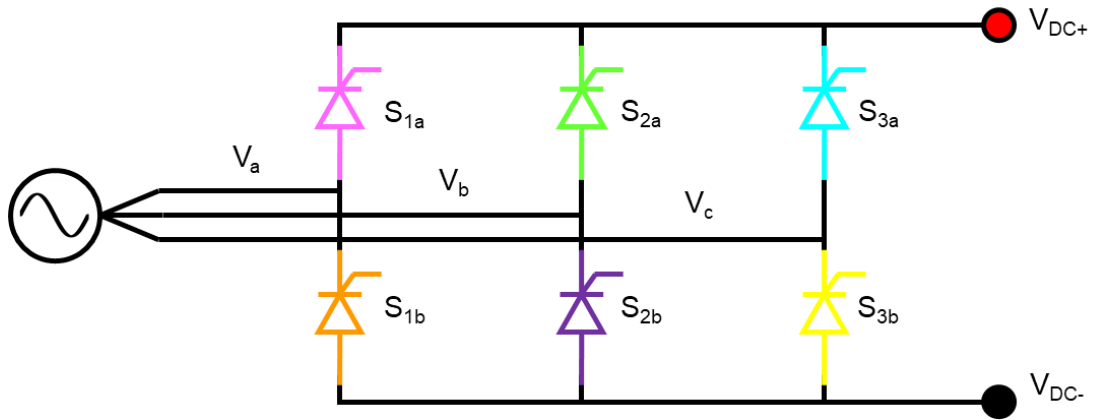


Figure 2-7: General structure of three-phase full-bridge converter with thyristors

Each switch can be put into a conducting state by triggering, or firing, the device via its control terminal. In the case of LCC systems, the device latches (i.e. the device, after being enabled by its gate) and remains in a conducting state until a zero-crossing of AC-side current occurs. Figure 2-8 shows the conduction period for each of the switching devices (S_{1a} , S_{1b} , S_{2a} , S_{2b} , S_{3a} and S_{3b}) in Figure 2-7 superimposed over a three-phase voltage waveform.

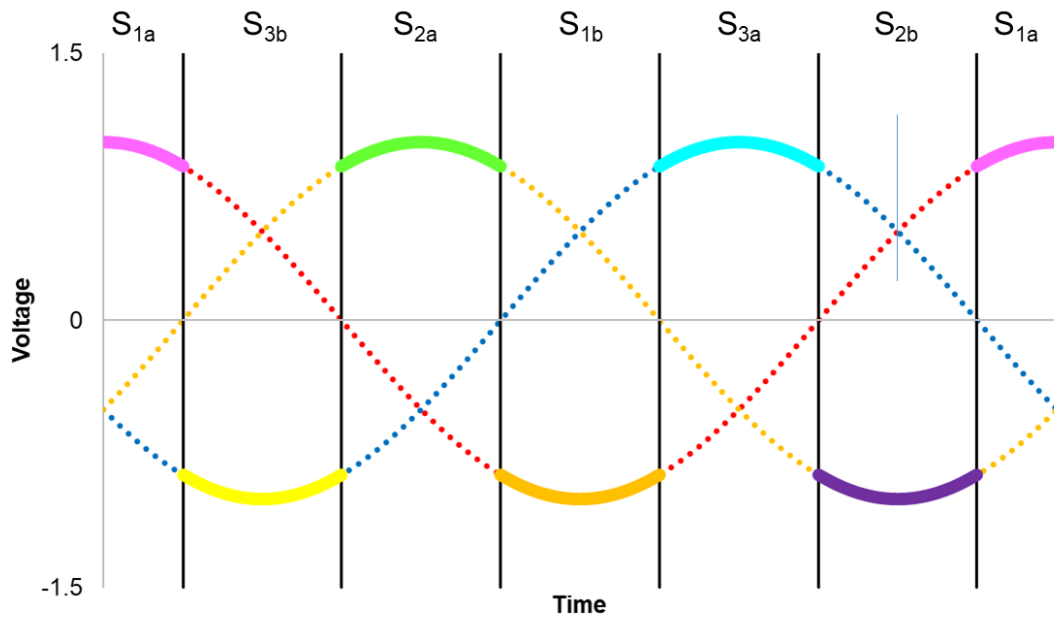


Figure 2-8: Conduction diagram for switches S_{1a} , S_{1b} , S_{2a} , S_{2b} , S_{3a} , S_{3b} superimposed on three-phase voltage waveform

Figure 2-9 represents the positive (+ve) and negative (-ve) conduction periods for a diode, or thyristor with firing angle of 0° , superimposed on top of a three-phase voltage, consisting of voltages V_a , V_b , and V_c , to yield the unsmoothed DC side voltage (V_{DC}).

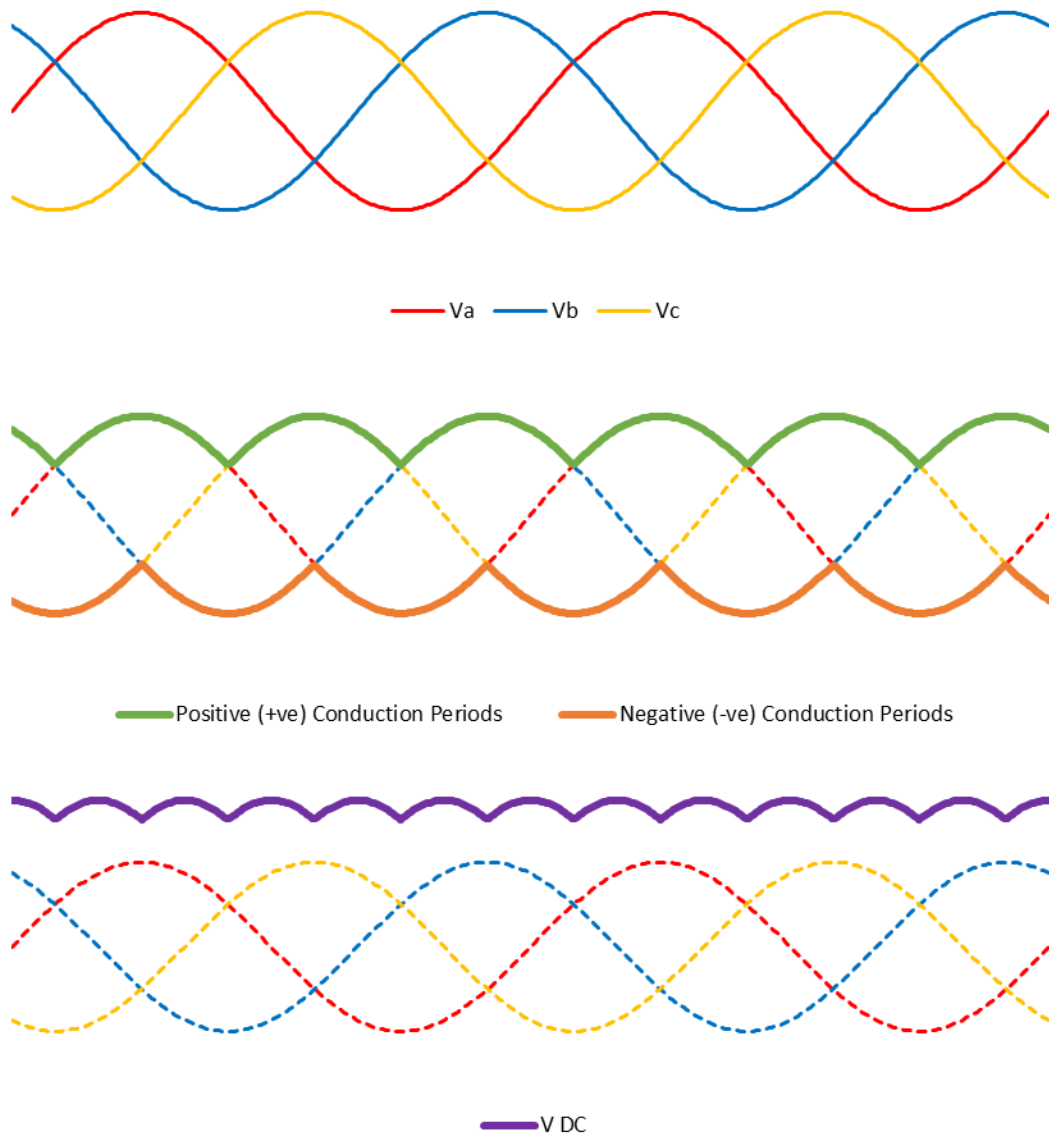


Figure 2-9: Conduction envelope for LCC converter

By delaying the switch-on time for the device (known as the firing angle), the DC-side voltage can be controlled. The mean DC terminal voltage ($\overline{V_{DC}}$) is defined in equation 2-1 where V_p is the peak AC line to ground voltage and α is the firing angle, in degrees, of the power electronic device.

$$\overline{V_{DC}} = \frac{3\sqrt{3}V_p}{\pi} \cos \alpha \quad 2-1$$

LCC converters generate low-frequency harmonics, which include 5th (250 Hz), 7th (350 Hz) and 11th (550 Hz) orders for a six-pulse converter [1]. These harmonics are associated with the

switching of thyristors, which will naturally lag the AC side voltage. As such, it is common to operate LCC converters with a low firing angle, typically $15 - 20^\circ$, to try to minimise the magnitude of harmonics generated [79].

The presence of harmonics on the wider power system may lead to poor power quality due to distorted voltages which may cause damage to electronic equipment and heating of transformers and machines [80]. To remove these harmonics, AC-side filters are required at the terminals of the converter. The reactive power required by these filters can be up to 60% of the power transfer rating of an LCC-HVDC system [81]. Filtering also contributes to the large physical footprints of LCC systems, e.g. for a full converter station site, sizes are estimated at $54 \text{ m}^2/\text{MW}$ [82].

The current flow in an LCC scheme is unidirectional and therefore a change in DC voltage polarity is required to reverse the direction of power flow in these systems. Power flow reversal features are often required for HVDC interconnectors as seen with HVDC schemes between France and the south of England [83] [84]. The coordination of this change can make multi-terminal (i.e. systems with more than two converter station nodes) LCC applications ineffective and difficult to operate [85].

Additionally, operating LCC in weak networks (a weak network is a system with high impedance and is associated with voltage stability issues and power transfer limitations [79]) is challenging as the high rate-of-change in voltage (e.g. AC faults, switching of loads, energising of lines) may lead to commutation failures [86]. Commutation failure is where a power electric switch (e.g. a thyristor) fails to turn off and continues to conduct into the next AC cycle. Commutation failure may occur when there is a voltage depression at the inverter AC bus of more than 10% [87]. When the thyristor on the opposite pole of the same converter leg is enabled, this creates a short circuit across the DC bus as outlined in Figure 2-10 [79]. The installation of parallel LCC converters in an HVDC environment can have similar effects.

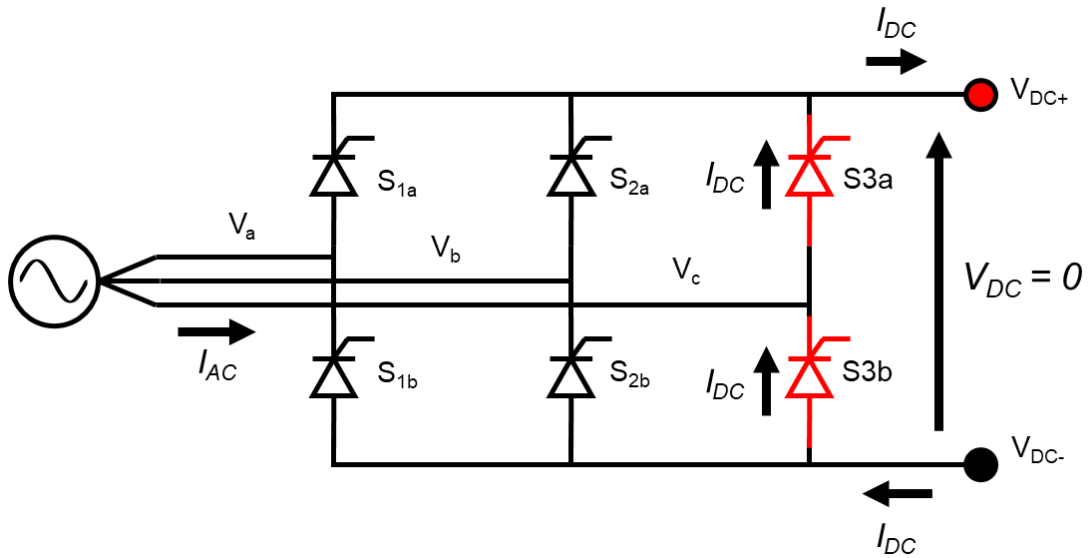


Figure 2-10: Short circuit conduction path caused by commutation failure of S3b [79]

While LCC systems offer the most efficient conversion technology, they create integration issues, especially as power grids move away from conventional rotating machines towards converter-interfaced (non-synchronous) based generation.

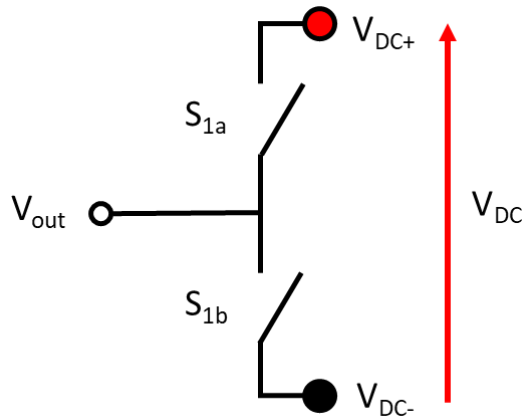
2.3.3 Voltage Source Conversion (VSC)

Voltage source converters (VSC) (also referred to as force-commutated converters) are based upon semiconductor technologies such as power MOSFETs (metal-oxide-semiconductor field-effect transistor) and IGBTs. This technology relies upon external control signals (hence the name force-commutated) to allow and block conduction of individual semiconductor devices at will. These control signals often switch devices at frequencies many hundreds of times faster than the fundamental (e.g. 50 Hz) for power applications (e.g. 2 kHz) [88]. The use of higher switching frequencies allows the low-pass filters required to remove these harmonics to be significantly smaller when compared to LCC – typically VSC sites are between 50% to 80% the area of a comparable LCC scheme [82]. As the switching frequency increases, the switching losses which occur every time a power electronic device is switched on or off, become more apparent [89]. There is, therefore, a trade-off to be made between switching losses and the size, cost and performance of filters.

To change the direction of power flow in an LCC system, the voltage polarity of the DC link needs to be reversed as the current can only flow in one direction in these systems. The ability to control the individual IGBTs independently of the AC system in VSC schemes allows the direction of the current to be changed relatively easily. Since the direction of the DC current

can be controlled, the polarity of the DC-side voltage can be fixed while still allowing the bidirectional flow of power. As such, the fixed polarity of VSC schemes makes multi-terminal DC grids more achievable as the coordination of converters to change voltage polarities is not required [79].

Figure 2-11 presents the basic structure of one ‘leg’ of a two-level VSC converter with the associated truth table in Table 2-1. Within the converter, it is of utmost importance that switches on the same leg (e.g. S_{1a} and S_{1b}) are not simultaneously closed otherwise a short circuit is created.



S_{1a}	S_{1b}	V_{out}	Comment
0	0	0	Blocked (Open circuit)
0	1	$-V_{DC}$	–
1	0	$+V_{DC}$	–
1	1	–	Invalid (Short circuit)

Figure 2-11: Basic two-level converter leg

Table 2-1: Truth table for output voltage for various switching states

Sinusoidal pulse width modulation (SPWM) allows the average voltage produced by the converter to be created and controlled. For a balanced system, the output voltage (v_{out}) is presented in equation 2-2 where $m(t)$ is the modulation function, expressed in equation 2-3, and V_{DC} is the DC bus voltage.

$$v_{out} = \frac{V_{DC}}{2} \times m(t) \quad 2-2$$

$$m(t) = M \sin(\omega t + \phi) \quad 2-3$$

The modulation function can be manipulated in terms of magnitude (M), angular velocity (ω) and phase (ϕ). This modulation function is compared to a high frequency triangular carrier signal which produces a square wave output with variable ‘on’ and ‘off’ durations (Figure 2-12). This square wave represents the control signal for one of the switches of the converter (e.g. $S_{1a} = 1$), while its neighbour receives the conjugate value (e.g. $S_{1b} = 0$). Using three modulation functions, with appropriate phase offsets, allows three-phase voltages to be

produced. Since the switching of devices occurs at high frequency, it is easy to remove the high order harmonics, using filters, to achieve near-sinusoidal voltages and currents.

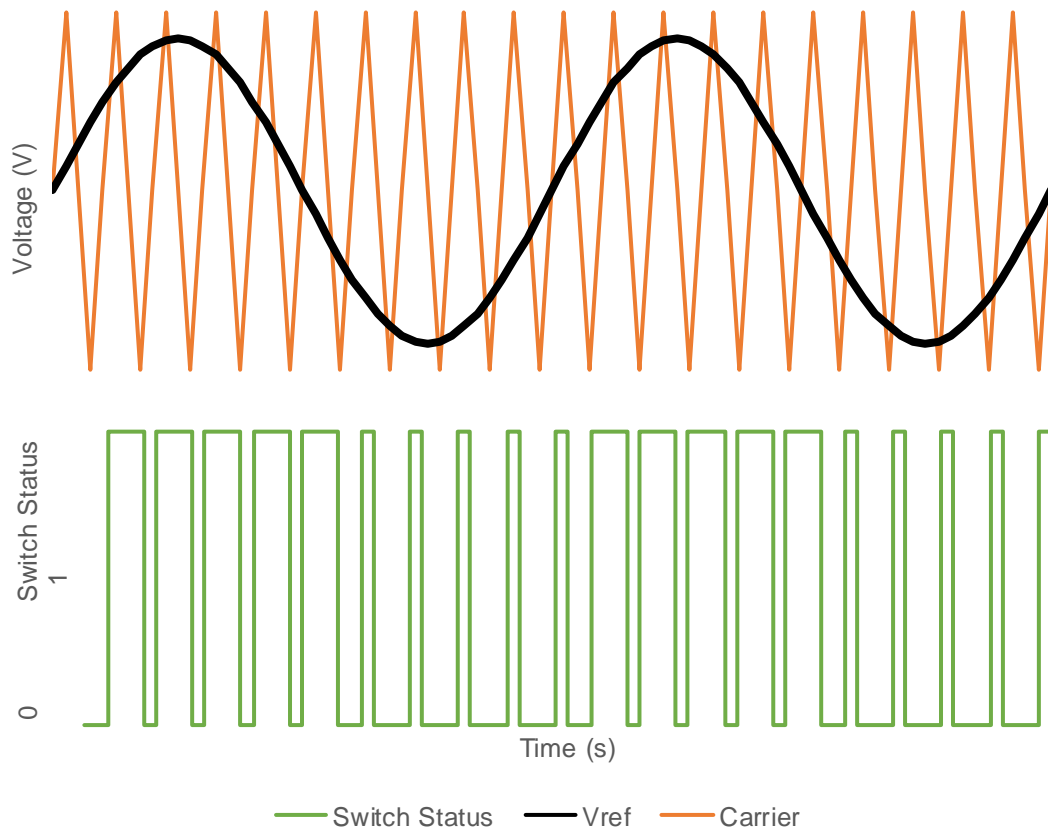


Figure 2-12: Voltage reference and triangular carrier with associated PWM switching output

As the turn on and turn off times for all the switches can be manipulated independently from the AC system (unlike with thyristors where the device can only be enabled by a control signal and not disabled), this converter type can provide full control of both real and reactive power supplied from the converter when acting as an AC source to a supplied system (that is, it can control the angles between the supplied AC-side voltage and current as required). VSC converters are therefore more suitable than LCC schemes for connection in weaker grid areas and distribution networks [90] because the reactive power required during commutation is minimal [91]. Additionally, since they do not require a line voltage for commutation, VSC schemes may also offer black start provision – black start is the procedure used to restore power to a “dead” system in the event of a complete or partial de-energisation of an electricity supply system [92]).

Historically, up until 2010, VSC converter designs were developed to power capacities of up to 400 MW and DC voltages of ± 400 kV [93] [94]. This was achieved by series connecting multiple IGBT devices, which had individual voltage ratings of up to approximately 4.5 kV [95], to form the DC voltage [96] as outlined in Figure 2-13. The challenge with series connecting IGBTs was ensuring that all the devices switch simultaneously. A small delay in switching would result in the full DC voltage being placed across a single IGBT which would often lead to failure of the device.

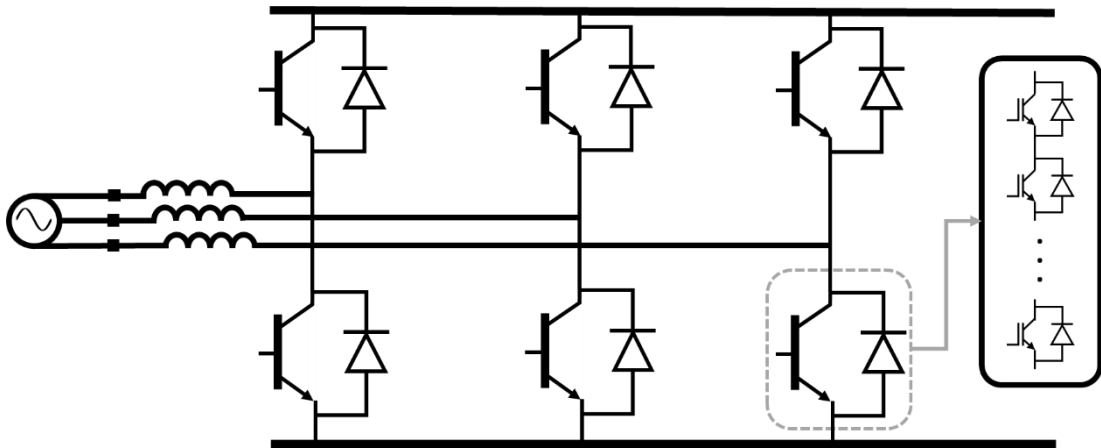


Figure 2-13: Example of the series connection of IGBTs to achieve higher DC-side voltages for a conventional two-level VSC converter

2.3.4 Comparison of HVDC Technologies

A comparison between the key parameters of VSC and LCC HVDC conversion systems is provided below in Table 2-2. In summary, while VSC systems offer increased controllability, a reduced site footprint and higher power quality, LCC HVDC links are capable of delivering significantly higher power transfers and are more tolerant against DC faults

Table 2-2: Summary of key parameters of LCC and VSC [97] [98] [99]

	LCC	VSC (including MMC)
DC voltage	± 800 kV (more recently ± 1.1 MV)	± 640 kV
DC power rating	10 GW	3 GW
Switching device	Thyristor	IGBT
Reactive power requirements	Up to 60% rated power	None; full control of real and reactive power
AC filtering requirement	Large filter banks	Significantly reduced (none/minimal for MMC)
Losses (as percentage of station power rating)	$\sim 0.8\%$	$\sim 1.0\%$
Footprint [82]	Large (e.g. $54 \text{ m}^2/\text{MW}$)	Typically, 50-80% the size of an LCC site (e.g. $41 \text{ m}^2/\text{MW}$)
Fault handling	Robust	Very vulnerable other than FB-MMC but at the expense of increased operational losses (as will be described in Section 2.3.5).
Multi-terminal capability	Proven to be challenging	Regarded as being simpler due to fixed voltage polarity
Black start capability	No	Yes - with appropriate control systems
Control complexity	Reduced due to self-commutation and lower switching speed	Increased over LCC due to force-commutation. MMC adds further complexity

2.3.5 Modular Multilevel Converter (MMC)

The modular multilevel converter (Figure 2-14) is the result of essentially cascading several VSC converters or 'cells' to create a bridge 'arm' and therefore allowing the voltage stress across each switching device to be reduced. There are many topologies and cell arrangements proposed in literature and deployed commercially. The general converter arrangement is outlined below in Figure 2-14 where L_{arm} is the arm inductance for filtering and current limiting purposes and n is the total number of submodules.

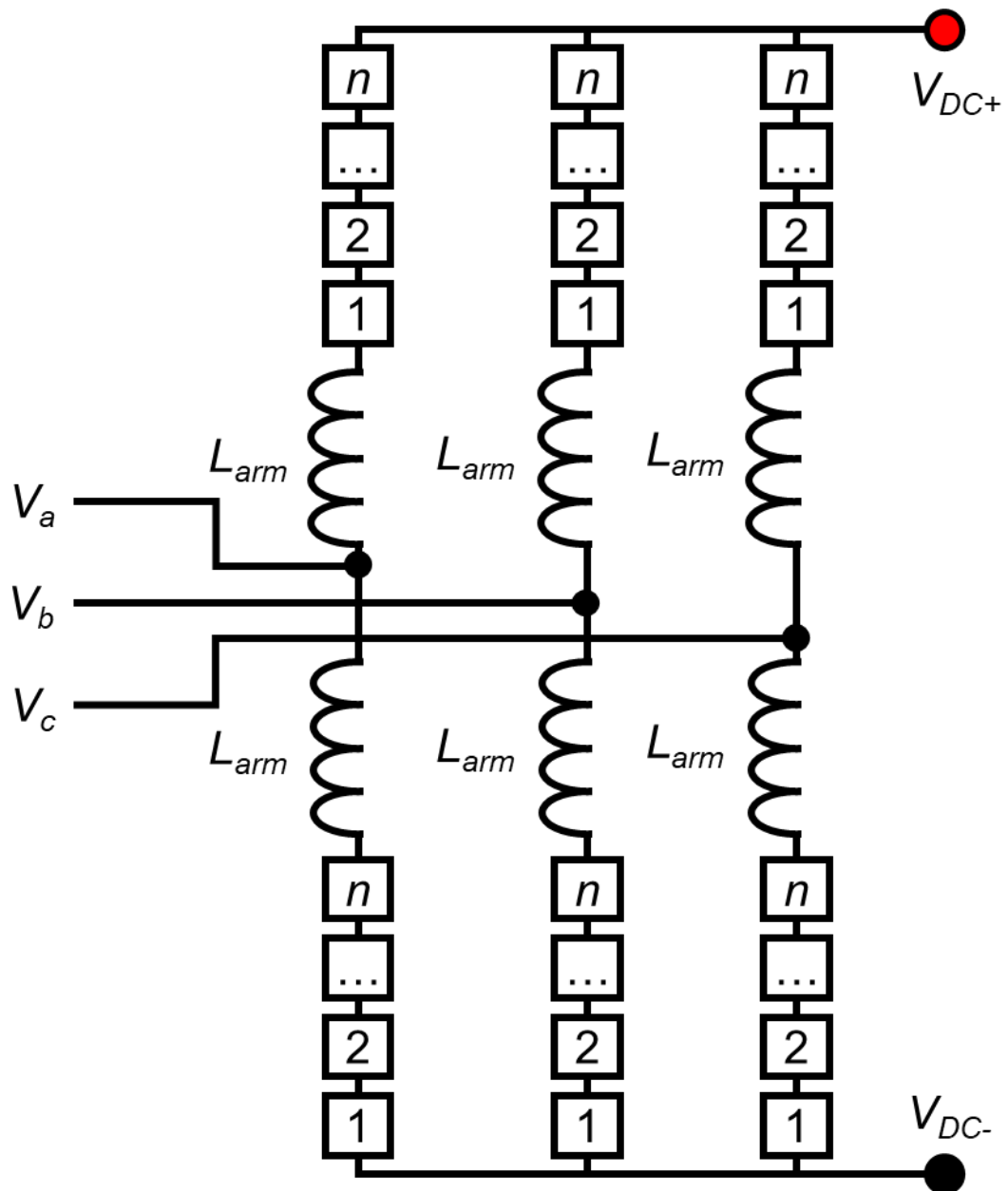


Figure 2-14: Three-phase MMC topology with n submodules in each arm.

There are several advantages to this approach, including:

- in-built redundancy in the system;
- improved AC side power quality (reduced harmonics);
- increased power and voltage ratings over conventional VSC topologies;
- a reduced converter station footprint (i.e. a higher energy density); and
- increased efficiency over conventional VSC topologies.

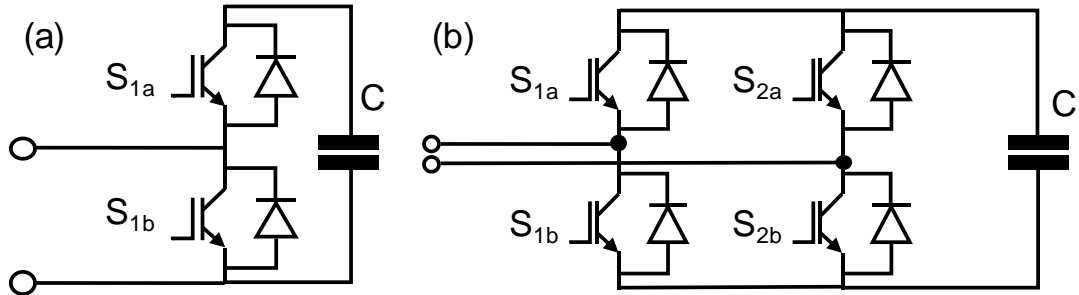


Figure 2-15: MMC cell construction (a) half-bridge (HB) and (b) full-bridge (FB)

Figure 2-15 presents two basic cell structures for the half-bridge (HB) and the full-bridge (FB) converter. The HB structure is a more efficient conversion method when compared to the FB-MMC as current flows through fewer power electronic devices therefore reducing the conduction loss of the system. This topology has similar vulnerabilities to a conventional two-level VSC systems during DC-side faults due to the placement of the freewheeling diodes - as will be outlined in detail later. The greatest advantage of the FB arrangement is its ability to control and block current flow during DC-side faults but this is at the cost of increased conduction loss during steady-state operation. During DC-side faults, FB-MMCs can impose a negative voltage, supplied by the energy stored in the capacitors, preventing fault current flowing from the AC system into the DC-side fault [100]. The extra losses associated with the FB-MMC during normal operation makes the technology unattractive with current thinking favouring HB-MMC technologies for multi-terminal DC systems [88].

The output voltage of each arm (V_{arm}) of an MMC is given in equation 2-4 where n is the number of cells in the arm and $V_{submodule}$ is the voltage across the capacitor of each submodule.

$$V_{arm} = \sum_{i=1}^n V_{submodule} \quad 2-4$$

In high voltage applications, converters may have between 200-400 cells [88]. As each submodule represents a discrete voltage step, each MMC submodule switches significantly more slowly than a conventional VSC scheme with switching frequencies in the range of 100 – 200 Hz [88], unlike conventional two-level VSC where devices commonly switch between

1 – 2 kHz. The output AC voltage from an MMC much more closely resembles a pure sinusoid than its VSC counterpart. Therefore, the filtering requirement of MMC is further reduced when compared to standard VSC systems – and in some cases zero. A typical output from an MMC is presented in Figure 2-16 and compared against the voltage trace produced by a standard two-level VSC converter.

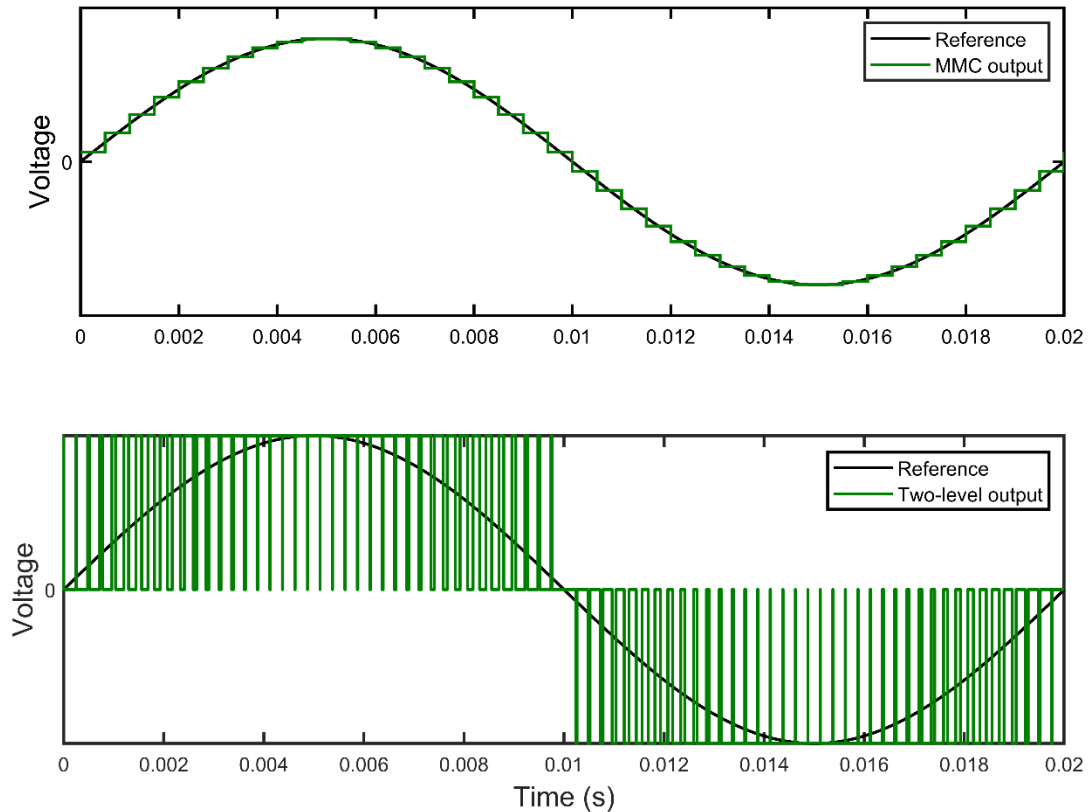


Figure 2-16: Example output voltages for an MMC and a two-level VSC converter

2.4 HVDC

While this thesis is concerned with MVDC, it is worth highlighting the drivers behind the adoption of HVDC technologies as much of the knowledge is transferable. This section describes why HVDC development is currently an attractive proposition for grid operators for certain applications. According to [1], HVDC transmission projects fall into one or more of the following four categories.

- i. transmission of bulk power;
- ii. interconnection of systems either with different frequencies or that are unsynchronised;
- iii. addition of power infeed (e.g. an offshore wind farms [101]) without increasing short circuit level of the receiving AC system; and

- iv. improvement of AC system power quality via fast control of HVDC.

As alluded to previously in Section 2.2.2, HVDC is widely used for transmission system reinforcements and interconnections. When selecting a DC solution over a conventional AC approach, there are two critical distances which ultimately govern the decision: the critical distance for losses (Figure 2-17) and the critical distance for capital investment (Figure 2-18).

When comparing the ohmic losses of HVDC transmission circuits against equivalently rated AC circuits, HVDC systems are generally found to be more efficient for reasons outlined previously. However, the process of converting from AC to DC, and vice versa, represents a source of loss when considering an HVDC system as a whole. For this reason, the losses in AC systems are lower than HVDC at short distance, however in the example presented in Figure 2-17 it is observed that once transmission distance reaches approximately 250 km (for a transfer of 1.2 GW), HVDC represents a more efficient means of power transmission.

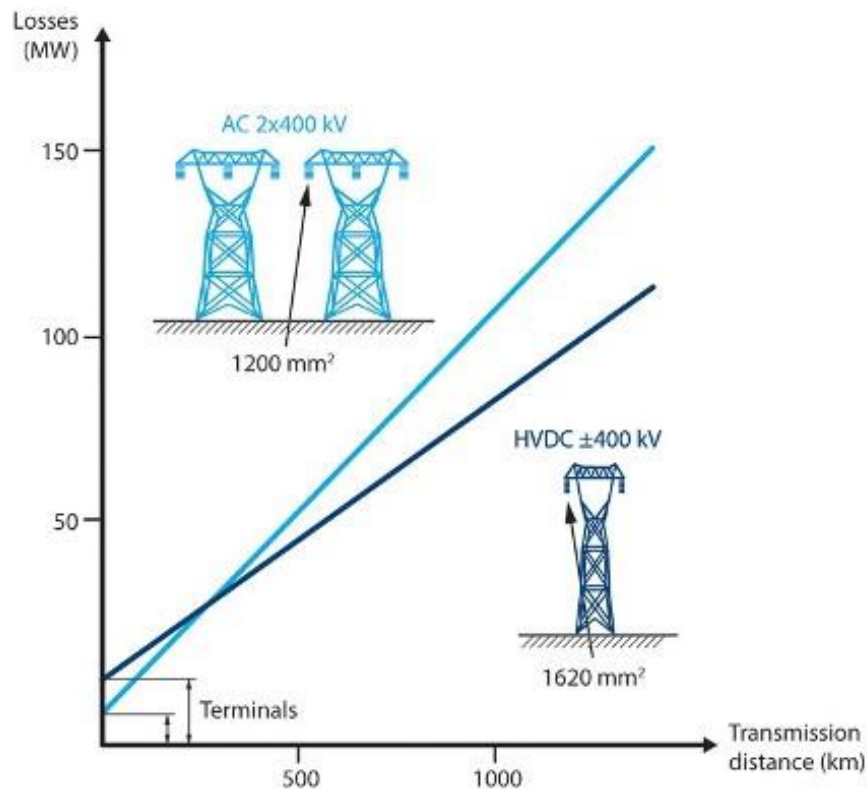


Figure 2-17: Comparison of losses against transmission distance for HVDC versus HVAC for a 1.2 GW overhead line system [102]

While the losses of a system are important, the cost of the solution must also be considered. The investment required to create a DC converter station is much greater than an equivalently rated AC connection, however, the cost of DC conductors for a given transfer capacity is lower

than an equivalently sized AC conductors as less material and no reactive compensation is required. Over a certain line length (known as the “critical distance”), typically 50 km for subsea cables and 600 km for overhead circuits, DC starts to offer a more cost-effective means of power delivery in terms of both operational and capital expenditure. Other metrics such as controllability and grid conditions must also be considered when comparing DC and AC solutions.

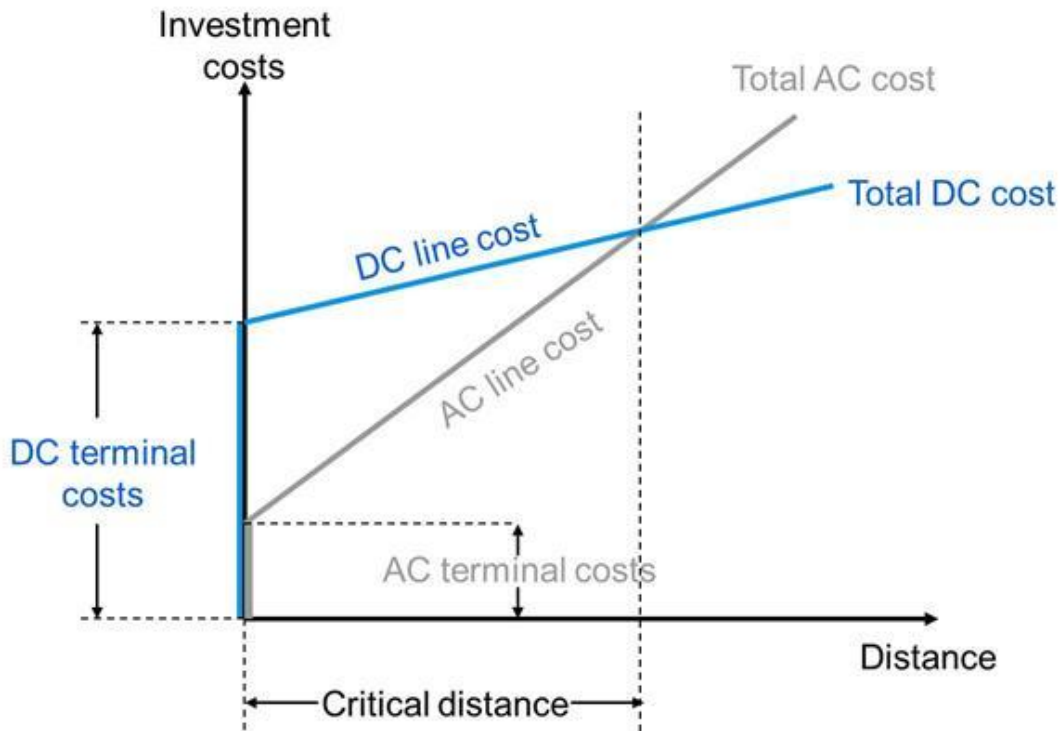


Figure 2-18: Investment cost comparison between DC and AC systems [102]

The first commercial HVDC link (Gotland 1) was commissioned in 1954 by ABB. The 96 km subsea cable connected between the Swedish Island of Gotland and the Swedish mainland. The link was initially of 20 MW rating with a nominal DC voltage of 100 kV – the exact electrical topology of the link appears to be undocumented from the available published literature on the project. The system originally deployed mercury arc valves (MAV) until it was upgraded in 1970 when thyristors were connected in series with the MAVs to increase the rated voltage to 150 kV [103].

As well as hosting the first LCC installation, Gotland also claims host to the first VSC link. Commissioned in 1999, the 50 MW link operating at ± 80 kV was deployed to mitigate against the poor power quality on the AC-system in the region caused by existing wind generators

(40 MW). Two underground cables of 70 km were installed to connect the south of Gotland to the city of Visby in the north-west of the island [104].

Since these pioneering installations, the number of HVDC installations worldwide has increased with more than 150 systems (including back-to-back schemes) in operation with many more projects in development. Figure 2-19 displays the four operational HVDC links within the UK as of early-2018 on the left and the number of HVDC links expected to be in operation by 2030 on the right; with many of the proposed links now in operation, under construction or in planning.

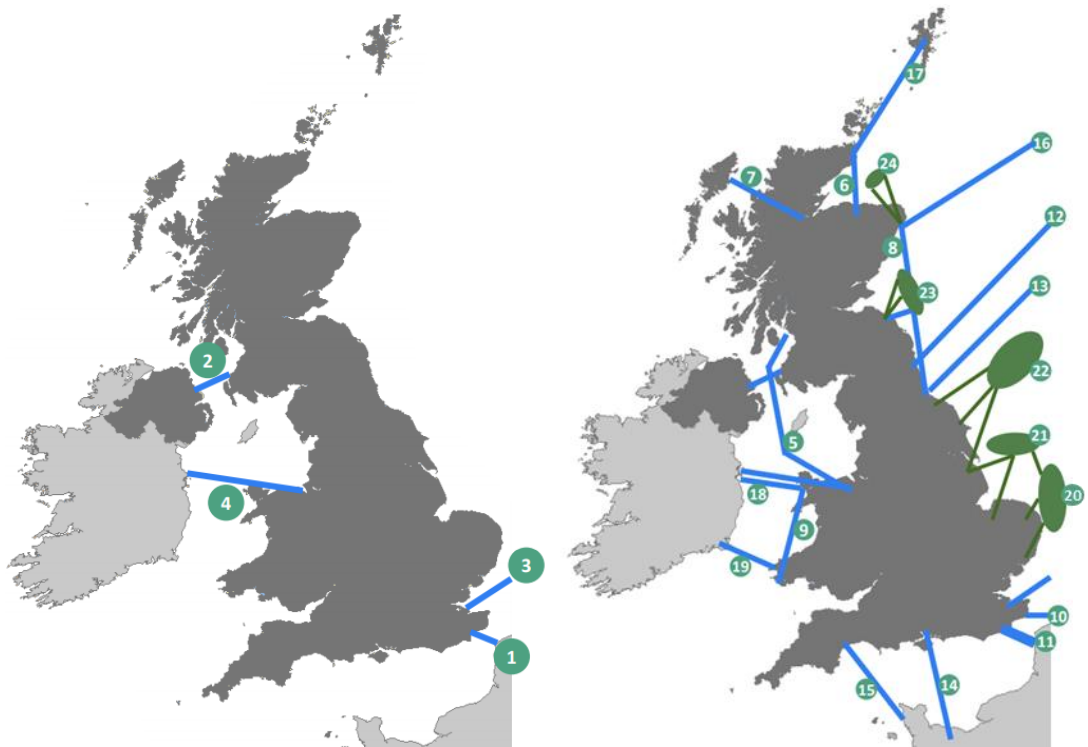


Figure 2-19: HVDC in the UK for mid-2018 (left) and by 2030 (right) [97]

The key advantages of HVDC can therefore be summarised as:

- the elimination of charging current and skin effects (reduction of losses);
- the interconnection of independent AC synchronous grids (primarily for bulk energy sharing/trading applications);
- greater power transfers are possible using DC than AC for a given voltage/insulation level;
- full control of real and reactive power flows (if VSC is used);
- the creation of natural “firewalls” between systems so that disturbances occurring in one system area are not reflected to the other (although this can of course still happen

if one system is supplying critical infeed to the other and the supplying system fails);
and

- increased infeed capacity for a supplied system without significantly changing the sending and receiving systems' fault levels.

While HVDC systems have many advantages over equivalent AC systems, it should be highlighted that there are several notable examples of the technology not performing as expected. One such example is the £1.3 billion Western HVDC link, mentioned previously, which has experienced multiple cable faults since its delayed delivery. At the time of writing, the project is being investigated by the GB energy regulator, OFGEM (Office of Gas and Electricity Markets), to determine whether any licence conditions were breached by National Grid Electricity Transmission and/or Scottish Power Transmission [105] [106].

2.5 Summary

This chapter has provided a review of AC power systems and has introduced their typical design. AC has historically been preferred over DC due to the ease of transforming between voltage levels. DC systems for transit applications have been popular since the early 1900s, however the use of DC for utility-scale power system applications was minimal until the 1950s with the introduction of the world's first HVDC link.

Since then, DC technologies have increasingly played an important role in transmission systems especially with the shift towards a low-carbon energy system (e.g. to interface remote hydro schemes with load centres). HVDC, particularly via subsea cabling, is fast becoming the prevalent method to quickly achieve transmission network reinforcements in GB (e.g. the Western Link and Caithness-Moray). The technology starts to become commercially and technically attractive for cable circuits which are longer than 50 km and overhead lines greater than 600 km [107]. A comparison between key parameters of VSC and LCC HVDC conversion systems was provided in Table 2-2.

As HVDC technology becomes more prevalent in transmission networks and while more low-carbon generation continues to connect to distribution networks, the question of whether DC in distribution networks makes sense technically and commercially is starting to be investigated by network operators. This question will be explored in more detail in Chapter 4.

Chapter 3

Review of Power System Protection Fundamentals

3.1 Introduction

Protection schemes safeguard power networks from the effects of faults (most commonly short circuits – types of faults are discussed in the next section) by disconnecting defective elements – typically within 100 ms for transmission networks. If a fault remains on a system indefinitely there is a high risk of equipment damage and wide-area system blackout, and this would also pose a hazard to people and buildings in the vicinity of the faulted power system component.

This chapter introduces the role and need for power system protection. Section 3.2 outlines why power system protection is required by examining the sources and effects of faults. Equipment required to detect and isolate faults from the power system is described in Section 3.3. Performance requirements are also introduced in this section. Commonly applied fault detection techniques are presented and discussed in Section 3.4. An overview of protection schemes deployed as part of a distribution network is outlined in Section 3.5. With the shift towards DC technologies, as outlined in the previous chapter, challenges associated with the protection of DC systems is introduced in Section 3.6.

3.2 Electrical Faults

No matter how much effort is put into preventing them, faults will always occur. The art of power system protection is to detect and react to faults while minimising their impact when they inevitably materialise. A power system fault may arise at any voltage and power level due to a diverse range of causes, including;

- vandalism (such as metal theft) [Figure 3-1];
- wildlife (animals e.g. spanning conductors);
- vegetation encroachment (tree branches spanning conductors) [Figure 3-2];
- assets reaching their end of life (insulation degradation);
- weather events (lightning, wind, solar storm, snow, ice);
- poor equipment installation (improper termination or cable joints);

- substandard manufacturing of devices (insulation damage, poor connections); and
- accidental damage (e.g. contractors cutting through underground cables) [Figure 3-3].



Figure 3-1: Attempt to forcefully remove equipment from substation [108]



Figure 3-2: Tree branch spanning all conductors on an overhead line [109]



Figure 3-3: Excavator cutting through an underground cable causing a short circuit [110]

The likelihood of a fault occurring on a circuit is primarily linked to the physical properties of the network. For example, an overhead line in an exposed location will be very likely to experience a greater number of faults over its operational life than an underground cable. This is because the overhead line is prone to risks such as inclement weather conditions, animals/vegetation spanning conductors and lightning events whereas the cable is protected from such phenomena by being underground or in a duct. A series of tables are presented to highlight the likelihood and characteristics of different event types. Table 3-1 outlines the percentage distribution of recorded disturbances by fault cause for two Nordic countries (Finland and Iceland) based on 2012 field data which resulted in an interruption to supply. Table 3-2 presents the distribution of faulted assets during the same period. These statistics cover transmission voltages ≥ 132 kV. In these tables, a grid disturbance is defined as an outage, forced or unintended disconnection or failed reconnection as a result of faults in the power grid [111]. There is not a great deal of publicly available data relating to fault statistics.

Table 3-1: Causes of grid disturbances for two Nordic countries leading to a supply interruption (2012) [111]

Fault cause	Percentage distribution of disturbance (%)	
	Finland	Iceland
Lightning	18	0
Other environmental causes (e.g. Ice, snow, vegetation, wind, pollution, forest fires etc.)	33	63
External influences (e.g. Vandalism, birds and animals etc.)	1	2
Operation and maintenance (e.g. fault in protection setting, human error etc.)	5	3
Technical equipment (e.g. Installation error, vibration, aging, corrosion etc.),	8	10
Other (e.g. faults in external networks, a major fault within customers premises)	5	23
Unknown	30	0

Table 3-2: Faulted asset percentage distribution for two Nordic countries (2012) [111]

Faulted asset	Percentage distribution of faulted assets (%)	
	Finland	Iceland
Overhead line	63.9	16.2
Underground cable	0.1	0.0
Power transformer	2.2	1.3
Instrumentation transformers (CTs and VTs)	9.5	0.0
Circuit breakers	3.4	75.6
Disconnecter	1.7	0.0
Surge Arrester and spark gap	0.0	0.0
Busbar	7.5	0.0
Control equipment	9.0	1.3
Other substation faults	0.0	0.0
Compensation equipment faults	0.0	0.0
Other faults	1.1	5.6
Total number of faults (absolute number)	445	40

The vast majority of faults are short circuits. However, other situations (e.g. open circuits, unbalanced operation, sustained overloading, islanding) must also be guarded against – many of these other conditions may have a root cause of a short circuit, but other phenomena can and do cause undesirable conditions, and must be protected against. For example, an open circuit fault will cause current to reduce to zero while voltage remains around its nominal value. A typical open circuit fault could be a broken conductor [112] [113]. They can be difficult to detect but may be detected via unbalance in a three-phase system [114]. However, most faults involve short circuits.

During a short circuit, the voltage difference between faulted conductors and/or ground at the point of fault reduces to near zero (depending on the resistance of any arc involved between the conductor(s) and ground, if ground is involved) while the current contribution rises to a value limited by the impedance between the source and the point of fault as well as the ability of the source to supply current. Short circuits can be either symmetrical or asymmetrical events. A symmetrical event is where voltage and currents remain balanced across all three phases such as in phase-phase-phase-ground and phase-phase-phase faults. An asymmetrical fault is where an unbalance exists between phases (e.g. phase-ground, phase to phase).

A variety of fault types are outlined in Figure 3-4 for a three-phase AC system with DC faults for a two-wire system illustrated in Figure 3-5. Table 3-3 presents a typical distribution of short circuit event types for a conventional overhead AC distribution system.

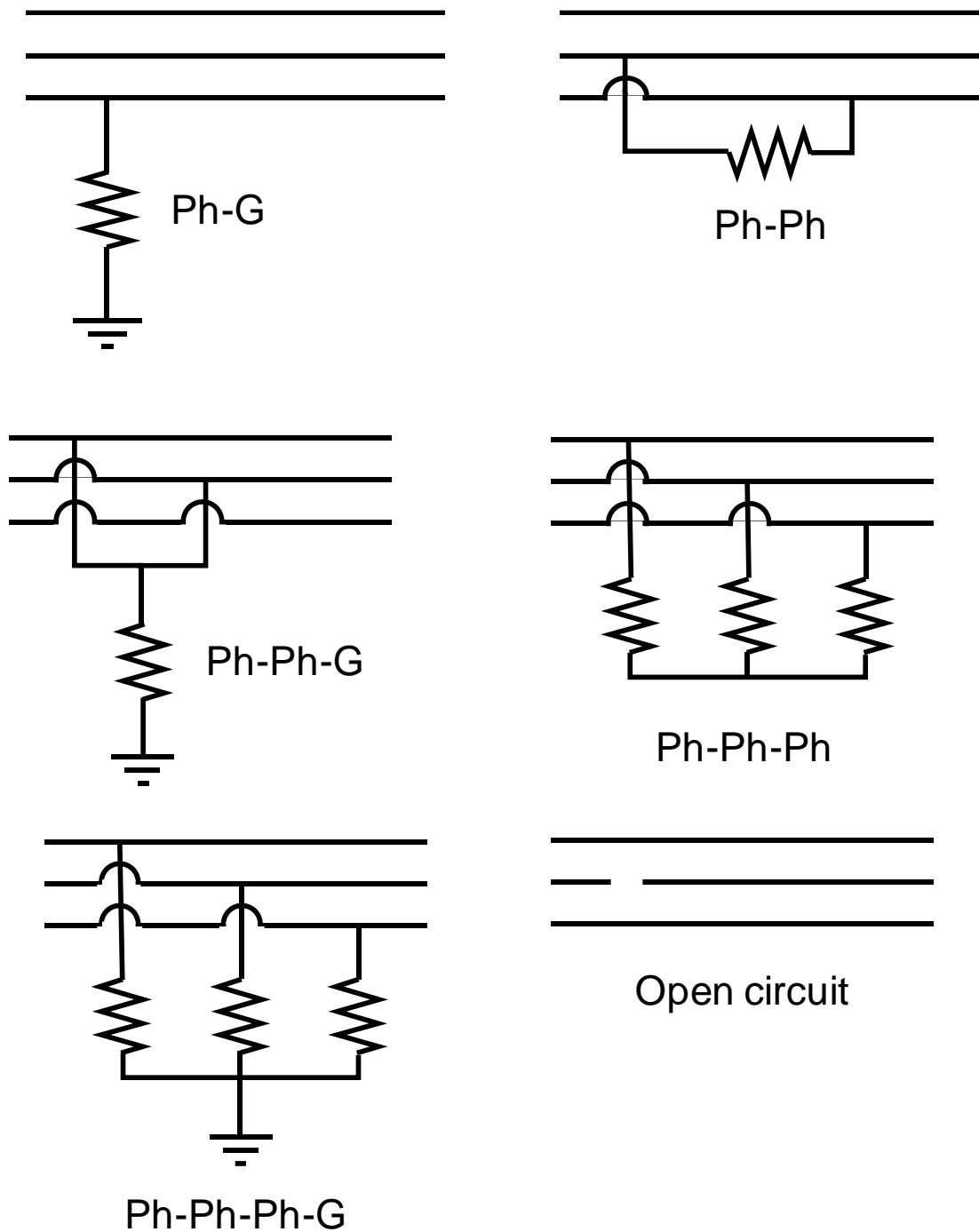


Figure 3-4: Main fault types in a three-phase AC system

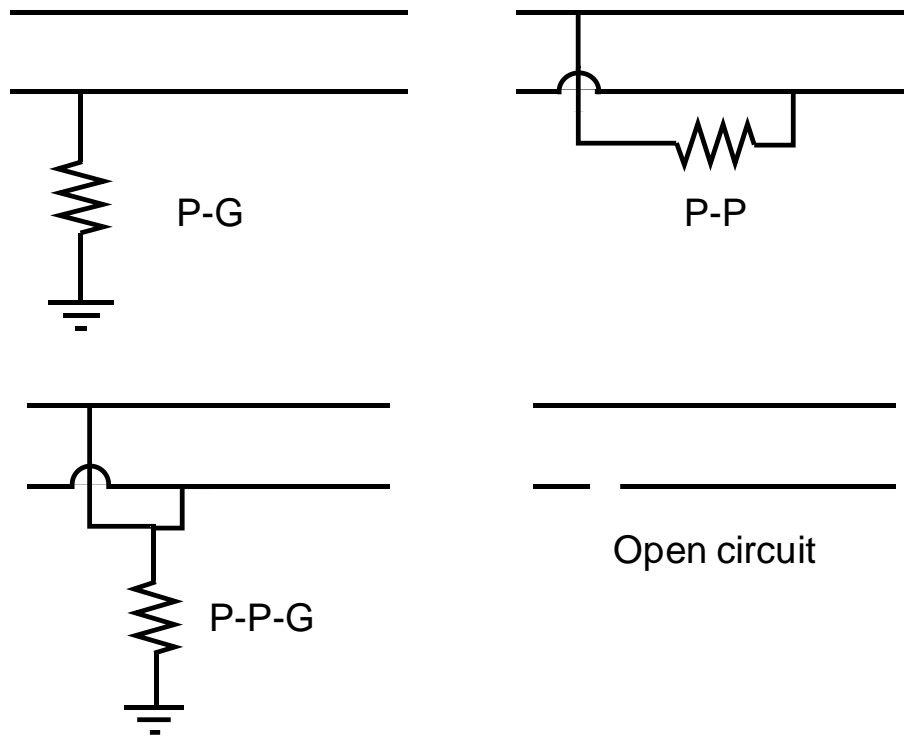


Figure 3-5: Main fault types in two-wire DC system

Table 3-3: Approximate probability distribution of AC short circuit fault types (for overhead systems) [115]

Fault Type	Probability of Fault (%)
Single Phase to Ground	70 – 80
Phase-Phase-Ground	10 – 17
Phase to Phase	8 – 10
Three Phase	2 – 3

3.3 The Protection System

Although faults cannot be prevented, it is important that they are identified and disconnected from the system quickly to maintain a safe, reliable and functional electricity grid and to avoid excessive damage. All network-connected devices (e.g. generators, transformers, compensation equipment, lines, cables and loads) should be protected by a minimum of at least one system. To detect different fault types, enhance security and to protect against the failure of an element or subsystem within an individual protection system, it is commonplace for network elements to be protected by multiple devices. These devices can either provide primary (main) or backup protection (required when an element of the main protection system(s) fail) against faults [116] [117].

3.3.1 Protection System Performance Requirements

Throughout this thesis, reference will be made to the four performance requirements of power system protection; selectivity, sensitivity, operation time and stability [118].

- 1) **Selectivity** – the ability of a protection system to select whether to operate or not for a given set of measured input values. This is also sometimes referred to as discrimination.
- 2) **Sensitivity** – the ability of the system to identify faults which may appear very similar to normal operating conditions.
- 3) **Operation time** – the time between the fault inception and the trip signal being sent to appropriate devices.
- 4) **Stability** – the capability of a protection scheme to remain inoperative under certain fault conditions allowing other protection devices to clear the event.

These criteria are placed into context in Section 3.4 where the main types of protection schemes used in power networks are described.

3.3.2 Instrumentation for Protection Systems

Protection systems generally rely upon a measured input of system current and/or voltage. To obtain voltage and current measurements from the power system, voltage transformers (VT) and current transformers (CT) are employed. The ratios of CTs and VTs are selected by considering the system voltage level and loading (or, more precisely, the capacity of the protected equipment, as sometimes this is higher than prevailing maximum load levels to cater for future load growth). Instrument transformers scale the primary side voltages and currents to a level more readily interfaced with protection relays. The secondary value of a CT is usually referred to a 1 A or 5 A scale (for nominal primary system ratings) while the secondary voltage of a VT is generally referenced to 110 V rms phase-phase (for the nominal system phase-phase rms) voltage [115]. This allows for the standardisation of protective relays and instrument transformers for a range of voltage and power levels [119] [120]. A typical distribution VT may have ratings of 33,000:110 V or 11,000:110 V while a CT may have a ratio of 750:5 A or 400:5 A [121].

3.3.3 Protection Relays

According to the IEEE Standard for Relays and Relay Systems Associated with Electric Power Apparatus [122], a relay is defined as:

“... an electric device designed to respond to input conditions in a prescribed manner and, after specified conditions are met, to cause contact operation or similar abrupt change in associated electric control circuits. A relay may consist of several relay units, each responsive to a specified input, with the combination of units providing the desired overall performance characteristic of the relay. Inputs are usually electrical but may be mechanical, thermal, other quantities, or a combination of quantities.”

Protection relays are therefore responsible for the detection of faults and decision-making relating to whether to trip immediately, trip with a time delay (typically for remote faults in backup mode that should be cleared by other main protection systems) or not trip at all for a given set of input measurements. The principle of protection relaying is to disconnect the fewest possible number of customers/assets when a fault occurs while isolating the faulted asset.

Relays have developed over several decades from electro-mechanical devices through to static (analogue electronic with no moving parts), digital and ultimately to numerical or Intelligent Electronic Devices (IED) used at present [123]. All of these technologies are in present-day operation on the electricity system, with electromechanical devices still used in certain applications (typically lower voltages) due to their cost, simplicity and reliability.

3.4 Protection Schemes

There are various methods for detecting faults on power systems. Typically, this is achieved using measurements of currents and/or voltage although other detection techniques are used. The temperature of a rotating machine or transformer may also give an indication as to the status of the plant, although this may be more applicable to condition monitoring rather than fast-acting fault protection. Frequency, as mentioned in Chapter 1, is a widely used method of detecting faults on the power system. Rate-of-change-of-frequency (RoCoF) relays are used to detect whether a loss-of-mains event has occurred. Low Frequency Demand Disconnect relays (LFDD) are used to limit the fall in frequency during extreme events [124]. In the GB power system these relays start to disconnect demand should system frequency fall below 48.8 Hz [125]. The tripping of these relays was witnessed during an event on the GB system on the 9th August 2019. Approximately 1.1 million customers were disconnected which resulted in 1 GW (5%) of load being disconnected from the system [126]. The root cause of the event was linked to lightning strikes which caused several generators to disconnect.

Figure 3-6 shows the main elements within a typical protection scheme.

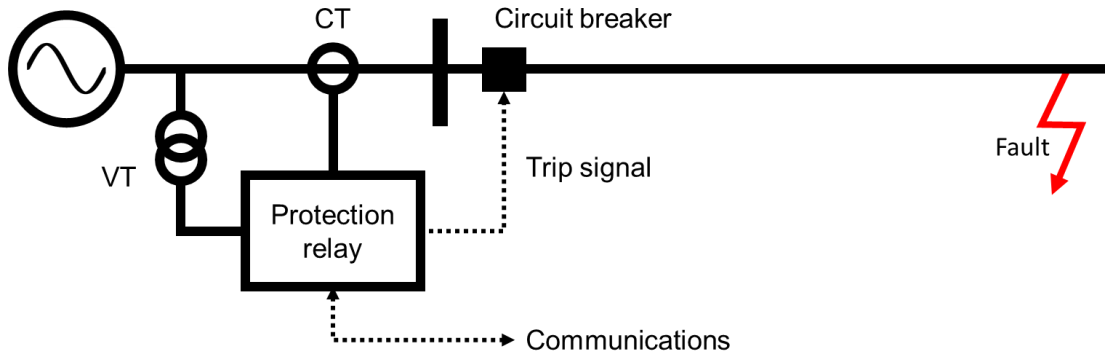


Figure 3-6: Typical protection topology

Protection schemes generally fall into one of two categories: unit or non-unit. A unit scheme protects a predefined section and is not sensitive to faults outside of the protected region. Unit schemes often require communication links or pilot wires to operate - especially when protecting cables and overhead circuits. An example of a unit scheme which does not require communications is transformer protection as all measurements are local to the relay and there is no need to exchange information between substations. This protection method measures the difference between the current entering and leaving a transformer while taking the turns ratio of the transformer into account. Should the currents entering and leaving the transformer not be consistent, it can be assumed that a fault resides within the transformer [118].

Non-unit schemes, while designed to protect a specific zone or item or equipment, cannot provide coverage for a precisely defined section of the power system. This is because non-unit schemes typically derive measurements from a single point on the system and therefore changes in operating conditions (e.g. variations in fault level, different fault resistance and return path impedances) make it impossible to be certain of whether a fault resides within a specific and exactly defined protected zone, or not. However, non-unit schemes provide necessary, valuable and effective backup protection through their inherent overlapping adjacent zones of protection [127]. While such schemes cannot normally detect the exact location of a fault, they normally are set up such that for faults relatively close to the measurement point, relatively fast tripping operation is initiated (i.e. the scheme operates in “main protection” mode), while for faults deemed to be relatively further away, a delayed operation is configured such that the protection will provide backup in the event of failure of adjacent protection systems. The boundary between “close” and “further away” is usually configured (using relay settings) to be around the boundary between the main protection equipment/zone and other equipment/zones for which backup operation is desired. Communications can also be used, in a variety of ways, to enhance the performance of non-

unit schemes. However, any non-unit scheme should be capable of operating (even in a degraded mode) when communications is lost; which is not always the case for unit protection schemes, which typically are rendered ineffective if communications facilities are lost.

To ensure reliability, measurement equipment (i.e. use of different cores on CTs), protection relays and other ancillary equipment are normally duplicated (and sometimes even triplicated at transmission voltages) to ensure that faults of all types can be detected and isolated [118]. It is mandated that unit and non-unit protection relays are both used to provide backup should the main protection (or communications used by main protection) fail. Other failures (e.g. of circuit breakers) would also be detected and reacted to, either by overlapping non-unit protection, or by dedicated circuit breaker fail protection.

While many protection systems exist, a short summary of three widely deployed approaches to power system protection is presented in the following subsections. Overcurrent and differential protection methods are highlighted in Section 3.4.1 and Section 3.4.2, followed by Section 3.4.3 which introduces distance protection relays. Distance protection will form the basis of the proposed fast-acting backup protection solution for embedded DC links developed in this thesis, so will be examined in relatively more detail than the other main types of protection.

3.4.1 Overcurrent Protection

This type of protection functions when the measured current exceeds a predefined threshold. At higher voltage levels, overcurrent protection is generally deployed as backup protection. Figure 3-7 outlines a typical overcurrent scheme employing a relay that has an input from a current transformer. The relay typically compares the measured current with a threshold either mechanically, via analogue electronics or via software. Fuses also offer overcurrent protection and are deployed extensively at 11 kV and LV. Overcurrent typically represents the cheapest form of power system protection [127].

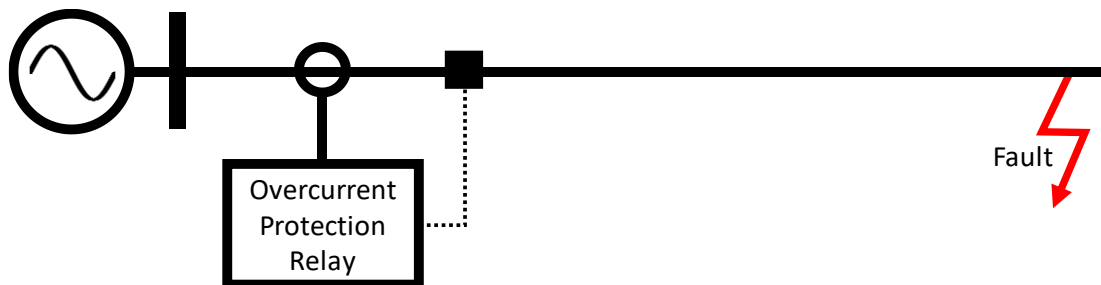


Figure 3-7: Overcurrent protection system topology

A simple time delay can be applied to an overcurrent scheme such as that used in a definite time (DT) relay. This approach will trip the relay after a pre-determined time should a current threshold be exceeded. Figure 3-8 presents a simple network with three busbars. The network is protected by three DT overcurrent relays – one at each busbar. A grading margin of 0.4 s is applied between the relays with the relay at busbar C set to trip with a time delay of 0.3 s. Fault levels at each busbar are also presented. Figure 3-9 presents the time/current characteristic for the scheme.

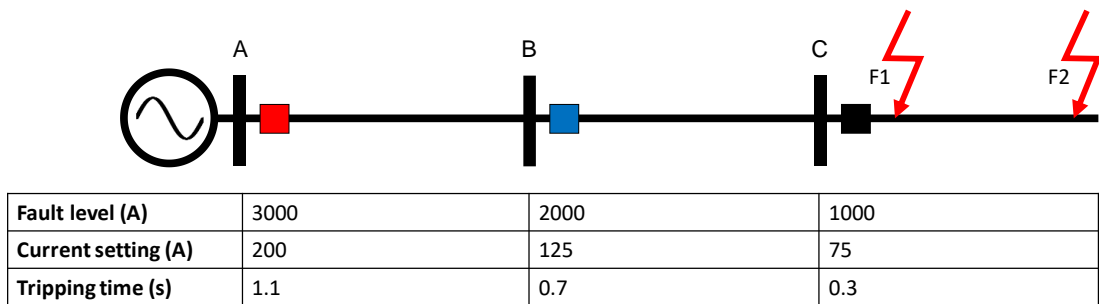


Figure 3-8: Overcurrent protection for three serially connected feeders.

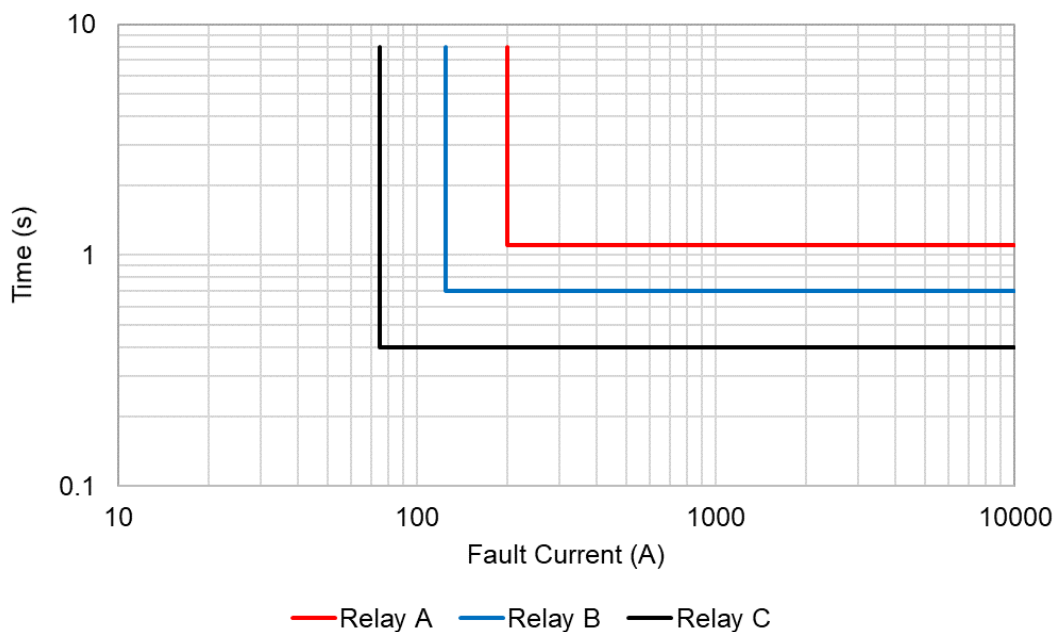


Figure 3-9: Time/current characteristics for relays A-C

From Figure 3-9 it is clear that a fault at position F1 would be disconnected after the same time delay as fault F2. This has the somewhat negative consequence that faults with the highest currents will be cleared in the same time as faults that are marginally over the tripping threshold – which can be problematic in that high short circuit currents may be allowed to

persist for relatively long times – increasing the risk of severe damage/fire and other undesirable consequences.

To counteract this problem, an inverse time characteristic, such as those in an inverse definite minimum time (IDMT) relay, can be employed. This characteristic reacts more quickly for a large fault current than for a smaller measured value. The IDMT tripping characteristic can take multiple forms as outlined in equations 3-1, 3-2 and 3-3 where t is the operation time of the relay, TMS is the time multiplier setting, I_s is the relay setting current and I_m is the current measured by the relay (supplied via the secondary of the CT).

$$\text{Standard inverse (SI)} \quad t = TMS \times \frac{0.14}{\left(\frac{I_m}{I_s}\right)^{0.02} - 1} \quad 3-1$$

$$\text{Very Inverse (VI)} \quad t = TMS \times \frac{13.5}{\left(\frac{I_m}{I_s}\right) - 1} \quad 3-2$$

$$\text{Extremely inverse (EI)} \quad t = TMS \times \frac{80}{\left(\frac{I_m}{I_s}\right)^2 - 1} \quad 3-3$$

Figure 3-10 presents the standard inverse (SI), very inverse (VI), extremely inverse (EI) and definite time (DT) characteristics graphically. High set, or instantaneous, overcurrent parameters can be optionally specified to provide an immediate trip when it is known that a fault is “definitely” on the main protected line and not the next line. The measured fault current must be sufficiently higher than the maximum current expected by any “downstream” relaying devices. The setting current for instantaneous elements is typically set to 130% of the fault current expected at the next downstream relay’s location [118] [128].

Overcurrent relays are generally the least stable, sensitive and selective of the three protection schemes outlined, but are widely used at lower voltages as they are an effective and economic solution for applications where the consequences of faults are not critical to the stability and security of the overall power system.

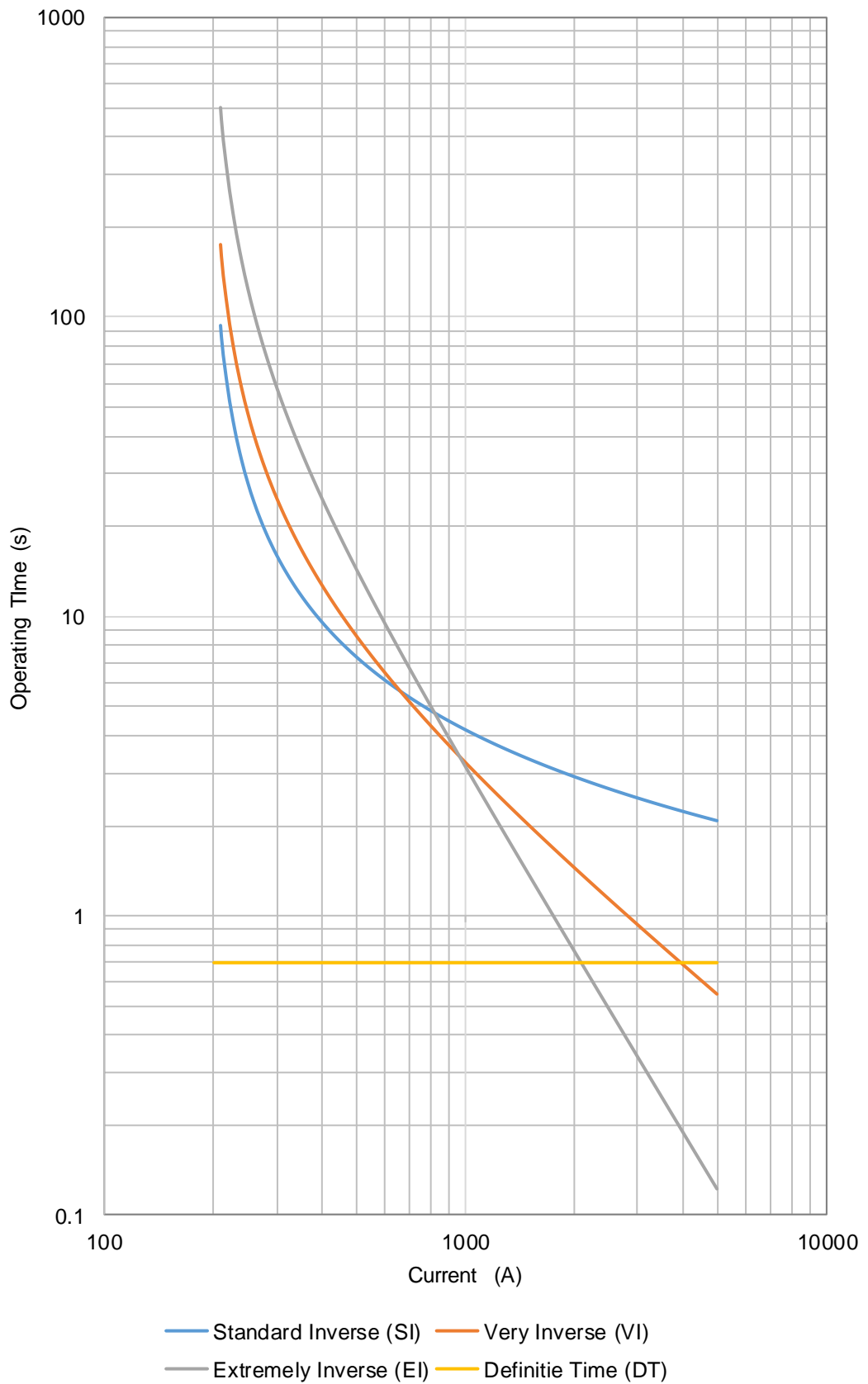


Figure 3-10: IDMT (IEC 60255) and DT relay characteristics ($I_s = 200$ A; $TMS = 1.0$)

3.4.2 Differential Protection

Differential protection schemes detect faults within a predefined network section and are not sensitive to faults external to their protection zone. Figure 3-11 represents a differential protection scheme which monitors a section of line – differential protection is also widely used to protect transformers, generators and busbars. When a fault occurs within the protected section, the current entering the line at point I_{in} is unequal to the current leaving the system at I_{out} . This imbalance creates certainty that the fault resides within the protected zone and therefore a trip signal is issued to circuit breakers.

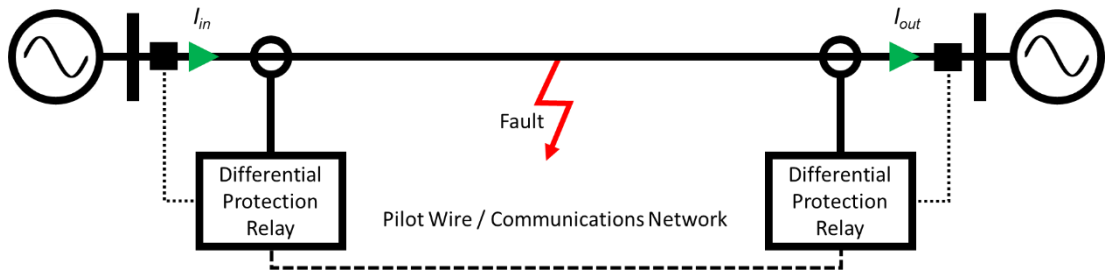


Figure 3-11: Differential protection system connection topology

Differential protection, particularly for overhead lines and cable circuits, requires communications for example via radio frequencies, power line carrier (PLC), optical fibre, pilot wires, etc. The use of communications can introduce a time delay between measuring a local value and comparing it against the remote measurement. GPS/Galileo time synchronisation is often applied to ensure that time-concurrent measurements are compared. Alternatively, a measurement or estimate of the propagation delay is used and measurements are synchronised using this information [118] [129] [130]. Due to the requirement for multiple measurements and the need for communications, differential protection is often expensive to deploy.

Differential systems are highly sensitive for faults which reside inside of their protected zone but are not sensitive to faults external to their zone and are therefore very secure and stable. Differential protection will not detect overload conditions, although modern multi-function protection relays may run additional functions alongside the main differential protection algorithm [131].

3.4.3 Distance Protection

The backup scheme proposed in this thesis is based upon distance protection. Distance protection is a well-established method in both transmission and higher voltage distribution systems (generally ≥ 33 kV). The subsequent subsections will provide an overview of distance protection principles, introduce the basic principles of impedance calculation, and provide an overview of a selection of communication-assisted distance protection schemes. More information surrounding distance protection and the protection methods outlined previously can be found in various protection textbooks [115] [118] [132].

3.4.3.1 Distance Protection Principles

The tripping time of a distance protection relay is determined by the distance (which is largely proportional to the line impedance – neglecting fault resistance) between the relay measurement point and the fault location. Distance relays rely upon the measurement of both voltage and current from which the apparent impedance is derived (Figure 3-12).

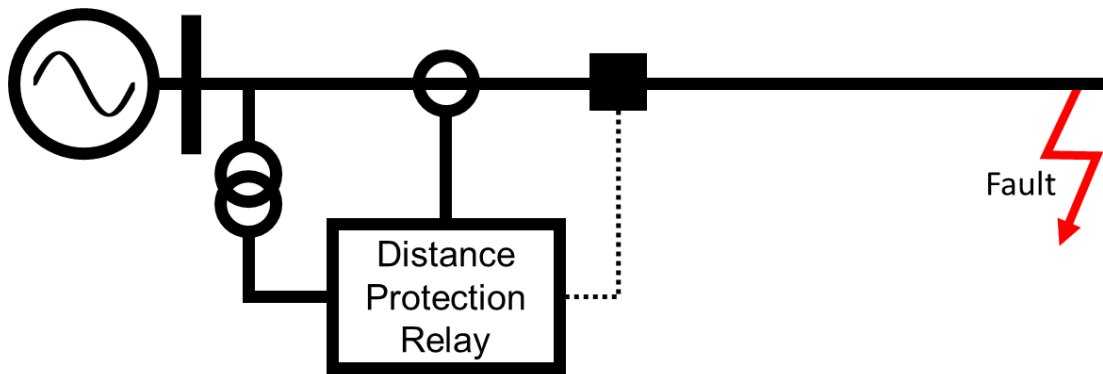


Figure 3-12: Distance protection system topology

A fault relatively near to the measurement point will result in a lower calculated apparent impedance than a fault relatively further away from the measurement point. This principle allows operational zones, typically three (and sometimes more), to be defined as presented in Figure 3-13 [133]. Distance protection is not a type of unit protection due to uncertainty in fault location near to zone boundaries (uncertainty is caused by measurement errors, differences in line impedance (e.g. due to temperature) and fault impedance).

- Zone 1 generally reaches to approximately 80% of the first protected feeder (Line RS in Figure 3-13) to prevent overreach into Zone 2 which would be caused by errors in the transducers, the relay itself and in the estimation of line parameters.
- Zone 2 is typically set to 120% impedance of the protected line (120% of Line RS).

- Zone 3 typically reaches to 120% of the combined impedance of lines RS and ST [118].

Suggested distance protection clearance times for a distribution network operator are presented in Table 3-4. These times are designed to allow a remote circuit breaker closer to the fault to clear the fault first, except in the case of a zone 1 fault, where the local breaker would be tripped as quickly as possible. This time-delayed zone approach is designed to reduce the number of customer interruptions associated with a downstream fault. Distance protection is also directional and can differentiate between faults “in front” or “behind” the measurement point.

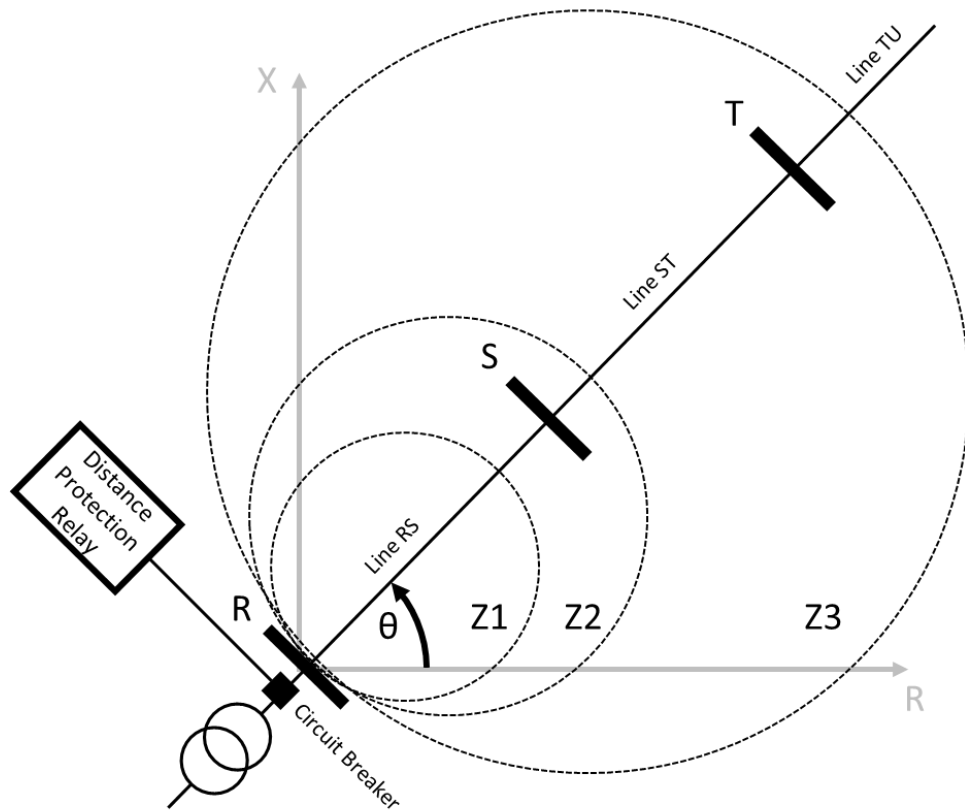


Figure 3-13: Distance protection zone diagram using Mho characteristic

Table 3-4: Example of distance protection clearance times for a Scottish DNO [57]

Zone	Maximum permissible clearance time (s)
Z1	0.150
Z2	0.500
Z3	1.300

Different tripping characteristics may be specified. These include the standard “Mho” (an offset circular characteristic), quadrilateral, lenticular and plain impedance characteristics. These tripping regions generally cover the positive resistive and inductive quadrants as in Figure 3-13.

Distance protection represents an affordable ‘unit-like’ scheme without the need for remote communication, although it is acknowledged that communications can enhance distance schemes [118] as will be outlined in Section 3.4.3.3. The sensitivity of distance relays may be reduced for high resistance faults however they are generally more selective than overcurrent schemes. Another important benefit of distance protection is that, unlike overcurrent schemes, distance protection is theoretically not affected by variations in fault levels, as the ratio between voltage and currents during faults should be preserved regardless of the “strength” or fault level of the system.

3.4.3.2 Overview of Fault Impedance Calculations and Tripping Characteristics

Distance protection relays consist of six impedance sensing elements per protection zone which are categorised as either phase elements (i.e. A-B, B-C and C-A) or ground elements (i.e. A-G, B-G and C-G) [134]. Each element measures the positive phase sequence impedance between the relay and the point of fault. Sequence components are used to represent imbalance, perhaps caused by load imbalance or a non-symmetrical fault, in a power system using positive-, negative- and zero-sequence phasors, as a set of three balanced systems [134].

The transformation between standard three-phase values and sequence component values is outlined in equation 3-4 for voltages, although the same transformation is valid for currents, where V_1 represents the positive-sequence, V_2 the negative-sequence and V_0 the zero-sequence voltages. V_a , V_b and V_c have their usual meaning, a is a complex number defined in equation 3-5 and a^2 in equation 3-6. Equation 3-7 describes the inverse transformation allowing the conversion from sequence components back to standard voltages [135].

$$\begin{bmatrix} V_1 \\ V_2 \\ V_0 \end{bmatrix} = \frac{1}{3} \begin{bmatrix} 1 & a & a^2 \\ 1 & a^2 & a \\ 1 & 1 & 1 \end{bmatrix} \begin{bmatrix} V_a \\ V_b \\ V_c \end{bmatrix} \quad 3-4$$

$$a = e^{j(\frac{2\pi}{3})} = \frac{1}{2} + j\frac{\sqrt{3}}{2} \quad 3-5$$

$$a^2 = e^{j(\frac{4\pi}{3})} = e^{-j(\frac{2\pi}{3})} = -\frac{1}{2} - j\frac{\sqrt{3}}{2} \quad 3-6$$

$$\begin{bmatrix} V_a \\ V_b \\ V_c \end{bmatrix} = \frac{1}{3} \begin{bmatrix} 1 & 1 & 1 \\ a^2 & a & 1 \\ a & a^2 & 1 \end{bmatrix} \begin{bmatrix} V_1 \\ V_2 \\ V_0 \end{bmatrix} \quad 3-7$$

Sequence components allow a standard electrical network (Figure 3-14) to be translated into a network of sequence components where Z_s is the source impedance and Z_L is the impedance from the protection relay to the fault. It is assumed that positive- and negative- sequence components are equal for the purpose of the following calculations. Figure 3-15 presents the sequence component network for a phase-phase fault. Different sequence component networks are used for the analysis of other fault types.

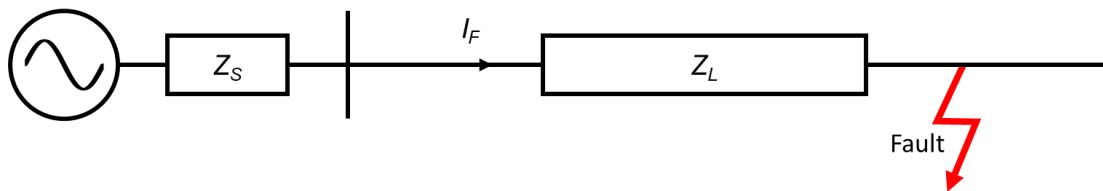


Figure 3-14: Standard electrical network with fault location indicated

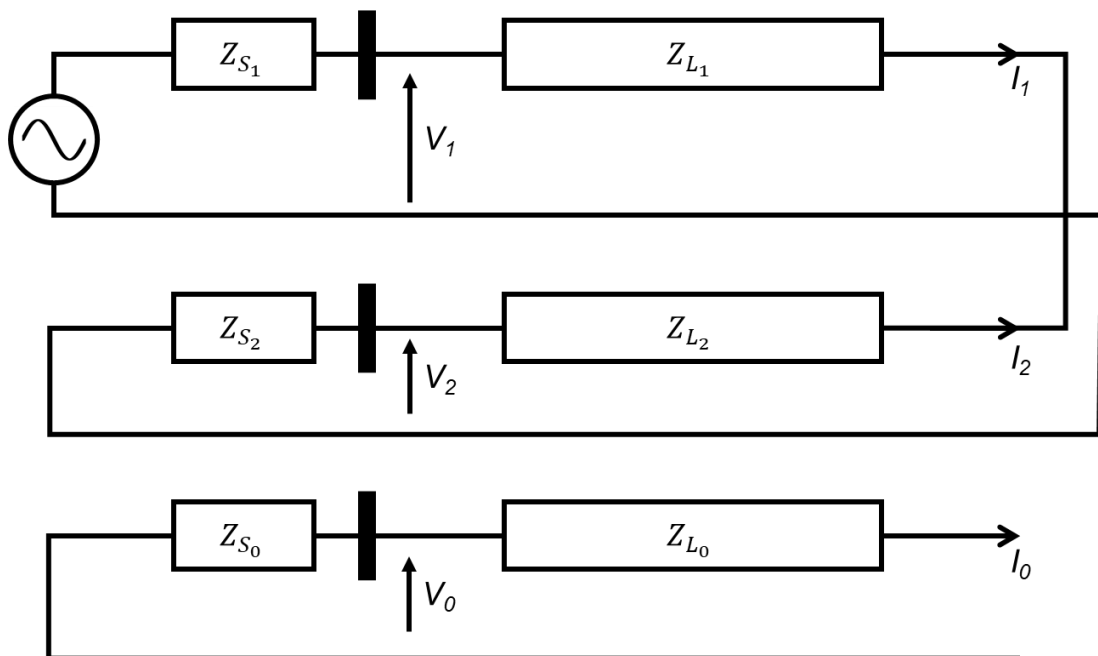


Figure 3-15: Sequence component network for phase-to-phase fault [134]

From the matrix outlined previously in 3-4, the sequence voltages are outlined in equations 3-8, 3-9 and 3-10.

$$V_1 = \frac{1}{3}(V_a + aV_b + a^2V_c) \quad 3-8$$

$$V_2 = \frac{1}{3}(V_a + a^2V_b + aV_c) \quad 3-9$$

$$V_0 = \frac{1}{3}(V_a + V_b + V_c) \quad 3-10$$

Applying Kirchhoff's theorem, which states that the sum of all the voltages around a closed loop in a circuit must be equal to 0, to Figure 3-15 yields equation 3-11. Since it is assumed that positive- and negative- sequence impedances are equal, the following equations determine the positive-sequence impedance in terms of positive- (Z_{L_1}) and negative- (Z_{L_2}) sequence voltages and currents – equation 3-14.

$$V_1 - I_1Z_{L_1} + I_2Z_{L_2} - V_2 = 0 \quad 3-11$$

$$V_1 - I_1Z_{L_1} + I_2Z_{L_1} - V_2 = 0 \quad 3-12$$

$$V_1 - V_2 = Z_{L_1}(I_1 - I_2) \quad 3-13$$

$$Z_{L_1} = \frac{V_1 - V_2}{I_1 - I_2} \quad 3-14$$

Using the sequence-component transformation matrix outlined previously in equation 3-7, the term in equation 3-17 can be derived. This transformation is also valid for currents – equation 3-18.

$$V_1 - V_2 = \frac{1}{3}(V_a + aV_b + a^2V_c - V_a - a^2V_b - aV_c) \quad 3-15$$

$$V_1 - V_2 = \frac{1}{3}(V_b(a - a^2) - V_c(a - a^2)) \quad 3-16$$

$$V_1 - V_2 = \frac{1}{3}(a - a^2)(V_b - V_c) \quad 3-17$$

$$I_1 - I_2 = \frac{1}{3}(a - a^2)(I_b - I_c) \quad 3-18$$

The impedance of phase elements can be computed via the substitution of equations 3-17 and 3-18 into equation 3-14 as in equation 3-19 and simplified in 3-20 to yield an expression for the BC phase element where Z_{L_1} is the positive-sequence impedance between the relay and the fault location.

$$Z_{L_1} = \frac{\frac{1}{3}(a - a^2)(V_b - V_c)}{\frac{1}{3}(a - a^2)(I_b - I_c)} \quad 3-19$$

$$Z_{L_1} = \frac{V_b - V_c}{I_b - I_c} \quad 3-20$$

A similar approach can be taken to determine the positive sequence impedance for ground elements. Figure 3-16 presents the sequence network for a phase-ground fault.

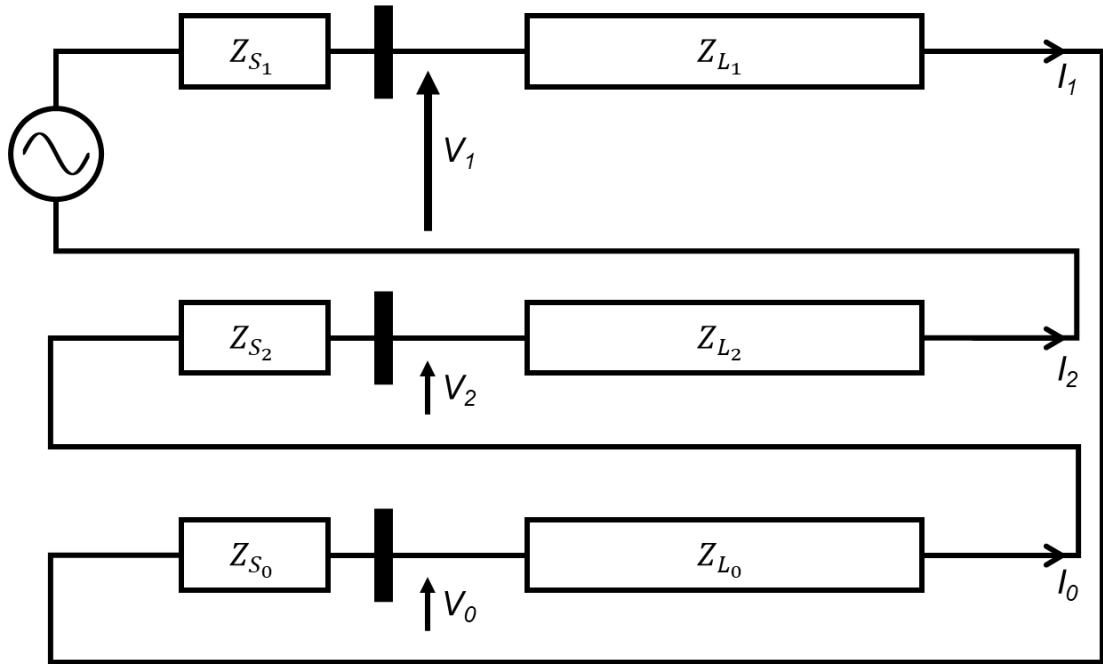


Figure 3-16: Sequence component network for phase-to-ground faults [134]

Again, from Kirchoff's theorem, and assuming that the positive and negative impedances are equal, the equation representing the circuit in Figure 3-16 is outlined in 3-21.

$$V_1 - I_1 \alpha Z_{L_1} + V_0 + V_2 - I_2 \alpha Z_{L_2} = 0 \quad 3-21$$

$$V_1 + V_2 + V_0 = I_1 Z_{L_1} + I_2 Z_{L_1} + I_0 Z_{L_0} \quad 3-22$$

From the transformations outlined previously in equation 3-4, the voltage terms can be simplified to V_a to give equation 3-24.

$$V_1 + V_2 + V_0 = V_a \quad 3-23$$

$$V_a = I_1 Z_{L_1} + I_2 Z_{L_1} + I_0 Z_{L_0} \quad 3-24$$

Adding and subtracting the term $I_0 Z_{L_1}$ to equation 3-24 (essentially adding and subtracting 1), as in equation 3-25, allows the term to be further rearranged in equations 3-26 and 3-27

$$V_a = I_1 Z_{L_1} + I_2 Z_{L_1} + I_0 Z_{L_0} + I_0 Z_{L_1} - I_0 Z_{L_1} \quad 3-25$$

$$V_a = Z_{L_1}(I_1 + I_2 + I_0) + I_0 Z_{L_1}(Z_{L_0} - Z_{L_1}) \quad 3-26$$

$$V_a = Z_{L_1}(I_1 + I_2 + I_0) + I_0 Z_{L_1} \left(\frac{Z_{L_0}}{Z_{L_1}} - 1 \right) \quad 3-27$$

Again, substituting in I_a in for the sum of the sequence currents yields equation 3-28.

$$V_a = Z_{L_1} \left\{ I_a + I_0 \left(\frac{Z_{L_0}}{Z_{L_1}} - 1 \right) \right\} \quad 3-28$$

Using the transformation for I_0 allows the residual current (I_{res}) to be calculated as the sum of the phase currents.

$$I_0 = \frac{1}{3}(I_a + I_b + I_c) = \frac{I_{res}}{3} \quad 3-29$$

Substituting equation 3-29 into equation 3-28 yields equation 3-30.

$$V_a = Z_{L_1} \left\{ I_a + \frac{I_{res}}{3} \left(\frac{Z_{L_0}}{Z_{L_1}} - 1 \right) \right\} \quad 3-30$$

The residual compensation factor (K) can, therefore, be defined.

$$K = \frac{1}{3} \left(\frac{Z_{L_0}}{Z_{L_1}} - 1 \right) \quad 3-31$$

Finally, rearranging equation 3-30 for Z_{L_1} and substituting in K yields the positive phase sequence impedance for the phase A ground element as outlined in Equation 3-32

$$Z_{L_1} = \frac{V_a}{I_a + K I_{res}} \quad 3-32$$

A summary of the calculations required to determine the positive-sequence impedance for all phase and ground elements are presented below in equations 3-33 through 3-40 [134].

$$\text{Phase A-B} \quad Z_{L_1} = \frac{V_a - V_b}{I_a - I_b} \quad 3-33$$

$$\text{Phase B-C} \quad Z_{L_1} = \frac{V_b - V_c}{I_b - I_c} \quad 3-34$$

Phase C-A	$Z_{L_1} = \frac{V_c - V_a}{I_c - I_a}$	3-35
Phase A-G	$Z_{L_1} = \frac{V_a}{I_a + KI_{res}}$	3-36
Phase B-G	$Z_{L_1} = \frac{V_b}{I_b + KI_{res}}$	3-37
Phase C-G	$Z_{L_1} = \frac{V_a}{I_b + KI_{res}}$	3-38
Compensation factor (K)	$K = \frac{1}{3} \left(\frac{Z_{L_0}}{Z_{L_1}} - 1 \right)$	3-39
Residual current (I_{res})	$I_{res} = 3I_0 = I_a + I_b + I_c$	3-40

Once the positive phase-sequence impedances have been determined for all phase and ground elements, the values are individually compared against the tripping characteristics for each operational zone of the relay. Tripping characteristics may take various “shapes” such as the Mho, lenticular and quadrilateral as outlined in Figure 3-17. Different tripping characteristics have different benefits, for example, the lenticular characteristic may be used if there is a danger that the Z3 comparator of a standard Mho characteristic may trip during periods of high loading. For similar reasons, the quadrilateral characteristic allows for independent setting of resistive and inductive reaches.

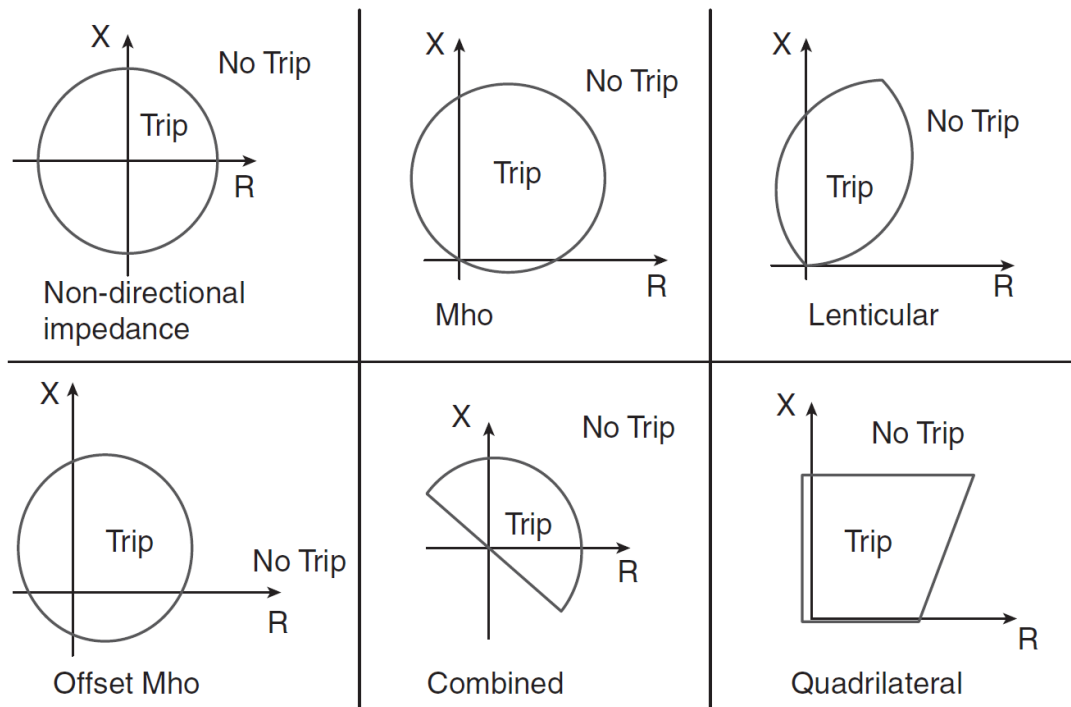


Figure 3-17: A selection of commonly used distance protection characteristics [128]

If the calculated impedance is found to be inside a Z1 tripping region, the relay will trip immediately as the fault is definitely on the first protected line. For non-instantaneous zones (e.g. Z2 and Z3), a timer is started when an impedance value resides within the tripping area. As the timer counts up to the pre-set tripping delay, the impedance is continually calculated to determine if the fault is still present on the system. Should the impedance transit to outside of the tripping characteristic, the timer is reset as it can be assumed that the fault is cleared by another protection system closer to the fault [134]. If the measured impedance remains in the tripping region for the duration of the pre-determined tripping delay, a signal is sent to open the CB.

The implementation of a distance protection relay is discussed in more detail in Chapter 6, however, a summary of the detection, comparison and tripping process is outlined in Figure 3-19 [136].

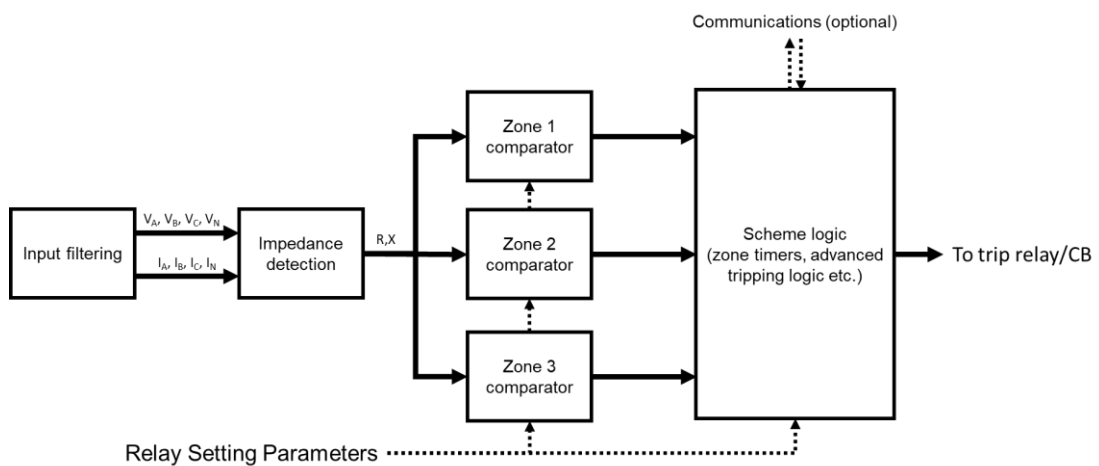


Figure 3-18: Flow chart summarising the operation of a distance protection relay

3.4.3.3 Advanced (Communication Assisted) Distance Protection Schemes

As alluded to previously, distance protection schemes can be enhanced through the use of communications. Using standard distance protection logic (Figure 3-19), fast tripping cannot be achieved for the full length the protected lines as presented in Figure 3-20. For faults at either end of the line, the tripping of CBs at either end of the line is not instantaneous. For example, a fault near to busbar A, as outlined in Figure 3-20, would be cleared quickly by Z1_A but after a delay by Z2_B.

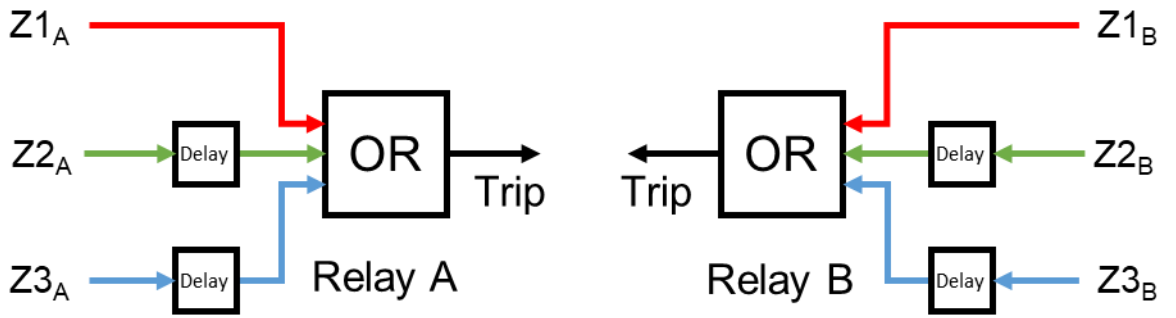


Figure 3-19: Standard distance protection tripping logic [137]

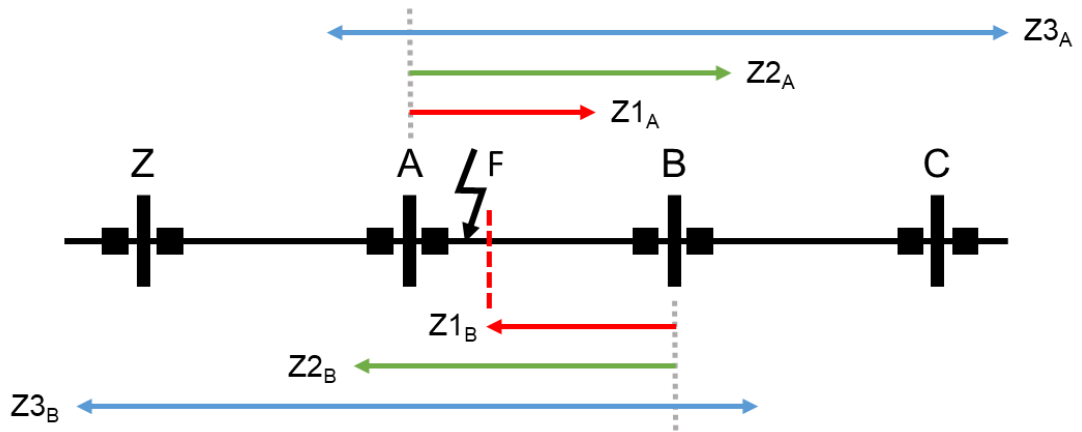


Figure 3-20: Simple network protected by distance protection relays [137]

There are various improvements which can be made to distance protection schemes to enhance their performance and provide fast-tripping for the full length of a line. The concepts of direct transfer tripping (DTT), permissive under-reach transfer tripping (PUTT) and permissive over-reach transfer tripping (POTT) will be introduced.

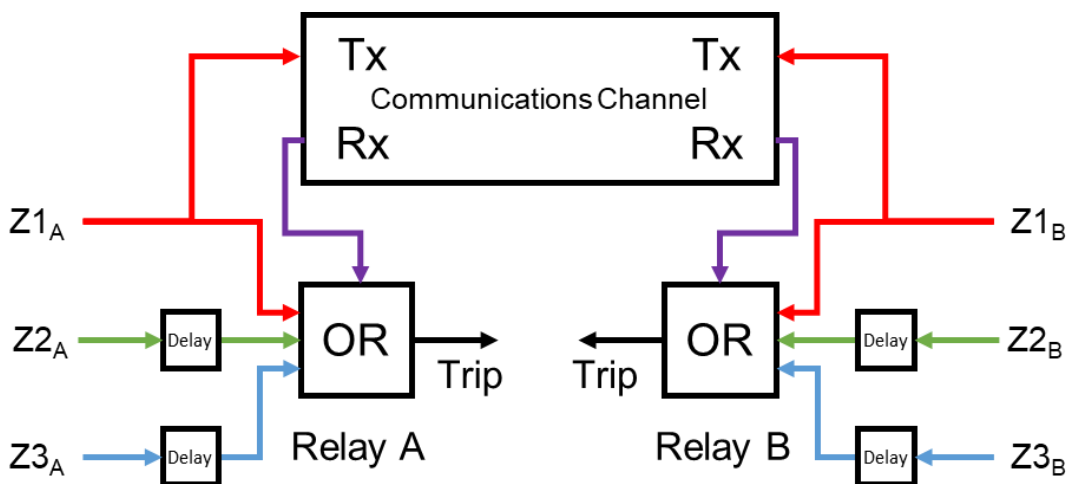


Figure 3-21: Distance protection tripping logic with direct transfer trip [137]

To provide fast tripping for the entire length of a line (e.g. the line connecting busbar A to B in Figure 3-20), a direct transfer tripping scheme may be introduced as presented in Figure 3-21. DTT schemes rely on a communication link to be established between two distance protection relays. When a fault is detected, for example in $Z1_A$, the trip signal is sent both to the local CB but also, via the communications link, to the remote relay at the other end of the protected line – this signal is known as a DTT. There is no measurement correlation between relays at either end of the line and the remote relay trips immediately when the DTT signal is received [138]. DTT schemes are very simple but the security of the system could be considered as being low when compared to the PUTT and POTT methods.

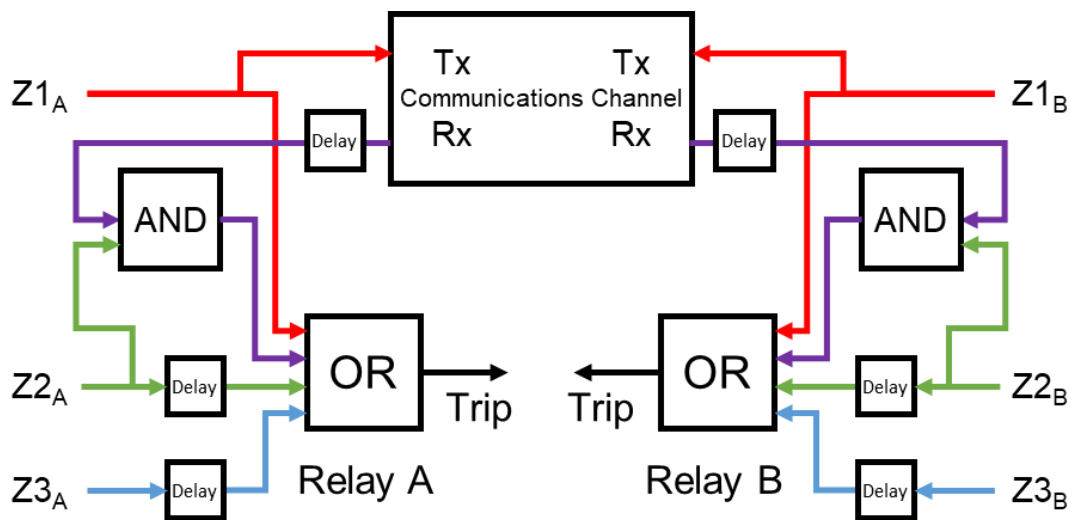


Figure 3-22: Distance protection tripping logic with permissive under-reach functionality [137]

Unlike with a DTT system, a Permissive Under-reaching Transfer Tripping (PUTT) scheme is required to detect the fault at either end of a line before a fast-trip signal is issued. This is achieved via the exchange of $Z1$ trip signals. Should a fault be detected in $Z1_A$, a signal is also sent to relay B as well as the local CB at busbar A. If a $Z2_B$ signal and the $Z1_A$ PUTT signal is present at relay B, it is assumed that the fault resides in the protected line AB. The CB at busbar B is therefore permitted to trip immediately [139].

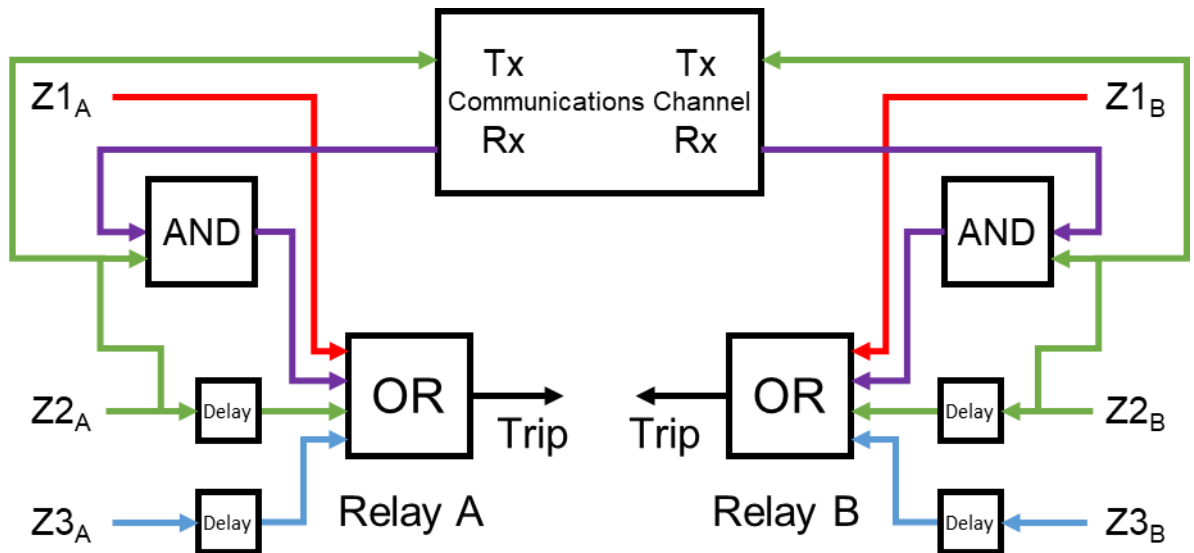


Figure 3-23: Distance protection tripping logic with permissive over-reach functionality

A Permissive Over-reach Transfer Trip (POTT) system (Figure 3-23) communicates Z2 information rather than Z1 as would be used in a PUTT scheme. In this case, if a fault is detected by both relays in Z2 (which covers 120% of the protected line) the fault must reside on the protected line. Again, since it is known and corroborated that the fault is on the protected line section, tripping can be instantaneous [140].

3.5 Protection of AC Distribution Networks

The coordination of protection devices within distribution networks is an important, and sometimes complex process due to the scale of the system which spans multiple voltage levels. Coordination of protection devices is defined as the grading of relay settings to achieve selectivity [132]. In other words, a coordinated protection system is designed so that when a fault occurs, the protective device closest to the fault will operate to clear the fault while leaving the rest of the system intact. A brief overview of the standard protection practices of the DNO SSEN is presented in this section [57]. Figure 3-24 provides an overview of a generic distribution protection system. Generally, as network voltage decreases, the number of customers impacted by an outage also reduces. Consequently, protection schemes for distribution networks are generally more involved and layered as voltage and connected demand increases. Consequently, the cost associated with the protection system also increases.

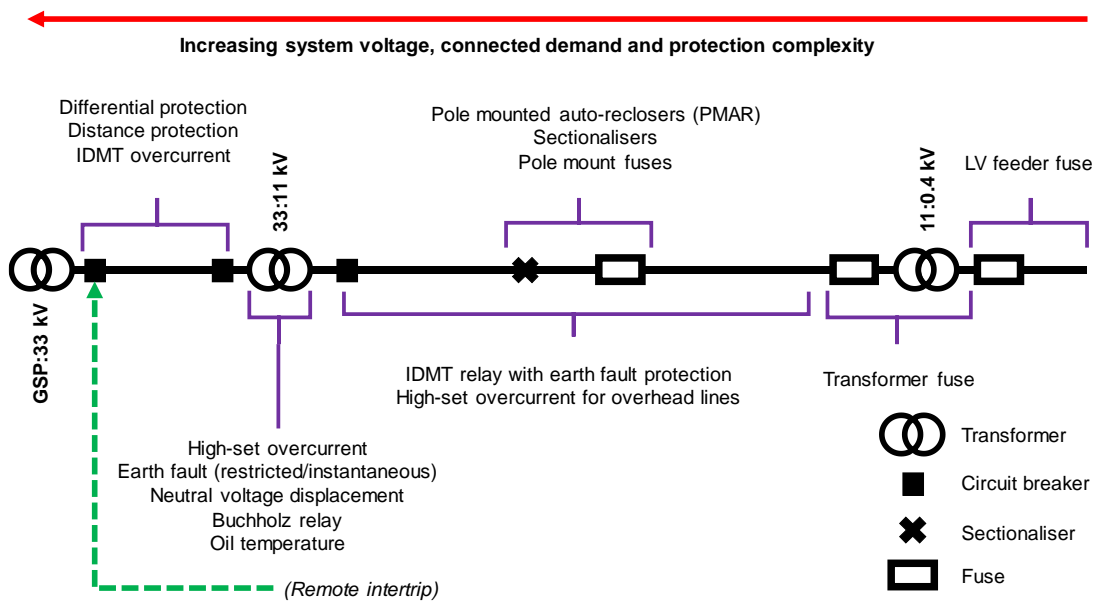


Figure 3-24: Simplified diagram summarising protection of a typical distribution networks

Low voltage feeders are commonly only protected by fuses or moulded case circuit breakers (MCCB) providing a time and current graded scheme designed to act for downstream network faults. Secondary (11 kV to LV) transformers are protected by fuses on the incoming high voltage side.

11 kV cable circuits are predominantly protected via IDMT overcurrent and ground fault relays with clearance times of up to one second (although normally faults should be cleared with times of significantly less than this). Overhead 11 kV circuits are protected in a similar way with instantaneous ‘high-set’ overcurrent protection also applied to provide a quicker trip for faults that can be deemed to be definitely on the protected line (as the fault current is significantly higher than the fault current at the remote end of the line). A ‘high-set’ is an extra parameter in a relay which is set above a certain “high” threshold. For fault currents above this threshold, it can be assumed that the fault is definitely on the first/main protected line and tripping can be instant.

11 kV overhead line (OHL) circuits commonly employ devices called auto-reclosers and sectionalisers. Since most faults on overhead systems are temporary (circa 80% [115]) the use of an auto-reclosing device, such as a pole-mounted auto-recloser (PMAR), allows a line to be re-energised automatically. When a fault current is detected by an auto-recloser, the unit will open. The device will then attempt several delayed reclosures until either fault current is no longer detected (i.e. the fault has been cleared) or the maximum number of operations has been reached where it is then assumed that the fault is permanent [118]. A sectionaliser is similar

to an auto-recloser, however it cannot interrupt fault current and normally operates during the “dead-time” while an upstream PMAR or other device is open. Sectionalisers are therefore used in conjunction with upstream circuit breakers and reclosers. A sectionaliser will count the number of times the device is subjected to fault current and will open when a certain threshold is reached, which typically means that the fault is downstream and permanent in nature and therefore after a number of failed reclose attempts, the sectionaliser will open, isolating the fault but allowing supplies to be restored to consumers connected upstream between the sectionaliser and the fault interrupting device. Sometimes sectionalisers are used to “save” downstream fuses by opening before the fuse would melt (and therefore need to be replaced) [141]. Reclosing devices are not used on cable circuits as a fault on such an asset is highly unlikely to be temporary and are invariably permanent, and reclosing could cause further damage to the cable, and more importantly, its surroundings, which could be a tunnel (e.g. a railway tunnel), on a bridge crossing, underneath a public footpath, etc.

Primary transformers, 33:11 kV, are generally protected by high-set overcurrent and ground fault (usually implemented using restricted ground fault methods with typically 150 ms operation times) relays. Neutral voltage displacement (NVD) relays are commonly deployed in the SSEN distribution network with tripping times of between 3 and 10 seconds. NVD relays are used to infer unbalanced faults or significant system imbalance on three-wire systems where no neutral is present. VTs which are capable of transforming zero-sequence voltages, via a three-phase five-limb VT or three single-phase VTs, are used in NVD relays [142] with the primary side of the VTs being star connected and solidly earthed while the secondary side is ‘open delta’ as demonstrated in Figure 3-25 [143].

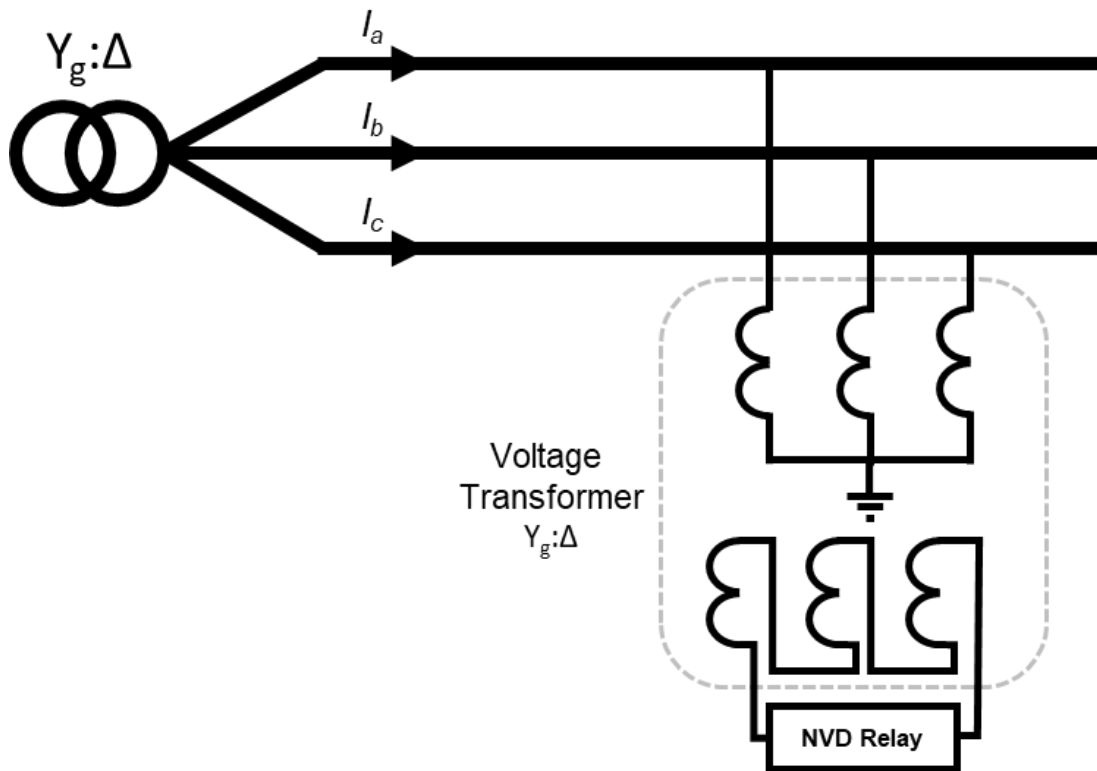


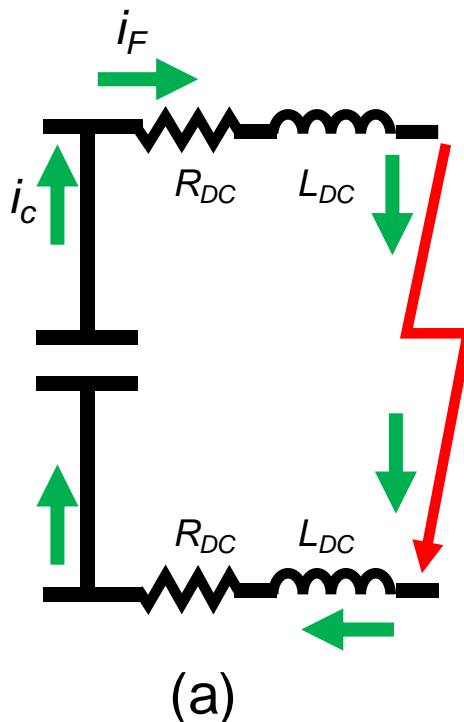
Figure 3-25: NVD relay connection topology

Protection of 33 kV feeders and transformers is typically a combination of the following: differential protection (which should operate within 150 ms), distance protection (with trip times specified previously in Table 3-4), IDMT overcurrent and ground fault protection (up to 3 s). Auto-reclosing techniques may also be applied to overhead 33 kV networks.

3.6 Protection of HVDC Systems

While the protection of AC assets is undoubtedly a complex task, the zero-crossing of current greatly assists with the physical interruption of AC current and interruption will typically occur at or around the zero-crossing. Since DC systems do not naturally benefit from zero-crossings, the challenge of extinguishing the electrical arc formed when the contacts of a DC circuit breaker open under fault (and even load) conditions is significantly increased [144]. One of the greatest challenges with DC links and future DC networks is therefore associated with the protection of the system [145] [146].

Fault currents in DC systems consist initially of the capacitive discharge from the DC conductors and any DC side smoothing capacitance (i_c) as outlined in Figure 3-26 (a). The freewheel diodes start to conduct essentially forming an uncontrolled rectifier when the DC-side voltage drops below the AC-side voltage [88] – Figure 3-26 (b). This is followed by infeed from the AC-side grid (i_{ga} , i_{gb} , i_{gc}) via the converter bridge (i_{DC}) - Figure 3-26 (c) [147] [148] [149] [150] [151]. Figure 3-27 outlines the typical DC voltage and current response during a balanced DC-side fault. Figure 3-28 shows the same event with the three DC fault stages, (a)-(c), highlighted.



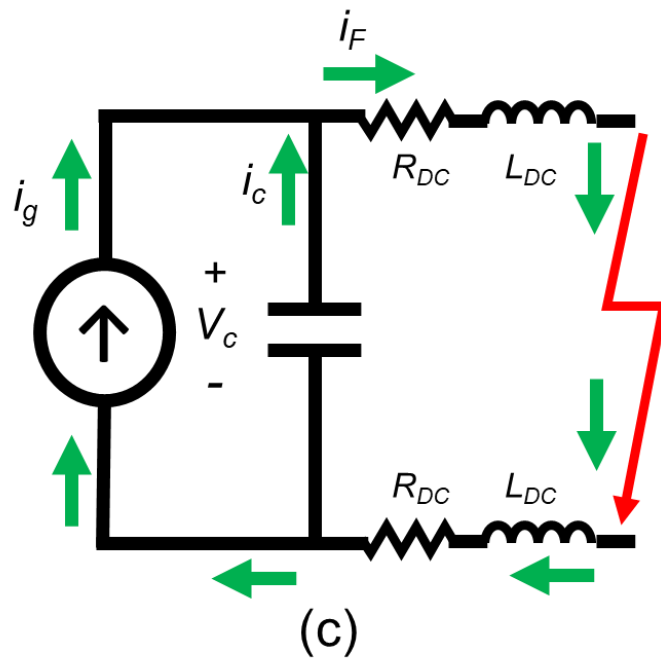
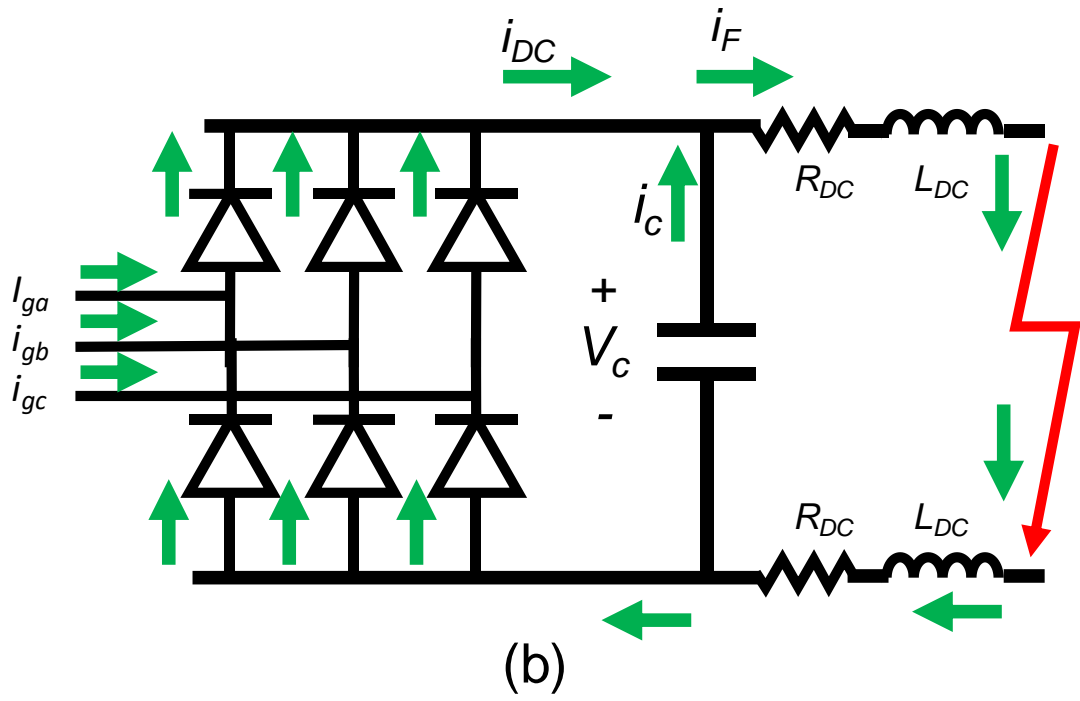


Figure 3-26: VSC fault current paths during (a) capacitor discharge followed by (b) diode freewheeling and (c) grid current feeding [152]

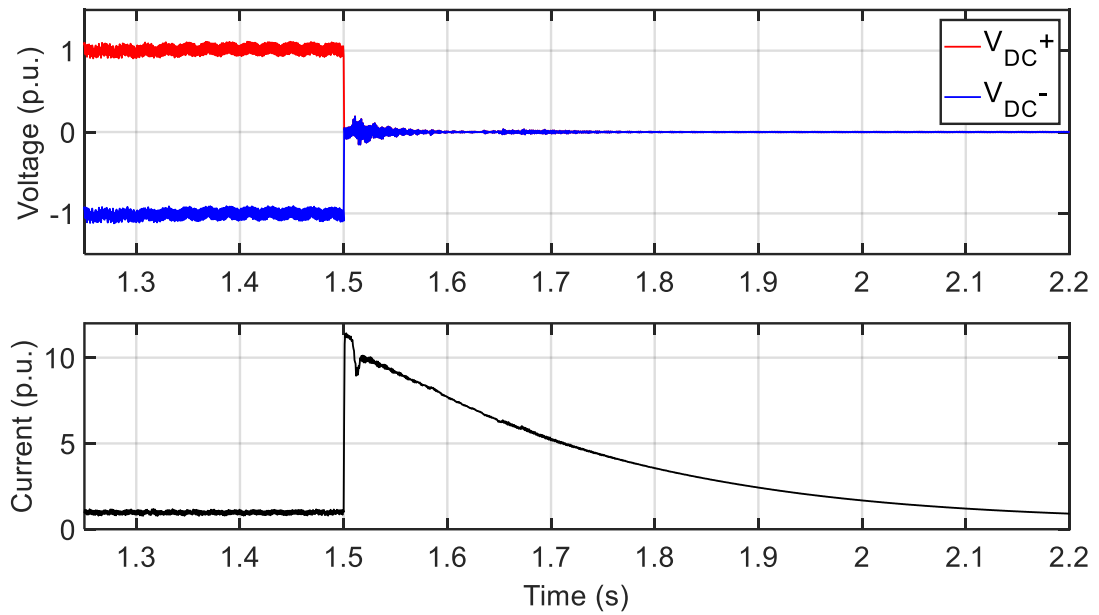


Figure 3-27: Example of DC-side voltages and current during an uncleared pole-to-pole fault at the converter terminals (0 km) for a ± 100 kV, 2,00 MVA, 75 km VSC HVDC link

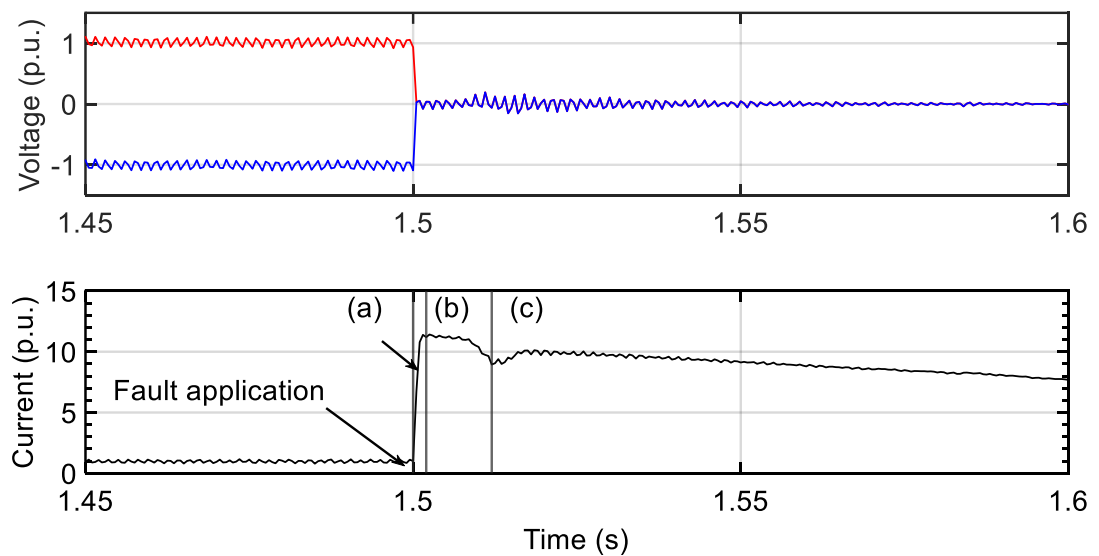


Figure 3-28: DC-side voltage and current during a DC-side fault with converter fault stages identified

Circuit breakers which are capable of interrupting DC currents are technically more complex, significantly larger and more expensive than an AC equivalent as they need to include additional components to extinguish any arc which may form during opening. There are three main approaches proposed for the design of DC circuit breakers: mechanical, solid-state and hybrid. Mechanical CBs, Figure 3-29 (a), act in a similar way as standard AC CBs, albeit they

are comparatively much larger. Mechanical DC CBs are often supplemented with additional electrical resonant circuitry which attempts to force a zero-crossing of current to assist with the extinguishing of any electrical arc formed during the opening of the mechanical element of the CB. These CBs are physically very large but they offer the lowest on-state loss of the three methods presented – they do however have the slowest interruption times, which is typically several tens of milliseconds.

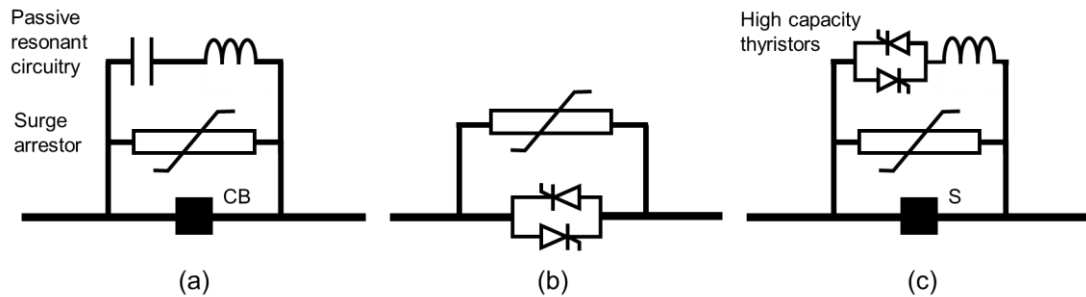


Figure 3-29: Simplified example topologies of (a) mechanical switch resonant circuit, (b) solid-state and (c) hybrid DC circuit breakers [153]

The solid-state DC CB, Figure 3-29 (b), is essentially an inline, series-connected, power electronic switch. These breakers have very quick interruption times, typically a few microseconds, however, this approach has high losses during normal operation due to the voltage drop across the power electronics which are connected in series with the power circuit [154] [155] [156].

The final DC interruption technology is the hybrid breaker. The hybrid breaker is a combination of the solid-state and mechanical-breaker as outlined in Figure 3-29 (c). During normal operation, the switch, S, is closed. This is a mechanical switch which therefore has a low on-state resistance during normal operation. When a fault occurs on the DC system, the high capacity thyristors are enabled to provide a parallel path for the fault current. The series inductor helps to limit the fault current while the thyristors are in conduction. The mechanical switch is opened while the thyristors continue to carry the fault current. Once the mechanical switch is open, the high capacity thyristors are turned off and the current stored in the inductor naturally discharges through the surge-arrestor.

Despite the large volumes of academic and industrial research in the area of HVDC CBs, in point-to-point HVDC applications, the use of DC circuit breakers is often avoided as AC-side interruption times are suitable fast. To prevent damaging power electronic devices during faults, point-to-point HVDC links should be isolated generally within 60 - 100 ms [157]. As this disconnection time of 60 - 100 ms is readily accomplished using established AC circuit

breaker technology, disconnection can be achieved by opening the AC-side CBs at either end of the DC link. This approach avoids the need to interrupt DC currents while using well-understood and more affordable AC CB technology. The speed of protection for HVDC point-to-point links is therefore generally limited by the speed of AC circuit breaker operation.

The fault current provided by the AC grid during DC faults in LCC systems can be brought under control typically within a single AC cycle by adjusting the firing angle of the thyristors. The design of thyristors permits a short-term overcurrent making them more likely to survive fault conditions. VSC topologies, for DC-side faults, are not as robust as their LCC counterparts. While the switching of IGBT devices can be blocked near instantaneously upon fault detection, the freewheel diodes placed across the IGBTs creates a current path which leaves the converter in an uncontrolled rectifying state as presented previously in Figure 3-26.

To increase the survival time of the power electronics used in VSC HVDC links during fault conditions, bypass thyristors are often employed [158] [159]. These thyristors, installed in parallel with each IGBT/diode, have a lower on-state voltage drop than the freewheel diode and therefore take a larger share of current during a fault – allowing additional time for AC-side circuit breakers to open before damaging the IGBT package.

The protection of multi-terminal VSC HVDC represents a further challenge. It is widely acknowledged that the protection time for DC grids is expected to be an order of magnitude faster than AC systems and point-to-point HVDC [160] [161] [162] with 5 ms disconnection times being suggested by industry [163]. Faster disconnection times are required for multi-terminal systems as the fault propagation speed is much faster than when compared to point-to-point and AC systems. This is due to the low DC-side impedance and the lack of inductance to limit the rate-of-change of current in a DC system [164] [165]. This issue is compounded when multiple sources supply fault current to DC-side faults as is the case in a multi-terminal scheme. Consequently, the development of fast-acting and low-loss CBs for HVDC grids has been a major focus of recent industrial and academic research [166] [167] [168]. Solutions generally propose that a voltage or current of opposing polarity is injected upon the fault current to create an artificial zero crossing. This zero-crossing reduces the strain on DC breakers and diminishes the likelihood of a sustained DC arc forming as described previously [163].

National Grid ESO outlines generic protection methods for HVDC point-to-point links in [47]. In this document, it is specified that the operator of an HVDC facility is responsible for the protection of all converter station plant, including:

- AC busbars;
- AC harmonic filter banks;
- converter station transformers;
- DC neutral point;
- DC busbars;
- DC filters; and
- DC conductors (e.g. cables or overhead lines).

It is stated that each plant item should employ two main and one backup protection method. There is no mention that remote, offsite, backup protection is required other than the ability to send a direct transfer trip (DTT) from the converter station to a remote circuit breaker.

3.7 Summary

This chapter has introduced the types and causes of electrical faults experienced by power systems. Power system protection is the process of detecting faults on a system and removing them in an appropriate manner. Protection schemes can be evaluated with reference to stability, sensitivity, selectivity and operation time. It is worth reiterating that no matter how advanced protection schemes become, they will never prevent faults from occurring on the power system in the first place. A review of three standard fault detection methods has been conducted with protection practices of a Scottish DNO briefly outlined.

As levels of embedded generation continue to rise and “smart grid” technologies develop, network operators must ensure that protection schemes remain stable, sensitive and selective [169] [170] [171] [172]. This shift will likely see more DC elements introduced across generation, power-delivery and demand systems. While DC power systems offer increased flexibility over the conventional ‘all AC’ approach, DC presents a challenge from the perspective of power system protection.

Chapter 4

Medium Voltage Direct Current Applications in Distribution Networks

4.1 Introduction

The use of HVDC and LVDC has increased significantly since the 1960s with both technologies being extensively explored academically and industrially [2] [173]. At low voltage, electronics (e.g. laptops, phone chargers etc.) usually employ DC interfaced to the grid via switch-mode power supplies [174]. As outlined previously, the properties of HVDC has made the technology commonplace for long-distance high voltage power transfers due to the reduction of line losses when compared against AC. However, the role and characteristics of MVDC both physically and electrically are comparatively less well explored.

Until recently, the cost of power electronic conversion systems has been too great to be considered a viable solution for distribution network applications. However in recent decades, the cost of power electronic converter systems has fallen significantly – driven by the push towards non-synchronous, converter-interfaced, generation such as wind and solar photovoltaic [175] [176]. To highlight the price reduction of power electronics, Figure 4-1 displays the cost per installed watt, in \$/W, for solar PV inverters between 2013 and 2019 for residential (3 – 10 kW), commercial (10 kW – 2 MW) and utility-scale (>2 MW) installations [177] [178].

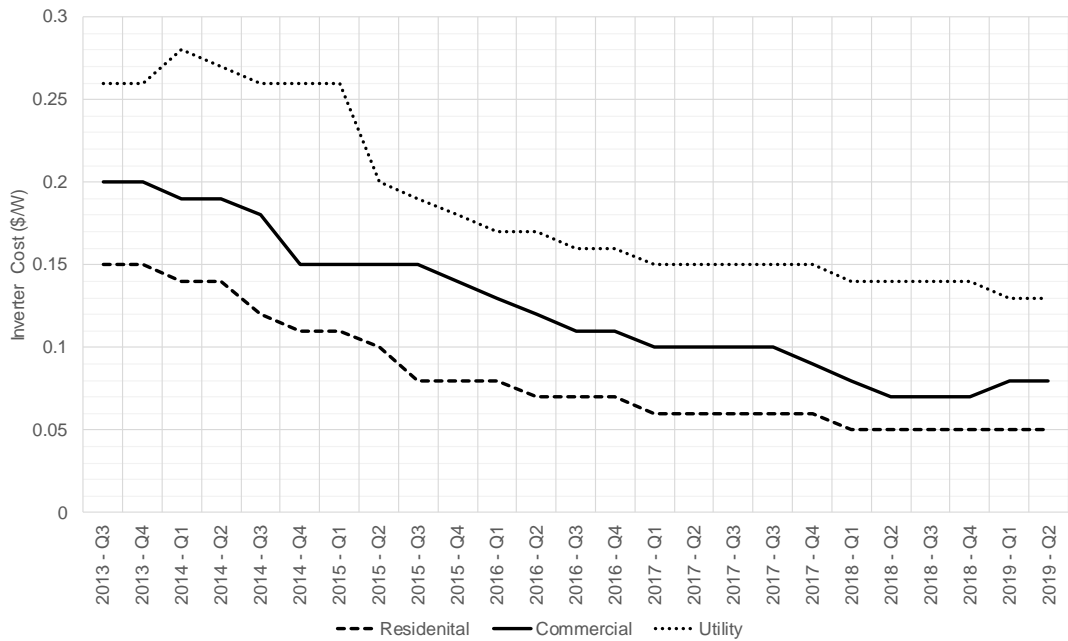


Figure 4-1: Cost of solar PV inverters for various installation scales [177] [178]

This chapter introduces MVDC with an emphasis on utility-scale power distribution applications. The general characteristic of MVDC are presented in Section 4.2.

Section 4.3 critically reviews academic and industrial literature in the field of MVDC applied to power distribution systems with a focus on protection, particularly backup protection. Section 4.4 describes three MVDC deployment trials taking place around Europe. The drivers behind the projects will be outlined alongside system topologies and implementation costs. A chapter summary follows in Section 4.5.

4.2 MVDC Characteristics

Notionally, MVDC would reside in the 5 kV – 50 kV range. This allows the repurposing of conventional AC HV distribution networks (e.g. 3.3 kV, 11 kV and 33 kV) for DC application. It is acknowledged that according to the standards IEC 60038 [179] (Table 4-1) and BS 7671:2018 [113] that any ‘ripple free’ DC voltage over 1,500 V is technically classed as high voltage. However, given that new HVDC and ultra-HVDC (UHVDC) schemes may operate anywhere between 380 kV and 1.1 MV [180], it seems appropriate that MVDC resides below this range. In literature [181] [182], commercial products [183] [184] and field trials [185], VSC technologies appear to be the preferred technology for MVDC distribution applications. This thesis therefore assumes that VSC technologies are employed for MVDC solutions primarily due to their increased control capability and their ability to more readily change the direction of power flow [186] when compared to LCC. Additionally, since VSC

converter stations have a smaller physical footprint than LCC, they are more suited for distribution applications where substations are generally required closer to load centres where land prices are higher.

Table 4-1: IEC 60038 voltage definitions

IEC Voltage Range	AC RMS Voltage (V)	DC Voltage (V)
High voltage	> 1,000	> 1,500
Low voltage	50 to 1,000	120 to 1,500
Extra-low voltage	< 50	< 120

MVDC converters for grid applications reside between medium voltage machine drives (used within wind turbines, traction, mining etc.) which generally operate at voltages between 1 – 14 kV [187] and HVDC operating at hundreds of kilovolts. Although the power ratings of large machine drives, typically between 1 – 80 MVA, are not dissimilar to that which an MVDC network solution would require, the voltage capability of converters needs to be increased to reduce resistive losses which would be significant when transmitting high currents over multi-kilometre line lengths [20] as demonstrated in Figure 4-2. In this figure the power losses, as a percentage of load, are presented for various DC voltages and circuit lengths. In this example, conductors have a resistance of 0.2 Ω /km.

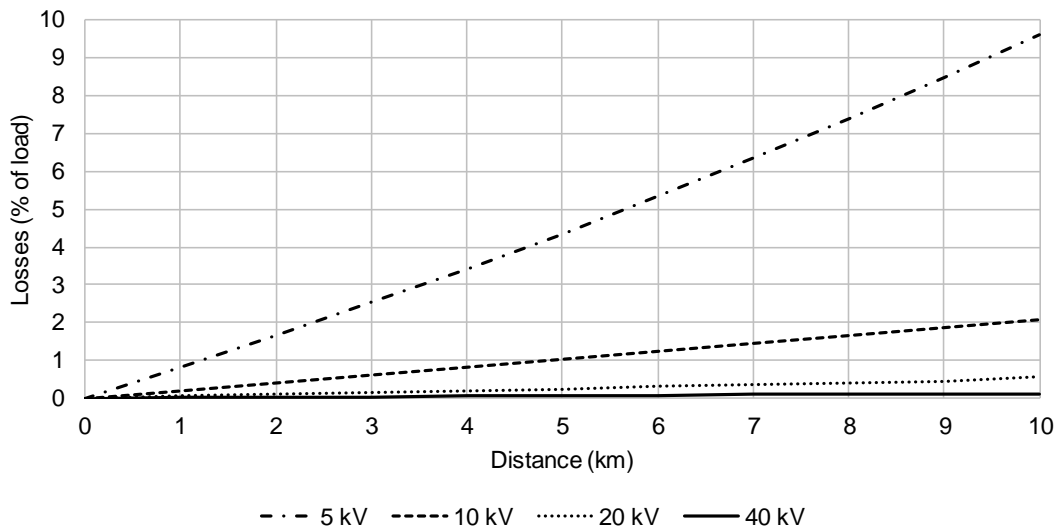


Figure 4-2: Losses associated with supplying a constant power 1 MW load at different DC supply voltages and circuit lengths (0.2 Ω /km)

Innovation projects such as [7], [188], [189], [190] and [191] all represent utility-scale projects where DC technologies are being proposed to support future demand and generation growth.

Equipment vendors have recently started to promote MVDC solutions for land-based power distribution applications too [183] [192]. Internationally, MVDC has been also been mooted for shipboard [193], rail traction [194], mining [195] and generation collection network [196] [197] applications.

4.3 Review of Academic/Industrial MVDC Research

In the late 1990s, there was a significant volume of literature produced which studied the design and protection of machine drives operating at medium voltage DC [198] [199] [200] [201]. Some of the first references to propose the use of DC technologies for power distribution applications are to be found in a pair of conference papers published in 2000 by Bloh, De Doncker et al. [202] [203]. These papers refer to ‘MVDC transmission’ and both review, benchmark and optimise different power electronic switching strategies for a ‘transformerless’ 5 kV DC system, rather than the more common arrangement which uses a front-end converter transformer to smooth harmonics. These papers examine methods to minimise the harmonics generated by the converter by trialling various switching schemes. The papers do not mention a power rating of the modelled converters nor the AC system voltage to which they connect. No discussion of power system protection is made.

Between 2004 – 2011 a series of patents [204] [205] were published on the Siemens’ SIPLINK (Siemens Multifunctional Power Link) system – essentially a back-to-back VSC (AC-DC-AC) converter which facilitates the controls of real and reactive power flow between two asynchronous AC systems. The SIPLINK system had a power rating of between 1 – 30 MVA, a DC operating voltage of 1 kV and was based on IGBT technology switching at 3 kHz.

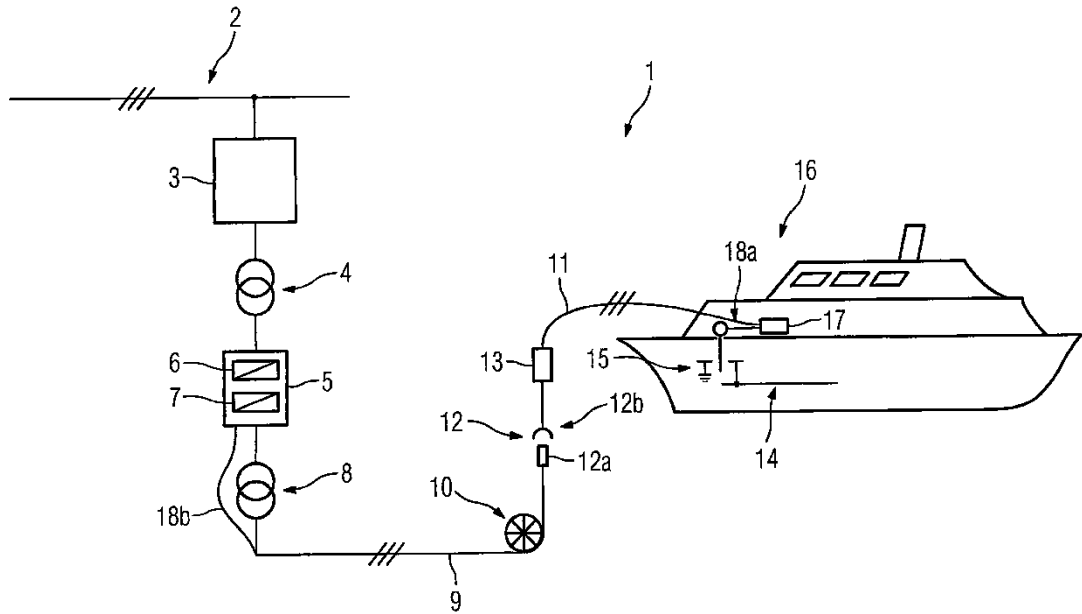


Figure 4-3: SIPLINK interconnection between land and ship power system via back-to-back power electronic converter (reproduced from [204])

The SIPLINK system (Figure 4-3) was originally designed to interface large ships with land-based power systems however it was proposed in a paper [206] that the technology could be repurposed to allow the interconnection between adjacent distribution networks. This paper outlines the key benefits of MVDC interconnection including the ability to interconnect different (and previously separate) AC systems without increasing fault levels and to allow the interconnection between grids of differing frequency. (HVDC frequency converters are used to interface between the 50 Hz and 60 Hz power systems in Japan for example [207] [208]). The paper acknowledges that ‘long-distance’ power transmission is not possible due to the relatively low operating voltage of the link and the associated ohmic power losses (due to high currents required for any form of meaningful power transfer). Other than the paper stating that each converter has a module for protection and control, no specific details are provided regarding the protection approach deployed. The two patents describe system arrangements but lack technical detail relating to protection, other than stating that protection would be achieved by fuses. A similar patent by ABB [209], again, lacks technical details as to the design of the main and backup protection systems.

MVDC has been considered for all-electric ship applications [210]. All-electric ships, where propulsion and service power are provided via a common electrical system rather than propulsion and electricity being independent [211], are said to offer greater efficiencies, reliability, flexibility and reduced operational cost over conventional mechanically-propelled

vessels with multiple examples in present-day operation [212]. MVDC expertise and standards in this area appear to be considerably more advanced than when compared to land-based utility power networks – for example, a document produced in 2010 by the IEEE Standards Association [213] recommends best practice for the design of shipboard MVDC systems. With regards to protection, this document states that backup short circuit protection should exist between each generator and its associated AC-DC converter. The transaction paper [214] presents the modelling, simulation and experimental validation of MVDC shipboard system. Comment is made as to the design of a DC capable circuit breaker, however, fault detection strategies to trip the circuit breaker are not considered. An adaptive protection scheme for all-electric MVDC ships is presented in [215] and, again, does not refer to backup protection.

MVDC has been proposed for offshore, and to a lesser extent onshore, collection networks for wind turbine power parks [216]. Figure 4-4 presents an example topology where an MVDC link connects to an offshore platform. Turbines are interfaced with DC-DC converter rather than a transformer as would be the case under standard deployment

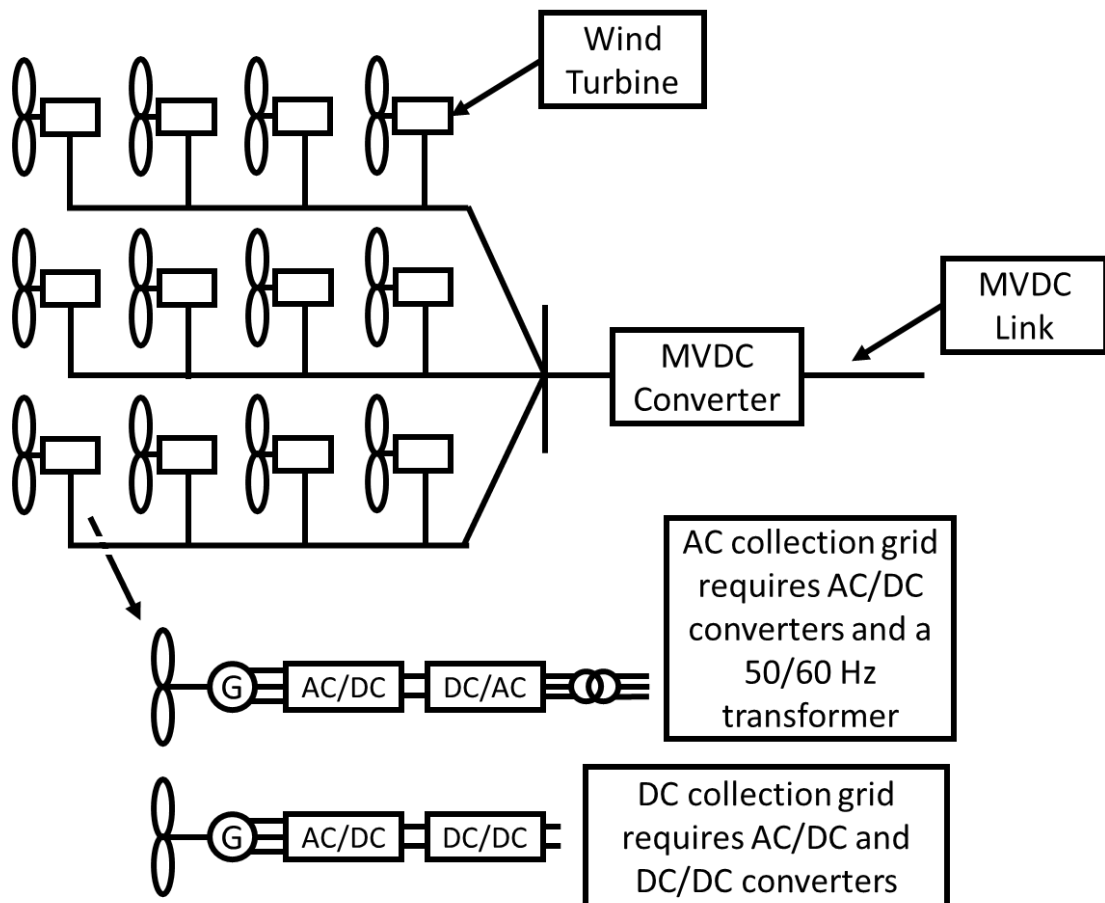


Figure 4-4: Example MVDC collection network for offshore wind applications [216]

An examination of efficiency savings offered by MVDC when compared to conventional 33 kV windfarm collection networks is performed in [217] for several topologies. It was found that for a 90 MW windfarm situated 15 km offshore a 20 kV DC system was 2.4% more efficient than the standard AC approach. The paper did not fully detail the configuration of the DC system. Analysis and design of an MVDC grid for offshore wind farm applications is discussed in [218]. This paper describes the converter behaviour during faults (as outlined in Chapter 3) but does not consider a fault detection methodology, as acknowledged by the authors. In 2018, an industry report was published which compares the different technology options available for offshore DC collection networks [196]. The report places the technology readiness level (TRL) of DC protection at 7/8 however positions the commercial maturity of the solution as low due to high costs of protection components. It is unclear whether the high TRL refers to CB technology or to protection solutions more generally. The document states that MVDC protection technology is not fully developed but makes no mention of protection schemes nor detection techniques.

The design of an MVDC substation is proposed in [219] with loads being supplied via either a DC-DC or DC-AC converter from a central 20 kV DC bus bar. No comment on protective relays is given other than reiterating that the area needs significant research and development for MVDC technologies to be applied more widely. Similarly, [220] makes the case for MVDC to be used for distribution feeders and concludes that MVDC could be beneficial but states that technical requirements of protection systems would require further research. An MVDC technology summary is provided in [221] which outlines where MVDC could play a role in the future. The paper presents the idea of MVDC becoming the enabling technology in future cities but also for generation collection networks – no reference of fault detection methods nor protection schemes is provided.

In 2017 a centralised protection system for MVDC microgrids was proposed in the transaction paper [222]. The proposed solution considers both main (differential) and backup (directional overcurrent) protection of an MVDC microgrid. The network model does not include any supply points derived from conventional AC grids and therefore limits the replicability of the solution in hybrid AC-DC distribution systems.

Zhang et al. propose the use of MVDC to release capacity for charging of electric vehicles [223]. The paper proposes the connection between two distribution lines by converting a segment of the network to DC. It is suggested that loads, such as electric vehicle charging, could be supplied from the DC link with a controlled contribution from each line. Methods to

repurpose existing AC conductors for DC are discussed in addition to voltage control strategies. As with several other papers, protection is not considered.

The operation and performance of an MVDC link is discussed in [224]. This paper states that MVDC links may interfere with the detection and discrimination of existing AC-side protection systems and potentially cause the mal or non-operation of relays. However, detailed studies are not presented. Faults on the DC-link are not considered.

From a literature review of MVDC, no backup protection approaches which are readily applicable to hybrid AC-DC distribution systems appear to be evident. The literature review was extended to the protection of HVDC schemes to determine best practice in this area.

A conference paper published in May 2019 describes the AC and DC protection methods for an LCC HVDC link in Italy [225]. The paper states that all primary equipment is covered by main protection with an instantaneous trip time and a time-delayed backup. A transfer trip scheme is used to allow the opening of the relevant TSO's CB in the event of CB failure at the HVDC stations. This document has similarities with the National Grid ESO document detailing the protection requirements for HVDC converter stations outlined previously [47]. The detection of faults on the DC link is not considered from AC measurements.

Alam et al. provide a comprehensive analysis of how VSC-HVDC links may cause distance protection relays to operate incorrectly, or not at all, for symmetrical and non-symmetrical AC-side faults [226]. No solutions to the identified issues were proposed and faults on the DC system are not considered. A paper presented at PowerTech 2017 observed similar behaviour [227]. Again, this paper does not propose a method for dealing with such faults, neither does it examine faults on the DC link. Papers [228] and [229] offer similar findings.

From a review of academic and industrial publications, it has been determined that there is a lack of consideration to backup protection solutions to secure against faults residing on the DC-side of embedded MVDC links. Backup protection methods from the perspective of the HVDC system appear to rely upon a direct transfer trip originating from the HVDC protection controller, therefore requiring communications. While communication links are commonplace at transmission level, they are less available in a distribution environment and their performance may not be suitable for tripping signals, particularly in a rural setting. A backup protection scheme which is not reliant on communications but rather informed by AC measurements would, therefore, be of benefit when considering the deployment of DC technologies within networks in the future. While the protection of the DC systems and components (e.g. converters) may be mentioned in several of the reviewed papers, there does

not appear to be any literature addressing specifically, and in detail, the ability of AC protection systems to provide backup protection for adjacent DC links, nor relating to system-wide protection (including backup protection) of land-based hybrid AC-DC systems.

4.4 Review of Deployed MVDC Technologies in Distribution Systems

This section provides an overview of several MVDC deployment activities with an emphasis on land-based distribution networks. The Angle-DC project is outlined and discussed followed by a summary of the back-to-back ‘Flexible Power Link’ installed by Western Power Distribution. The multi-terminal MVDC campus demonstration project at Rheinisch-Westfälische Technische Hochschule (RWTH) University Aachen, Germany is also highlighted.

4.4.1 Angle-DC – SP Energy Networks

The UK energy regulator, OFGEM, via their Network Innovation Competition (NIC) awarded funding to the DNO SP Energy Networks to develop and deliver an MVDC demonstration project - Angle-DC [188]. The project budget of £14.8 million is being used for the design and installation of a 3 km MVDC link which connects two adjacent network sections, with the aim of increasing the export capability of the area thus allowing greater penetration of distributed renewable generation [188] [230] - Figure 4-5. The two areas which the link interconnects are identified as already having high levels of installed distributed generation with significant load and generation growth predicted. At the same time, the surrounding 33 kV network is understood to be operating close to design limits in terms of thermal capacity. To facilitate control of power flows and voltages at either end of the link, MVDC was selected as the candidate technology.

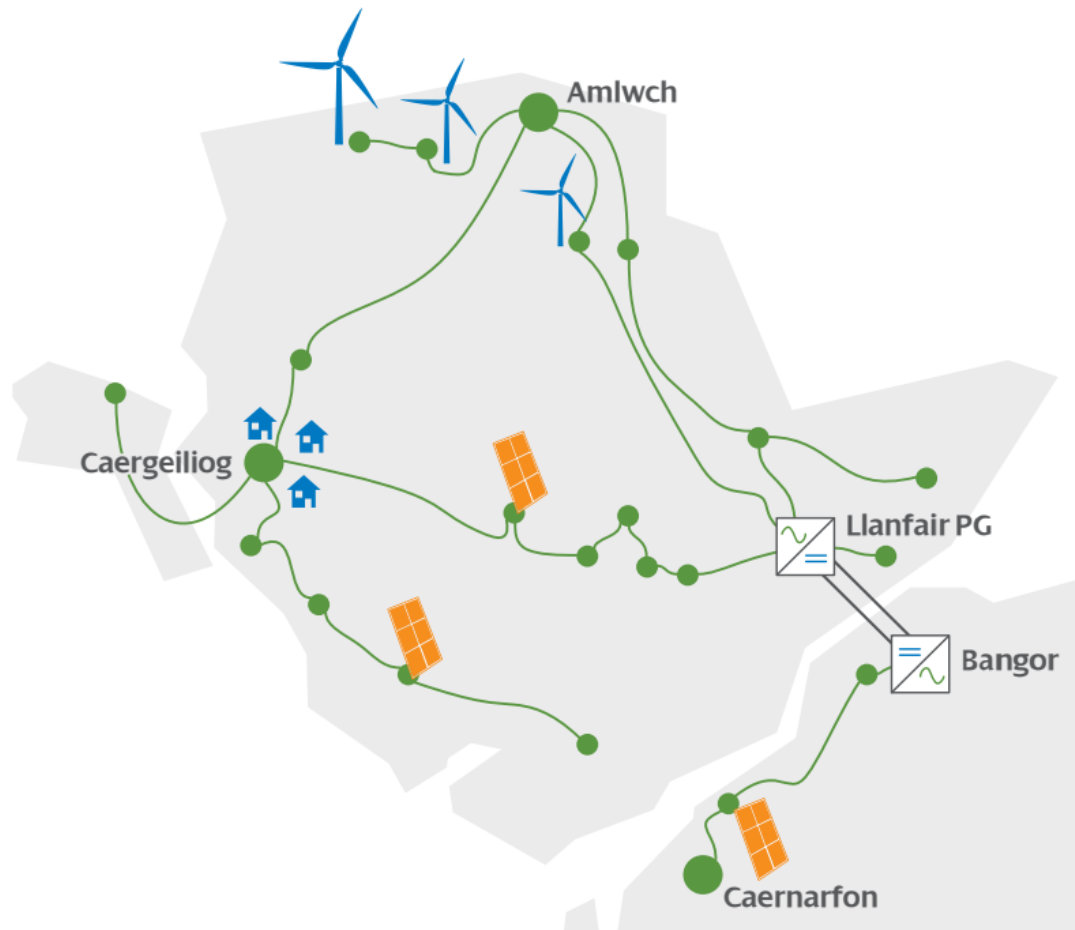


Figure 4-5: Illustration of Angle-DC geographic topology [185]

The scheme, under-construction at the time of writing in early-2020, has a bipolar topology operating at a DC voltage of ± 27 kV with a transfer capacity of approximately 35 MW [231]. The installation will use existing AC-wayleaves and will repurpose AC conductor assets to DC. The selected voltage rating ensures that the insulation coordination of the existing AC assets is not breached when converting to DC operation. One DC pole is formed by combining all the AC conductors in one of the supply circuits. The other DC pole is formed by doing likewise with the second 3-wire circuit, as outlined in Figure 4-6. Since the two poles of the DC link take geographically different routes, the likelihood of pole-to-pole faults is essentially eliminated. With significant research examining the repurposing of three and four conductor AC circuits to DC [232] [233] [234], it is perhaps disappointing that this approach was not investigated. The technical specification for the project states that the resistance of the two DC poles may be different, however these values are not quantified [235]. The circuits are predominantly cable with small overhead sections to allow for transient faults to be experienced and examined [235]. The DNO was permitted by OFGEM to install an additional AC circuit in parallel with the link to help de-risk the solution - Figure 4-7. This circuit is to

provide backup should the MVDC link be removed from service as part of either a planned or forced outage – otherwise, it will remain de-energised while the DC link is in operation [185].

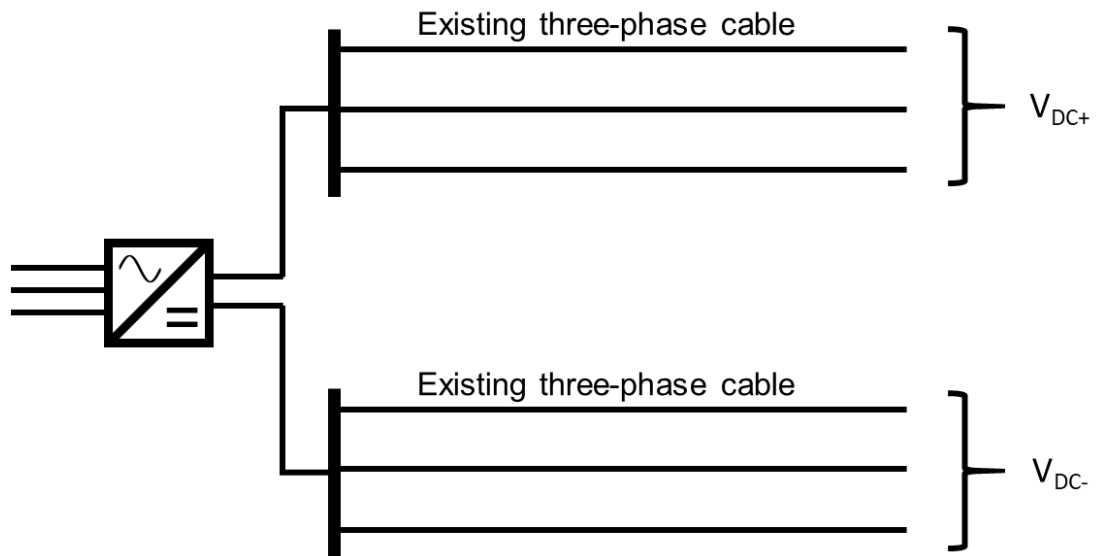


Figure 4-6: Angle-DC two three-wire AC circuits converted to two-pole DC system

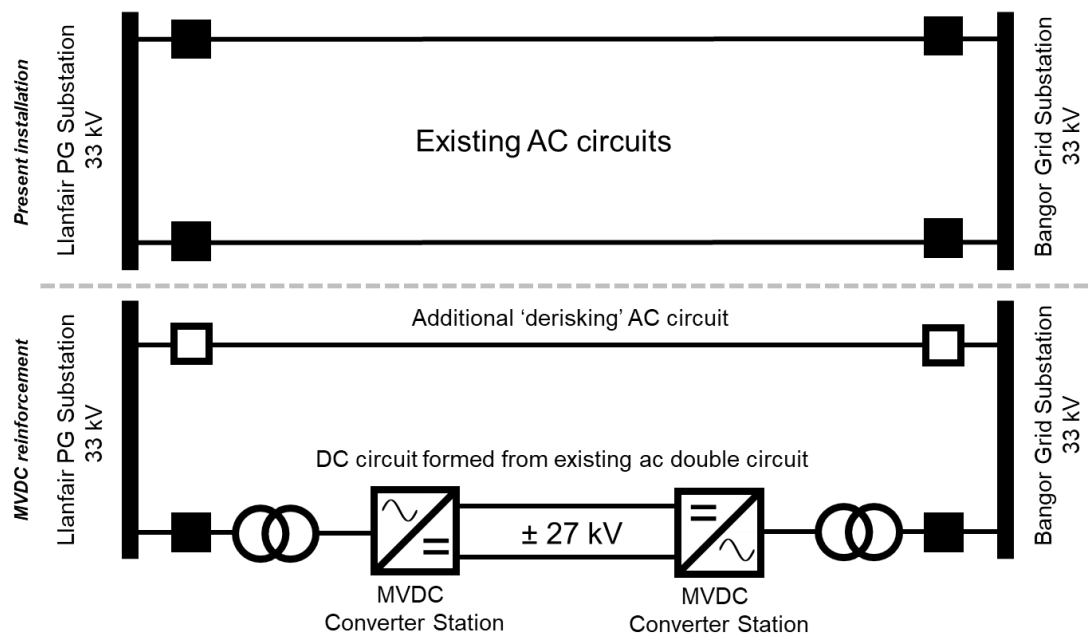


Figure 4-7: Angle-DC electrical topology

Each AC-DC substation is based upon twelve cascaded three-level neutral point clamped (NPC) converters as outlined in the simplified topology diagram in Figure 4-8. Cascading of these NPC converters essentially forms a simple multi-level arrangement but with the benefit of using readily available three-level machine drives. Three-level NPC converters can produce

a positive, negative and zero DC-side voltage. The converters deployed in the system are based on GE's MV7000 series machine drive architecture (specifically the MV7306-3) [236]. Each 'mini-converter' or module connects to a 2.1 kV AC supply derived from a specially designed multi-winding transformer. The DC voltage produced by each module is 4.5 kV ($4.5 \text{ kV} \times 12 \text{ modules} = 54 \text{ kV} \Rightarrow \pm 27 \text{ kV}$ bipole) with each having a power rating of 2.85 MVA [13].

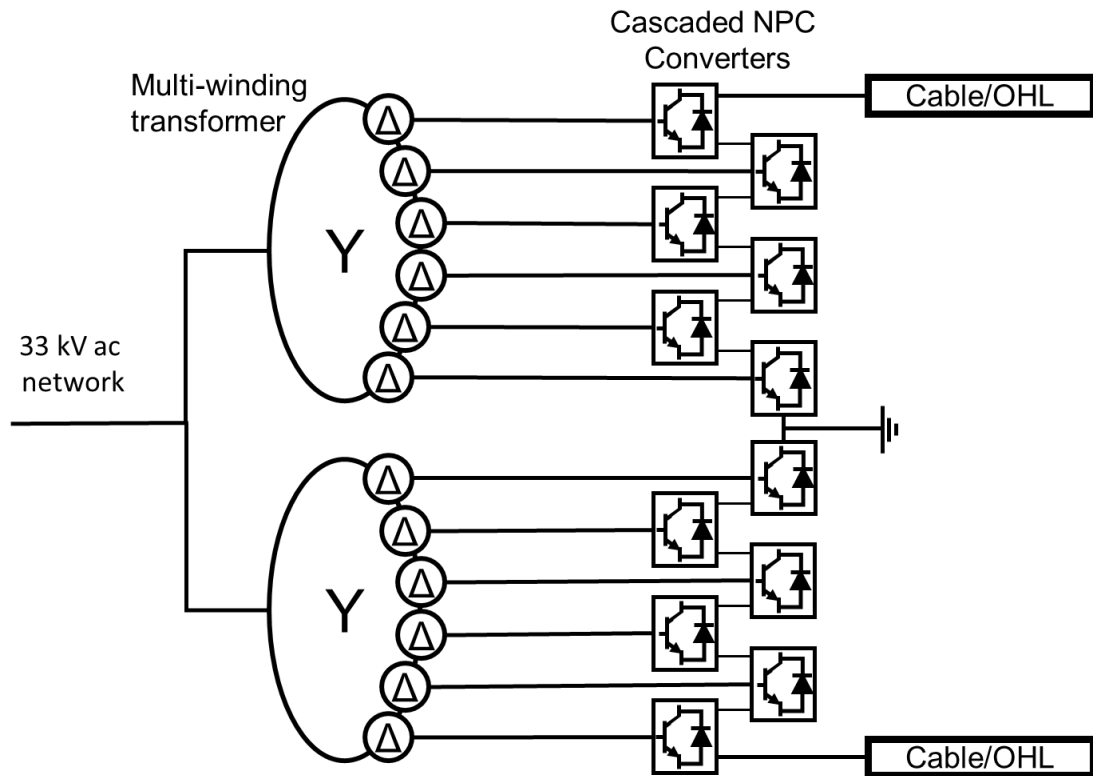


Figure 4-8: Angle-DC simplified station topology

Initial estimates by the network operator suggest that a 20% reduction in losses is to be expected upon successful energisation representing a £630k saving per annum [188]. SP Energy Networks claims that it has identified a further 30 sites where the technology could be applied within its network, however, a list of these locations has not been published. SP Energy Networks hope to move the technology readiness level of such a solution from stage five towards stage eight during this trial period. TRL is a metric where level one represents the fundamental basics/principles stages of a technology and level nine represents a technology being a business as usual solution [237]. TRL assesses how technically ready a solution is for deployment and the commercial availability of the solution [238].

While technology readiness level of the solution by the end of the project is expected to be high, especially considering commercial maturity of the machine drives being employed, at a

project budget of £14.8m (each kilowatt of transfer capacity essentially costs £423) the technology performance level (TPL) requires some improvement to reduce the installed cost of MVDC solutions, as SP Energy Networks acknowledges. TPL is defined as how well a technology performs and its economic ability to gain a market presence [238]. According to the Angle-DC funding proposal, the uptake of embedded MVDC depends largely on the cost of power electronics. SP Energy Networks estimates that the price of these devices will drop by up to 55% between now and 2040 [8] - it is unclear if this figure considers inflation.

The control of the Angle-DC link is discussed in [239]. This paper outlines a three-level control hierarchy for operating during a loss of communications. The paper recommends a series of active power setpoints for various levels of communication availability, however the paper does not discuss the detailed control of the DC link.

Initial design challenges surrounding the project are highlighted in [231]. These include the derating of the system during a permanent fault and the electromagnetic compatibility with adjacent rail signalling infrastructure. The paper proposes that during a permanent fault of one of the six conductors which form the two DC poles, the complimentary conductor on the 'healthy' pole should also be removed via mechanical isolation. The power rating of the link is reduced to 67% of the rated power until the fault is repaired [235]. This approach is illustrated in Figure 4-9.

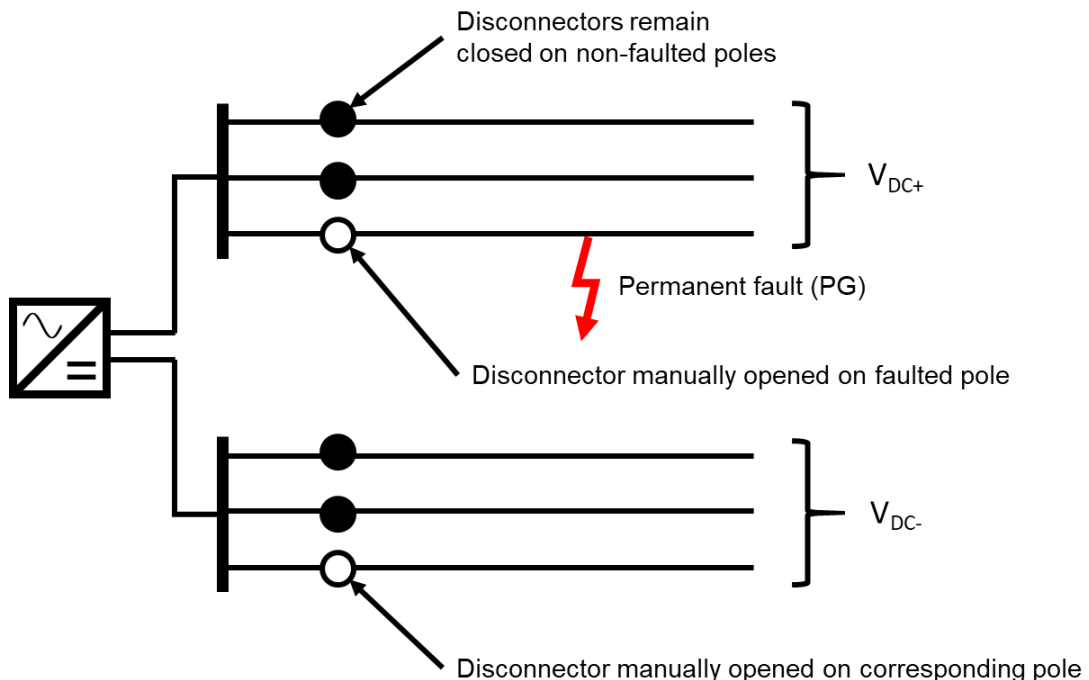


Figure 4-9: Angle DC circuit reconfiguration under permanent pole-ground fault

The electromagnetic compatibility of MVDC systems is considered as part of the project as both the DC poles of the link run in parallel with rail signalling infrastructure [231]. The rail operator (Network Rail) had raised concerns that the magnetic fields created by the DC link could cause signal cabling and track-side equipment to operate incorrectly. The results from the electromagnetic compatibility (EMC) studies before and after the energisation of the MVDC link have not yet been published.

As mentioned previously, the likelihood of pole-to-pole faults has been minimised as each pole of the DC link takes a physically different geographic route. It may be hypothesised that pole-to-ground faults on the DC link are detected by measuring a current flow in the ground return path of the converters. However, there is no specific mention of protection techniques in published Angle-DC literature for primary or backup protection.

4.4.2 Flexible Power Link – Western Power Distribution

While the Angle-DC project is to deploy a DC link over 3 km, the Flexible Power Link (FPL) project will trial the use of a controlled back-to-back (i.e. AC-DC-AC) converter in the confines of a distribution substation with the primary aim of improving voltage regulation in the network [189]. The project is led by Western Power Distribution (WPD) which is the DNO in the UK responsible for the Midlands, South-West England and Wales region. The FPL project is part of a wider £13.1 million, regulator funded, Network Equilibrium project which aims to investigate the role of improved voltage control within distribution networks to increase penetration of low carbon technologies.

The FPL consists of a 20 MVA (5 MVA_r) back-to-back VSC converter which connects across a NOP between two different 33 kV distribution network areas as presented in Figure 4-10. In the project application, submitted to OFGEM, WPD states that it is unable to operate the network with the NOP closed primarily due to concerns surrounding raising fault level which may result in switchgear operating above rated interrupting capacities [240].

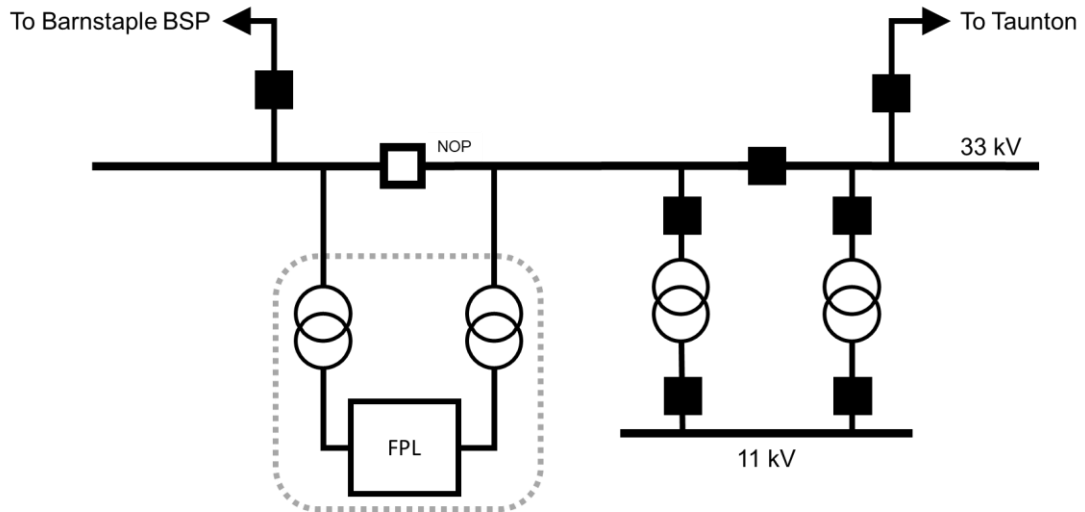


Figure 4-10: FPL network topology [241]

The FPL is interfaced to the distribution network via two 33 kV (Δ):3.25 kV (Y) /3.25 kV (Δ) (Dy11d0) three-winding transformers where each transformer connects to a different side of the NOP. Figure 4-11 displays an overview of the electrical topology for the FPL. The nominal DC-side voltage of the system is ± 2.5 kV. The power electronic switching technology selected for the FPL is the IGCT (Integrated Gate-Commutated Thyristor). When compared to the more common IGBT, the IGBT generates lower losses in applications where the converter is operating at part loading or in strongly fluctuating control conditions [242] (e.g. wind power parks, DC links where power transfer changes regularly). IGCTs are therefore more suited for applications where power transfers are more predictable and consistent in nature.

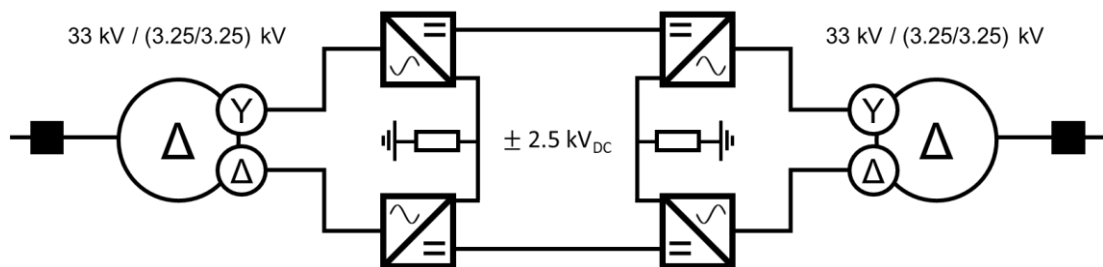


Figure 4-11: Simplified FPL electrical topology

WPD anticipates that the link will have the potential to unlock 36 MW of latent grid capacity, for DG connections via active power flow and voltage management at either side of the back-to-back link, however initial results from the study suggest that the link has only released 20 MVA of capacity to date [243]. (The concept of using controllable MVDC links to increase the ability of a network to host DG is demonstrated in the Appendix section). As with Angle-

DC, the project employs adapted, commercially available technologies. In this case, the AC/DC interface technology is based upon flexible AC transmission system (FACTS) devices produced by ABB [240], specifically the PCS6000 series converter.

The FPL device is a containerised solution (Figure 4-12) which allows for offsite construction and therefore reduced installation time in the substation environment. Additionally, the containerised approach allows the FPL to be easily moved to another site should network conditions change. The budget cost to deliver the FPL was £6.95 million and therefore represents an implementation cost of £348 per installed kilowatt of transfer capacity. The difference of £75 per installed kilowatt between Angle-DC and FPL is assumed to be because of the following reasons,

- the reduced voltage rating of the FPL decreases the insulation requirement of equipment (since the DC link in the FPL is very short, essentially a bus bar, ohmic losses are low and therefore there is no need to increase system voltage);
- civil infrastructure is only required at one site whereas the Angle-DC implementation requires a duplication of groundworks at both substation sites;
- the cooling solution can be shared between converters rather than designing and installing two ventilation and cooling systems as in the case in Angle-DC;
- the containerised nature of the FPL allows for offsite construction and testing (a project report estimated that this alone saved £150,000 [244]);
- reduced transformer complexity of the FPL solution; and
- additional de-risking AC assets were installed under the Angle-DC deployment which were not required in the FPL trial.



Figure 4-12: Crane installation of FPL container at WPD’s Exebridge substation [245]

Three papers have been published on the FPL link. The first publication [246] presents the steady-state modelling of the FPL device but does not consider system protection. [247] states that the FPL “has a local control and protection system” – no specific details of the scheme are provided. The only mention of backup protection of the FPL is made in [248]. This paper states that overcurrent, ground fault and busbar protection relays were installed on the AC terminals of the FPL, however, no setting guidance is provided for the relays. This backup scheme is designed to detect faults on the converter equipment, including the DC system, and disconnect the link in less than 100 ms. These backup protection relays are connected to the FPL’s CBs and leaves the device open to damage should this CB fail. A DTT scheme was therefore implemented to protect against this scenario however specific details of the implementation of this could not be found in the available literature.

It is worth highlighting that since the FPL is a back-to-back converter and is installed within a containerised structure the likelihood of a DC fault occurring is reduced as the DC system is protected from external environmental hazards.

4.4.3 DC Campus – FEN Campus RWTH Aachen

While Angle-DC and the Flexible Power Link both represent projects where MVDC technologies are embedded within distribution networks, they only consider the application of point-to-point links rather than a wider MVDC system with multiple sources of demand, generation and storage. Papers published in 2012 present the detailed design of an MVDC

network at the Melaten Nord Campus of RWTH Aachen University, Germany. The proposed system consists of five terminals operating at a voltage of 10 kV (configured as a bipolar ± 5 kV system) with the power ratings of converters ranging between 1 – 5.5 MW [182] [249] [250]. Figure 4-13 and Figure 4-14 present the system topology and electrical single line diagram of the proposed installation. The all-cable network is to operate as a private grid within the existing campus electrical network and will distribute energy between several large-scale laboratories.

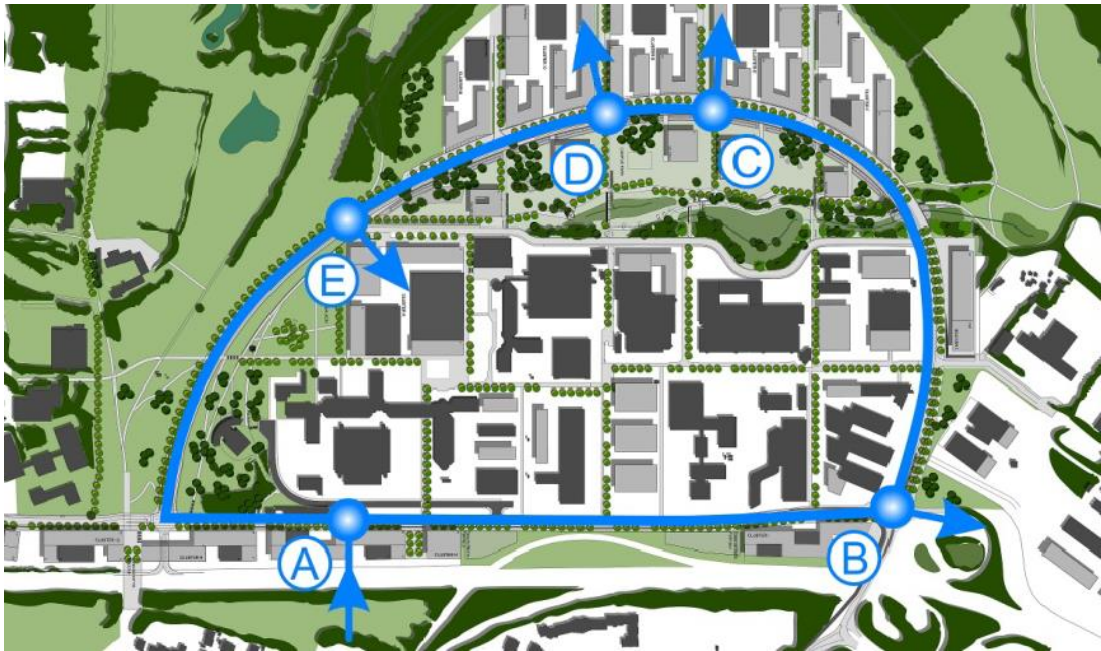


Figure 4-13: Proposed RWTH Aachen MVDC topology [249]

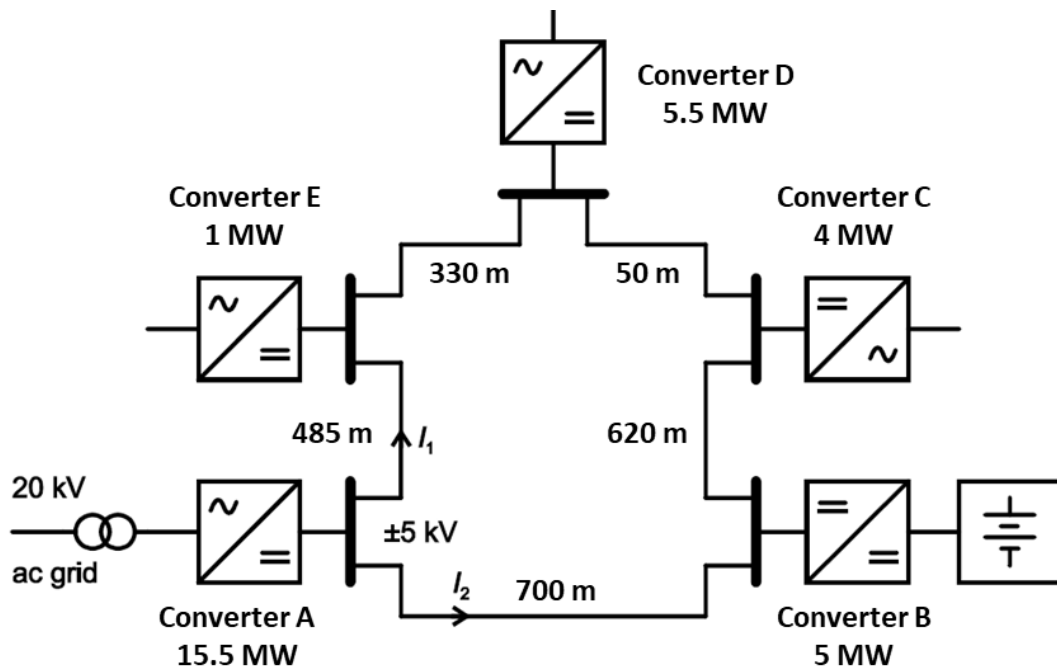


Figure 4-14: Proposed RWTH Aachen MVDC electrical topology [249]

As part of this project, the team within RWTH Aachen have developed a medium-voltage DC-DC dual active bridge (DAB) converter. A DAB, essentially a DC transformer (albeit a significantly more complex system than a conventional AC transformer), allows two DC systems which operate at different voltage levels to be interfaced. This is achieved by converting the DC voltage to high frequency AC via a standard H-bridge arrangement. This voltage is stepped up/down via a high frequency AC transformer and then converted back to DC using another H-bridge as outlined in Figure 4-15 [251]. The use of the high frequency intermediate step allows the transformer to be more compact, lighter and more affordable as less material is required than a similarly rated conversion at 50 Hz [252].

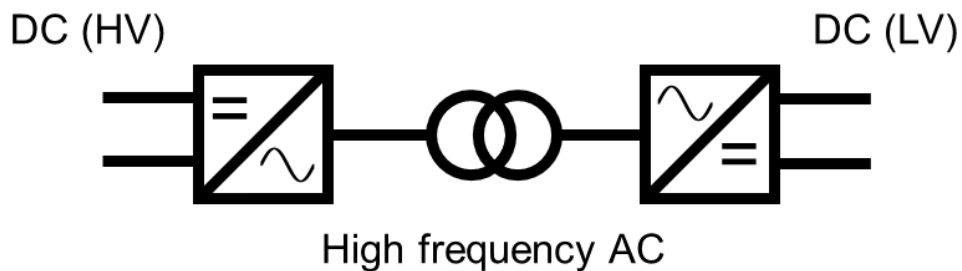


Figure 4-15: Dual active bridge conversion stages

The installation of the MVDC campus network, initially a three-terminal scheme which incorporates the DAB, commenced in late March 2018. The final system is to span 2.3 km

with a capacity of 6.2 MW. A press release from late-2019 reports that the MVDC campus research grid had been energised and is now in active operation [253].

No information about the performance of the system has been published at the time of writing due to the early stages of operation. Few details relating to the physical implementation and the technical design of the installed project are currently available in the literature.

4.5 Summary

This chapter has provided an overview of literature and demonstration projects relating to MVDC technologies. It has been shown that MVDC systems are well established in some areas (in particular, for marine applications); however, the technology is relatively unexplored in the context of utility-scale power distribution.

A review of published conference proceedings, journal papers and patents has shown that MVDC technologies are of interest from both academic and industrial perspectives. The role of MVDC is currently being investigated for use within distribution networks including Angle-DC, Flexible Power Link and the MVDC campus project at RWTH Aachen. These three projects represent different types of MVDC installation: back-to-back, point-to-point and a multi-terminal network. These trials are all under development and therefore conclusions from these demonstration projects have not yet been drawn - however it is clear from more recent funding awards that DSOs in GB are increasingly interested in exploring the operational aspects of introducing DC technologies onto their networks [7] [254].

Appendix A (at the end of the thesis) presents several load flow studies conducted by the author on two Scottish distribution networks showing the benefits of introducing MVDC links (both back-to-back and point-to-point) to increase the potential for adoption of low carbon generation and demand technologies.

Published literature on deployed MVDC systems does not fully present the methods by which the converters and DC system are protected. This is likely due to the control and protection systems being considered as specialist knowledge by equipment vendors and incorporated into products. Through the limited information available it has become apparent that protection, specifically backup, in hybrid AC-DC systems is not considered in appropriate detail.

DC faults have already been highlighted in Chapter 2 as being potentially damaging to VSC power electronic conversion systems. While primary protection and backup protection techniques exist at a converter station level, it appears that no consideration is made for the failure of station protection or circuit breakers from a remote protection perspective (as is the

case with AC power system protection where backup is provided both locally and on a network-wide basis). This deficiency could represent both a safety issue but also an unwanted and unpredictable operational expense associated with downtime and the repair of damaged equipment if a fault were allowed to persist due to local failure of all (main and backup) local protection systems. Literature does consider the impact of HVDC links on distance protection for AC faults however the response of these devices for DC events does not appear to have been explored or documented in significant detail.

The review of published material presented in this chapter has identified that MVDC is a topic of interest to facilitate future electricity networks with high penetrations of renewables, however, it can be concluded that a greater focus on the protection aspects of embedded MVDC links is required – particularly in the case of backup protection systems.

From the findings presented through this literature and technology review, the research question which forms the basis of this PhD is therefore clear, and as stated in the introductory elements of this thesis.

Chapter 5

A Fast-Acting Backup Protection System for Embedded MVDC Links

5.1 Introduction

For MVDC technologies to become more established in distribution networks, effective main and backup protection systems will be required for all elements of the network. In particular, the protection required to detect DC-side faults must be extremely fast acting [161] otherwise the power electronic devices are likely to be irreversibly damaged [150] [255]. Existing practice for the protection of point-to-point HVDC links involves sending a direct transfer trip to remote CBs in the event of a fault not being cleared by the converter station's local breakers. This relies on the converter control system detecting the fault and the communications system delivering the trip signal correctly to the remote CB, rather than depending on the direct measurement of electrical parameters at the remote CB. Detection of DC-side faults via remote AC measurements could potentially be more reliable, secure and cost-effective (and potentially more cyber-secure) than the DTT approach. Communication systems may also introduce a delay into the protection systems which might lead to unacceptably long clearance times [256].

Since the current available to supply DC-side faults is limited by the AC-DC converter, it is unlikely that remote overcurrent protection would provide a suitably fast backup to the converter's main protection and it may not even be able to be applied as the fault current may be no more (or even less depending on several factors – AC infeed, line length, converter capability, the position of fault on DC link, etc.) than nominal current. Additionally, time grading a remote overcurrent relay for these applications may prove to be challenging as at 33 kV overcurrent is already extensively used as a backup protection method (with tripping delay of up to three seconds [57]).

This chapter focuses on determining the apparent impedance measured by a remote AC-side distance protection relay during DC-side faults. A detailed summary of distance protection has

been provided in Chapter 3. To summarise, a distance protection relay calculates the apparent impedance associated with a system event via measurement of current and voltage. From known system parameters (e.g. line impedances), operational zones can be created, each with a different tripping time specified, to allow for both main and backup protection functionality.

Following a study of the system impedance during various fault events, this chapter presents a novel method to provide fast-acting, remote backup protection, with no requirement for communications, for DC pole-to-pole and pole-pole-ground events should the primary protection scheme of an MVDC link fail to detect or respond to a DC event.

5.2 Study Methodology

The study methodology employs a series of simulation platforms and steps which are outlined in the following subsections. Due to the nature of power system faults and the behaviour of power electronic converters during such events, it is necessary to develop a full switching model of an MVDC link - rather than a simplified converter model. The implementation of a 10 km MVDC link is initially discussed in Section 5.2.1 with the associated control approach (which is active during steady state, non-fault conditions) outlined in Section 5.2.2. The fault management approach for the converter is introduced in Section 5.2.3 followed by a summary of the employed modelling procedure in Section 5.2.4.

5.2.1 Converter Topology

For the modelling reported in this chapter, a two-level symmetrical monopole VSC converter is employed for the following reasons:

- VSC offers significantly more controllability than LCC;
- VSC links, when compared to LCC, perform better in weak grid environments [91];
- two-level VSC has a reduced control requirement when compared to more complex MMC structures; and
- more advanced topologies look very similar under fault conditions to a two-level converter as demonstrated in Figure 5-1 for a HB-MMC.

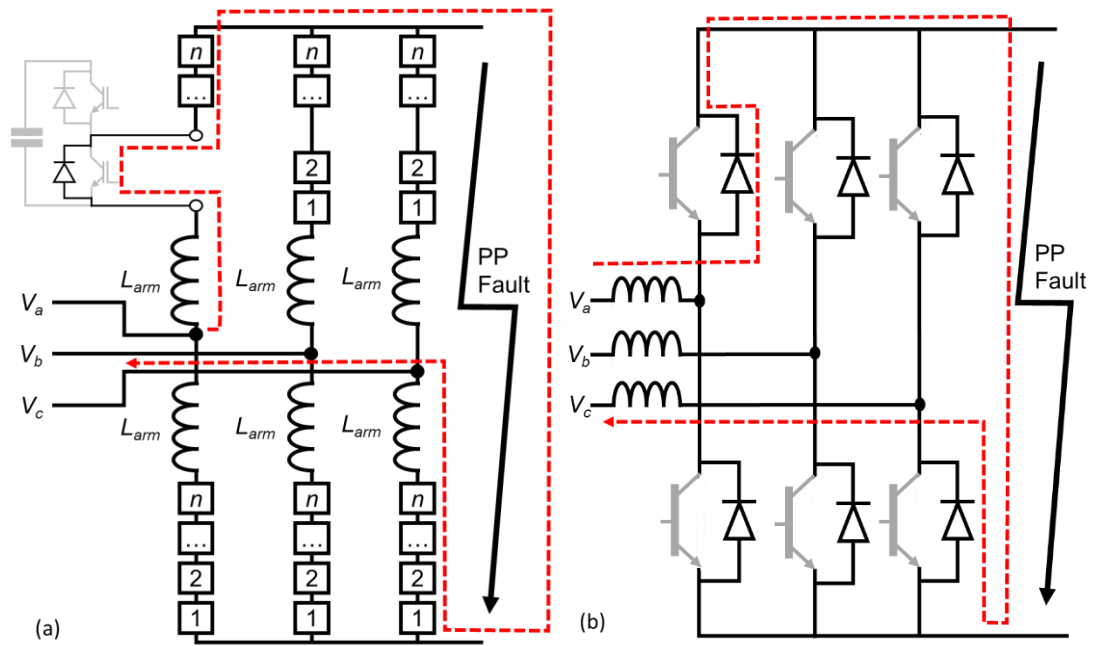


Figure 5-1: Comparison of the uncontrolled fault path through IGBT diodes for a (a) HB-MMC and (b) a standard 2-level converter [150]

5.2.2 Control Structure

Literature extensively covers the general control structure for VSC converters for generation, HVDC and machine drive applications [257] [258]. Figure 5-2 presents a control overview diagram for the modelled MVDC link. The converter control deploys a standard inner current control approach as outlined in Figure 5-3 where the inner controller takes direct-quadrature (d - q) reference frame current setpoints (a setpoint being represented by * in diagrams) from the outer loop controllers presented in Figure 5-4 [258].

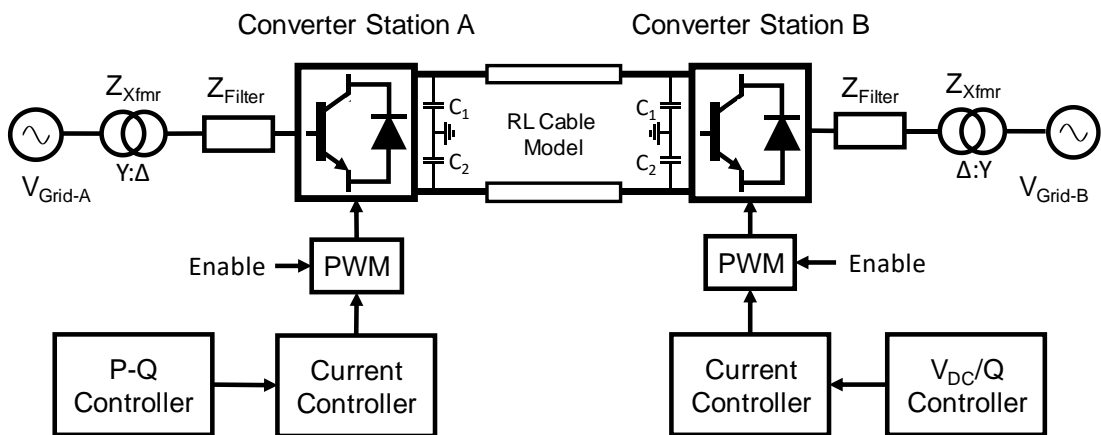


Figure 5-2: MVDC link control topology

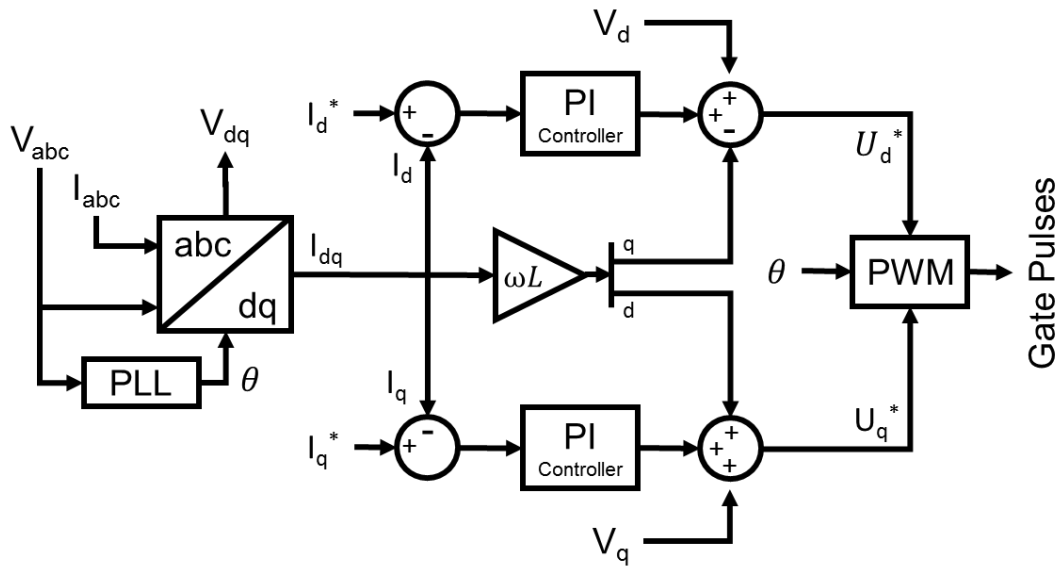


Figure 5-3: Standard inner current control loop

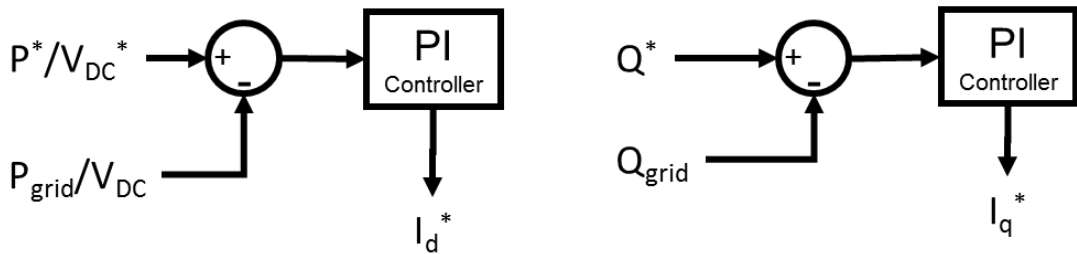


Figure 5-4: Outer loop controllers

Using the outer control loops, Converter Station A is set to maintain a real and reactive power (P - Q) reference, while Converter Station B regulates the DC-side voltage (V_{DC}) and reactive power (Q) under non-fault operating conditions [258]. This basic control strategy is commonly applied to HVDC links. In summary, if the power to be transmitted through the DC link is to be increased, Station A would request the new power setpoint. This increased power setpoint will result in a rise in DC-side voltage due to the charging of the DC cable capacitance and DC capacitor. Station B measures the increased DC voltage and increases the power exported to the V_{Grid-B} network to regulate the DC voltage to the desired setpoint.

Note that the operating control strategy described in this subsection is for pre-fault conditions and is only used to create a pre-fault power transfer across the DC link. When a fault occurs on the DC link the converter controller transits to a fault protection mode.

5.2.3 Behaviour of Converters During Fault Conditions

5.2.3.1 AC Faults

At present, there is no obligation for an MVDC links to provide fault current for AC-side faults as there are no requirements in the GB distribution code imposed on DNOs for such a technology [259].

For AC faults modelled in this thesis, it was assumed that the converter remains connected to the AC system but does not contribute any current during AC faults. It is recognised that significant fault infeed from a converter could influence relays' impedance measurements for AC faults, but given the fault level of the test network (500 MVA) and the power rating of the MVDC converter (35 MVA), the vast majority of fault infeed will be from the wider AC system with the MVDC link having negligible impact on distance protection zones.

5.2.3.2 DC Faults

Section 5.2.2 summarises the operation of the converter under steady-state operation, however the management of the converter during DC-side faults must also be considered. The fault conduction path of a two-level VSC converter is presented again in Figure 5-5 to aid discussion.

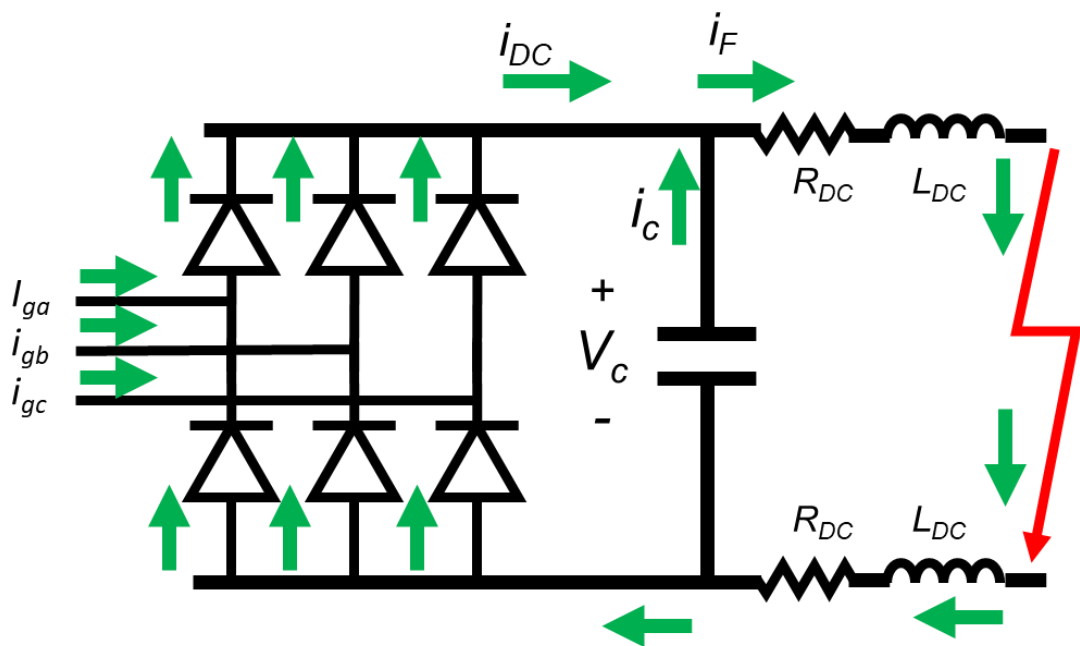


Figure 5-5: Example of the uncontrolled fault path within a VSC converter

While grid-connected converters can provide limited and controlled fault current contribution to AC-side faults via the converter's IGBTs [149], their performance during a DC fault is

effectively uncontrolled [148] [260] for most converter topologies and can only be overcome at the expense of significant power losses by employing full-bridge converter structures as highlighted in previously in Section 2.3.5 [167]. Faults on DC links are commonly detected by measuring a current which exceeds the rating of the converter flowing from the AC grid into the DC converter, the collapse of the DC system voltage or via an overcurrent at the DC terminals [261] [262]. Detection times are typically much less than 10 ms for point-to-point DC links [165] [263]. When a DC-side fault occurs on a DC link and is detected by the converter controller, the first step taken by the protection system is to block commutation of the switching devices by disabling the IGBT control signals. This prevents the power electronic devices being subjected to high fault currents which would only be limited by the AC system fault infeed capability and converter filter impedances [150]. The DC-side capacitors discharge forcing the freewheel diodes, placed across the IGBTs, into conduction as displayed in Figure 5-5. The converter essentially becomes an uncontrolled rectifier with current only being limited by the AC side impedance between the source and the converter [151].

Bypass devices (presented in Figure 5-6), often high capacity thyristors, with a lower on-state resistance than the freewheel diodes, may be installed in parallel with the IGBT/diode to provide a path for fault currents and to allow time for protection to operate [158] [159]. The AC-side CB of the converter should open to isolate current infeed to the link. This needs to happen quickly (typically in around 100 ms for HVDC applications) to protect the parallel diodes from overheating and potentially failing completely [264].

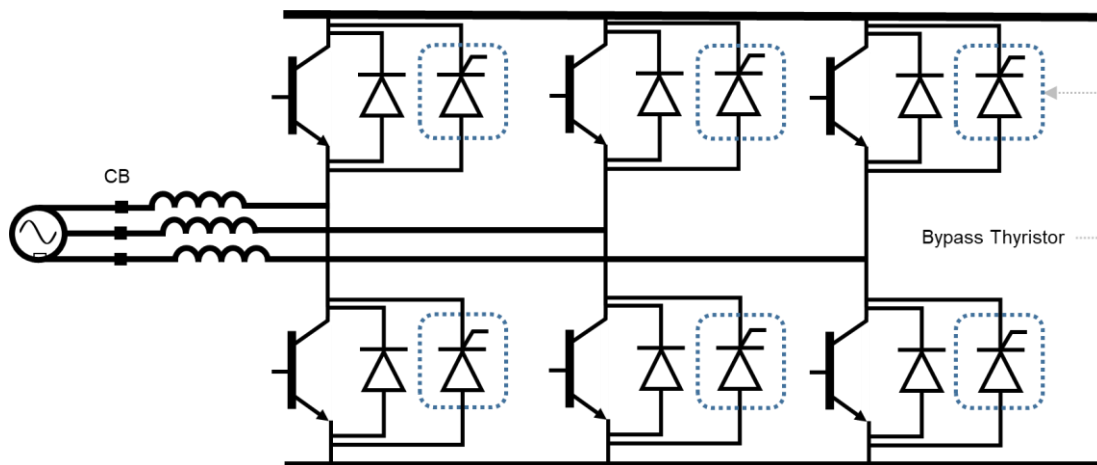


Figure 5-6: Bypass thyristors installed in parallel with IGBTs

For the modelling in this thesis it is assumed that the bypass thyristors are activated when the absolute value of instantaneous currents entering the converter is equal to or greater than the

user-definable current threshold (I_{max}). I_{max} is set as 110% of the rated converter current for the subsequent simulations. Should an overcurrent be detected on any phase, the bypass thyristors will be enabled to create a parallel conduction path across the IGBT diodes. The bypass thyristors and, now to a much lesser extent, the freewheel diodes will conduct fault current until the converter is isolated via AC-side breakers. Figure 5-7 presents an overview of the bypass controller.

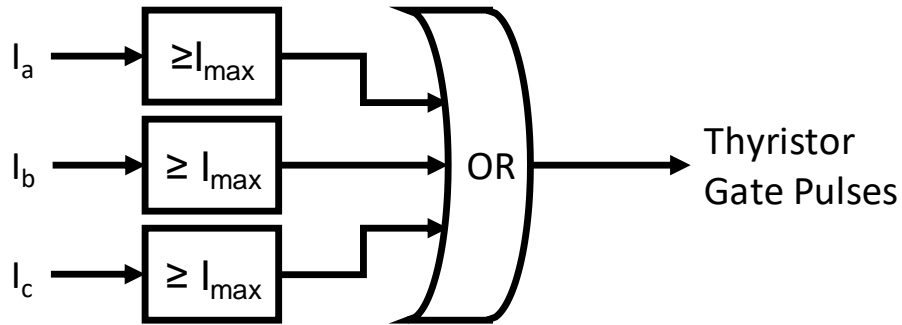


Figure 5-7: Overview of bypass thyristor controller

Should any of these steps fail (converter controller failure, trip signal failure, maloperation of AC-side CB), the converter could be left in a damaging (e.g. freewheel diodes are typically not rated for continuous operation) uncontrolled rectifying state as described.

The fault detection and isolation process for a converter can be summarised in Figure 5-8.

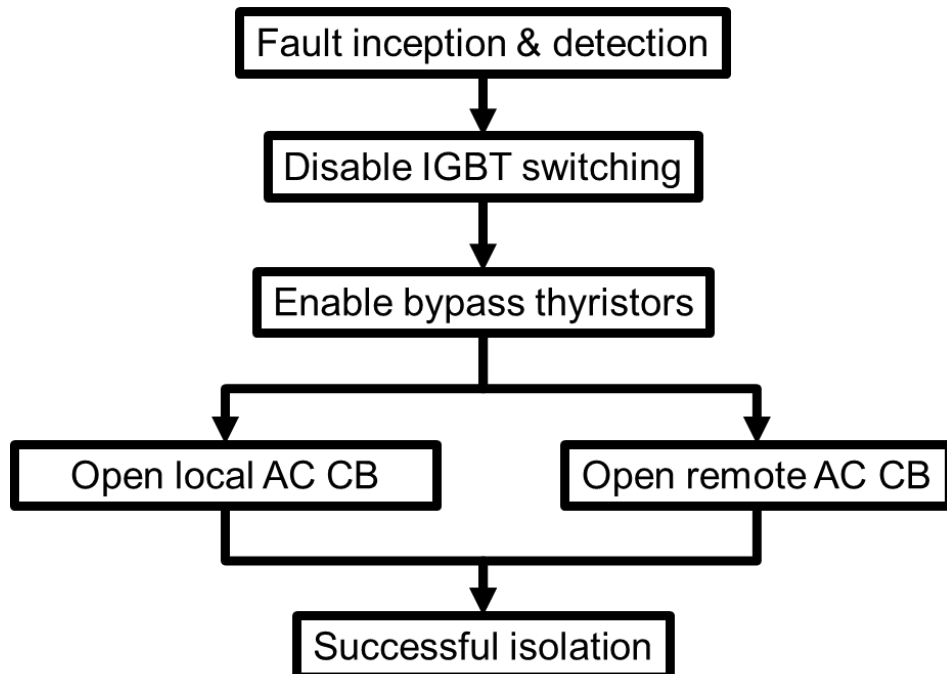


Figure 5-8: Summary of converter control actions during a fault upon the DC link

5.2.4 Modelling Procedure

A two-stage simulation process is employed to determine the apparent AC-side impedance during a DC-side fault. Sampled voltages and currents are generated via switching level software simulations of fault events. When a fault is detected, the converter behaves as outlined in Section 5.2.3. In summary, switching of the IGBTs would be blocked and the freewheeling diodes would conduct fault current until isolation via AC-side breakers. The generated voltage and current traces are then used as inputs into a distance protection relay simulator where the apparent impedance of events can be determined.

The Dynamic Protection Modelling Controller (DPMC) [265] software package is used to determine the impedance of the network during steady state and fault conditions. This software was developed to assist National Grid in the post-fault investigation of power system performance following various faults and events. The relay models within DPMC are based upon and validated against commercially available devices, and validation was carried out using secondary injection to ensure that actual relay versus DPMC performance matched for all tested cases studies. The software uses sampled three phase voltages and current values from either fault records or simulation along with a relay setting file as input. Tripping output (or not) and operating times of the relay are calculated according to the setting file logic and the modelled algorithms within the relay. In the case of distance protection studies, DPMC generates an R-X locus diagram for visual interrogation of how the apparent impedance evolves as the fault progresses. Figure 5-9 summarises the developed simulation approach.

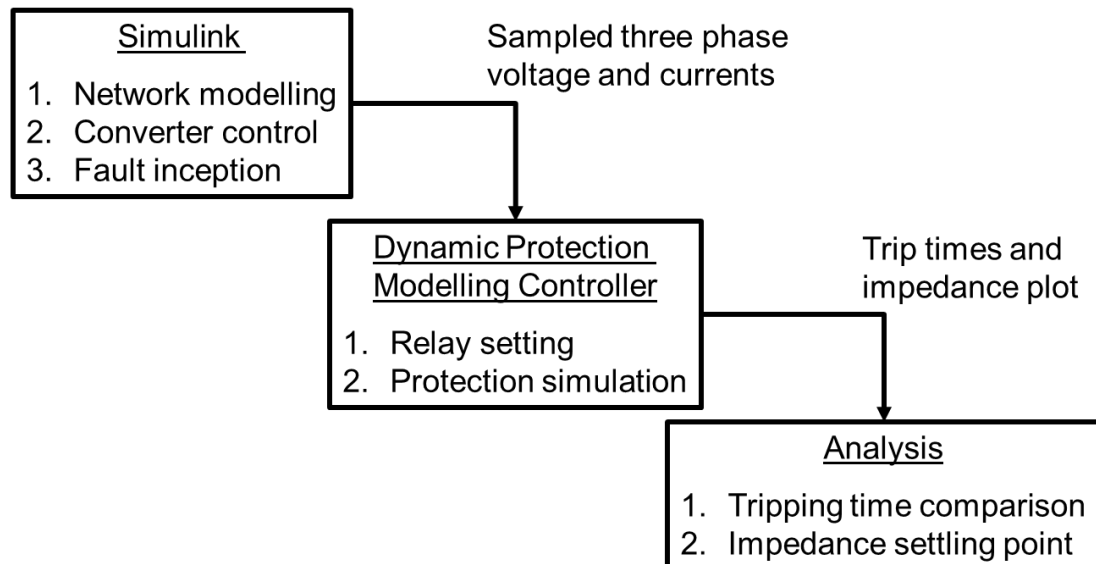


Figure 5-9: Simulation methodology

5.3 Case Study

In this section the apparent impedance, as measured at the relay location, for both AC- and DC-side faults will be determined. Section 5.3.1 introduces the test network and the parameters of the MVDC link. The protection settings for the distance relay are determined in Section 5.3.2 for standard AC zones of operation. The impedance measured by the relay for AC- and DC-side faults is presented in Section 5.3.3.

5.3.1 Test Network

The network section modelled is based upon an area of the 33 kV network in the South of Scotland where the benefits of introducing embedded MVDC links has been shown via simulation as outlined in the Appendix section [266]. The converter has a power rating of 35 MVA operating as a two-level symmetrical monopole with DC voltage (V_{DC}) of ± 27 kV, which is broadly equivalent to 33 kV rms line-line (53.9 kV peak-peak) voltage from an insulation perspective. The per-unit impedance of the converter filter is 10% with a wye-delta transformer of 20% impedance connected to the AC network which helps to limit fault currents during DC-side faults and improve power quality during normal operation. The base quantities of the modelled system are 33 kV and 35 MVA with the base impedance calculated as 31Ω . The test network used for modelling is presented in Figure 5-10 where the characteristic impedance of all lines is $(0.17 + j0.3) \Omega/\text{km}$ [56]. Key network and converter parameters used in the model are summarised in Table 5-1. AC conductors are modelled as lumped element R-L components while the DC cable is implemented as a single π -section with the shunt capacitance modelled via the DC capacitors [267].

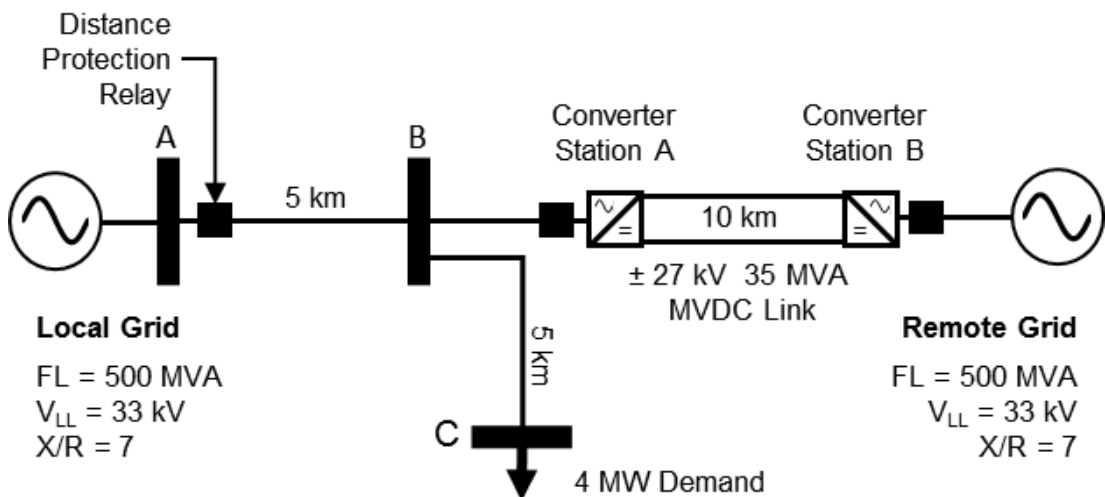


Figure 5-10: Test network

Table 5-1: Summary of modelled parameters [56]

Parameter	Value
Local & remote grid voltage (line-line)	33 kV
Local & remote grid X/R ratio	7
Local & remote grid fault level	500 MVA
A-B line length	5 km
B-C line length	5 km
MVDC line length	10 km
AC conductor impedance	(0.17 + j0.3) Ω/km (0.35 ∠ 60.5°) Ω/km
DC conductor resistance	0.17 Ω/km
DC conductor inductance	0.95 mH/km
MVDC link voltage	± 27 kV
MVDC link power rating	35 MW
DC link capacitor value (C1, C2)	1 mF [268]
Filter impedance (Z_{Filter})	10%
Transformer impedance (Z_{Xfmr})	20%
Transformer vector group	Yd11
Transformer rated power	35 MVA

5.3.2 Relay Setting Parameters

Relay settings are assigned in accordance with [136] [131]. Tripping delays are selected to ensure that fault clearance occurs inside of the maximum permissible clearance times outlined previously in Table 3-4. Key distance zone setting parameters are outlined in Table 5-2 (note that the impedances are referred to the primary circuit and therefore do not take CT nor VT ratios into account). In this example it was assumed that the MVDC link was constructed via the repurposing of existing AC conductors that connected between busbar B and the remote grid. The Z3 reach was therefore calculated via equation 5-1. In reality, it is likely that the reach of Z3 would be reduced to be 120% of the impedance of line AB and line BC.

$$Z3 = 120\% \times 0.35(5 + 10) = 6.3 \quad 5-1$$

Table 5-2: Summary of relay setting parameters

Parameter	Value
Mho Phase (°)	60.5
Z1 (Ω)	1.4
Z2 (Ω)	2.1
Z3 (Ω)	6.3
Z2 Fault Delay [phase & ground] (s)	0.3
Z3 Fault Delay [phase & ground] (s)	1.1

The angle (θ) of the mho characteristic is established by considering the ratio between the downstream line reactance and resistance as specified by equation 5-2 where X_{line} is the reactance of the protected line and R_{line} is the resistance.

$$\theta = \tan^{-1} \left(\frac{X_{line}}{R_{line}} \right) = \tan^{-1} \left(\frac{0.3}{0.17} \right) = 60.5^\circ \quad 5-2$$

5.3.3 Fault Impedance Analysis

The behaviour and performance of the distance protection relay is now be outlined, initially for AC-side faults (on lines A-B and B-C) and then for pole-to-pole-to-ground (PPG) DC-side fault. Faults on the remote AC-side system are not considered as any fault current provided by the MVDC link would be limited to the power rating of the converter which would essentially appear as the converter operating at maximum demand to the distance protection relay at busbar A.

5.3.3.1 Analysis of Distance Relay Settings and Fault Performance

To verify the correct setting of the distance protection relay for standard AC system faults (i.e. Z1, Z2 and Z3), six fault studies were conducted, covering a wide range of fault locations and types. Transient simulations were carried out using a model implemented in Matlab Simulink (SimPowerSystems). Faults are applied after the beginning of the simulation at 0.5 s in all cases.

Table 5-3 (where G indicates the detection of a fault to ground and P signifies a phase fault) presents which of the internal comparators of the distance protection relay leads to the tripping of the CB for each fault study. For the scenarios conducted the relay operates within the maximum clearance times specified previously.

Table 5-3: Simplified relay log for Z1, Z2, Z3 AC-side faults

Scenario		Time of Trip (s)	Tripping Element					
			Z1		Z2		Z3	
Fault Location	Fault Type		G	P	G	P	G	P
Line AB midpoint (Z1)	A-B-C-G	0.5144		◆				
Busbar B (Z2)	A-B-C-G	0.8229				◆		
Busbar C (Z3)	A-B-C-G	1.6221						◆
Line AB midpoint (Z1)	A-G	0.5178	◆					
Busbar B (Z2)	B-C	0.8183				◆		
Busbar C (Z3)	C-A-G	1.6254						◆

5.3.3.2 DC Side Fault Analysis

For PPG DC-side faults, it is assumed that the converter's AC-side CB at Station A fails to operate for the event, which therefore requires backup protection operation. Both Station A and Station B block commutation upon the initiation of the fault with the remote converter station disconnecting from the AC network within four AC cycles (80 ms). Fault inception is at 0.5 s and occurs at the midpoint (5 km) of the DC link. Faults at either end of the DC link are considered later.

Figure 5-11 and Figure 5-12 present the (primary referred) AC-side voltage and currents as measured at the distance relay in addition to the DC-side voltage and currents measured at Station A. In the simulation, converter initialisation occurs up to 0.15s, then a pre-fault transfer of 30 MW from converter A to B is established.

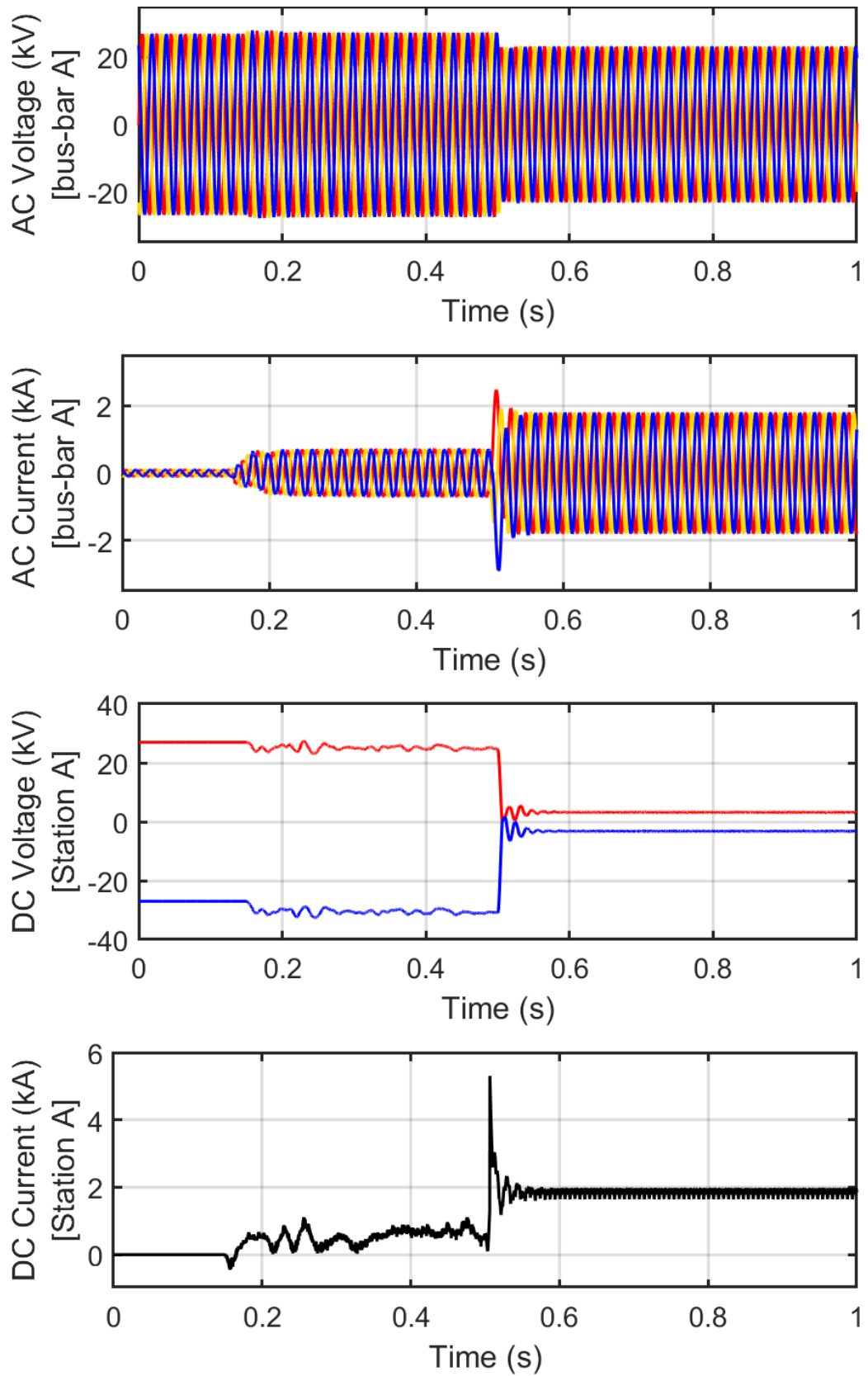


Figure 5-11: Voltage and current characteristics for AC and DC systems during PPG fault at the mid-point of the DC link

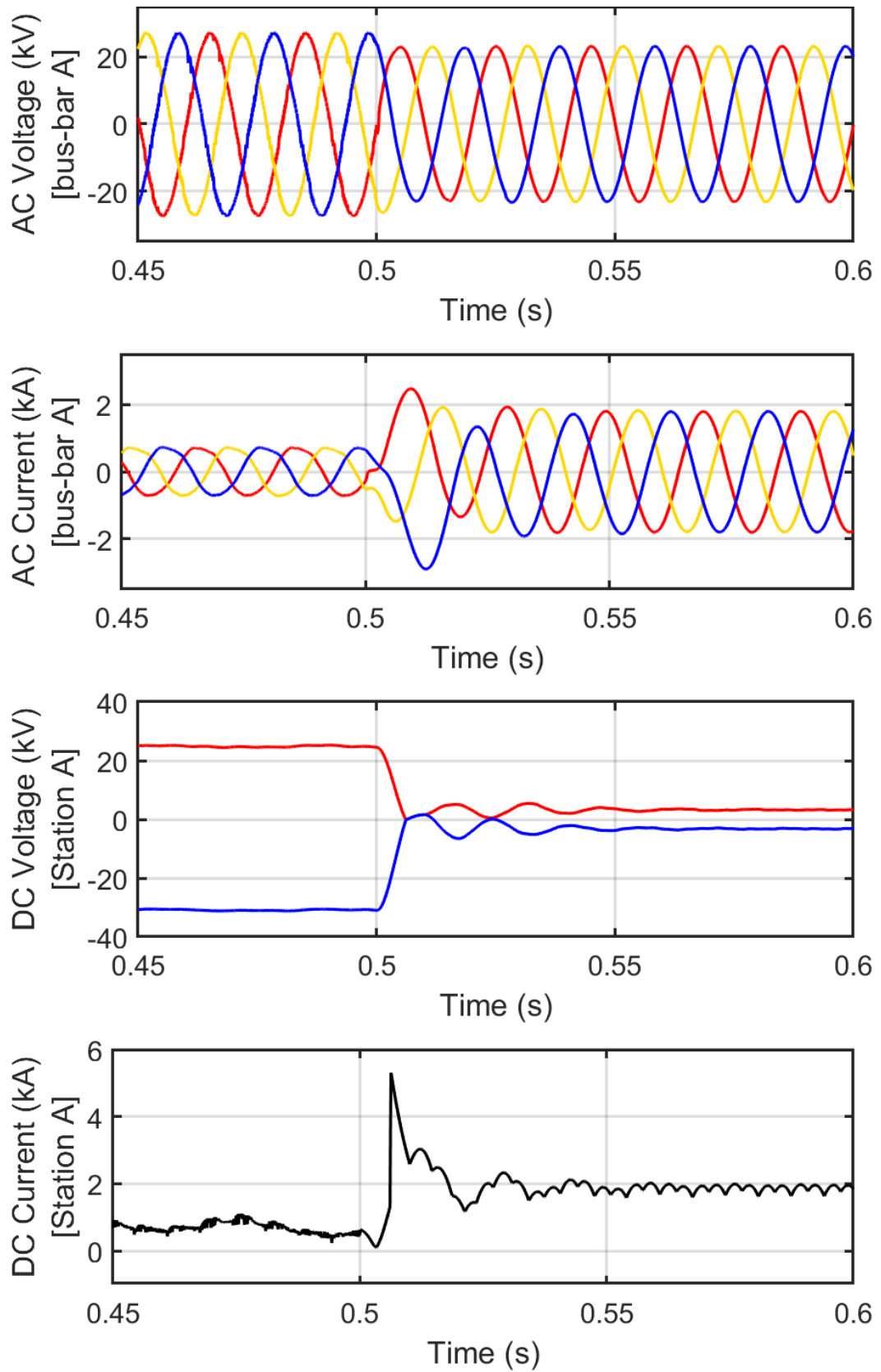


Figure 5-12: Voltage and current characteristics for AC and DC systems during PPG fault at the mid-point of the DC link (0.45 s to 0.6 s)

The impedance locus diagrams displayed in Figure 5-13 represent the time-varying impedances calculated by the distance protection relay during the fault at the midpoint of the DC link. Each subplot shows a different calculation of the impedance based on phase to phase and phase to ground measurements (i.e. A-G, B-G, C-G, A-B, B-C, C-A). These subplots also show the standard distance protection zones (i.e. Z1 - Z3) as outlined previously in Section 3.4.3. The “trails” represent the “history” of the calculated impedance over time starting from the time of fault inception – for example for AG, one can see that the measured impedance has “entered” from the right and transited (via an approximately circular loci) to its “steady state” – this evolution of measured impedance is due to the initial fault and the measurement algorithm (e.g. discrete Fourier transform etc.) within the relay stabilising during and after the initial transient/discontinuity in the measured voltages and currents. The impedance loci during the fault reside significantly outside the standard AC protection zones of the distance protection relay. The loci do however evolve towards a sustained value of approximately $(2.5 + j10.8) \Omega$ for a PPG fault.

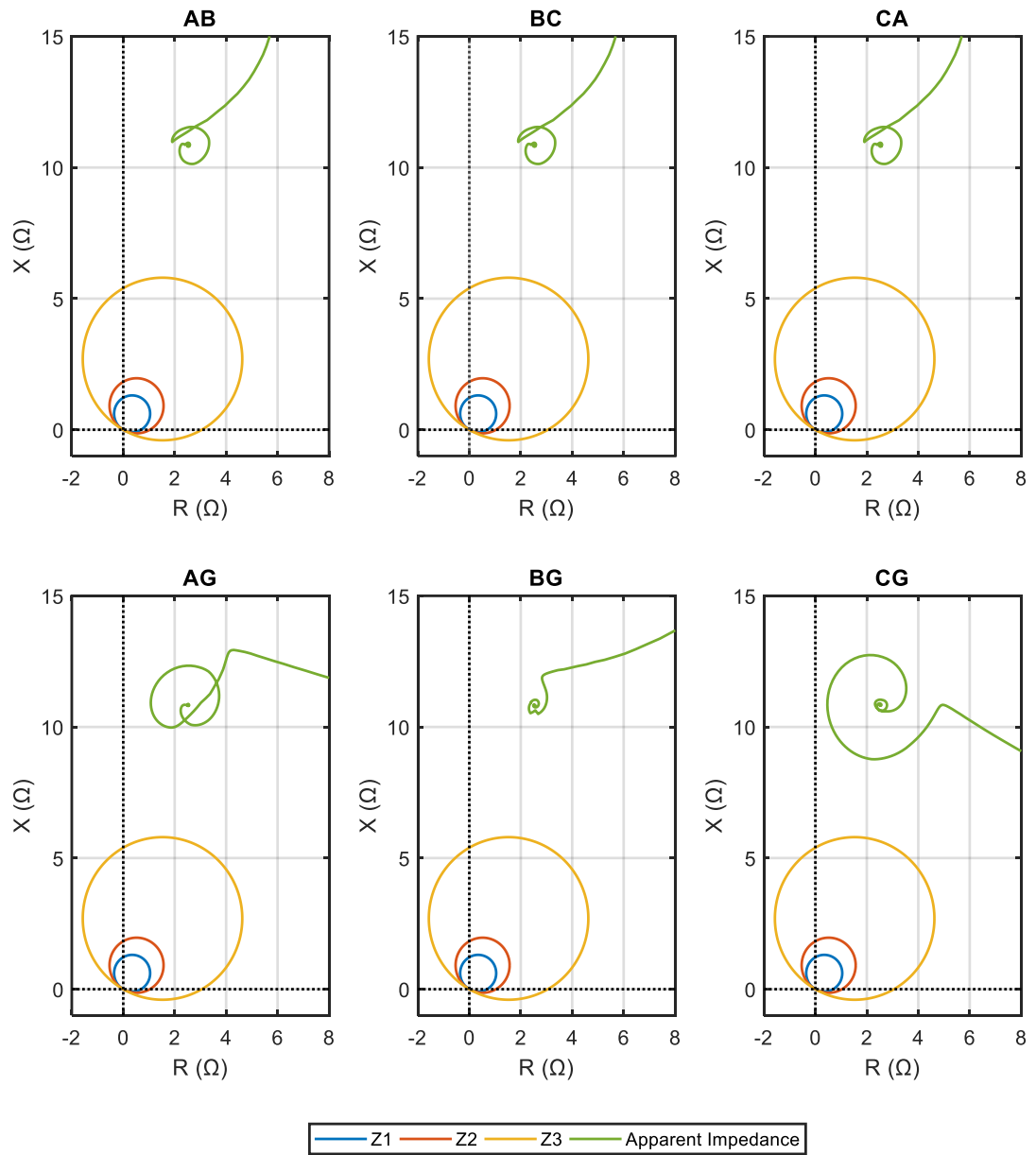


Figure 5-13: R-X diagram for a PPG fault at the midpoint (5km) of the DC link

5.4 Fast-Acting Backup Protection Function

5.4.1 Proposed Solution

The highly inductive nature of the fault outlined previously in Figure 5-13 creates a degree of certainty as to where the impedance loci of a DC-side PPG event settles. This settling point resides significantly outside of the resistive, load-serving, operational area during load conditions. The inductive nature of the fault is associated with the significant amounts of inductance (i.e. converter filter and converter transformer) placed between the distance protection relay and the converter. This highly inductive characteristic could allow a distance protection relay to detect DC-side PPG/PP faults and trip quickly, using appropriate logic, should primary protection fail.

As mentioned previously, conventional overcurrent protection is unlikely to provide reliable and fast backup disconnection as the current infeed to the fault is expected to be very low (again due to the significant impedance in the system). In the case of the simulated response for a PPG fault (Figure 5-11) this hypothesis is confirmed as the fault current is only approximately two times greater than load current with the DC link operating at maximum power export.

Many modern digital distance protection relays include customisable zones where the setting characteristics can be manipulated as per network requirements. It is hypothesised that a fast-trip quadrilateral characteristic, shown as zone 4 (Z4) in Figure 5-14 could potentially provide sufficiently quick backup protection to an embedded MVDC link for a DC-side PPG and PP faults.

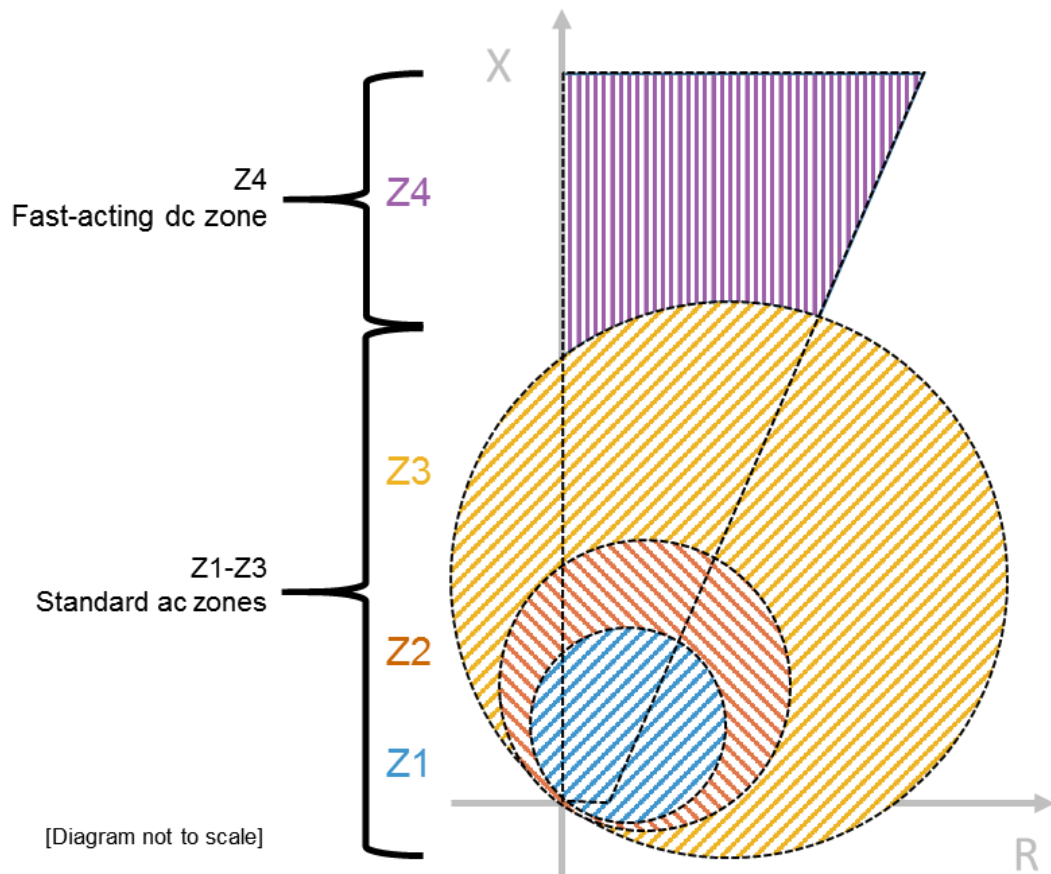


Figure 5-14: R-X diagram showing conventional Z1-Z3 tripping zones and fast-acting Z4 quadrilateral area for detection of DC-side faults.

For a DC-side fault, it is important that the relay only trips for the area outside of the Z3 Mho characteristic but within the bounds of the Z4 quadrilateral (the area shaded with purple vertical lines in Figure 5-14). Under conventional relay setting, this would not be an issue as the time grading (i.e. tripping delay) increases with the increasing zone number. However, for the solution proposed a fault detected in Z4 should react much more quickly than both Z2 and Z3. A fault which resides in either Z2 or Z3 but also within the quadrilateral Z4 characteristic should trip with the time delays associated with Z2 and Z3 to ensure correct discrimination. The logic tripping expression for the fast-acting Z4 area ($Z4_{TRIP}$) is therefore presented in equation 5-3. Note that since Z2 is a subset of Z3, a Z2 condition is not required in the tripping logic.

$$Z4_{TRIP} = \overline{Z3} \cdot Z4 \quad 5-3$$

From the R-X plots outlined previously (Figure 5-13), it is established that DC-side faults appear as symmetrical events to the distance relay for a PPG fault. With the majority of AC faults on the distribution system being non-symmetrical events [269], it is proposed that all Z4

comparators (i.e. AB, BC, CA, AG, BG, CG) must be active to permit the fast DC trip zone. Since it has been determined that balanced DC-side faults appear symmetrically across the comparators, the introduction of this additional check increases the certainty of a DC-side fault being detected and therefore a fast-trip should be issued. The stability of such a backup scheme is vital due to the wider geographical area and the larger number of customers liable to be disconnected should the Z4 scheme trip (but of course, this is required if there is a genuine uncleared fault on the DC link).

Figure 5-15 presents the impedance measured by the distance relay during a simulated power export of 35 MW (100%) from Converter Station A towards Converter Station B. The impedance lies significantly outside of the standard and fast-acting Z4 protection zones for the distance delay. As the loading on the link is reduced the measured impedance will increase and will not enter the Z4 protection area during steady-state operation.

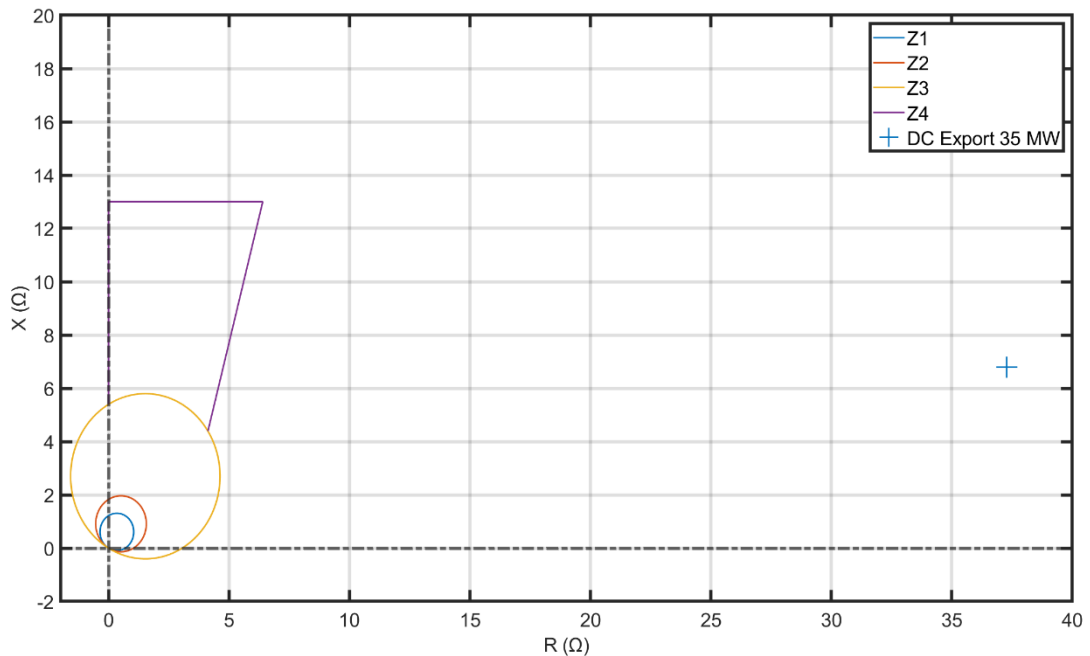


Figure 5-15: Impedance measured by the distance protection relay during 100% real power export from Converter Station A to Converter Station B

5.4.2 Relay Setting Parameters

The maximum (primary referred) resistance and reactance of the system, as measured by the distance protection relay, for a fault located at the remote end of a DC link is calculated via equations 5-4 and 5-5. A 20% grading margin is added to the apparent impedance to calculate the reach of Z4 ($Z4_{Reach}$) as in equation 5-6. This uncertainty allows for errors in line length and transducer error but also considers the nonlinearities associated with the AC to DC

conversion system such as those associated with the conduction ($i-v$) curve of power electronic devices.

$$R_{Z4} = \Sigma[R_{L_{ac}}, R_{X_{fmr}}, R_F, R_{L_{dc}}] \quad 5-4$$

$$X_{Z4} = \Sigma[X_{L_{ac}}, X_{X_{fmr}}, X_F] \quad 5-5$$

$$Z4_{reach} = 1.2 \times \sqrt{R_{Z4}^2 + X_{Z4}^2} \quad 5-6$$

R_{Z4} and X_{Z4} are the maximum expected resistance and reactance associated with a DC-side fault at busbar B, as measured at the relay location. $R_{L_{ac}}$ and $X_{L_{ac}}$ represent the resistance and reactance of the AC conductors between the distance relay and the converter's AC-side CB. $R_{L_{dc}}$ is the resistance of the DC conductors between converter Station A and Station B. R_F and X_F are the resistance and reactance of the AC filters at Station A. Finally, $R_{X_{fmr}}$ and $X_{X_{fmr}}$ are the resistance and reactance of the converter transformer. Note that the reactance of the DC line is not included in the calculation of X_{Z4} as there should be no AC component within a DC system and therefore no reactance.

The quadrilateral line setting angle for the solution employs equation 5-2 but using the resistance and reactance values determined by equations 5-4 and 5-5. The angle of the Z4 reach can be computed as per equation 5-7.

$$\theta = \tan^{-1}\left(\frac{X_{Z4}}{R_{Z4}}\right) \quad 5-7$$

For the network presented previously in Figure 5-10, setting parameters are calculated as follows. Note that the transformer winding resistance has been assumed to be negligible for these case studies.

$$R_{Z4} = [(0.17 \times 5) + 0.3 + (0.17 \times 10)] = 2.9 \Omega$$

$$X_{Z4} = [(0.3 \times 5) + 6.28 + 3.14] = 10.9 \Omega$$

$$Z4_{reach} = 1.2 \times \sqrt{2.9^2 + 10.9^2} = 1.2 \times 11.28 = 13.5 \Omega$$

$$\theta = \tan^{-1}\left(\frac{10.9}{2.9}\right) = 75.1^\circ$$

A summary of all the relay setting parameters is outlined in Table 5-4. A tripping delay of 100 ms is used for Z4 to provide time for the converter's main protection scheme to detect and block (assumed maximum 20 ms) and isolate the fault through opening the AC-side breaker

(assumed maximum 60 ms), with a discrimination margin of 20 ms (in effect, clearance would be after a further 80 ms or so due to circuit breaker action).

Table 5-4: Summary of relay setting parameters

Parameter	Value
Mho line angle (°)	60.5
Quadrilateral line angle (°)	75.1
Z1 reach(Ω)	1.4
Z2 reach (Ω)	2.1
Z3 reach (Ω)	6.3
Z4 reach (Ω)	13.5
Z4 resistive reach (Ω)	2.9
Z2 delay (s)	0.300
Z3 delay (s)	1.100
Z4 delay (s)	0.100

5.4.3 DC Fault Simulation Studies

To validate the relay setting configuration, a series of simulated PPG and PP events were applied at three locations on the DC line: at the terminals of converter A (0 km), the middle of the DC line (5 km) and at the terminals of converter B (10 km). Faults are applied at 0.5 s with a fault resistance of 0.1 Ω . The tripping times and associated detection zones for these DC-side faults are presented in Table 5-5. Figure 5-16 presents the associated R-X locus diagrams for a PPG fault at the midpoint of the DC link.

Table 5-5: Relay Log DC-Side Faults

Scenario		Time of Trip (s)	Tripping Zone			
Location	Fault Type		Z1	Z2	Z3	Z4
0 km	PPG	0.634				◆
5 km	PPG	0.637				◆
10 km	PPG	0.639				◆
0 km	PP	0.635				◆
5 km	PP	0.637				◆
10 km	PP	0.638				◆

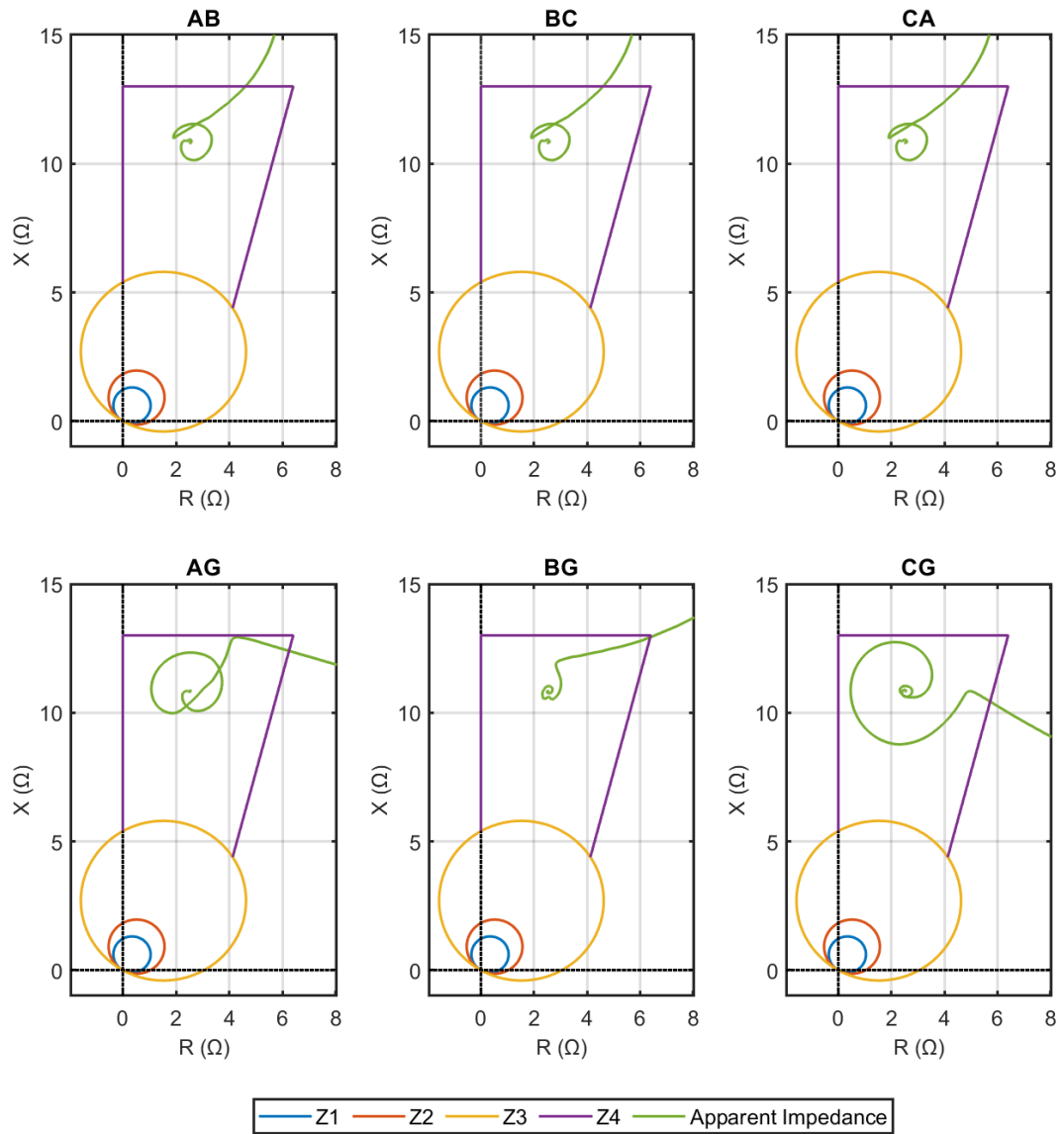


Figure 5-16: R-X diagram for a pole-to-pole-to-ground fault at DC link midpoint

It is observed from Figure 5-16 and Table 5-5 that the relay correctly identifies all PPG and PP faults with a maximum tripping time of 0.639 s, 0.139 s after fault inception in the case of the PPG fault at 10 km. This time incorporates the (user-configurable) 100 ms Z4 delay outlined previously to allow for grading with the embedded MVDC link's main converter protection scheme. Effectively, the relay detects the presence of the fault residing inside Z4 in 40 ms. The tripping time could potentially be shorter if desired, through specifying a shorter delay time.

The final impedance settling points are presented in Figure 5-17 for PPG faults and in Figure 5-18 for PP events. It is shown that the relay is sensitive to all PPG and PP faults along the

length of the MVDC link. These plots confirm that the measured AC-side impedance only increases horizontally along the resistive axis proportionally to the increasing distance between the measurement point and fault location for DC-side PPG and PP faults. Accordingly, for any resistive fault, the locus of the apparent impedance would be shifted to the right with the magnitude of the shift being proportional to the fault resistance.

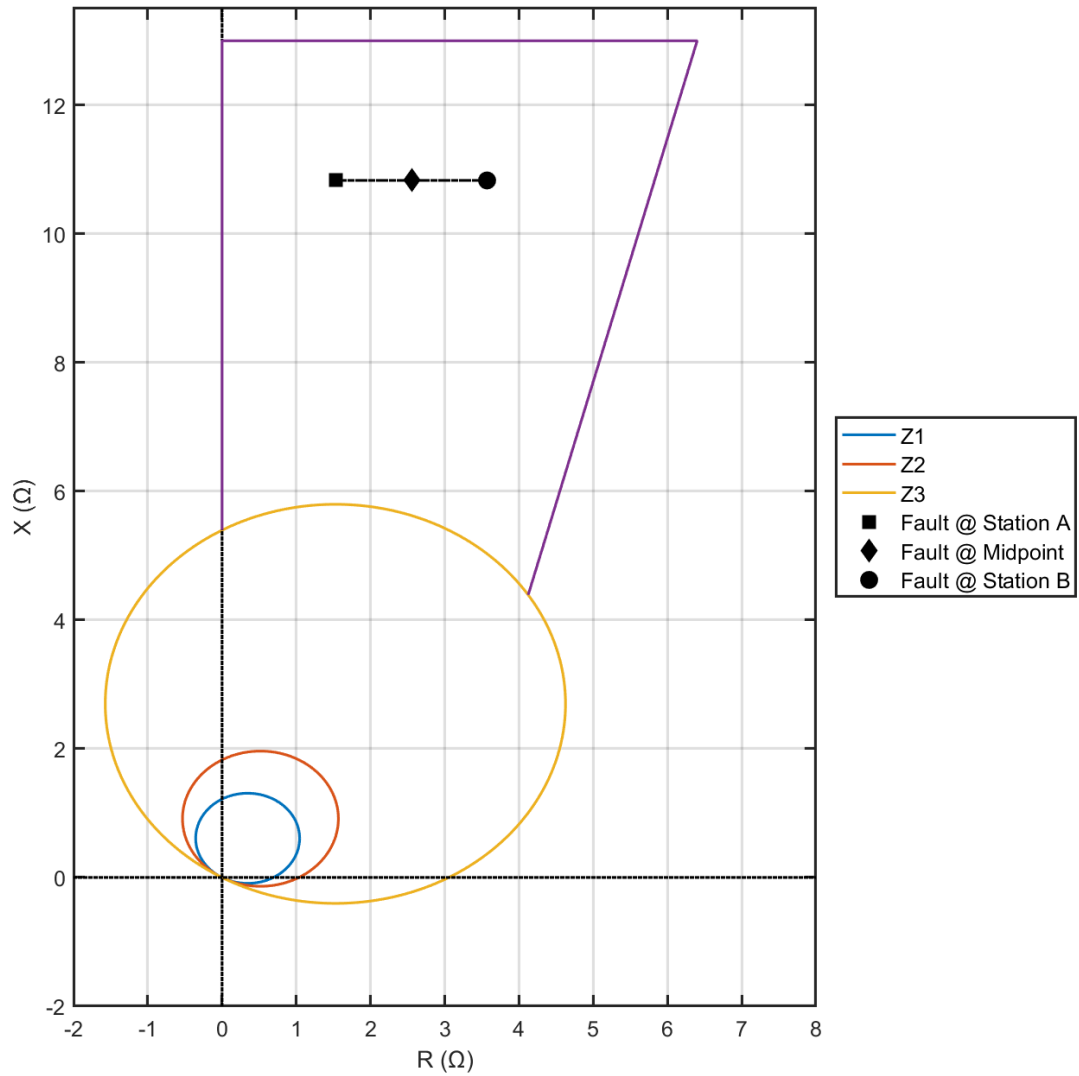


Figure 5-17: Final apparent fault impedance settling points for PPG events at Station A, mid-point and Station B

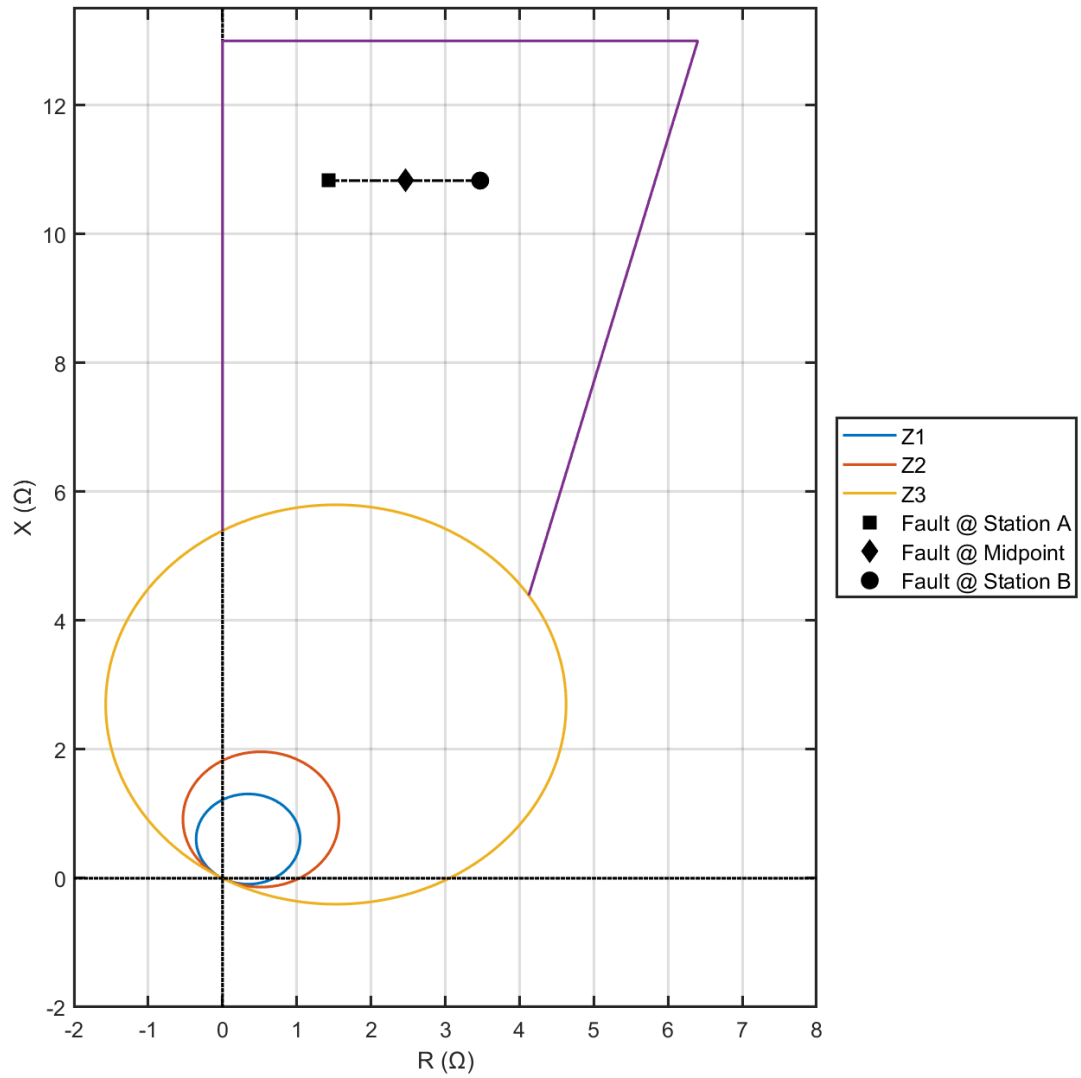


Figure 5-18: Final apparent fault impedance settling points for PP events at Station A, midpoint and Station B

5.5 Discussion

Fast-acting distance protection offers an innovative method of providing fast backup protection to the main converter protection for DC-side PPG and PP faults under a symmetrical monopole operating topology.

The back-up protection reported here would not be capable of detecting single pole-to-ground faults for a symmetrical monopole. When a PG fault occurs, the link effectively becomes a monopole with a metallic/ground return. The transfer current remains constant, as the system is still controlled, while the DC voltage tends towards twice the nominal pole-to-ground voltage (i.e. 54 kV in the case of a ± 27 kV system) as outlined in Figure 5-19 [270]. From the AC-side, there is no change in the AC voltage or currents and therefore the distance relay would not be sensitive to such faults.

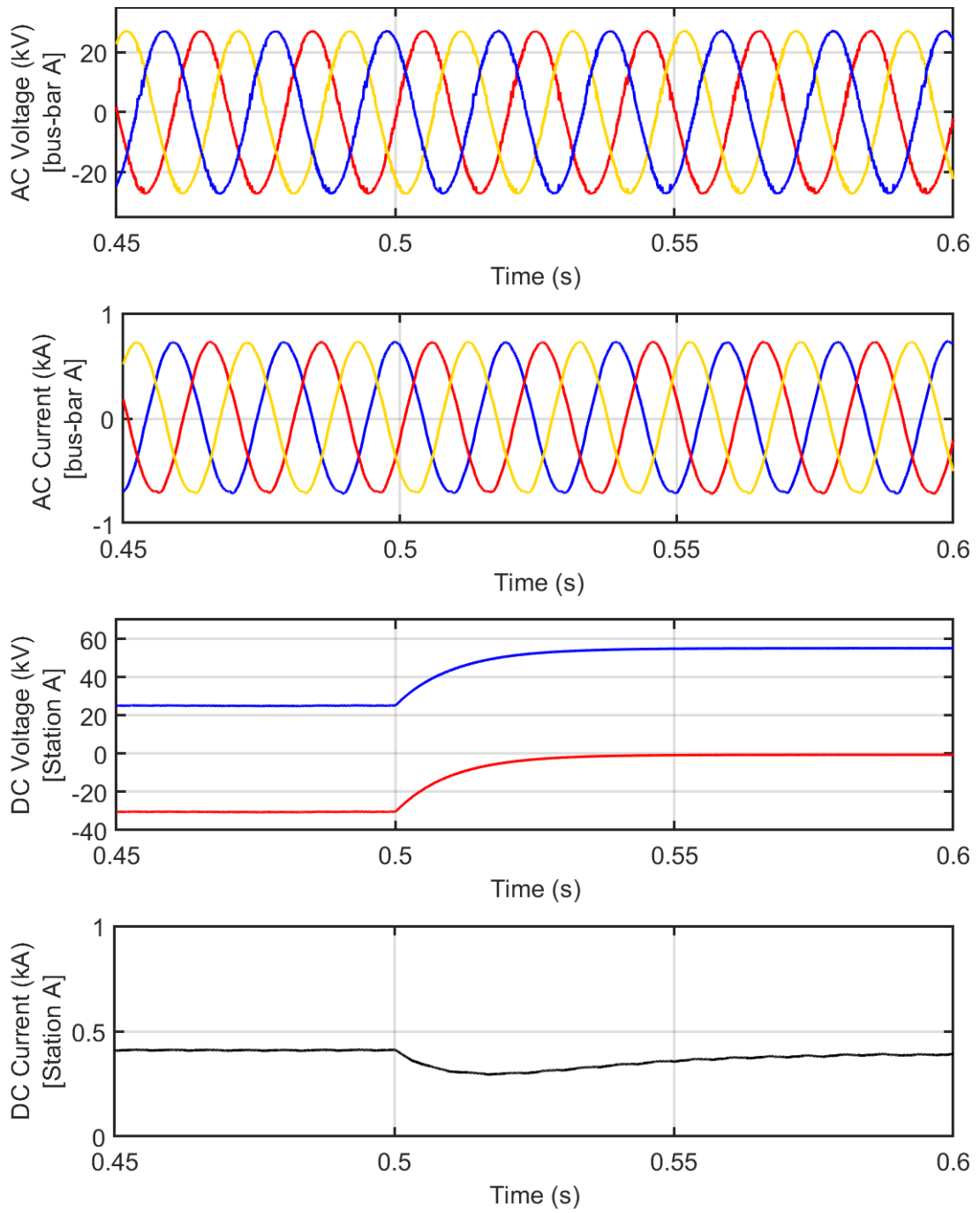


Figure 5-19: AC and DC voltages and currents for PG fault at the mid-point of the DC link

Depending upon network topology, it may be undesirable to permanently trip the CB at the AC distance relay (i.e. at busbar A in Figure 5-10) in the event of a DC-side fault, however, the approach outlined could also provide a transfer trip to a more local CB or potentially even a load-interrupting switch (which may be usable as fault currents are relatively low) to minimise the isolation of healthy AC circuits in an interconnected network.

A quadrilateral impedance characteristic has been used for these studies, as it is easy to implement on standard commercially available relays. It may be preferable to define a more customized shape (i.e. via specific R-X coordinates to create a specific boundary) to improve performance. This could readily be achieved via modifications to distance protection relay configuration and setting software as will be explored in detail in towards the end of Chapter 6.

5.6 Conclusion

The role and effectiveness of existing network protection strategies must be investigated for situations where DC interconnectors, with converter interfaces, are introduced within existing networks. This chapter has presented the results of such an investigation into the impacts on power system protection performance from the introduction of embedded MVDC links into distribution networks and shown how existing AC-side distance protection can be modified to provide backup protection, should a fault on the DC link not be cleared by the main protection for that link.

Through simulations presented in this paper, the impedance for DC-side PP and PPG faults, as measured remotely from the AC network, are determined. Using this characteristic, a fast-acting backup protection scheme has been demonstrated. The developed solution is trialled for faults at various locations on the DC link with the protection performing as expected.

Studies have shown that existing AC distance protection relays, with suitable modifications to their zones/settings, have the potential and ability to discriminate and react quickly to faults upon a DC link in a backup mode.

Chapter 6

Physical Validation of DC Fault Impedance and of the Fast-Acting Protection Scheme

6.1 Introduction

Simulations in Chapter 5 have demonstrated that conventional AC-side distance protection relays can detect and issue trip signals to provide fast-acting backup protection for balanced faults residing on an embedded MVDC link. While the results from software simulation-based investigations appear promising, it is good practice and important from a research perspective to validate that the sampled voltages and currents produced via the transient simulations are a realistic representation of a converter's behaviour under symmetrical DC-side faults, and that the protection system developed through the research will perform as expected. Due to the low volume of research produced by the academic community surrounding the topic of AC-side system performance during DC-side faults, the response of the AC system during a DC faults will first be validated in this chapter.

The performance of a commercially available distance protection relay will be examined and tested in a hardware-in-the-loop (HiL) simulation environment. The requirement for additional algorithms, outlined in the previous chapter, will be demonstrated and implemented on the relay. The use of a customisable R-X coordinate based setting approach will also be trialled.

In summary, this chapter will discuss and present the findings from three experimental processes as outlined.

1. Verification of AC system performance for DC-side faults – Section 6.2
2. Validation of the fast-acting backup protection concept using a commercial distance protection relay and demonstrating the relay's correct functionality and sensitivity for AC faults – Section 6.3
3. A user-customisable R-X coordinate-based setting approach – Section 6.4

6.2 Validation of AC System Response During DC Faults

6.2.1 Objective of Tests

The protection solution outlined in Chapter 5 is based upon transient simulations derived from software. This has the implication that results are of course subject to mathematical models of electrical components used by the software in addition to simulation platform characteristics which may, or may not, accurately reflect the true behaviour of a physical system during normal and faulted conditions. A test environment was designed and constructed to allow the AC-side impedance associated with a DC fault to be validated via physical measurement of three-phase voltages and currents.

The following subsections outline the design of the test system and define the anticipated response, through simulation, for the test system. The experimental procedure and results are then presented followed by a discussion of results.

6.2.2 Description of Test System used in Experiments

The test system was based on a 35 MVA converter which connected between two 33 kV distribution networks via a line of 10 km - similar to the Angle-DC project. To reduce the currents associated with faults and to keep system voltages to a safe and manageable level, a three-phase 42 V_{rms} AC test network was used for the laboratory experiments. The use of a low voltage system allows for straightforward measurement of instantaneous voltage and currents.

There were several challenges associated with the scaling of an MVDC converter to levels that will be suited to a laboratory environment. The test setup therefore did not contain any actively switched power electronics but rather used a three-phase, six pulse, full-bridge diode rectifier to represent an AC-DC converter for the reasons outlined below:

- VSC converters block commutation during DC side faults and essentially respond as an uncontrolled rectifier once the DC-side voltage is lower than the rectified voltage level (as discussed previously);
- a diode bridge arrangement reduces prototyping time by negating the requirement to design and build of a VSC converter control system;
- the experimental cost could be reduced due to diode bridges being inexpensive compared to actively switched devices in addition to fewer electrical components and controllers being required; and

- the response of a diode rectifier supplying DC-side faults is generally well-reported in literature.

While it is acknowledged that a diode-rectifier does not have the same control capabilities as an actively switched VSC system during steady-state operation (e.g. the ability to independently control real and reactive power), the system can be considered as representative of an MVDC link for symmetrical DC-side faults.

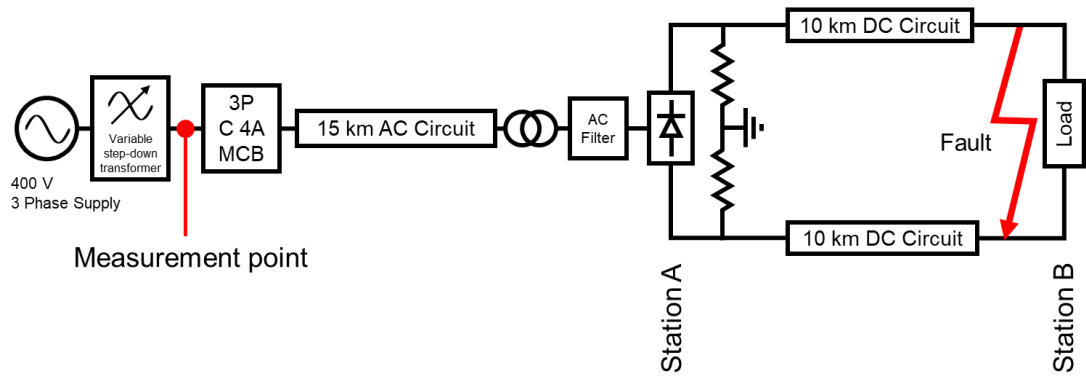


Figure 6-1: Single line test network diagram

Figure 6-1 presents the test network built and used in the laboratory. A 400 V, three-phase, supply was stepped down via a three-phase variable autotransformer (commonly referred to as a Variac) to a phase-phase rms voltage of 42 V. Measurements of instantaneous voltage and current were taken at the position outlined in the diagram.

A three-pole, 4 A MCB (miniature circuit breaker) with C-type tripping characteristic was used both to protect the low voltage system as well as to provide a point to physically isolate the low voltage system from the supply [271]. MCBs with C-type tripping characteristics are designed for devices with higher inrush currents (e.g. inductive loads such as motors and lamp ballasts etc.) of between five and ten times rated current [261] whereas a standard B-type MCB, found in most domestic properties, facilitate a lower current inrush of between three and five times rated current. The MCB also allowed the AC voltage to be set, via the Variac, prior to full energisation of the downstream test network.

Cables (both AC and DC), the transformer and AC converter filters were emulated using lumped-element $R-L$ components. A three-phase uncontrolled diode bridge was used to convert the three-phase AC to DC. No DC-side capacitance was included in the system as capacitors store energy which would have introduced an unnecessary hazard into the experimental setup. Since the capacitor discharge during DC-side faults occurs for only a short period, it was deemed that the exclusion of these components would have negligible

effect on the final fault impedance. The DC system was grounded via a midpoint created by two high value resistors (50 k Ω) which connect in series between the two DC poles.

A two-pole contactor was used for fault inception. The use of a contactor allowed for faults to be applied to the system from a safe distance via a hardwired remote control. The contactor (an electrically controlled mechanical switch - essentially a relay for higher power applications) connected the fault resistance of either 0 Ω or 1 Ω at the rectifier terminals or at the load terminals to simulate faults at either end of the 10 km DC link.

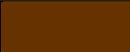
The measurement of three-phase voltages and currents was achieved using a Fluke 435 Series II Power Quality and Energy Analyser [272] operating in the 'Power Wave' recording mode. This mode samples voltage and current values at a frequency of 3,750 Hz and logs the results to an SD card. The data on the SD card was downloaded on to a computer where the recorded traces could be converted to a tabulated text file using software (Power Log 430 – II) provided by the manufacturer. Current measurements were achieved via clamp-on current transformers.

A summary of the electrical parameters for the test network is presented in Table 6-1. The electrical topology for the experimental setup is outlined in Figure 6-2. Note that the conductor colours of the experimental test network are outlined in Table 6-2 and follow the colour coding convention defined in BS 7671 [273]. Figure 6-3 and Figure 6-4 display two- and three-dimensional visualisations of the mechanical design of the test system. Images of the test setup follow in Figure 6-5 to Figure 6-7 with points of interest numbered. The component values selected for this setup were selected to be similar to values used in the modelling of a grid-scale converter, while making sure that the components were readily available from suppliers and existing laboratory equipment.

Table 6-1: Component values for experimental setup

Component	Value
AC line resistance	0.16 Ω /km
AC line inductance [per phase]	1.2 mH/km
Transformer inductance [per phase]	35 mH
Converter filter inductance [per phase]	20 mH
Rectifier current rating [274]	25 A
Rectifier voltage rating [274]	600 A
DC line resistance [per pole]	0.16 Ω /km
DC line inductance [per pole]	1.2 mH/km
DC load	33 Ω
DC midpoint grounding resistance [per pole]	50 k Ω
Fault resistance	0.0 / 1.0 Ω
Fault contactor (2 pole) current rating (230 V coil)	20 A
3 pole MCB – network protection	4 A – Type C
1 pole MCB – control protection	1 A – Type C

Table 6-2: Circuit wiring colour codes [273]

Colour					
	Brown	Black	Grey	Blue	Yellow - Green
3-phase AC	L1	L2	L3	Neutral	Ground
3-wire grounded DC	Positive	–	Negative	Mid-Point	–

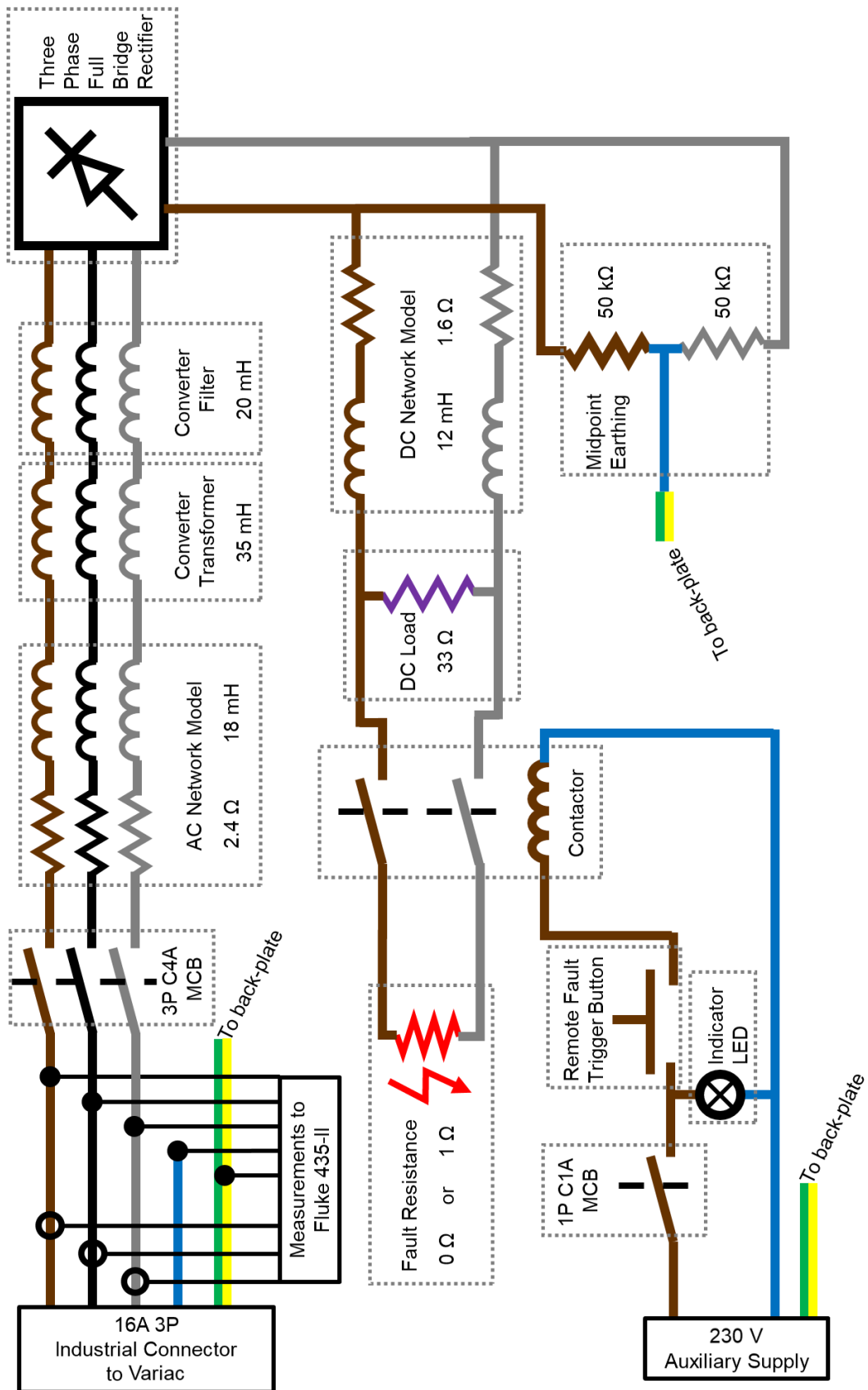


Figure 6-2: Electrical schematic of test setup

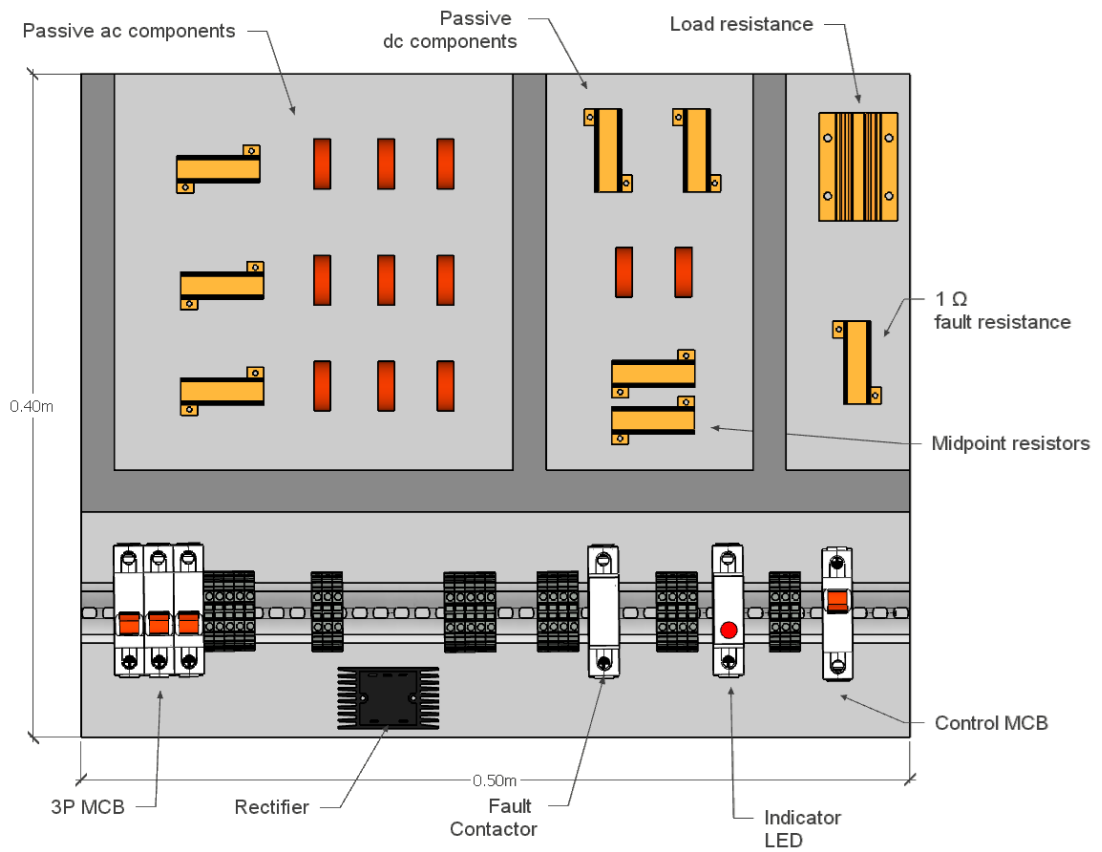


Figure 6-3: Plan view of mechanical layout

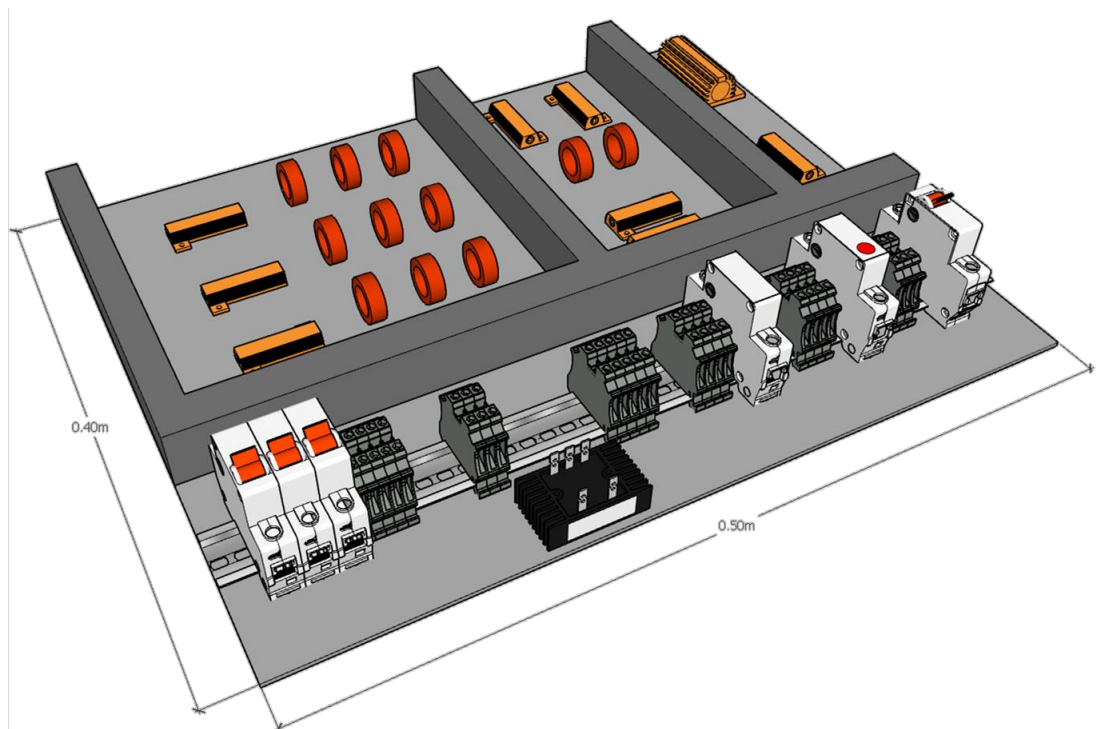


Figure 6-4: 3D view of mechanical layout

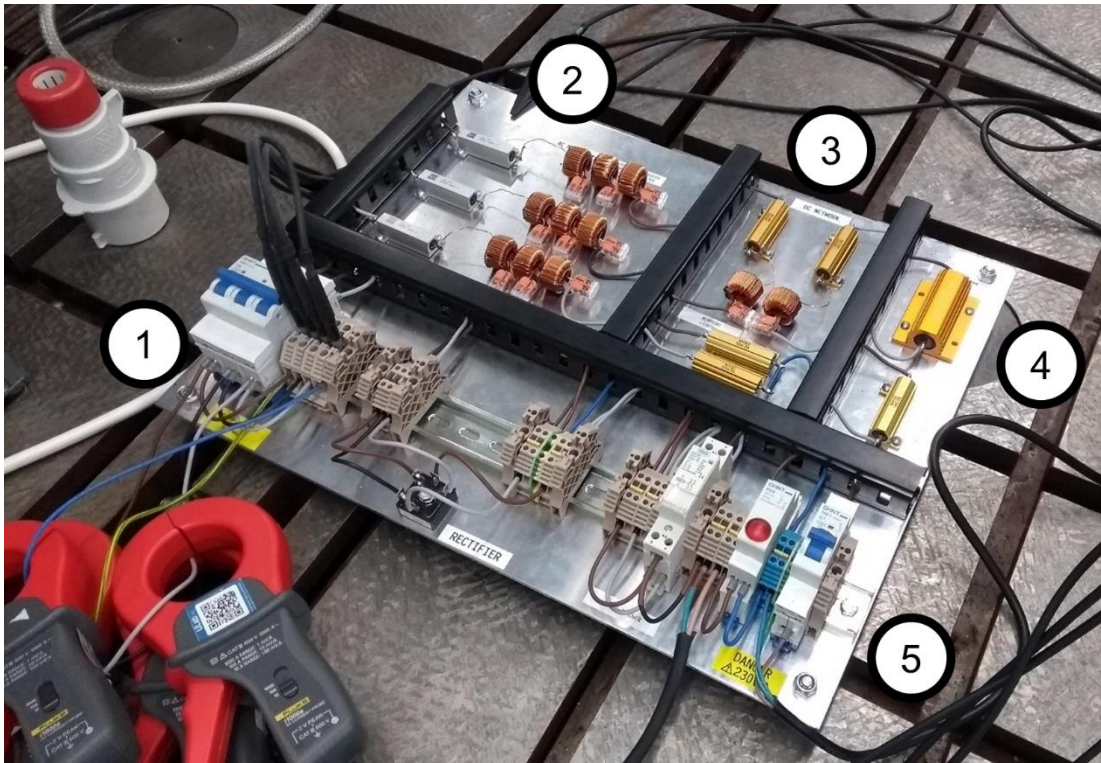


Figure 6-5: Laboratory test setup (1)

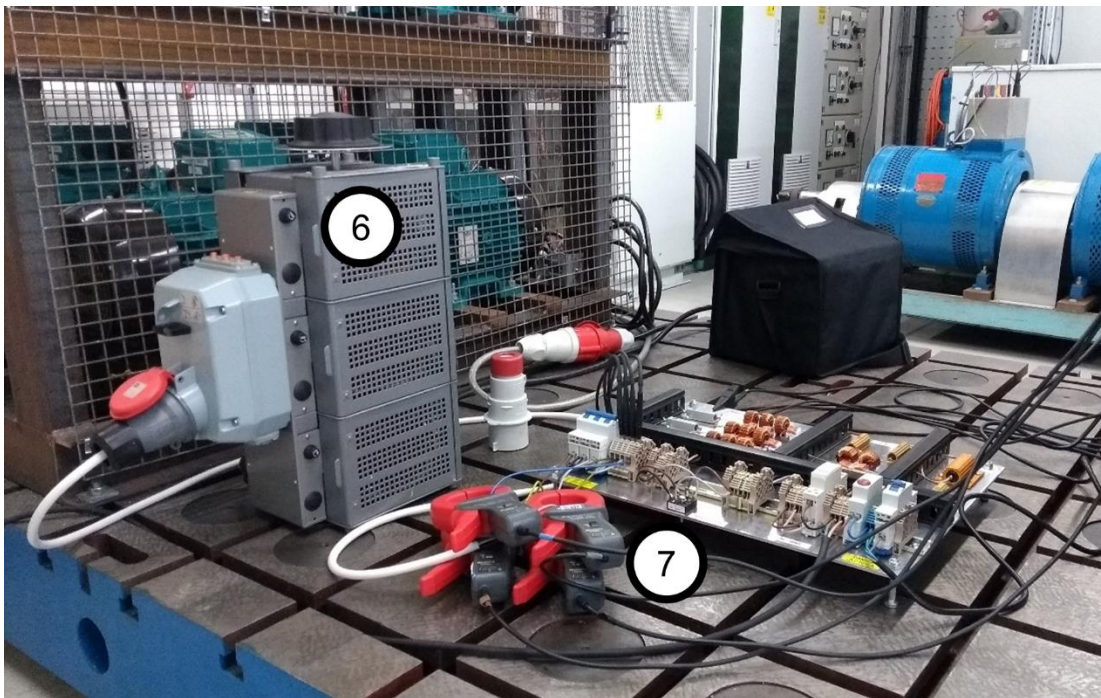


Figure 6-6: Laboratory test setup (2)

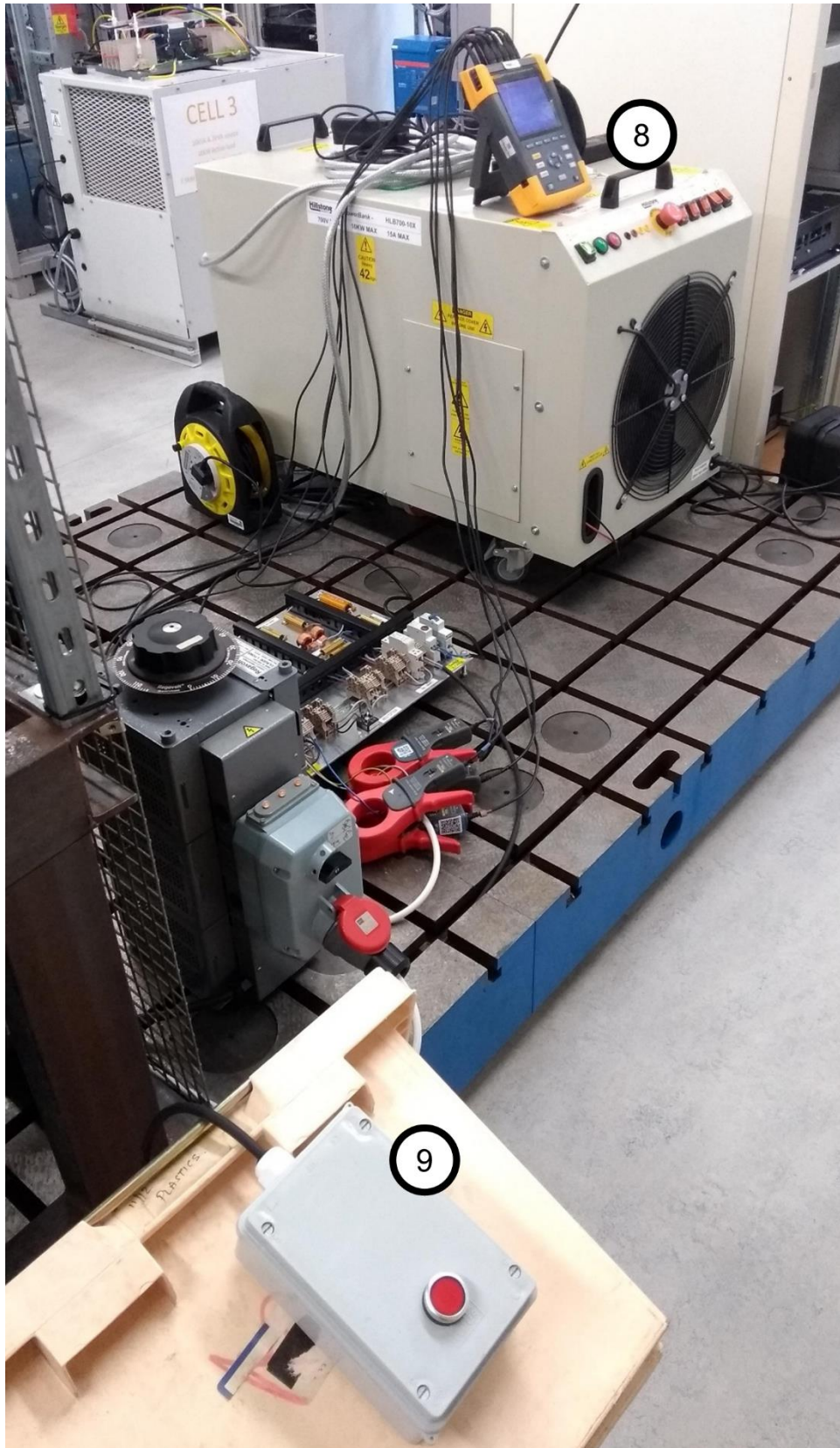


Figure 6-7: Laboratory test setup showing hardwired remote control for fault inception and instantaneous three phase voltage and current logger

Table 6-3: Description of numbered points from laboratory test setup images

ID	Description
1	LV AC isolation point and voltage measurement location
2	Passive components emulating AC network and converter assets
3	Passive components emulating DC network and DC grounding system
4	Passive components to emulate DC load and fault resistance
5	DC fault inception control circuitry
6	Three-phase controllable step-down transformer (Variac)
7	Split-core current clamps for current measurements
8	Fluke 435 Series II Power Quality and Energy Analyser
9	Hardwired remote control for fault inception

6.2.3 Simulated Response

Before determining the response of the system on the physical hardware test platform, the network was first simulated in Matlab Simulink to ensure that components were operated within their continuous rating. Although faults were only be placed on the system for short periods of time (<1 s) it was important that components did not impose non-linearities on to the system during fault transients.

Four scenarios were studied for faults placed at either end of the DC link with a fault resistance (R_f) of either 0Ω or 1Ω . To summarise, the four fault events were as follows:

- a) Location = station A (0 km), fault resistance = 0Ω
- b) Location = station A (0 km), fault resistance = 1Ω
- c) Location = station B (10 km), fault resistance = 0Ω
- d) Location = station B (10 km), fault resistance = 1Ω

The voltages and currents for each event were recorded and analysed in Matlab Simulink to determine the final settling point of the impedance for phase-phase and phase-ground elements. The calculation of R and X values was achieved in Simulink using the subsystem presented in Figure 6-8. This subsystem employs a Fourier transform to convert a pair of time-varying voltage and current measurements into a magnitude and phase. A complex division operation was carried out to obtain the measured impedance of the system in polar form. This value was transformed to cartesian form to provide the impedance in terms of R and X. Six of these subsystems were used in parallel to determine the impedance for all phase-to-phase and phase-ground elements.

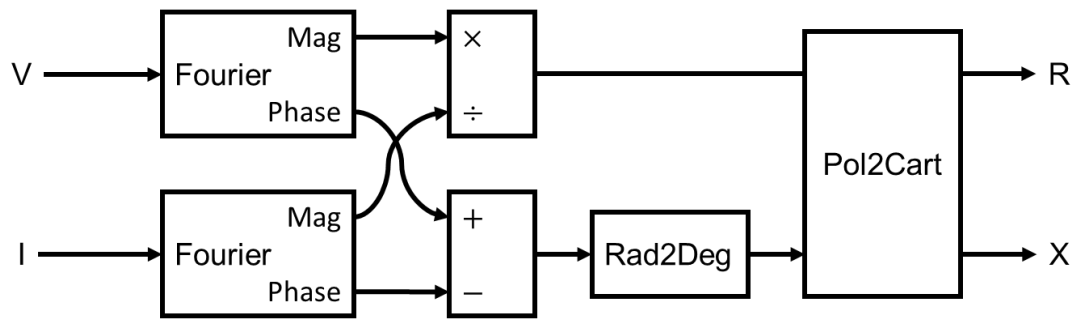


Figure 6-8: R-X detection subsystem

An example of the three-phase, time-sampled voltages and currents produced by the simulation model is presented in Figure 6-9. Note in this figure the voltage magnitude appears to remain unchanged during the fault event, this is primarily due to the fault current being very low and as such the voltage drop at the measurement point is negligible. The final R-X impedance values for each event are presented in Table 6-4 where the highly inductive characteristic (as measured by the AC-side for DC-side faults) can be observed for the four fault events as expected. The pre-fault impedance is also recorded in this table to demonstrate that the steady-state operation of the converter is significantly outside of the fault impedance area.

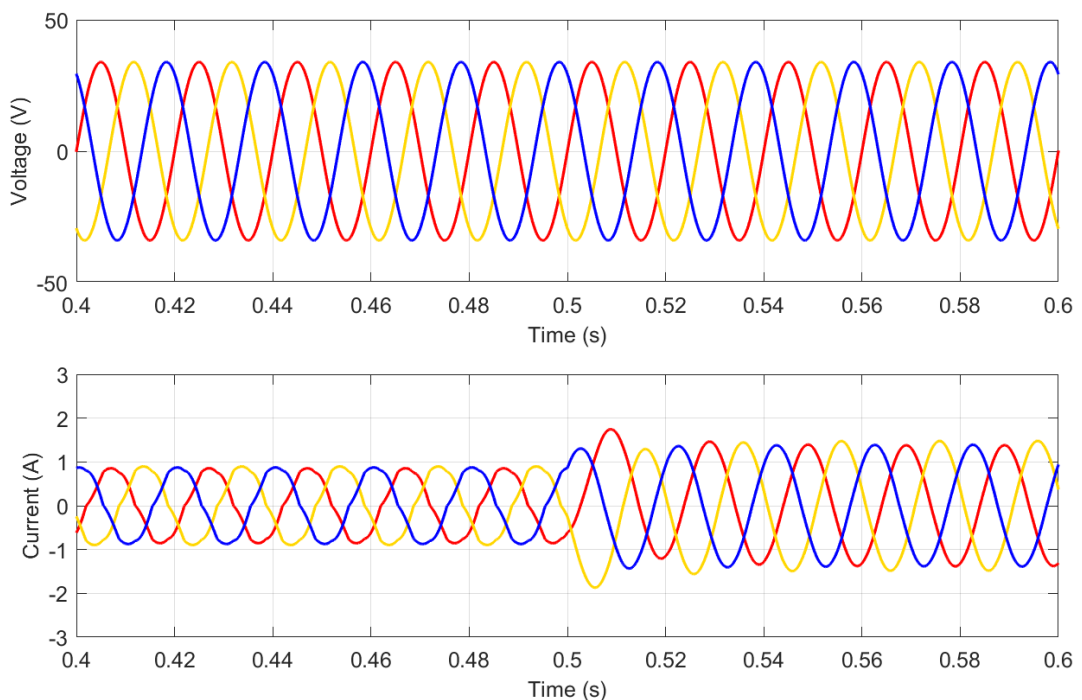


Figure 6-9: Simulated three-phase voltages and currents for a 1 Ω DC fault at Station A (fault application time = 0.5 s)

Table 6-4: Impedance measurements during DC-side faults and pre-fault conditions

	Fault Location	Station A		Station B		Pre-fault	
		$R_F (\Omega)$	$X_F (\Omega)$	$R_F (\Omega)$	$X_F (\Omega)$		
Distance Element	AB	$R (\Omega)$	5.67	6.27	7.55	8.14	28.3
		$X (\Omega)$	23.98	23.99	24.33	24.3	26.65
	BC	$R (\Omega)$	5.67	6.27	7.55	8.14	28.3
		$X (\Omega)$	23.98	23.99	24.33	24.3	26.65
	CA	$R (\Omega)$	5.67	6.27	7.55	8.14	28.3
		$X (\Omega)$	23.98	23.99	24.33	24.3	26.65
	AG	$R (\Omega)$	5.67	6.27	7.55	8.14	28.3
		$X (\Omega)$	23.98	23.99	24.33	24.3	26.72
	BG	$R (\Omega)$	5.67	6.27	7.55	8.14	28.2
		$X (\Omega)$	23.98	23.99	24.33	24.3	26.63
	CG	$R (\Omega)$	5.67	6.27	7.55	8.14	28.2
		$X (\Omega)$	23.98	23.99	24.33	24.3	26.76

6.2.4 Experimental Results

The four pole-to-pole fault events were then applied to the physical test system. As mentioned previously, faults were applied to the system via the hardwired remote control with instantaneous voltages and currents being recorded to an SD card via the Fluke measurement system. An example of the voltages and currents associated with a 1 Ω fault at Station A is presented in Figure 6-10 - note the similarity between measured plot in Figure 6-10 and the simulated plot in Figure 6-9. The small differences between individual voltage and current phases is associated with discrepancies in resistance and inductance values of physical components.

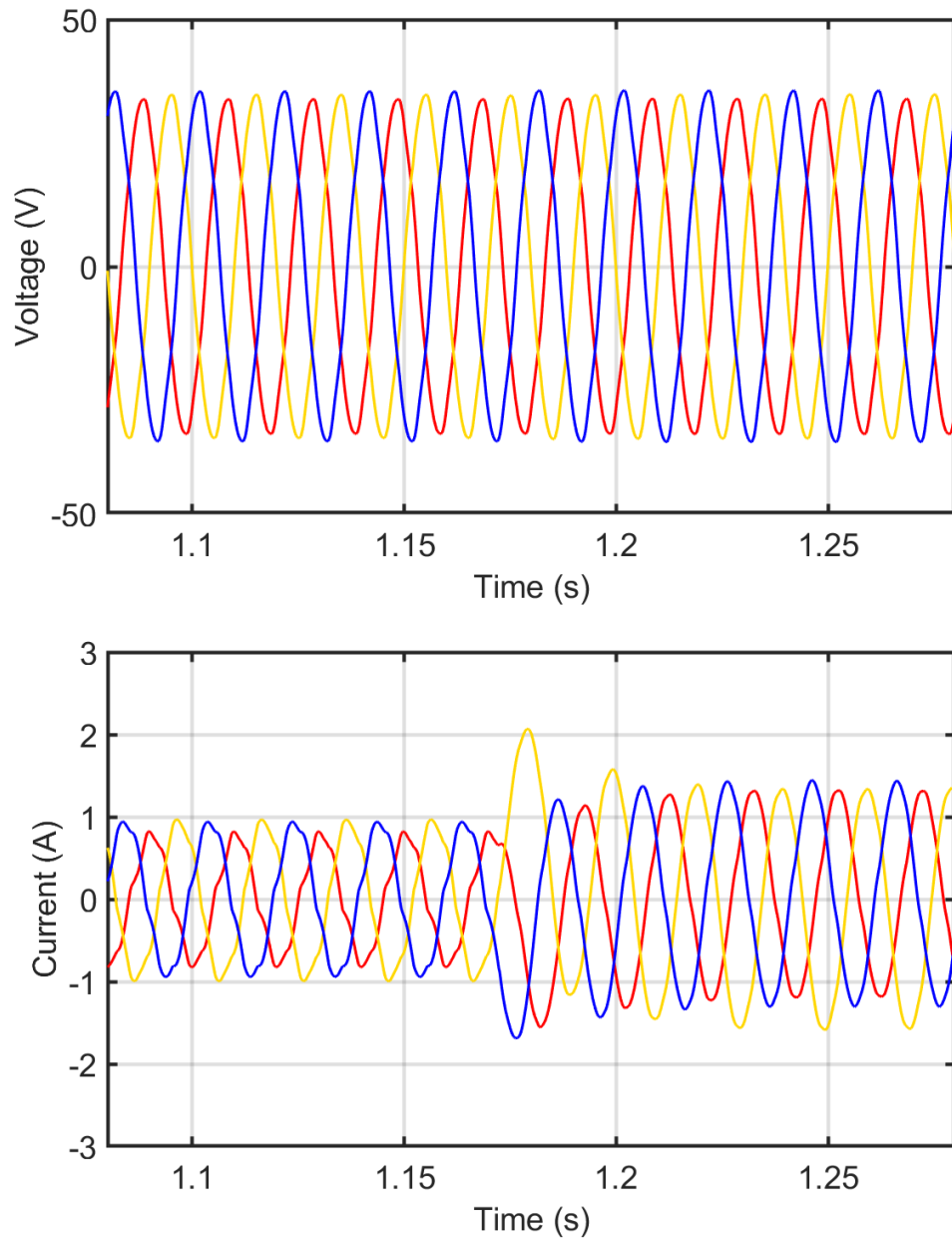


Figure 6-10: Experimental three-phase voltages and currents for a 1Ω DC fault applied at Station A (fault application time ≈ 1.18 s)

The final R-X impedance settling points for each fault event are presented in Table 6-5. Each experiment was conducted three times with the mean R and X value being recorded for each case. The final impedance settling points for all comparators (i.e. AB, BC, CA, AG, BG, CG) for each fault event are plotted in Figure 6-11 for both hardware and software tests.

Table 6-5: Final settling impedance for fault scenarios (mean value recorded)

Fault Location		Station A	Station A	Station B	Station B	Pre-Fault	
R_F (Ω)		0	1	0	1		
Distance Element	AB	R	7.08	7.73	9.02	9.69	31.8
		X	23.3	23.3	23.1	23.1	22.7
	BC	R	7.08	7.73	9.02	9.69	31.8
		X	23.3	23.3	23.1	23.1	22.7
	CA	R	7.08	7.73	9.02	9.69	31.8
		X	23.3	23.3	23.1	23.1	22.7
	AG	R	7.67	8.47	9.67	10.4	32.4
		X	25.8	25.8	25.6	25.6	24.7
	BG	R	7.79	8.41	9.67	10.4	32.5
		X	22.6	22.6	22.4	22.4	25.7
	CG	R	7.63	8.43	9.63	10.3	32.4
		X	25.9	25.9	25.8	25.8	25.3

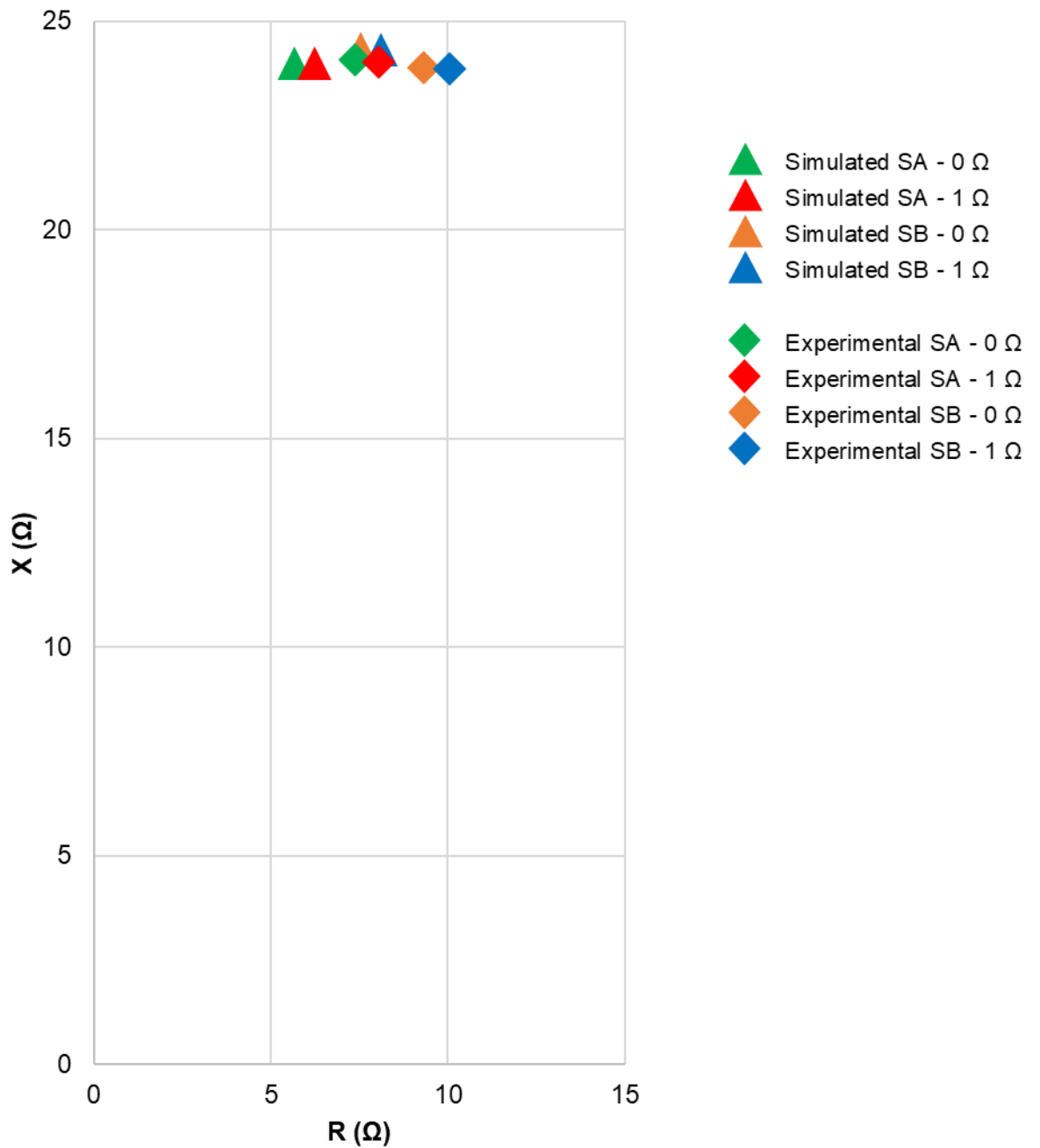


Figure 6-11: Simulated and experimental DC fault impedances

It is clear from Figure 6-11 that the experimental and simulated results of the system perform similarly for the four fault events studied. For clarity purposes, each point plotted in Figure 6-11 represents the mean value of the six comparators. It is noted, however, that there are discrepancies between the experimental and simulated results. This absolute error between the simulation and experimental results are quantified in terms of R and X in Table 6-6.

Table 6-6: Absolute impedance error between simulated and experimental faults

Fault Location	Z_F (Ω)	Simulated		Experimental		Absolute Error	
		R (Ω)	X (Ω)	R (Ω)	X (Ω)	R (Ω)	X (Ω)
Station A	0	5.67	24.0	7.39	24.1	1.72	0.08
Station A	1	6.27	24.0	8.08	24.0	1.81	0.03
Station B	0	7.55	24.3	9.34	23.9	1.79	-0.45
Station B	1	8.14	24.3	10.05	23.9	1.91	-0.45

Based on the absolute error between resistance and reactance values, the impedance error is calculated in Table 6-7 and presented as a percentage error. It was found that the maximum error between simulated and experimental fault impedances of 7.67%. Considering that the experimental setup employed current transformers (with an error tolerance of 2% [275]) as well as a measurement device which was only calibrated for measurements of >50 V [272], the results between experimental and simulation investigations appear to be consistent with one another.

Table 6-7: Mean fault impedance across all distance elements for simulated and experimental results

Fault Location	Z_F (Ω)	Absolute Error (Ω)		Absolute Error (Ω)	Error (%)
		R	X	Z	
Station A	0	1.72	0.08	1.721	6.98
Station A	1	1.81	0.03	1.812	7.31
Station B	0	1.79	-0.45	1.843	7.23
Station B	1	1.91	-0.45	1.965	7.67

6.2.5 Discussion

From the experiments conducted in this section it has been determined that a highly inductive characteristic, as measured via AC-side voltage and currents, is expected for DC faults. This aligns with the hypothesis produced during simulation in Chapter 5. Additionally, it has been confirmed that the AC impedance for faults on the DC system move along the resistive axis for increasing distance from the measurement point. When considering the limitations associated with component tolerances and the measurement system, the results from the experimental setup support the simulation results. Given that the highly inductive settling point of the system has now been confirmed, the protection approach outlined previously in Chapter 5 can now be validated on a commercial protection relay.

6.3 Deployment of Protection Scheme on an Actual Distance Protection Relay

6.3.1 Introduction

In the work reported in this section, the backup protection scheme developed in Chapter 5 was deployed on a commercially available distance protection relay in a HiL test environment. The trials conducted in this section benchmark the performance of the solution for both standard AC-side zone faults as well as DC-side pole-to-pole events to ensure that the stability of the device is not impacted by the introduction of the fast-acting Z4 tripping region.

6.3.2 Description of Experimental Setup

The 33 kV test network used in the studies is outlined in Figure 6-12. In this example two 10 km circuits were fed from busbar B. The first circuit is an AC line which supplies a 4 MW resistive load. The second circuit connects between busbar B and busbar D via an MVDC link operating under a symmetrical monopole topology. (Under conventional AC operation it is unlikely that these busbars would be connected due to concerns surrounding increased fault level). The link was rated at 35 MW with an operating voltage of ± 27 kV and was formed via the repurposing of existing AC conductors. All conductors use the same characteristic impedance of $(0.17 + j0.3) \Omega/\text{km}$ and were modelled as lumped element $R-L$ series components.

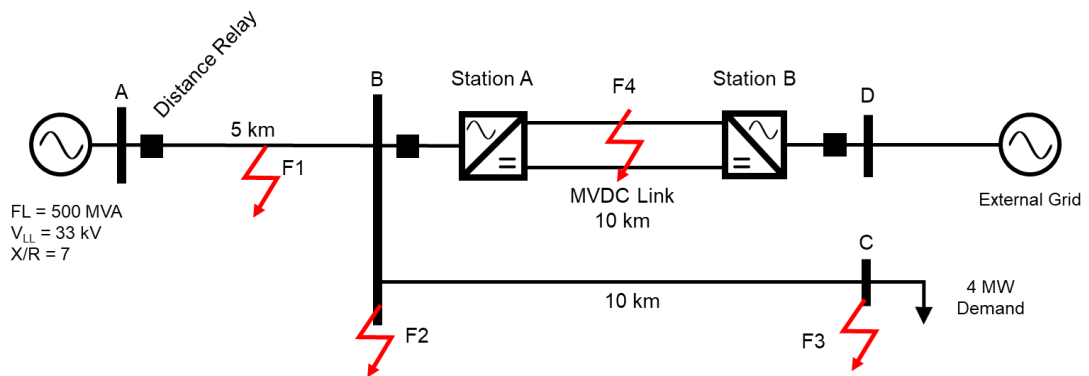


Figure 6-12: Test network with four fault locations indicated

The steady-state control for the converters was based on a standard $P-Q / V_{DC}-Q$ arrangement as described previously in Section 5.2.2. During AC-side faults it was assumed that the MVDC link did not contribute any current into the fault as, at present, no grid codes exist in GB which govern the connection and fault ride through requirements of an MVDC link connected to a distribution network [60]. The converter had a per unit transformer impedance of 20% (6.22Ω

/ 20 mH) in addition to an AC filter of 20%. Note that quantities were referred to a 33 kV, 35 MVA and 31 Ω base.

During a DC fault, the converter should block commutation of switching devices and open the AC-side converter CBs at either end of the MVDC link. It was assumed for these studies that the CB at Station A failed to open for DC faults leaving the link in an uncontrolled rectifying state. Therefore, the fault had to be cleared by the fast-acting backup protection algorithm, outlined in Chapter 5, implemented on the distance protection relay in Figure 6-12.

A series of fault studies were investigated to determine whether the relay could identify faults on the MVDC link and distinguish them from standard AC-side events. Figure 6-12 also outlines four fault locations, one in each protection zone, which were studied. Faults were modelled as symmetrical three-phase to ground events for AC-side disturbances and pole-to-pole-to-ground for DC-side events. It was assumed that the converter controller at Station B correctly isolates the infeed from the external grid during faults. The link had a pre-fault power transfer of 5 MW towards the external grid.

Voltages and currents recorded at busbar A during offline simulations were used as the input for a series of real-time HiL simulations. Sampled (100 μ s) three-phase voltages and currents were produced via Simulink simulations and stored to a comma separated value (CSV) file for each fault scenario. These files were suitable for upload into an injection amplifier which connected to the protection relay. A sample injection trace showing three-phase voltage and current is presented in Figure 6-13. These values were secondary referred via a VT with ratio of 33,000/110 V and CT ratio of 1750/5 A. All faults are applied at 0.5 s.

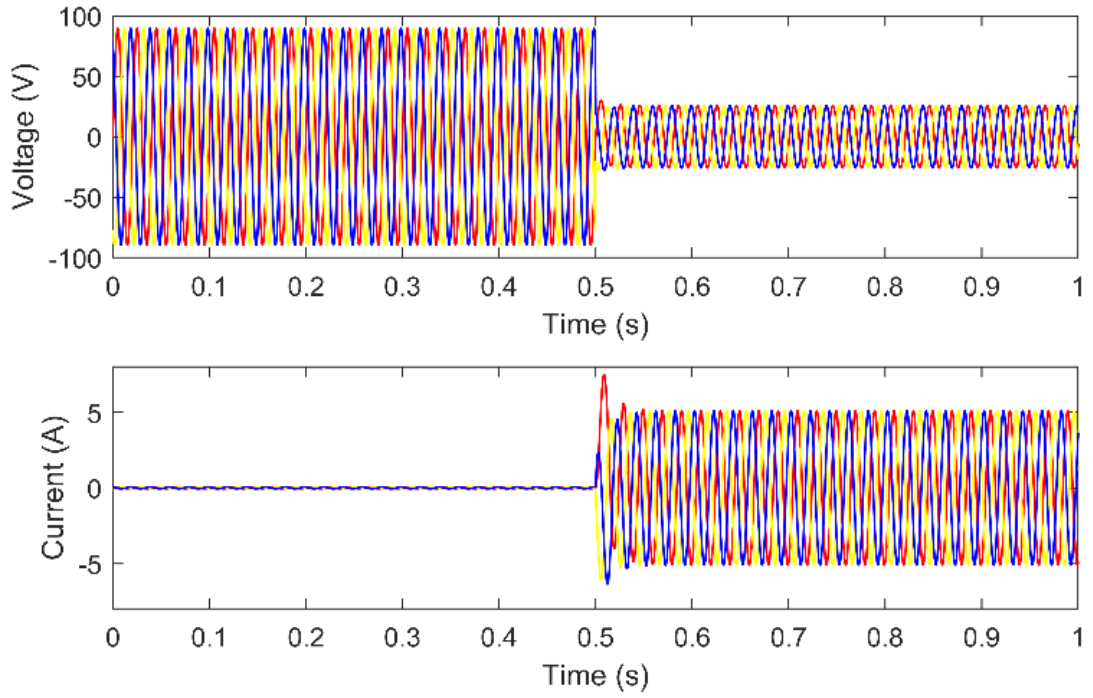


Figure 6-13: Three-phase, secondary-referred, injection voltages and currents for fault F1

The calculations for the fast-acting Z_4 resistive (R_{Z4}) and reactive (X_{Z4}) line reach settings (as determined in Chapter 5) are detailed below using equations 6-1 and 6-2 where a 20% grading margin was applied to account for uncertainties in circuit parameters, errors in transducers etc. The line impedance angle (θ) is calculated via equation 6-5. In the equations the variable R signifies a resistance and X a reactance in ohms (Ω). L_{ac} denotes the AC line, X_{fmr} the converter transformer, F the converter filter and L_{DC} is the DC line. It was assumed that transformer resistance is negligible for the cases studied.

$$R_{Z4} \approx 1.2 \times \sum [R_{L_{ac}}, R_{X_{fmr}}, R_F, R_{L_{dc}}] \quad 6-1$$

$$X_{Z4} \approx 1.2 \times \sum [X_{L_{ac}}, X_{X_{fmr}}, X_F] \quad 6-2$$

$$R_{Z4} \approx 1.2 \times [(0.17 \times 5) + (0.3) + (0.17 \times 10)] \approx 3.42 \Omega \quad 6-3$$

$$X_{Z4} \approx 1.2 \times [(0.345 \times 5) + 6.22 + 6.22] \approx 17.0 \Omega \quad 6-4$$

$$\theta = \tan^{-1} \left(\frac{X_{line}}{R_{line}} \right) = \tan^{-1} \left(\frac{0.3}{0.17} \right) = 60.5^\circ \quad 6-5$$

Table 6-8 outlines the setting parameters applied to the distance protection relay. Note that these values are primary referred and do not take CT and VT ratios into consideration. The numerical distance protection relay used in this section automatically calculated the

appropriate secondary values using the predetermined CT and VT ratios. Quadrilateral characteristics were implemented for all zones due to limitations in the relay's configuration software.

Table 6-8: Distance protection relay setting parameters

Parameter	Value
Line angle [Z1-Z3] (°)	60.5
Line angle [Z4] (°)	80.0
Z1 reach (Ω)	1.374
Z2 reach (Ω)	2.146
Z3 reach (Ω)	6.010
Z4 reach (Ω)	17.44
Resistive reach (All Zones) (Ω)	3.420
Z1 fault delay (phase & ground) (s)	0.100
Z2 fault delay (phase & ground) (s)	0.500
Z3 fault delay (phase & ground) (s)	1.300
Z4 fault delay (phase & ground) (s)	0.100

Figure 6-14 summarises the HiL test setup. The control computer was used to upload the sampled voltages and currents into the programmable test amplifier via a parallel communication interface. The sampled voltages and currents were produced via simulation, for each of the four fault events, in a CSV format with time resolution of 100 μ s.

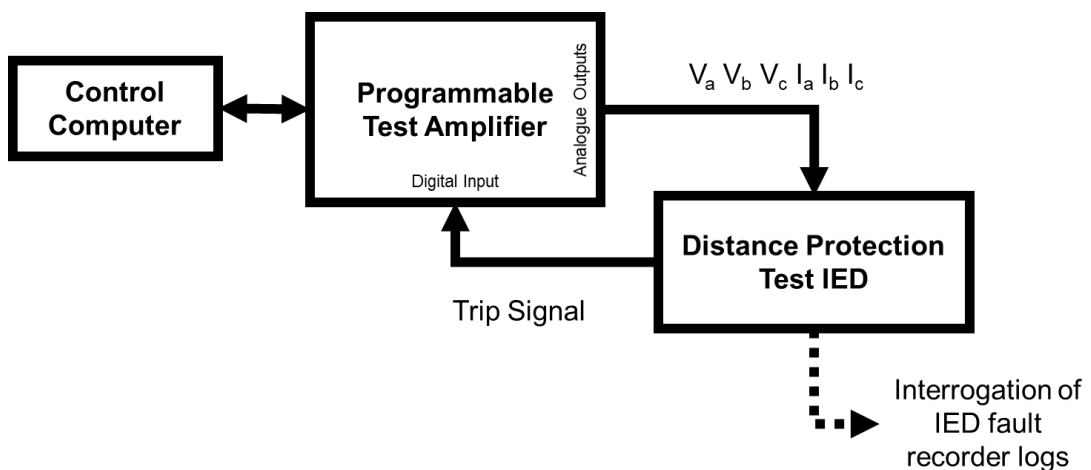


Figure 6-14: Real time hardware-in-the-loop test setup

The injection amplifier was connected to the distance protection relay via six shrouded test leads; three for voltage injections and three for current injections. The settings for the digital distance protection relay could be configured via the manufacturer’s relay configuration software and were applied to the relay by uploading the setting file via a serial interface.

The standard logic of a distance protection relay assumes that the tripping time increases with increasing zone. As stated previously in Chapter 5, amended tripping logic as presented in equation 6-6 was required to correctly time-grade the protection relay - thus ensuring stability for standard AC faults. Additionally, as stated previously in Chapter 5, the impedance of DC-side faults, as measured from the AC side, appears symmetrically across all six measurement comparators on distance protection relays. This logic presented in Figure 6-15 ensures that all of the Z4 comparators were active before a trip command was issued.

$$Z_{4Trip} = \overline{Z3} \cdot Z4 \tag{6-6}$$

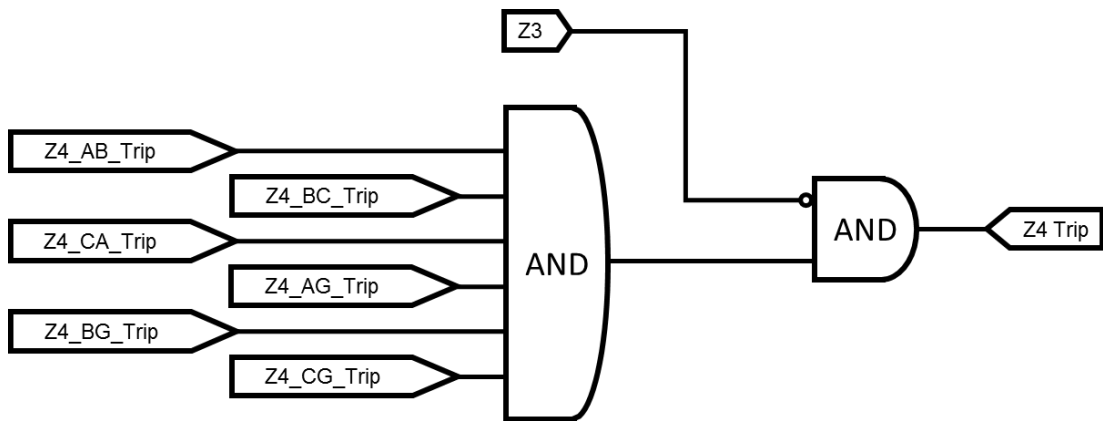


Figure 6-15: Additional tripping logic diagram

Experiments were initiated from the control computer where the three-phase voltages and currents were injected into the relay by the amplifier in real-time. The tripping output contact of the relay connected back to the monitored inputs on the injection amplifier to allow trip times produced by the relay to be recorded. Further interrogation of events was achieved via the relay’s human machine interface (HMI) or by downloading fault logs over the serial interface. Figure 6-16 and Figure 6-17 display the experimental setup in the Dynamic Power Systems Laboratory at the University of Strathclyde.

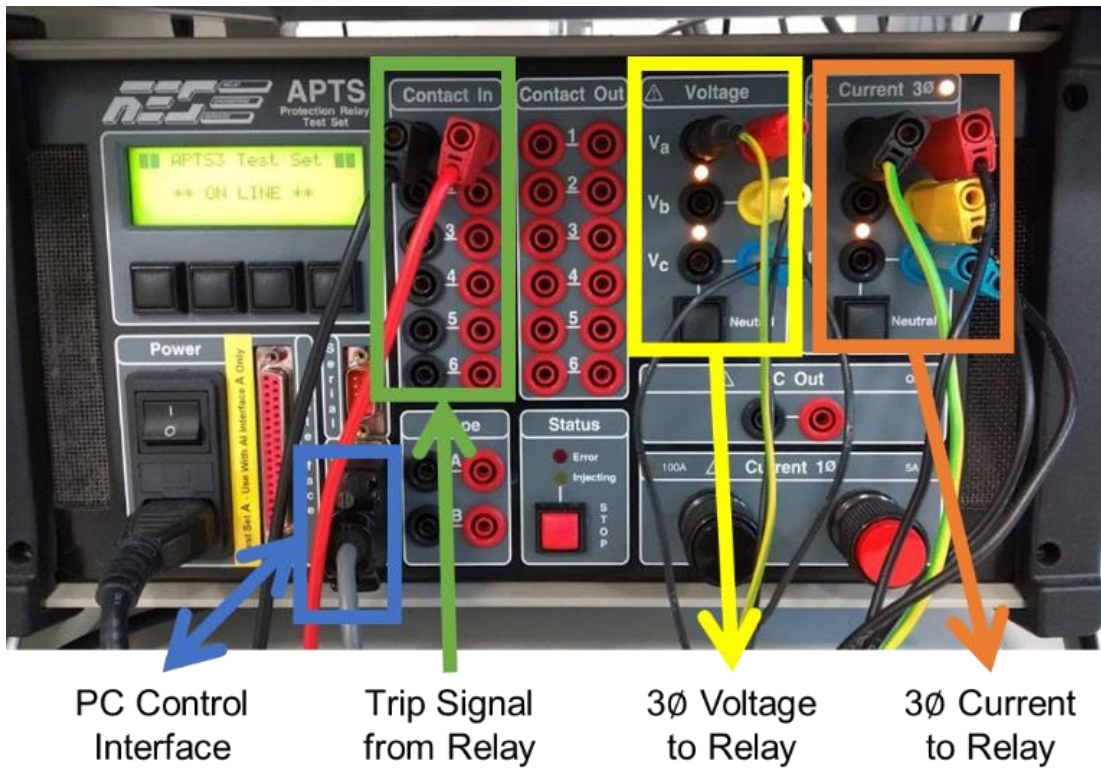


Figure 6-16: Hardware-in-the-loop injection amplifier

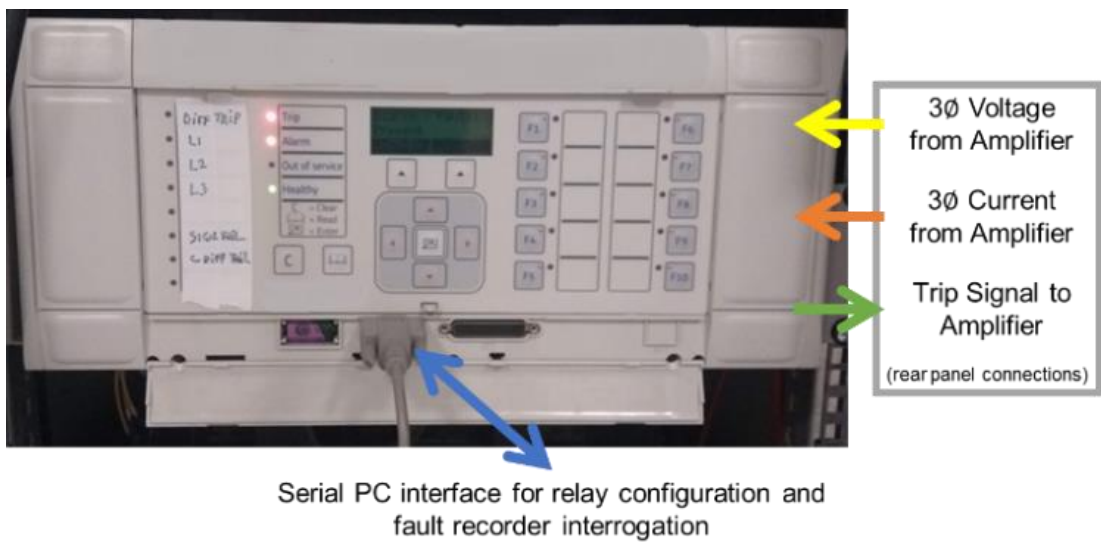


Figure 6-17: Anonymised commercially available relay used in HIL experiments

6.3.3 Experimental Results

Four injections tests were conducted to represent faults associated with each of the four fault locations as outlined previously. Faults were all applied to the system at 0.5 s. The relay trip time and active zone elements were recorded for each of the four fault scenarios and are presented in Table 6-9 alongside the expected tripping time of the relay. Note that it was not possible to mix Mho and quadrilateral characteristics with the relay used in this investigation due to limitations in the configuration software. It is observed that the trip times for all event scenarios are as expected. In the case of fault F4, which represents a fault on the MVDC link, the relay detects the fault inside of 35 ms and sends a trip signal to the CB 0.1344 s after fault anticipation.

Table 6-9: Relay log for fault simulations

Scenario	Distance Zone Triggered				Trip Time (s)	Expected Trip Time (s)
	Z1	Z2	Z3	Z4		
F1	◆	◆	◆	◆	0.5206	> 0.5
F2		◆	◆	◆	0.8166	> 0.8
F3			◆	◆	1.8220	> 1.8
F4				◆	0.6344	> 0.6

Simplified R-X diagrams, which show the impedance calculated by the distance protection relay for the phase element AB, for faults F1 to F4 are presented in Figure 6-18 - Figure 6-21.

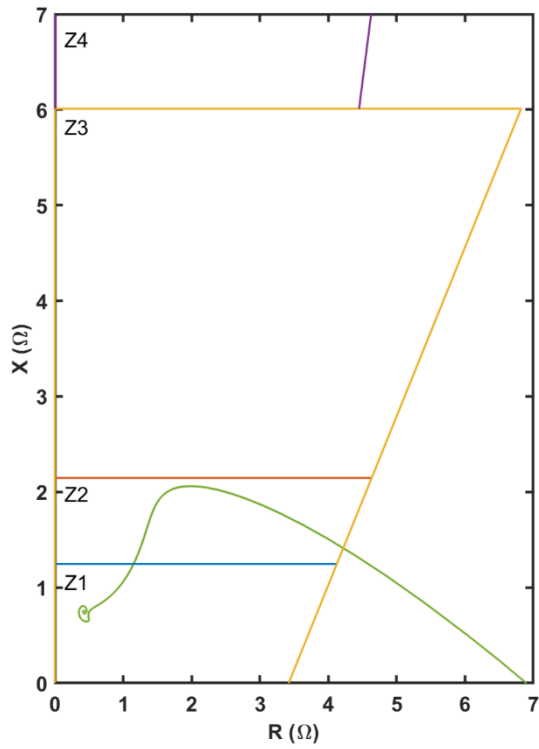


Figure 6-18: R-X diagram for fault F1

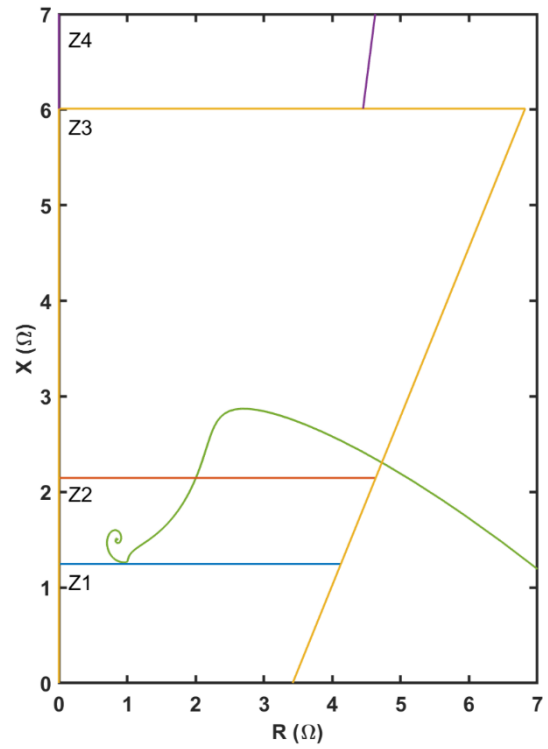


Figure 6-19: R-X diagram for fault F2

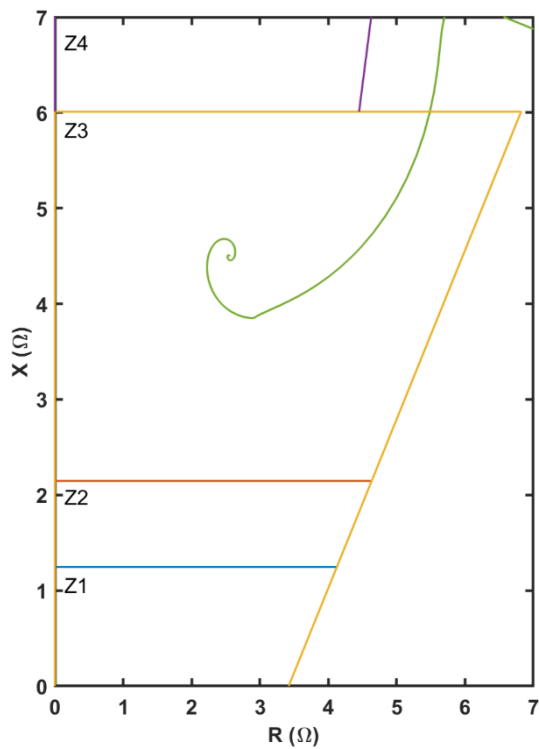


Figure 6-20: R-X diagram for fault F3

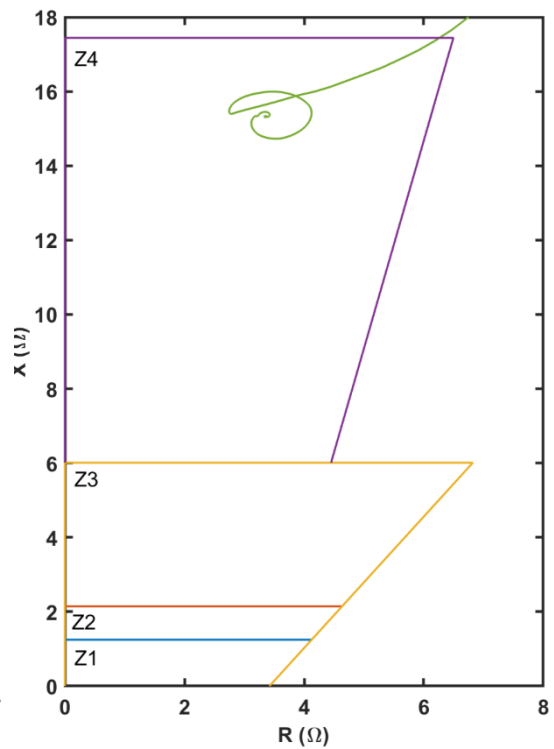


Figure 6-21: R-X diagram for fault F4

6.3.4 Discussion

From the experiments presented in Section 6.3, it has been determined that a commercially available distance protection relay can successfully respond to DC-side faults in a fast-acting manner while remaining sensitive to AC system events in Z1, Z2 and Z3. In the case of event F4, the relay detects the DC fault within 35 ms and trips the CB after a further user-definable delay of 100 ms.

The tripping logic of the relay required to be adjusted to avoid premature tripping for faults residing in Z2 and Z3 as presented in equation 6-6 in the form of a Boolean expression. This expression essentially blocks a Z4 trip when the relay detects a fault residing in Z2 or Z3, therefore, allowing a more appropriate disconnection time to be used. This modification to tripping logic can be readily implemented on numerical and digital protection relays.

The inclusion of additional setting parameters in relay configuration software would make the implementation of the fast-acting Z4 region much simpler for end-users – as will be explored in the subsequent section. For example, if the relay configuration software allowed the X setting value to be increased from 0 Ω , to circa 14 Ω , a fully independent Z4 to be created outside of Z1-Z3. The implementation of this is described in Section 6.4.

The fast-acting protection approach trialled in this section demonstrates that it is possible to use existing distance protection relays to provide backup protection for embedded MVDC links. This method also represents a potential cost saving as existing relaying equipment and measurement transducers can be reused in retrofit scenarios.

6.4 R-X Coordinate-Based Setting Approach

6.4.1 Overview of R-X Setting Approach

While the protection scheme has been verified on a commercially available digital distance protection relay, the Z4 tripping region could be considered as being unnecessarily large – especially given that the fault impedance lies towards the top of the Z4 region. This large area could, theoretically, cause an unwanted fast trip for AC faults occur at the boundary of Z3 and Z4 when in reality it should be cleared by downstream protection devices or after a more appropriate time delay. To alleviate this potential concern, an R-X coordinate-based setting approach, as outlined in Figure 6-22, will be introduced in this final experimental section.

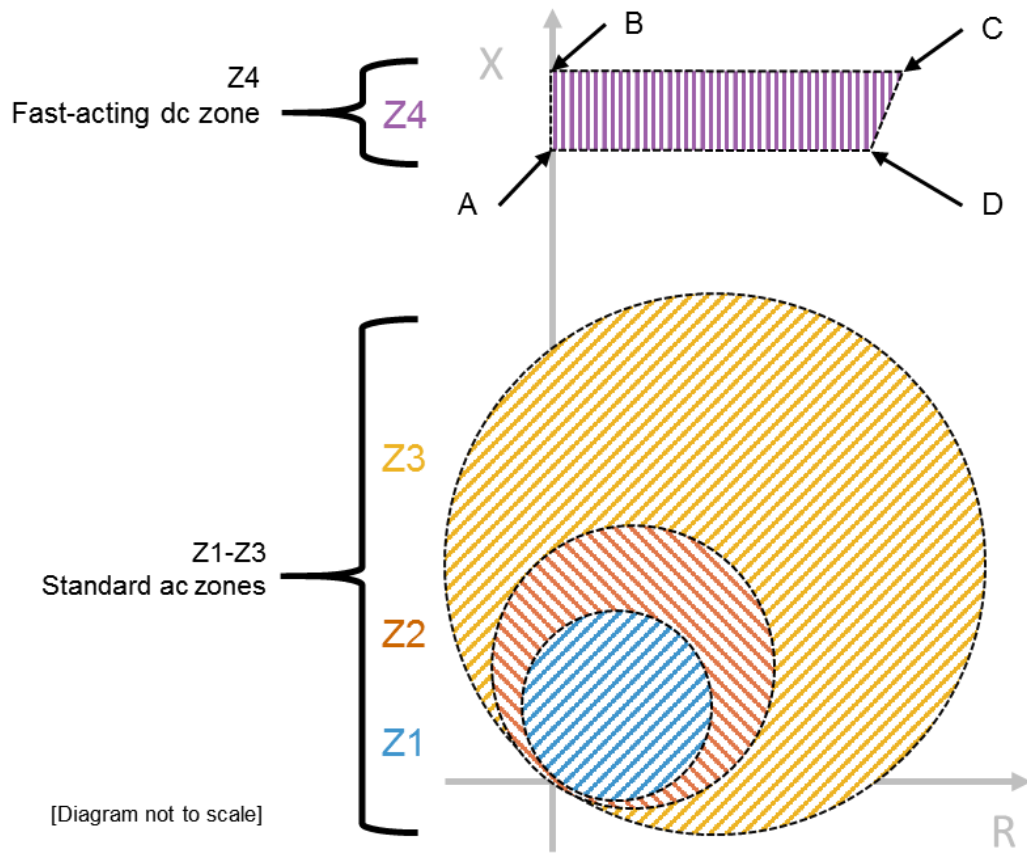


Figure 6-22: New Z4 tripping region using R-X coordinate points marked A-D

The coordinates for the fast-acting Z4 region are described in Table 6-10 for the points A-D. A grading margin of 20% is applied in line with standard protection practice to allow for uncertainties in transducers, line parameters and in relay operation. The values of R_{Z4} , X_{Z4} and θ can be determined using the process described previously in Chapter 5.

Table 6-10: Setting coordinate calculations

Point	R	X
A	0	$0.8 \times X_{Z4}$
B	0	$1.2 \times X_{Z4}$
C	$R_D + \frac{X_B - X_A}{\tan(\theta)}$	$1.2 \times X_{Z4}$
D	$1.2 \times R_{Z4}$	$0.8 \times X_{Z4}$

6.4.2 Description of Experimental Design

6.4.2.1 System Overview

To validate the outlined protection method, the protection algorithm was implemented on a low-cost (c. £40 in the year 2020) computing platform (in this work a Raspberry Pi Model 4 [276]).

A test network (presented later in Figure 6-31) was constructed using Matlab Simulink for a range of simulated AC and DC faults at different locations on the test network. The simulated voltages and currents were recorded in the form of COMTRADE (Common format for Transient Data Exchange for power systems) files. These COMTRADE files were imported into a real time simulation platform (in this case an RTDS Technologies system), where the playback function was used to re-play the simulated faults.

The voltage and current signals were sent from the RTDS to the Raspberry Pi based protection controller via a GTNET card using a UDP protocol. The Raspberry Pi calculates, using a Fourier transform, the associated impedances and compares them against the relay setting parameters to determine whether to trip, trip with a time delay or to not trip at all. If a tripping condition is met, a trip signal was sent back to the RTDS (via the same UDP connection), where the time of fault inception, the fault detection time and the received trip signal were all monitored and recorded. Further details surrounding the implementation of the distance protection relay are provided in Section 6.4.2.2. A diagram of the test setup is presented in Figure 6-23.

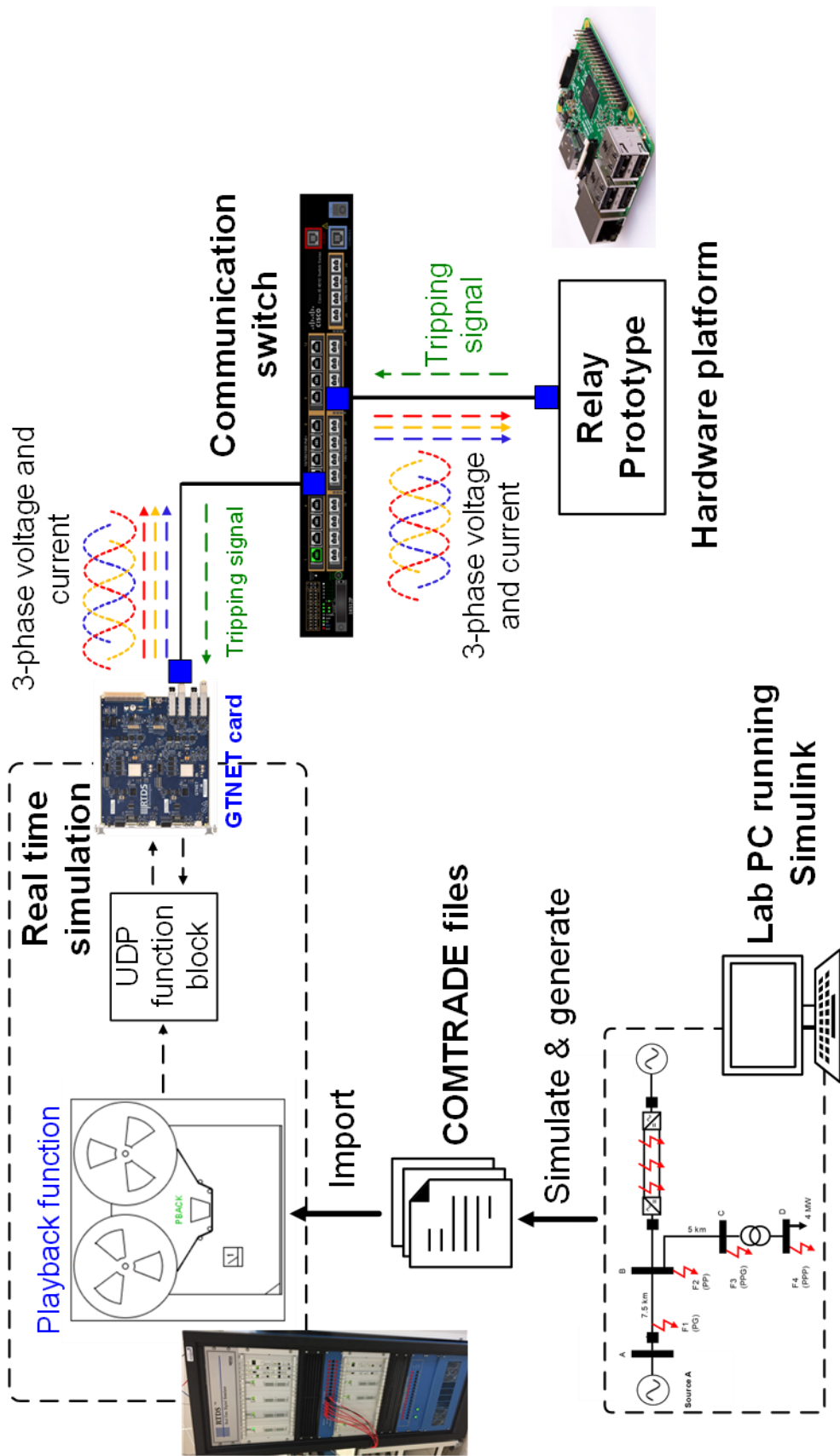


Figure 6-23: Experimental overview

6.4.2.2 Distance Relay Implementation Overview

A summary of the processing steps required to implement the distance protection relay for this investigation are outlined in Figure 6-24. More detailed logic diagrams are presented in Figure 6-25 to Figure 6-30 which provide further details about the implementation of the distance relay in software. It should be highlighted that distance protection relays are very complex and that the relay created through the steps presented in this section is simplified when compared to a commercial relay.

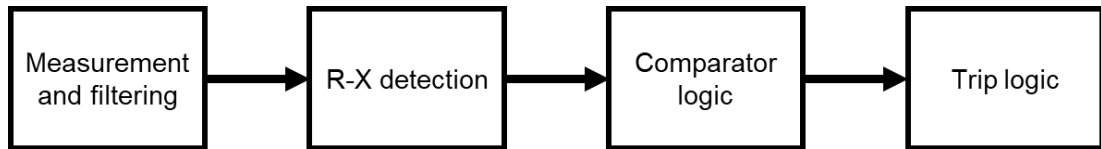


Figure 6-24: Summary of distance relay processing steps

Voltage and current quantities were initially measured and filtered using a standard low pass filter with a cut-off frequency of 100 Hz to remove unwanted harmonic content from these signals. The magnitude and angle of the voltages and currents were then calculated using a Fourier transform. Once the transform had been applied a complex division allowed the values for R and X to be determined.

The comparator subsystem within the distance protection relay was responsible for determining whether the calculated impedance resided inside or outside any zones of protection. Should the calculated impedance reside inside one (or more) of the operational zone(s) a signal was sent to the tripping logic. This logic determined whether the relay should trip immediately, trip with a time delay, or not trip at all.

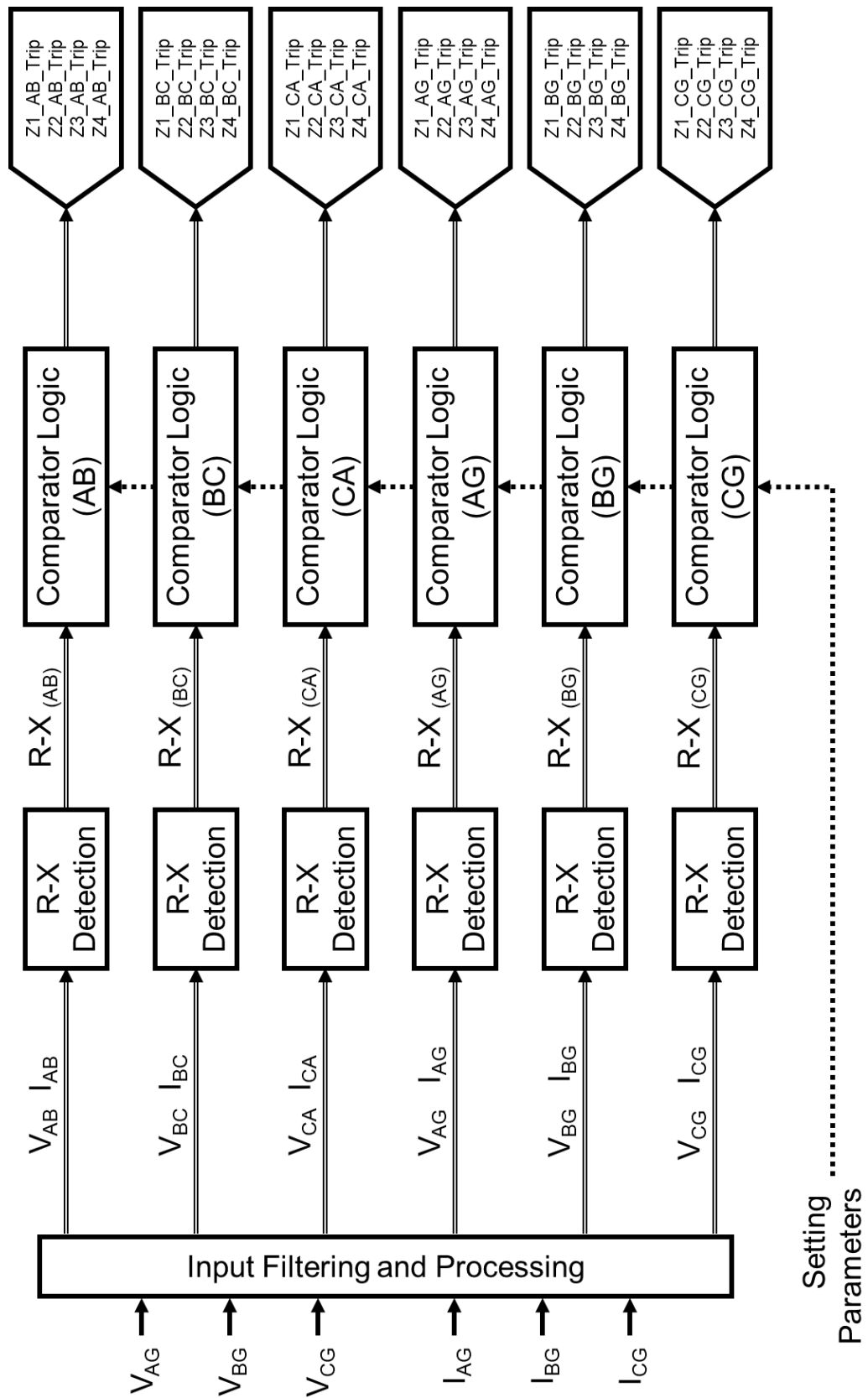


Figure 6-25: Distance protection relay design software flow diagram

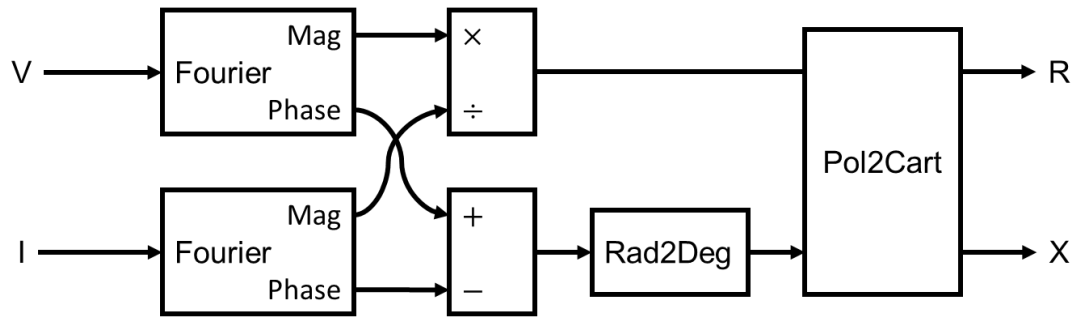


Figure 6-26: R-X detection subsystem

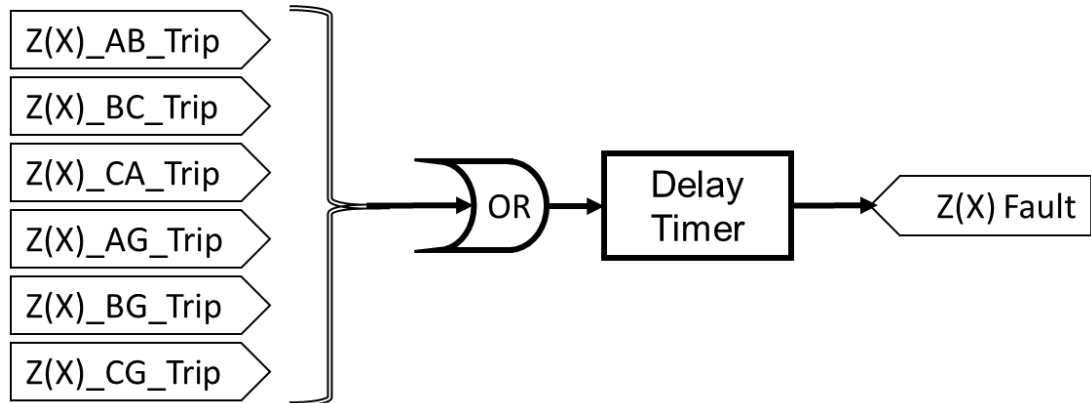


Figure 6-27: Trip logic for standard (Z1-Z3) zones including time delay

Note that the use of an 'AND' gate for the Z4 characteristic in Figure 6-28 means that the relay will not operate unless a Z4 fault is detected in all six comparators as discussed previously in Chapter 5.

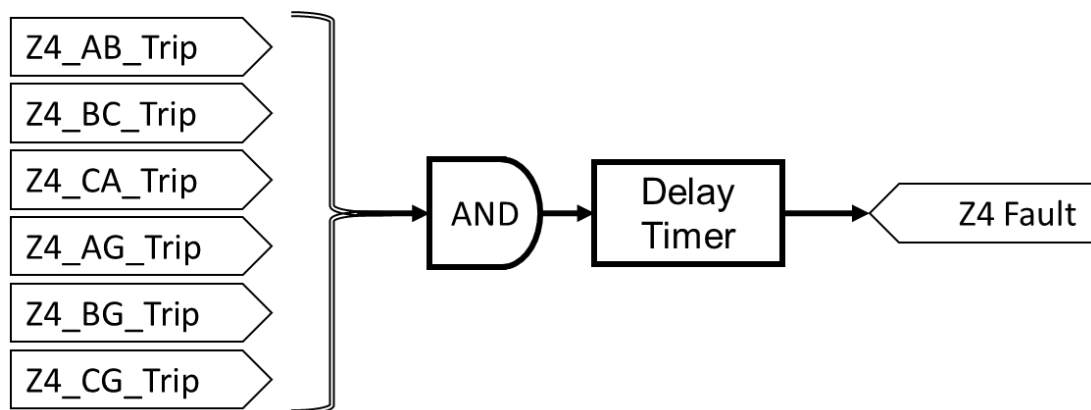


Figure 6-28: Zone 4 trip logic including cross-check

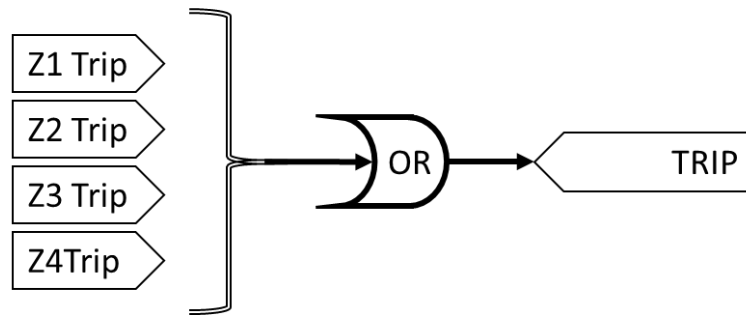


Figure 6-29: Trip output

The relay settings were input via user interface as outlined in Figure 6-30. The relay employed the standard Mho characteristic for Z1, Z2 and Z3 while Z4 used a customisable quadrilateral characteristic. The parameters for the standard operation mode were set by using an apparent impedance reach value and line angle. The quadrilateral characteristic for Z4 was defined via four coordinate points ($A(R)$, $A(X)$, $B(R)$, $B(X)$, $C(R)$, $C(X)$, $D(R)$, $D(X)$). Time delays for each operation zone could also be specified.

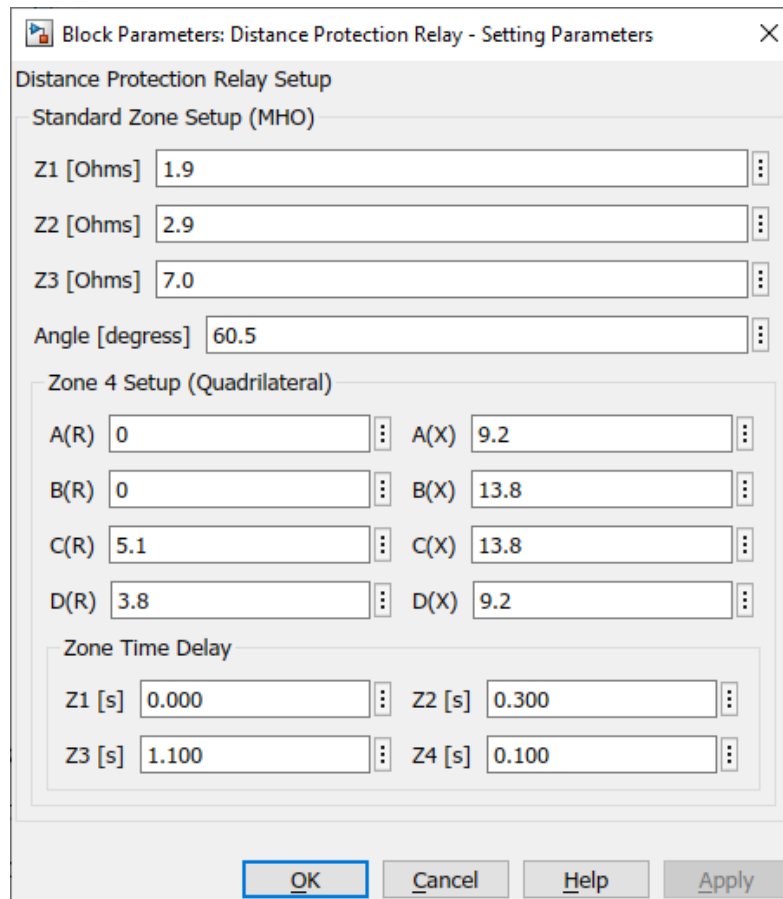


Figure 6-30: User interface for relay setting parameters

6.4.2.3 Modelling

As in previous investigations, the MVDC converter was modelled as a two-level, symmetrical monopole topology which employs standard P - Q , V_{DC} - Q control during normal operation (as outlined earlier in Figure 5-2). When a fault occurs on the DC link, the converter transitions to a protective mode where the switching of devices is blocked. A pre-fault power transfer of 25 MVA towards Converter Station B was established for all fault scenarios.

The test network is presented in Figure 6-31 with seven fault locations outlined (F1-F7) across the network along with the type of fault for F1-F4. Fault F4 was designed to test whether the fast-acting DC backup protection could be triggered by a symmetrical AC fault downstream of the 33:11 kV transformer. The remaining faults on the DC system were of pole-to-pole type and were applied at the terminals of both converter stations and at the midpoint of the DC link. All faults had a resistance of 0.1 Ω . Further network and converter modelling parameters are summarised in Table 6-11.

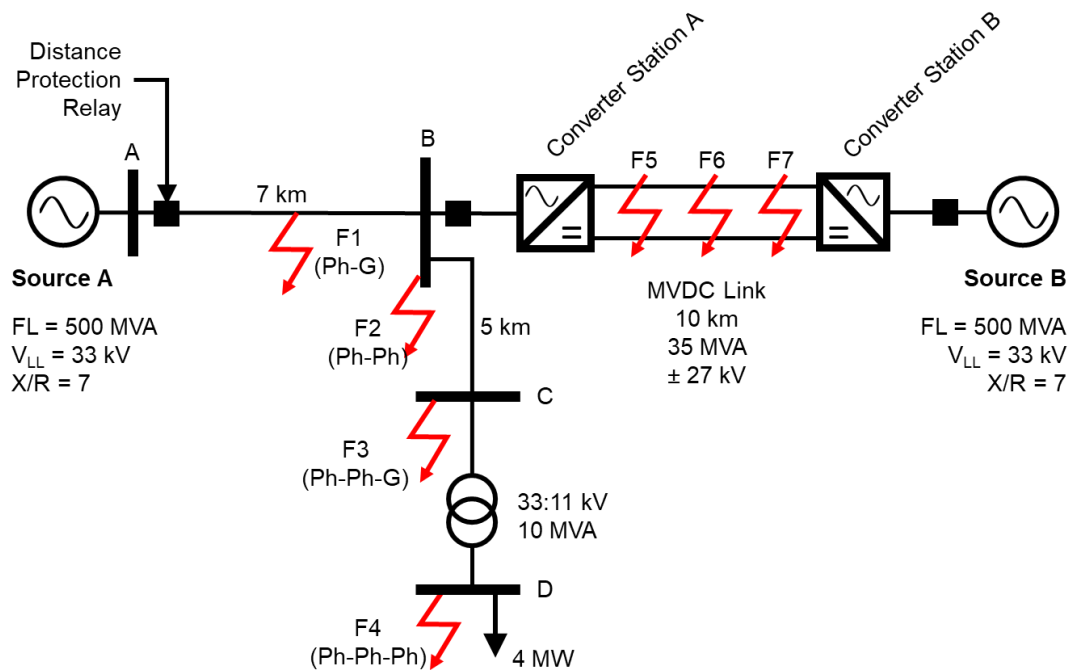


Figure 6-31: Test network with faults F1-F7

Table 6-11: Summary of modelled parameters

Parameter	Value
Line length A-B	7 km
Line length B-C	10 km
Conductor impedance	0.17 + j0.30 Ω/km
MVDC link line length	10 km
MVDC link voltage rating	± 27 kV
MVDC link power rating	35 MVA
MVDC filter impedance	10% (35 MVA base)
MVDC Transformer voltage rating	33:33 kV
MVDC Transformer power rating	35 MVA
MVDC Transformer impedance	20% (35 MVA base)
Transformer voltage rating	33:11 kV
Transformer power rating	5 MVA
Transformer impedance	8% (100 MVA base)

6.4.2.4 Relay Setting Parameters

For the network outlined in Figure 6-31 and Table 6-11, the settings for the original protection scheme, as described in Chapter 5, were calculated along with settings for the standard operating zones (i.e. Z1-Z3). The calculation of Z4 setting parameters are outlined in equations 6-7 to 6-10. Relay setting parameters are summarised in Table 6-12. Note that transformer winding resistance has been assumed to be negligible.

$$R_{Z4} = \sum[R_{Lac}, R_{Xfmr}, R_F, R_{Lac}] = (0.17 \times 7) + 0.3 + (0.17 \times 10) = 3.2 \Omega \quad 6-7$$

$$X_{Z4} = \sum[X_{Lac}, X_{Xfmr}, X_F] = (0.3 \times 7) + 6.28 + 3.14 = 11.5 \Omega \quad 6-8$$

$$\theta = \tan^{-1}\left(\frac{X_{Z4}}{R_{Z4}}\right) = \tan^{-1}\left(\frac{11.5}{3.2}\right) = 74.5^\circ \quad 6-9$$

$$Z4_{reach} = 1.2 \times \sqrt{R_{Z4}^2 + X_{Z4}^2} = 1.2 \times \sqrt{3.2^2 + 11.5^2} = 14.3 \Omega \quad 6-10$$

Table 6-12: Settings for fast-acting backup protection scheme outlined in Chapter 5

Parameter	Setting value
Mho angle (°)	60.5
Z4 quadrilateral angle (°)	74.5
Z1 reach (Ω)	1.9
Z2 reach (Ω)	2.9
Z3 reach (Ω)	7.0
Z4 reach (Ω)	14.3
Z4 resistive reach (Ω)	3.2
Z2 delay (s)	0.300
Z3 delay (s)	1.100
Z4 delay (s)	0.100

The coordinate setting points for the enhanced protection algorithm are calculated in equations 6-11 to 6-14 for the test network using the equations outlined previously in Table 6-10. The final settings for the R-X coordinate based distance protection algorithm are presented in Table 6-13.

$$X_A = X_D = 0.8 \times X_{Z4} = 0.8 \times 11.5 = 9.2 \Omega \quad 6-11$$

$$X_B = X_C = 1.2 \times X_{Z4} = 1.2 \times 11.5 = 13.8 \Omega \quad 6-12$$

$$R_D = 1.2 \times R_{Z4} = 1.2 \times 3.2 = 3.8 \Omega \quad 6-13$$

$$R_C = R_D + \frac{X_B - X_A}{\tan(\theta)} = 3.8 \times \frac{13.8 - 9.2}{\tan(74.5^\circ)} = 5.1 \Omega \quad 6-14$$

Table 6-13 Settings for R-X coordinate-based protection solution

Parameter	Setting value
Mho angle ($^{\circ}$)	60.5
Z1 reach (Ω)	1.9
Z2 reach (Ω)	2.9
Z3 reach (Ω)	7.0
Z4 A (Ω)	(0.0, 9.2)
Z4 B (Ω)	(0.0, 13.8)
Z4 C (Ω)	(5.1, 13.8)
Z4 D (Ω)	(3.8, 9.2)
Z2 delay (s)	0.3
Z3 delay (s)	1.1
Z4 delay (s)	0.1

6.4.3 Experimental Results

The trip times and associated tripping zone for the original protection solution and the R-X coordinate based protection method are presented in Table 6-14 for the seven fault scenarios. Faults are all applied at 0.5 s of simulation time. Figure 6-32 presents the times recorded by the real-time simulator for fault application, fault detection and trip time for fault F6 and the R-X based algorithm.

Table 6-14 Results for original and R-X tripping regions

Fault scenario	Expected Trip Zone	Original Method		R-X Coordinate Method	
		Trip Time (s)	Trip Zone	Trip Time (s)	Trip Zone
F1	Z1	0.519	Z1	0.519	Z1
F2	Z2	0.817	Z2	0.817	Z2
F3	Z3	1.616	Z3	1.616	Z3
F4	Z3	0.610	Z4	1.733	Z3
F5	Z4	0.610	Z4	0.613	Z4
F6	Z4	0.617	Z4	0.621	Z4
F7	Z4	0.622	Z4	0.627	Z4

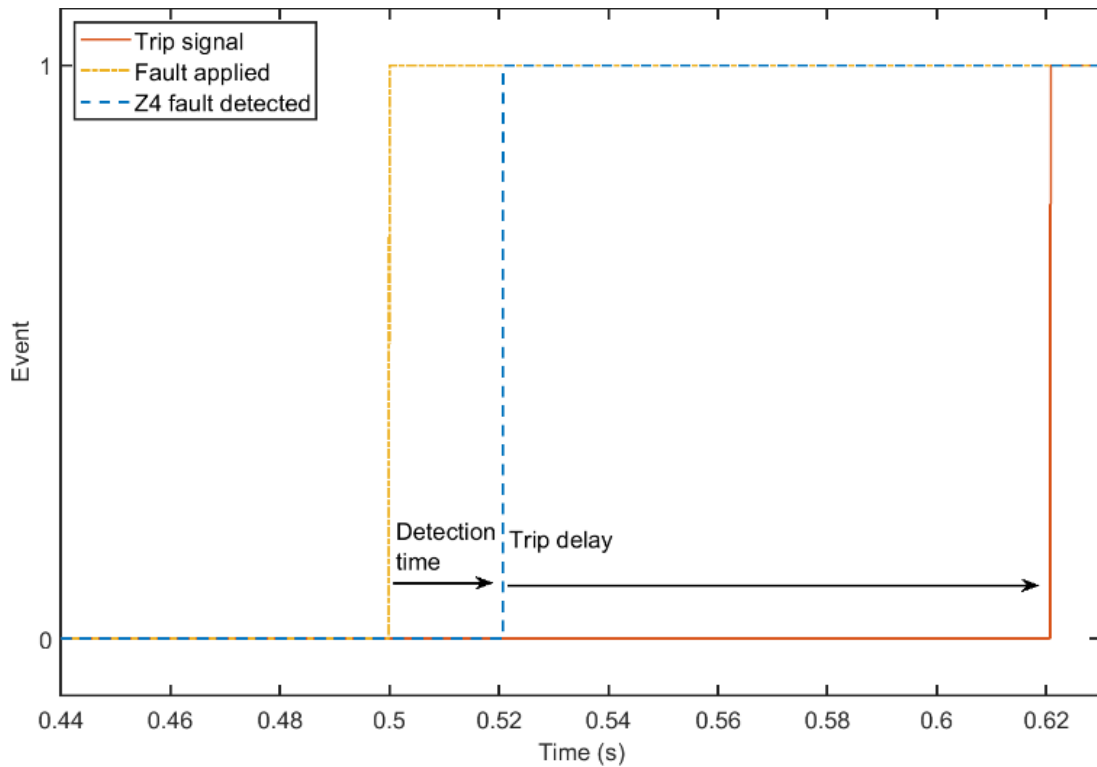


Figure 6-32: Fault inception and tripping times for fault scenario F6

From the results presented, it is observed that the original solution issues a Z4 trip for the event F4. This fault lies on the edge of Z3 and should be cleared by downstream protection devices, or by Z3 after a delay of 1.1 s. The R-X coordinate approach, however, correctly trips the Z3 comparator for fault F4 1.233 s after fault application. The R-X algorithm operates correctly for all tripping scenarios with all DC faults detected within 30 ms. During these experiments it has been assumed that the communication delay associated with sending signals between the real time simulation platform and the protection controller is negligible (i.e. <1 ms).

The tripping area of the original method was determined, via software, to be approximately $45.5 \Omega^2$ while the enhanced method was $20.4 \Omega^2$ as presented in Figure 6-33. This represents a reduction in the tripping area of 55%.

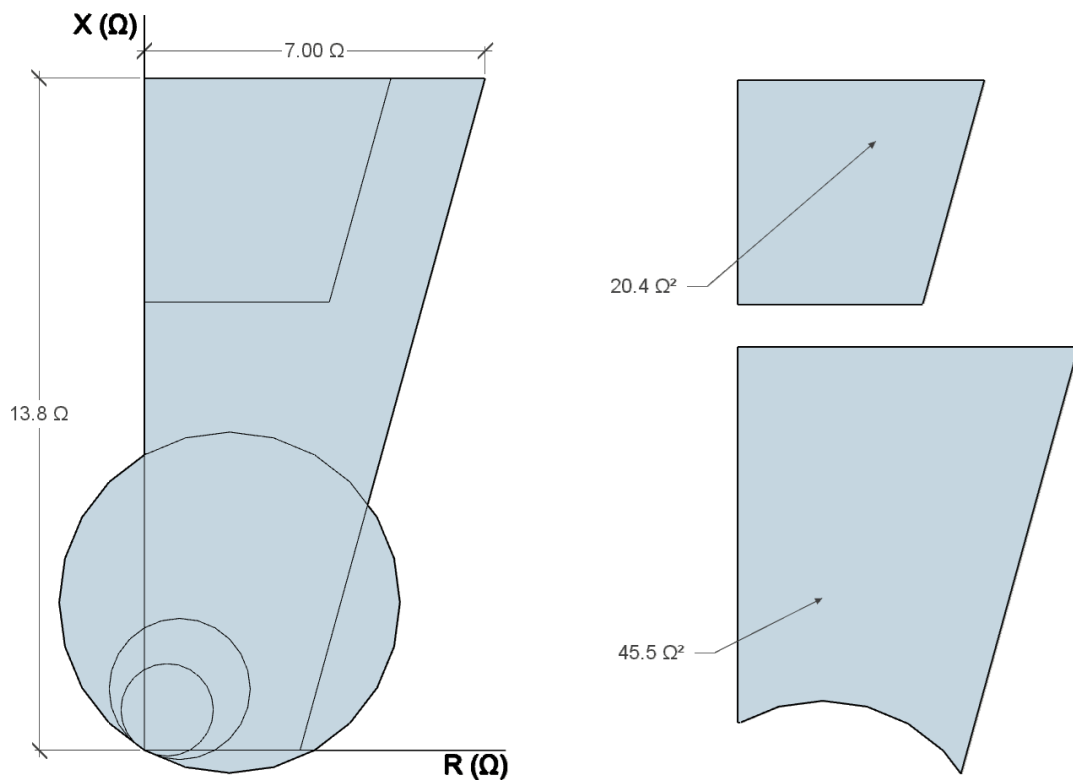


Figure 6-33: Z4 tripping area of original and R-X coordinate methods

6.4.4 Discussion

The R-X coordinate based setting approach has been demonstrated to detect accurately and respond to faults on an embedded MVDC link. The ability to implement the solution on low-cost hardware demonstrates that an R-X coordinate based setting system could be readily applied to commercially available protection relays in the future at minimal computational overhead.

This experiment has presented a method to increase the stability of the solution outlined in Chapter 5. The new method resulted in a reduction in tripping area of 55% for the test network when compared to the original solution.

It may be possible to extend the resistive reach of the Z4 region to provide protection for faults with higher resistance. The stability of this would need to be assessed for different network topologies and loading levels. Additionally, depending on the interruption time of the MVDC converter's CB, it may be possible to reduce the time delay for Z4.

6.5 Conclusions

This chapter has presented the results from three laboratory experiments designed to de-risk the fast-backup protection scheme outlined in Chapter 5.

The first experiment demonstrated that the simulated AC-side apparent impedance for DC-side faults is representative of the response expected from a physical system. The experiment used a low voltage test network where a maximum difference of 7.67% was found between computer simulations and the hardware test rig for the faults tested.

The use of commercially available numerical distance protection relays was trialled in the second experiment where correct tripping was observed for both AC and DC faults.

The final experiment aimed to reduce the fast-acting Z4 tripping area. The experiment employed a real time digital simulation platform which was used to playback a series of fault events. The R-X coordinate based protection algorithm was implemented on a low-cost computing platform (Raspberry Pi) which exchanged data with the real time simulation platform via a UDP network protocol. It was determined that the tripping area could be reduced by 55%, when compared to the original solution, while improving stability. Additionally, the test setup demonstrated that the R-X approach requires minimal computational effort and could potentially be implemented on a commercially available distance protection relay with minimal changes to relay firmware and configuration software required.

Chapter 7

Conclusions and Further Work

7.1 Conclusions

To facilitate reduced emissions and to enable the realisation of “net-zero” energy systems, power distribution networks must be able to host increased levels of embedded generation, demand and storage. MVDC is a candidate technology to enhance network utilisation by increasing power transfer capacities (for the same levels of voltage and insulation) and allowing more precise control over transfers of power between network sections. While DC technologies are being increasingly explored and deployed across all voltage levels, it has been shown through a literature review that a vulnerability exists in the backup protection of embedded MVDC links.

Backup protection to mitigate against DC-side faults on MVDC links is presently achieved via a direct transfer trip of a remote circuit breaker and therefore relies on a communications network rather than direct measurement of electrical parameters. Communication systems can introduce additional failure modes and are also often expensive to implement. Specifically, MVDC links are vulnerable if their protection scheme fails to detect or respond to a DC-side event and this could result in failure of the power electronic switching devices if not detected and cleared quickly enough.

In this thesis, a novel solution to the problem has been identified and demonstrated through simulation using verified distance protection relay models and via laboratory demonstrations. It has been shown that a fast-acting protection algorithm, which employs the commonly unused zone 4 setting parameters, can correctly identify and react to symmetrical DC faults. This fast-acting backup protection method does not require communications as is the case with current backup methods. No hardware changes to existing measuring apparatus are required to implement the solution.

Laboratory testing has confirmed that the physical response of an AC system during a DC fault matches the simulated response with further testing demonstrating that a commercially available relay could be configured to detect and respond appropriately to DC-side events.

The key conclusions of the works reported in this thesis are presented in the following subsections.

7.1.1 Analysis of DC Fault Impedance

Through simulation, it has been determined that symmetrical (i.e. PP and PPG) faults occurring on the DC-side of MVDC links present as highly inductive, in terms of the apparent impedance measured from the AC-side grid location. Additionally, the impedance appears balanced across all the individual phase to phase and phase to ground measurement elements. This impedance can be estimated via equations 7-1 and 7-2 outlined below.

$$R_{Z4} = \Sigma[R_{L_{ac}}, R_{X_{fmr}}, R_F, R_{L_{dc}}] \quad 7-1$$

$$X_{Z4} = \Sigma[X_{L_{ac}}, X_{X_{fmr}}, X_F] \quad 7-2$$

Note that pole-to-ground events on a symmetrical monopole arrangement present little observed change on the AC-system due to the grounding arrangement employed in their transformer and converter. The detection approach presented in these works is therefore only sensitive to symmetrical DC events.

7.1.2 Fast-Acting Backup Protection Scheme

From the analysis of the fault impedance, it has been found that the zone 4 tripping region of a standard numerical/digital distance protection relay could be employed, with additional fault detection logic, to provide suitable fast acting backup protection for an embedded MVDC link. A fast-acting trip should only be issued when the fault event appears across all six comparator measurements (i.e. AB, BC, CA, AG, BG and CG). Additional fault logic is required to maintain the stability of the relay under Z2 and Z3 faults as outlined in equation 7-3.

$$Z4_{TRIP} = \overline{Z3}.Z4 \quad 7-3$$

7.1.3 Hardware Verification of AC System Performance

A hardware test setup was designed and constructed to verify physically the characteristic impedance determined through software modelling. This test setup employed a low voltage, low current system where faults could be applied at either end of the DC link with a fault resistance of either 0 Ω or 1 Ω . The instantaneous values of voltage and current were recorded for several fault scenarios. Offline analysis allowed the impedance of the events to be calculated and compared against software simulation results. It was found that experimental results aligned with software simulation with a maximum error of 7.67% recorded. Given the

errors associated with the measurement apparatus and component tolerances, this error margin is deemed to be acceptable.

This experiment confirmed that a highly inductive impedance is to be expected on a physical system during a DC-side fault and therefore that the proposed protection approach is valid for non-fault blocking VSC converters.

7.1.4 Commercial Relay Demonstration

While the backup protection approach was confirmed through software simulation, which employed a validated model of a distance protection relay, it was also deemed important to demonstrate the method on a commercially available relay to show the applicability of the solution across different devices.

The test setup employed an injection amplifier and distance protection relay. A series of experiments concluded that the relay could be appropriately configured to detect (within 35 ms) and respond to DC-side events while remaining sensitive and stable to various AC zone faults. It was considered, however, that deploying a relatively large Z4 tripping area could be viewed as somewhat of a risk, especially with such a short tripping delay applied and that it may be beneficial to define the tripping region in terms of R-X coordinates. Accordingly, the scheme was refined as explained in the next section.

7.1.5 R-X Setting Approach

To reduce the large Z4 tripping area, an R-X setting approach was implemented on a low-cost compute platform and demonstrated in a real-time simulation environment. It was determined that the area of the Z4 trip region could be reduced, by 55% for the test network presented, while remaining stable for both conventional AC zone faults and for DC-side events. It is believed that this approach could be readily applied to existing distance protection relays via updates to the relay's firmware and configuration software.

7.2 Future Work

This thesis has identified a shortcoming in existing protection practice for DC systems connected both at high and medium voltage. The research recommends a method for detecting pole-pole(-ground) faults on a DC system from AC-side measurements and an associated fast-acting backup protection method. For such a system to be deployed as part of a protection solution there are a series of further research and demonstration tasks which require additional investigations. A summary of the initial future work packages in this area are identified in the following subsections.

7.2.1 Applicability to Other Converter Types

The research presented in this thesis has considered the use of a two-level symmetrical monopole converter arrangement as it represents one of the most cost effective and simplest methods to introduce controlled DC into AC distribution networks. More advanced MVDC converter topologies are available and require further investigation with regards to the AC-side response and measurement data that would be produced during a DC-side event. In theory, many converters such as the half-bridge MMC and the cascaded neutral point clamped converter have similar structures during fault conditions (i.e. similar to the symmetrical monopole as presented previously in Figure 5-1 for a HB-MMC). Therefore, the associated AC-side impedance should be similar between these topologies and the two-level symmetrical monopole arrangement used throughout the thesis for balanced DC-side faults. This assumption has been made by others working in this field of research [150].

7.2.2 Further Testing and Validation Activities

The experiments conducted during the research have investigated the following:

- the apparent impedance characteristics during a DC-side pole-to-pole event;
- the deployment of a fast-acting protection solution on a commercial distance protection relay based on voltage and current inputs from a software simulation model; and
- the development of a, user-configurable, R-X coordinate-based setting approach in a real-time environment.

The backup protection system investigated in this thesis has not been trialed in a closed, power HiL environment. In other words, the experimental trials have not involved the physical breaking of current during fault conditions to protect the converter. Future work in this area should aim to implement fully the solution in hardware (either at laboratory scale or in a field trial environment).

This may be achieved by using real-time measurements from the test platform developed previously in Section 6.2, passed either to the commercially available distance protection relay, such as in Section 6.3, or to the controller developed in Section 6.4. Trip signals from the protection relay should then be passed back to the physical test network to open a controllable circuit breaker (which may be implemented via a contactor in the laboratory environment) to disconnect the system in the event of a fault. An example of the proposed closed loop simulation is illustrated in Figure 7-1. This closed loop simulation approach should

also be applied to a full switching-based converter, rather than the simplified diode arrangement used in Section 6.2.

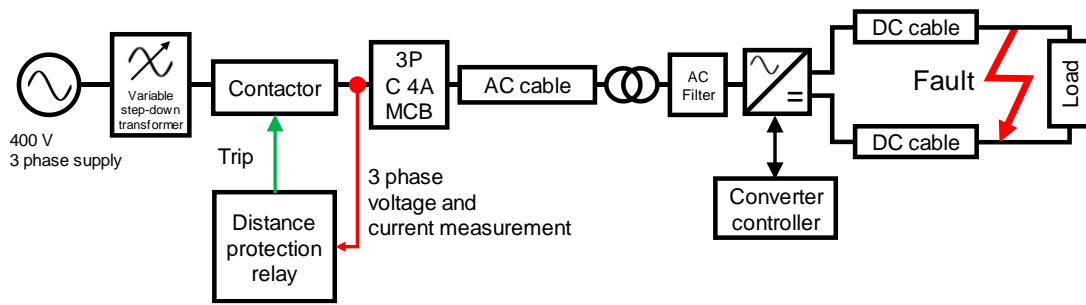


Figure 7-1: Proposed closed loop fault experimental setup

7.2.3 Converter Survival Time

Additional work is required to determine the survival time of an IGBT/diode device under fault currents expected in medium voltage applications. It has been assumed in this thesis that high-power, bypass thyristors are connected across the IGBT/diode arrangement within converters to handle fault currents during events – as is the case in some HVDC applications. More research is required to understand fully the critical failure time of the IGBT/diode devices to ensure that the fast-acting backup protection method can interrupt fault current in a suitable time. A tripping delay of 100 ms has been assumed, however it may be possible to reduce this delay time as the distance protection relays used in this thesis are able to detect the DC-side fault typically within two AC cycles.

7.2.4 Live Deployment

With the role of DC increasing in both the transmission and distribution systems, it would be interesting to deploy the protection scheme presented in this thesis on a live network - even if the trip signals from zone 4 were to be disabled. The author has experience of working for a TNO where sub-synchronous oscillation relays were installed at a windfarm where the trip contacts of the device were not connected to a circuit breaker. This allows the stability of the system under normal operation to be assessed and allowed for the fine tuning of setting parameters before live deployment. Another similar example of this was witnessed by the author during the commissioning of a multi-megawatt battery storage system (deployed under an enhanced frequency response (EFR) contract) where the response of the system was verified by the TSO operator with no power transferred between the battery and the grid.

With two innovation trials of MVDC being installed in the UK, both of which are connected at 33 kV with surrounding networks possibly already being protected by distance relays, there

is an opportunity to implement the protection approach on existing relays. This would provide valuable field data as to the performance of the method at low operational risk to the DNO should it not wish to send active trip signals to circuit breakers.

7.2.5 HVDC Back-Up Protection

The use of distance relays to provide backup protection for faults on an MVDC link has been considered in this thesis. While the approach appears to be valid for MVDC applications, the applicability to HVDC systems is not yet clear. In particular, the X/R ratio of transmission systems is generally higher than at distribution. It would therefore need to be determined if the standard protection zones already use the impedance region which is required for the fast-acting backup protection method.

It is unlikely that the approach outlined in the thesis will detect and respond quickly enough to be used for the protection of meshed, multi-terminal HVDC as protection times for these systems is an order of magnitude faster than the protection required for point-to-point applications.

7.2.6 Further Network Studies

The test networks presented in this thesis consist of small, but representative, sections of distribution network based on data from installed 33 kV systems. To understand the applicability of the solution developed during this research, faults and the protection approach should be investigated across a wider range of network topologies and asset impedances.

Finally, research is required to determine if the solution may be transferable to other distribution voltage levels - although in the UK distance protection is generally not deployed at voltages lower than 33 kV due to the lines being too short to provide accurately graded protection.

Supplementary Material A

MVDC Simulation Case Studies

A.1 Introduction

This appendix presents, via a series of load flow simulations, a selection of hypothetical case studies where MVDC links were introduced into existing distribution networks. Using two 33 kV network areas, the first being a rural region with high penetration of distributed generators and the second a large town, the introduction of controlled DC interconnectors was investigated with the aim of facilitating the uptake of future low-carbon demand and generation.

Section A.2 introduces the modelling methodology and highlights the data sources common to both investigations. The first case study is presented in Section A.3 and demonstrates how the introduction of relatively low capacity MVDC interconnectors can allow for significant increases in renewable generation capacity. Section A.4 presents the second case study. In this example an ‘inter-GSP’ ring is formed by placing MVDC converters across NOPs to allow the controlled transfer of power between three GSPs. This approach allows dynamic sharing of capacity across the region enabling future loads, such as high-power electric vehicle chargers, to be introduced using existing network infrastructure and wayleaves.

Section A.5 presents findings from the investigations while outlining some of the known regulatory integration challenges faced by the technology. Section A.6 summarises the findings of these MVDC integration case studies.

A.2 Modelling Methodology

The modelling conducted makes use of data extracted from the SP Energy Networks’ Long-Term Development Statement [56]. This document, produced annually, contains circuit data (e.g. conductor length, rating, resistance, inductance and susceptance etc.), transformer specifications, GSP loading statistics, and generation data for each ‘sub-region’ of their network. Reading these documents in parallel allows representative network models to be constructed in power system modelling software.

To conduct the case studies DIgSILENT PowerFactory 15 was employed due to the ease of implementing power electronic links and the speed at which large distribution networks can be created and simulated. The controlled MVDC links deployed in these case studies are all two terminal systems, i.e. a link is made up of one sending node and one receiving node. The control of these links is achieved via a P - Q controller at one converter station and a V_{DC} - Q control scheme at the other as is common in HVDC systems [257] [258] as per Section 5.2.2. If the power from the sending node was to be increased (via an increase of set-point at the P - Q controller), the voltage of the DC system would rise due to the charging of DC capacitances. The receiving end (V_{DC} - Q) controller detects the voltage increase and proportionately extracts more power from the link. Conversely, should the voltage of the DC link drop, the receiving end controller would reduce its power requirement until the DC side voltage returns to the system set-point.

For all DC conversion, it was assumed that existing AC conductors would be repurposed to DC with the thermal rating being equal to the existing AC rating. This means that any benefits gained from the introduction of controllable MVDC links were purely the result of increased system control. It is acknowledged that there are some interesting technical discussions surrounding the best way to repurpose AC wayleaves to a DC system especially with regard to conductor allocation, converter type and insulation coordination [232] [277].

Each converter station had an assumed fixed loss of 1% which represented switching, conduction and filtering losses associated with the power electronic converters. This loss figure is in line with losses expected from an HVDC converter station [278] [279].

All modelled primary transformers (33:11 kV) were capable of on-load tap changing with controllers set to a target voltage of 1 p.u at the 11 kV busbar as specified in ER P2/6 [280] and ER P2/8 [281]. The power output of generators was specified on a case by case basis to determine the hosting capacity of the network with, and without, MVDC interconnection. Loads were modelled as fixed real and reactive (constant power) demands at a voltage of 1 p.u.

For an acceptable solution to be found, all system voltages must be within $\pm 3\%$ of their nominal values while conductors must not exceed their continuous thermal rating.

A.3 Case Study 1: Increasing Renewable Capacity

A.3.1 Network Overview

Figure A-1 shows the test network for the initial case study. This region has significant levels of distributed renewable generation connected to various nodes across the area. The network consists of two GSPs, namely Coylton and Kilmarnock South, with the capacity of embedded generation connected downstream of the Coylton GSP exceeding the firm rating of the transformer, the firm rating of a substation being defined as the maximum demand that can be supplied when considering the failure of the largest transformer [282]. The network associated with Kilmarnock South GSP has significantly lower levels of generation than its counterpart but with a greater firm capacity.

Table A-1 outlines the ratings of the two GSPs and the amount of connected generation in each area. The table also highlights the amount of generation which had been allocated capacity by the DSO but which had not yet been connected to the system. This capacity was likely offered to generators under ‘non-firm’ connection agreements where the DSO may impose restrictions on generator output to maintain the system within operational limits [283]. Line lengths and winter continuous thermal ratings for the main distribution lines are presented in Table A-2. Thirteen primary substations are connected across the distribution network along with four large-scale windfarms. Parameters for these sites, including minimum and maximum demand and power ratings, are presented in Table A-3.

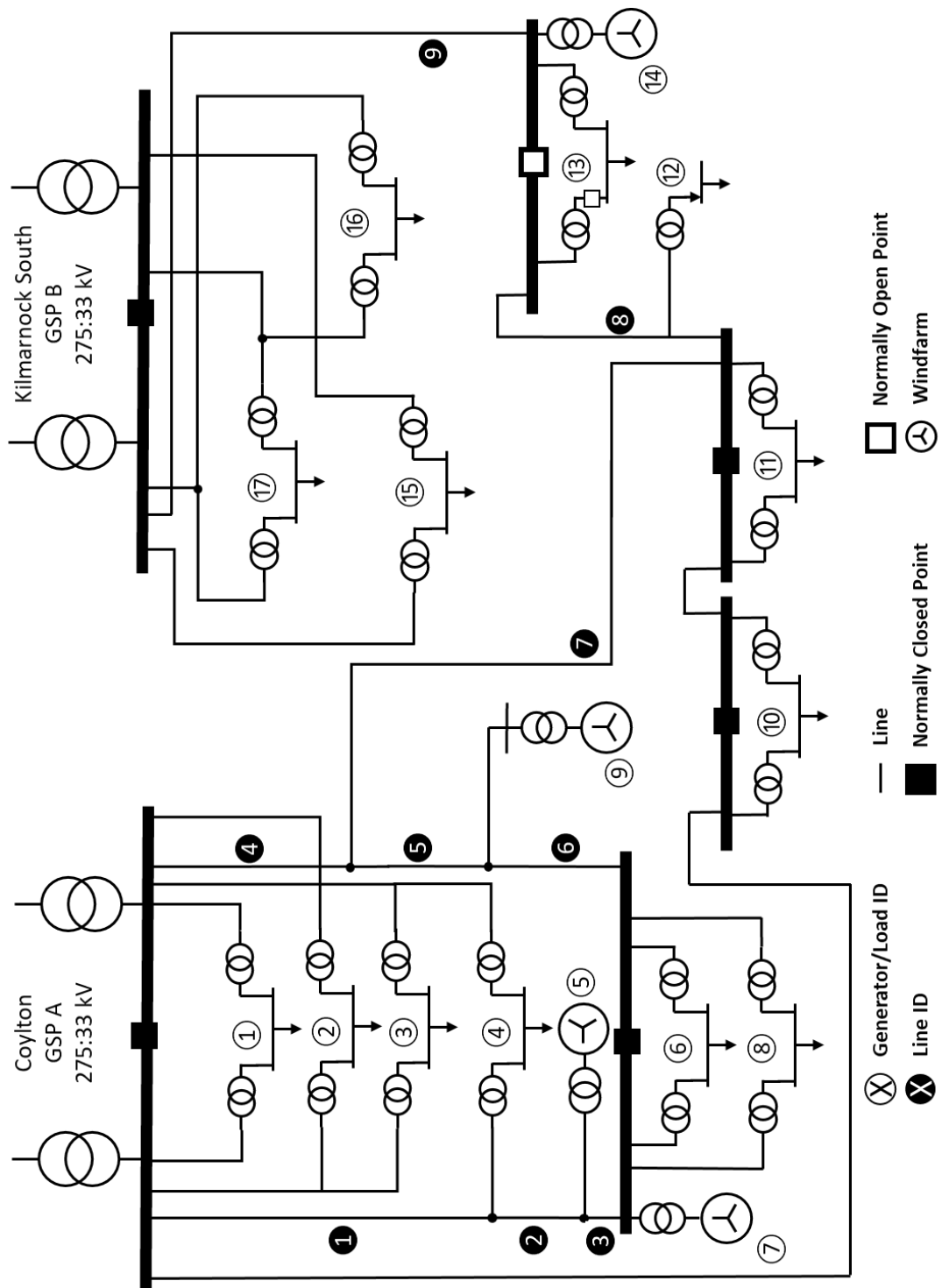


Figure A-1: Network topology for case study 1

Table A-1: Distributed generation connected and contracted to connect for associated GSP
[42]

GSP	Firm Capacity (MVA)	Connected (MW)	Contracted (MW)	Net Increase (MW)
Coylton	60	72.35	91.60	19.25
Kilmarnock South	120	16.10	30.40	14.3

Table A-2: Winter continuous thermal rating and circuit length for conductors [42]

Line	Rating (MVA)	Length (km)
①	20.86	8.01
②	38.81	8.48
③	41.2	0.01
④	38.81	6.29
⑤	29.43	13.68
⑥	20.86	0.025
⑦	20.86	6.25
⑧	24.63	12.56
⑨	20.86	0.21

Table A-3: Substation name, firm capacity, min/max loading and power factor for test network [56] [42]

ID	Name	Firm Capacity (MVA)	Maximum Apparent Power (MVA)	Minimum Apparent Power (MVA)	Power Factor
GSP A	Coylton	60	43.49	10.87	–
GSP B	Kilmarnock South	120	33.47	8.37	–
①	Lethanhill	10	4.08	1.02	0.98
②	Killoch	2	12.6	3.15	0.68
③	Cronberry	5	2.32	0.88	0.96
④	Cumnock	24	9.55	2.39	0.93
⑤*	Harehill WF	13	–	–	–
⑥	New Cumnock	5	2.78	2.39	0.76
⑦*	Harehill WF (ext)	33	–	–	–
⑧	Fauldhead	10	4.74	1.19	0.99
⑨*	Gallowrig WF	21.6	–	–	–
⑩	Drumley	10	6.7	1.67	1
⑪	Mauchline	10	5.7	1.44	0.99
⑫	Darvel	10	1.9	0.47	1
⑬	Newmilns	24	5.86	1.46	0.99
⑭*	Bankend Rig WF	14.3	–	–	–
⑮	Riverside	40	4.54	1.14	1
⑯	Monkton	21	13.35	3.34	0.99
⑰	Kilmarnock	24	15.14	3.79	0.99

* Denotes a generation node

A.3.2 Benchmark Studies

Initial load flows were conducted on the network section for minimum and maximum demand scenarios with all generators producing at 100% for both cases. 33 kV busbar voltages were all regulated to a voltage tolerance of $\pm 3\%$ of nominal as required. The percentage line loading for the lines under the two initial case studies are presented in Table A-4.

Table A-4: Key line loading for base network under maximum and minimum load

Line	Rating (MVA)	Loading (%)	
		Max Demand	Min Demand
①	20.86	42.2	37.2
②	38.81	60.3	60.3
③	41.2	25.7	26.6
④	38.81	70.4	82.9
⑤	29.43	131.9	142.7
⑥	20.86	75.8	91.8
⑦	20.86	59.2	47.4
⑧	24.63	8	1.9
⑨	20.86	40.4	59.3

Line ⑤ is the only recorded overload on the system and operates at 131.9% loading under the maximum demand conditions. This figure rises to 142.7% when network demands are at their minimum due to the power produced by distributed generation not being absorbed locally. The overload is partly due to the comparatively low impedance of this line when compared to neighbouring paths. Furthermore, lines ④ and ⑥ are also approaching their thermal limit under the minimum demand scenario.

While existing non-firm contractual mechanisms would manage the identified line overload, if curtailment becomes too great and occurs too frequently, then any prospective generators wishing to connect may deem the situation unworthy of investment. There is a case to be made that power flows must be managed more actively at distribution level to allow renewable and carbon targets to be met.

A.3.2.1 Introduction of MVDC Links

In looking for a solution to the overload of line ⑤, the line was converted to a symmetric monopole MVDC link operating at ± 27 kV similar to the Angle-DC MVDC implementation

[185]. The motivation behind this conversion was to limit the power passing through line ⑤ to its rated capacity. Line parameters were otherwise unchanged.

Simulations were conducted for both minimum and maximum demand scenarios with results presented in Table A-5. With the embedded DC link exporting 25 MW towards Coylton GSP, lines now remain within rated thermal capacity while voltages are within tolerance for the maximum demand scenario. However, at minimum demand, line ② records a 39.3% overload, essentially transferring the burden from line ⑤ to line ②.

Table A-5: Introduction of an MVDC link

Line	Rating (MVA)	Loading (%)			
		Base case		MVDC Line 5	
		Max Demand	Min Demand	Max Demand	Min Demand
①	20.86	42.2	37.2	24.1	20.3
②	38.81	60.3	60.3	91.6	139.3
③	41.2	25.7	26.6	53.3	98.2
④	38.81	70.4	82.9	34.8	55.0
⑤	29.43	131.9	142.7	84.3	99
⑥	20.86	75.8	91.8	22.6	42.2
⑦	20.86	59.2	47.4	54.9	36.3
⑧	24.63	8	1.9	8.2	1.9
⑨	20.86	40.4	59.3	40.4	59.3

A back-to-back converter rated at 20.8 MW was connected across the 33 kV normally open bus coupler, often referred to as a soft normally open point (SNOP) or a soft open point (SOP) [284], at bus ⑬ (Figure A-2) to alleviate the minimum load, maximum generation congestion identified on line ②. Two load flow calculations were conducted for both maximum and minimum demand with embedded link transferring 25 MW towards Coylton in both cases and the SNOP transferring 11 MW into the Kilmarnock South region for maximum system loading and 9 MW under minimum loading. The introduction of the SNOP combined with the embedded MVDC link allow all distributed resource to connect under minimum and maximum demand while operating within continuous line ratings and voltage limits. The conductor percentage loading figures for these studies are presented in Table A-6.

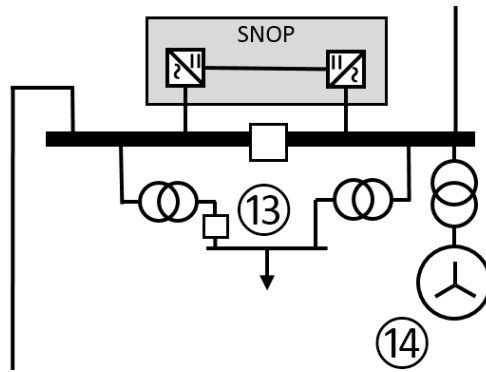


Figure A-2: 33kV SNOP connecting Coylton GSP to Kilmarnock South GSP

Table A-6: Loading results after the introduction of MVDC and SNOP

Line	Rating (MVA)	Loading (%)					
		Base case		MVDC Line 5		MVDC SNOP & MVDC Line 5	
		Max Demand	Min Demand	Max Demand	Min Demand	Max Demand	Min Demand
1	20.86	42.2	37.2	24.1	20.3	37.5	21.5
2	38.81	60.3	60.3	91.6	139.3	91.6	92.4
3	41.2	25.7	26.6	53.3	98.2	53.3	54.4
4	38.81	70.4	82.9	34.8	55.0	17.3	29
5	29.43	131.9	142.7	84.3	99	84.3	84.3
6	20.86	75.8	91.8	22.6	42.2	22.6	22.4
7	20.86	59.2	47.4	54.9	36.3	89.7	66.4
8	24.63	8	1.9	8.2	1.9	64.4	44.2
9	20.86	40.4	59.3	40.4	59.3	88.0	97.7

A.3.3 Facilitating an Increase in Renewable Generation

Analysis was carried out to investigate if the network could accommodate the additional generation seeking to connect (as described in Table A-1). A 20 MVA generator was connected at the junction between lines 4, 5 and 7 with a 15 MVA generator connected to the primary side of busbar 11. Load flow studies were carried out for the system with and without the MVDC links, outlined previously, for the minimum demand scenario. Line loadings for these studies are presented in Table A-7.

Table A-7: Results: line loading of base network and enhanced DC network under minimum system load

Line	Rating (MVA)	Loading (%)	
		Minimum demand	
		Base	MVDC Link and SNOP
①	20.86	53.7	44.6
②	38.81	64.6	92.4
③	41.2	30.3	54.4
④	38.81	118.3	95.6
⑤	29.43	137.5	84.3
⑥	20.86	83	22.4
⑦	20.86	65.9	32.6
⑧	24.63	1.9	41.1
⑨	20.86	124.2	81.4

While some lines are approaching their continuous thermal rating, the introduction of controlled MVDC links allowed the connection of 122 MVA of distributed generation on a network which could not support the presently installed 88.5 MVA. This represents a capacity release of more than 33.5 MVA without installing or uprating any conductors on the system.

A.3.4 Result Discussion

From this initial case study, the introduction of MVDC has improved the hosting capacity of the network by introducing power flow control into the network. This study was purely a load flow investigation and did not consider network security and redundancy metrics. This aside, the introduction of controllable MVDC appears to be a promising technology to increase the levels of renewable energy using existing AC conductors.

A.4 Case Study 2: Increasing Network Utilisation

A.4.1 Network Overview

Figure A-3 presents the single line diagram for the second case study. This network consists of eleven primary substations distributed across the region with ratings of between 21 MVA and 24 MVA. All lines had a winter maximum continuous rating of 20.86 MVA other than line 9 at 36.9 MVA. The network, based on real data, represents a suburban distribution network found in central/southern Scotland.

Table A-8 outlines the operating properties for the three GSPs in the region. A summary of the ratings and type of generators connected to the network can be found in Table A-9.

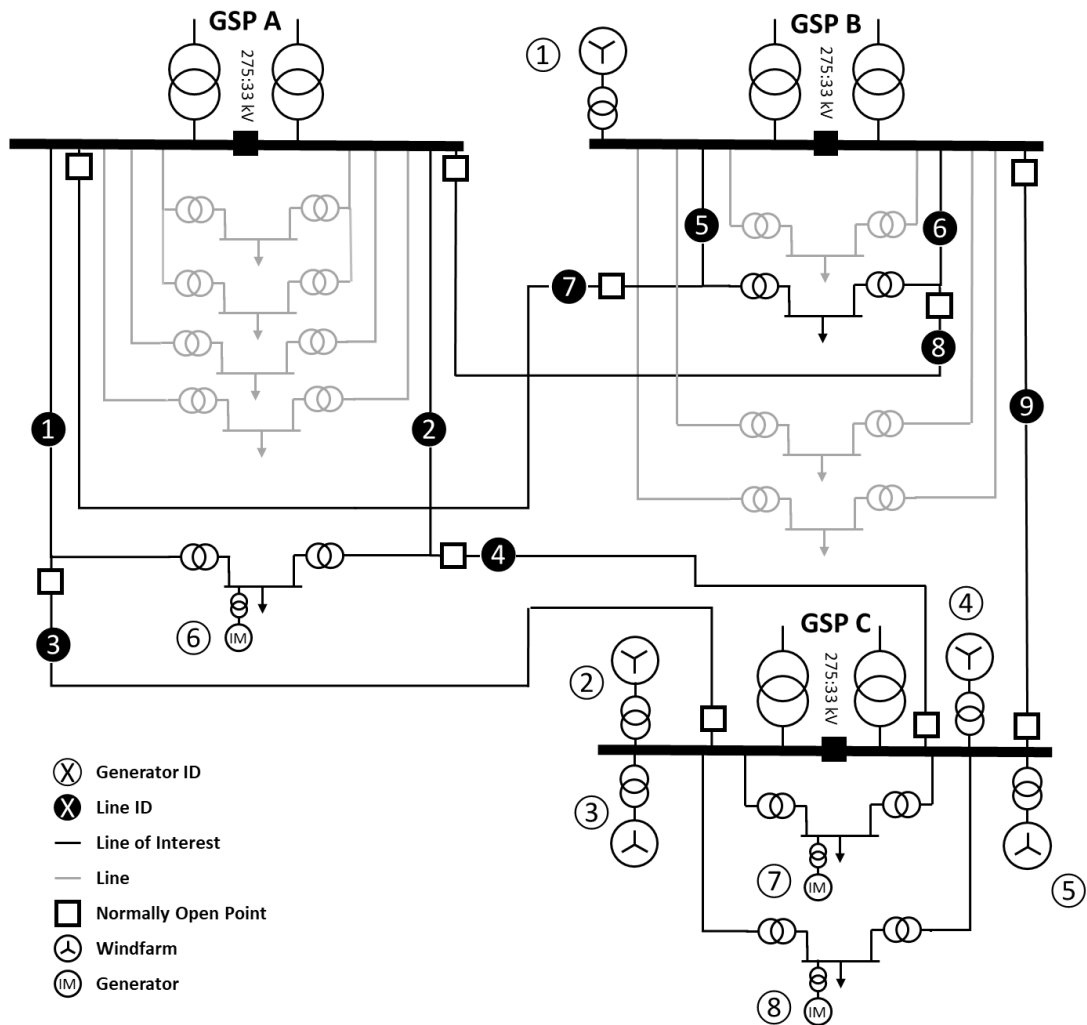


Figure A-3: Simplified distribution network comprising of three GSP all of which are interconnected via normally open points.

Table A-8: GSP properties

ID	Electrical Properties		
	Maximum Continuous Firm Rating (MVA)	Connected DG (MVA)	Mean GSP Loading (2016) (MVA)
A	120	0.5	34.2
B	120	12.3	23.6
C	120	110.3	-21.8 ^a

a. Negative values indicate an exporting node

Table A-9: Power rating of DG

ID	DG Rating (MVA)	Type
①	12.3	Onshore Wind
②	26	Onshore Wind
③	30	Onshore Wind
④	11.5	Onshore Wind
⑤	39	Onshore Wind
⑥	0.5	Run of River Hydro
⑦	2	Waste Incineration
⑧	4.2	Waste Incineration

Lines ③, ④, ⑦, ⑧ and ⑨ all represent normally open assets which provide N-1 security by interconnecting the three grid supply points within the network area. Conductors ⑦/⑧ and ③/④ form double circuit overhead routes while line ⑨ is a single circuit. As alluded to previously, these lines exist predominantly for fault restoration and maintenance purposes. Were these assets to be connected to the network, by closing of the NOPs, under normal operation, it is likely that the fault level would be greater than the designed limit of 1,000 MVA [15]. During normal operation these assets essentially sit idle and may be considered financially as ‘part-stranded’. (It is worth re-iterating that these assets are required by DNOs to meet network security standards set by the regulator and as part of their operating licence). In this investigation it was proposed that these non-load carrying assets be used to form an inter-GSP balancing network across the region using MVDC technologies.

A.4.2 Benchmark Studies

Using load and generation data for the distribution network, five deterministic benchmark studies (*a-e*), listed subsequently, were modelled to understand the network behaviour prior to introducing MVDC links into the system.

- a) Maximum demand and maximum generation.
- b) Minimum demand and maximum generation.
- c) Minimum demand and minimum generation.
- d) Maximum demand and minimum generation.
- e) Maximum demand (2040) and minimum generation.

Maximum generation scenarios assumed that all generators were producing at full power output resulting in 125.5 MVA of generation connected across the network. For minimum generation it was assumed all units were at zero output. Line and GSP loading percentages for the outlined scenarios are presented in Table A-10. The 2040 demand level for scenario *e* was in line with the 20% demand increase prediction made by the system operator, National Grid [285].

Table A-10: Network loading by scenario (negative indicates an exporting GSP)

Asset	Scenario				
	Percentage Asset Loading (%)				
	<i>a</i>	<i>b</i>	<i>c</i>	<i>d</i>	<i>e</i>
A	54.9	13.2	13.7	55.4	66.9
B	35.2	1.0	10.5	44.8	55.3
C	-83.0 ^a	-93.0	3.3	13.8	16.7
1/2	39.1	8.1	9.3	40.7	50.7
3/4	–	–	–	–	–
5/6	17.6	4.3	4.3	17.6	21.3
7/8	–	–	–	–	–
9	–	–	–	–	–

a. Negative values indicate an exporting node

While GSP A and B are lightly to moderately loaded for all scenarios, GSP C has a wide range of operation points from nearly full export to low levels of import depending upon the state of the embedded wind generation.

Using the existing normally open interconnection, the following section examines the possibility of increasing network capacity by repurposing the ‘part-stranded’ assets, identified earlier, to controlled MVDC links. The key benefit of this approach being that power can be dynamically balanced across the three GSPs without increasing system wide fault level.

A.4.3 Interconnection of GSPs via MVDC

Through conversion of the lines as outlined in Figure A-4, three MVDC symmetrical monopole links operating at ± 27 kV were inserted into the model to create an inter-GSP ‘balancing’ network. (Note that generation and primary substations were removed from the diagram for clarity purposes but remained connected for network studies). Switching losses were assumed to be fixed at 1% of converter load.

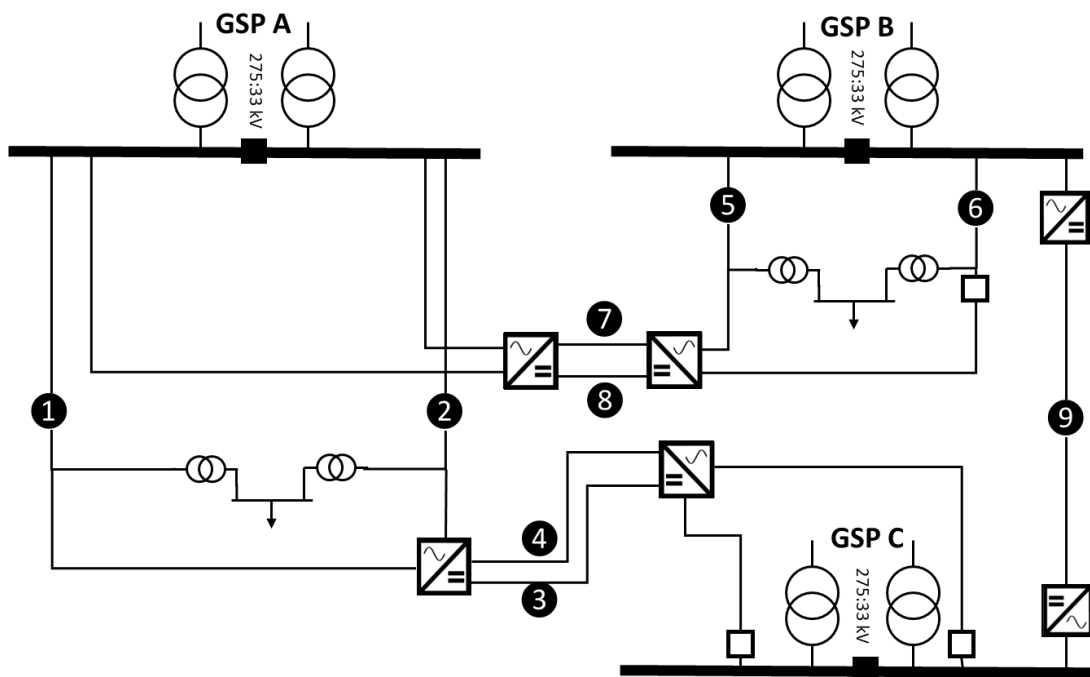


Figure A-4 - Network showing MVDC interconnection between GSPs.

As with the studies presented in Section A.3, the conductor ratings of DC assets were not increased – therefore, any benefit experienced by introducing controlled power electronic links was a result of increased network control. Note that because circuits 3/4 and 7/8 were double circuit overhead lines, the circuit ratings were combined when modelling to form a circuit with twice the capacity of the continuous AC winter rating (i.e. 2×20.86 MVA = 41.72 MVA).

Load flow studies for the following scenarios (*f-i*) were performed with the three MVDC links installed on the network. Results from the studies are displayed in Table A-11.

- f) Minimum demand and maximum generation with GSP export to be balanced across the region. i.e. each GSP aims to export the same power.
- g) Maximum demand and 99 MVA increase in renewable generation at GSP C such that the MVDC converters are at full export and that GSP C has reached its firm capacity.
- h) Minimum demand and increased renewables generation (of 87 MVA) at GSP C such that the MVDC converters are at full export and that GSP C has reached its firm capacity.
- i) A 40 MW point load, interfaced with an inverter, placed midway along the DC link ③/④ fed equally from GSP A and C under minimum demand and maximum generation conditions.
- j) Same scenario as *i* but with an additional 40 MW point load situated mid-way on DC link ⑨.

Table A-11: MVDC Balancing Network Studies

Asset	Scenario				
	Percentage Asset Loading (%)				
	<i>f</i>	<i>g</i>	<i>h</i>	<i>i</i>	<i>j</i>
A	-25.2	22.3	10.4	30.2	30.1
B	-25.4	8.5	-29.7	1.0	17.4
C	-27.5	-100	-100	-71.8	-55.2
①/②	89.4	64.1	89.4	56.9	56.9
③/④	100.0	100.0	100.0	50.0	50.4
⑤/⑥	16.4	17.6	4.3	4.3	4.3
⑦/⑧	21.1	0.0	0.0	0.0	0.0
⑨	100.0	100.0	100.0	0.0	54.4

A.4.4 Result Analysis

Study *f* demonstrates that MVDC interconnection allows dynamic sharing between GSPs to minimise export from the distribution network to the transmission system. This could be used to manage a planned or forced transmission system outage for example.

Studies *g* and *h* show that the creation of additional export capacity at GSP C via the controlled interconnection between GSPs A and C, to allow for further DG to be connected to the system. While keeping within the firm capacity of GSP C, under maximum generation and minimum demand scenarios, an additional 87 MW could connect to the system. Studies *i* and *j*

demonstrate that large point loads, such as large-scale EV charging hubs, could connect to the network and could be dynamically supplied from multiple GSPs.

Power flow analysis has quantified that inter-GSP MVDC allows for increased penetration of distributed generation – for the network studied an additional 99 MW of DG could connect during maximum demand periods and 87 MW under minimum demand. The use of existing ‘part-stranded’ assets, used for redundancy purposes, represents a promising solution to deliver additional network capacity using existing conductor wayleaves.

A.5 Discussion of Findings

The aim of the simulations presented in this appendix chapter has been to support the maximum amount of distributed generation on the network without operating network assets beyond their operational limits while avoiding curtailing generation. Security of supply requirements have not been considered within the modelling of the networks.

Using controlled MVDC links, the future DSO will have the ability to load a distribution network more dynamically to allow significant increases in power flows whilst not exceeding the firm capacity of grid supply point transformers. While conventional interconnection may offer some benefits, the lack of controllability of such largely passive grids means that the power flows are dictated by the ‘impedance map’ of the network.

While MVDC still has several technical and commercial barriers to becoming a ‘business as usual’ approach to network reinforcement, this appendix chapter has demonstrated the potential of the technology for unlocking latent capacity without adding ‘more copper’ to the network.

For simulation purposes it was assumed that line ratings remained the same under a DC conversion. In three-wire schemes the direct conversion to a two-wire DC yields a similar theoretical maximum power rating as AC. When converting a three-wire AC system into a two-wire DC system, a conductor is effectively left unused. The question remains open as to whether this third conductor could be more optimally used such as in the three-wire bipolar topology proposed in [286].

In Case Study 2, if the three MVDC links were introduced to the test network, the direct translation of costs would be £7.6 million for each of the double circuit lines and £7 million for the single circuit based upon the Angle-DC implementation cost. While it is appreciated that this is a rudimentary calculation, a £22 million investment is clearly a significant expense for a DSO.

Existing grid infrastructure is generally financially discounted over an operational time of many decades (30 to 40 years being commonplace). With power electronic machine drives, which often form the building blocks of MVDC systems, perhaps having a manufacturer warranty of five years, there is a challenge for DSOs and the system regulator, should MVDC solutions become more prevalent, in setting a commercially and technically appropriate target discount period. Modularity in design and confidence in the futureproofing of MVDC deployments is therefore critical to take MVDC from an innovation level to business as usual.

The simulations presented in this appendix chapter do not represent an optimal network solution but merely demonstrate the advantages of introducing controlled interconnection. Several other options exist which could take advantage of ‘part-stranded’ assets which interconnect GSPs. This approach may allow network operators to more quickly increase network capacity while avoiding the challenges of conventional AC reinforcements as outlined in Chapter 1. The electricity regulator in the UK has funded DNO investigations in the use of fault current limiters [25], distribution quadrature boosters [26] as well as the ‘soft normally open point’ [27] (a back-to-back converter topology) in the hope that latent capacity can be released on distribution networks at least cost to the consumer.

A.6 Conclusion

Existing distribution networks are under pressure due to increased embedded generation and demand patterns that are changing, and will be increasing, due to the electrification of transport and heating. The two case studies presented, based on network sections operated by the DNO SP Energy Networks, highlight the congestion that is now typical in rural and urban distribution networks in Scotland.

Power flow analysis using DIgSILENT PowerFactory 15 has demonstrated that assets may be operating outside of their thermal and/or voltage limits in places yet are underutilised elsewhere. This suggests that increased control of power flows is required - something that is challenging using conventional passive AC solutions.

The case studies presented have focussed on operating assets within thermal and voltage limits – and in that context, results are encouraging. Power quality and security factors have not been addressed and neither have the relative costs compared to conventional AC reinforcement.

These studies have set out the case for interconnection and consider the benefits of actively managing line loading and power flows. Design of present-day distribution networks and the

challenges faced by DNOs (and by DSOs in the future) in managing the increase of load and generation upon their system have been presented.

If power flows could be managed more effectively there is an opportunity to exploit existing infrastructure more fully, rather than constraining valuable renewable resource, without adversely affecting fault level as would be the case with traditional topologies.

References

- [1] Alstom Grid, HVDC for beginners and beyond, Alstom Grid, 2010.
- [2] IEEE/PES Transmission and Distribution Committee, “Existing HVDC Projects Listing,” IEEE HVDC and FACTS Subcommittee, 2013. [Online]. Available: <http://www.ece.uidaho.edu/hvdcfacts/Projects/HVDCProjectsListing2013-existing.pdf>. [Accessed 05 May 2017].
- [3] ARUP, “DC Power,” [Online]. Available: https://www.arup.com/-/media/arup/files/publications/f/5-minute-guide_dc-power.pdf. [Accessed September 2019].
- [4] Zap Map, “Charging Basics,” 02 December 2015. [Online]. Available: <https://www.zap-map.com/charge-points/basics/>. [Accessed 03 December 2015].
- [5] Zap Map, “Charging Point Statistics 2017,” 08 May 2017. [Online]. Available: www.zap-map.com/statistics. [Accessed 08 May 2017].
- [6] DC Systems, “Port of Amsterdam Smart Public Lighting on DC,” 2017. [Online]. Available: <https://dc.systems/projects/8-main/129-port-of-amsterdam-smart-public-lighting-on-dc-grid>. [Accessed September 2019].
- [7] SP Energy Networks, “LV Engine,” November 2017. [Online]. Available: https://www.ofgem.gov.uk/system/files/docs/2017/11/lv_engine_2017_nic_full_resubmission_-_clean_redacted.pdf. [Accessed September 2019].
- [8] DC Systems, “DC and sustainability in the Greenhouse,” 2011. [Online]. Available: <https://dc.systems/projects/8-main/157-dc-and-sustainability-in-the-greenhouse>. [Accessed September 2019].
- [9] Mark Murrill; B.J. Sonnenberg, “Evaluating the Opportunity for DC Power in the Data Center,” Emerson Network Power Energy Systems, Warrenville, Illinois, USA, 2010.

- [10] B. R. Shrestha, U. Tamrakar, T. M. Hansen, B. P. Bhattarai, S. James and R. Tonkoski, "Efficiency and Reliability Analyses of AC and 380 V DC Distribution in Data Centers," *IEEE Access*, vol. 6, pp. 63305 - 63315, 2018.
- [11] Scottish Government, "Energy in Scotland," Scottish Government, 2018.
- [12] SP Energy Networks, "Investment & Innovation," SP Energy Networks, February 2018. [Online]. Available: https://www.spenergynetworks.co.uk/pages/interactive_investment_map_gis.aspx.
- [13] V. Simonds and B. Hall, "Overcoming grid connection issues for community energy projects for Co-operatives UK and The Co-operative Group," Cornwall Energy, 2013.
- [14] H. Zayandehroodi, A. Mohamed, H. Shareef and M. Mohammadjafari, "Impact of distributed generations on power system protection performance," *Journal of the Physical Sciences*, vol. 6, no. 16, pp. 3873-3881, 2011.
- [15] W. El-Khattam and T. S. Sidhu, "Resolving the impact of distributed renewable generation on directional overcurrent relay coordination: A case study," *IET Renewable Power Generation*, vol. 3, no. 4, pp. 415-425, 2009.
- [16] D. Tzelepis and A. Dyśko, "Impact of distributed generation mix on the effectiveness of islanded operation detection," in *Sixth Protection, Automation and Control World Conference (PAC World)*, Glasgow, Scotland, 2015.
- [17] Adrianti and A. Dyśko, "Risk assessment analysis to find optimum ROCOF protection settings," in *12th IET International Conference on Developments in Power System Protection (DPSP)*, Copenhagen, Denmark, 2014.
- [18] C. Ten and P. Crossley, "Evaluation of ROCOF Relay Performances on Networks with Distributed Generation," in *IET 9th International Conference on Developments in Power System Protection (DPSP)*, Glasgow, UK, 2008.
- [19] National Grid ESO, "Electricity Ten Year Statement," November 2019. [Online]. Available:

- <https://www.nationalgrideso.com/document/157451/download>. [Accessed 19 April 2020].
- [20] K. Bell, “What happened to our electricity system on Friday August 9th 2019?,” UK Energy Research Centre, 14 August 2019. [Online]. Available: <http://www.ukerc.ac.uk/news/what-happened-electricity-system-fri-aug-9-2019.html>. [Accessed 18 April 2020].
- [21] DCODE, “DC0079 Frequency Changes during Large Disturbances and their Impact on the Total System,” 17 October 2017. [Online]. Available: http://www.dcode.org.uk/assets/uploads/Report_To_the_Authorityv3_1.pdf. [Accessed 18 April 2019].
- [22] J. Morren and S. D. Haan, “Impact of distributed generation units with power electronic converters on distribution network protection,” in *IET 9th International Conference on Developments in Power System Protection (DPSP 2008)*, Glasgow, UK, 2008.
- [23] F. Coffele, C. Booth, A. Dyśko and G. Burt, “Quantitative analysis of network protection blinding for systems incorporating distributed generation,” *IET Generation, Transmission & Distribution*, vol. 6, no. 12, pp. 1218 - 1224, 2012.
- [24] F. Coffele, Adaptive Protection Solutions for Future Active Power Distribution Networks, Glasgow, Scotland : University of Strathclyde, 2012.
- [25] United Nations Framework Convention on Climate Change, “Paris Agreement,” United Nations, Paris, France, 2015.
- [26] T. Macalister, “Longannet power station closes ending coal power use in Scotland,” *The Guardian*, 24 March 2016. [Online]. Available: <https://www.theguardian.com/environment/2016/mar/24/longannet-power-station-closes-coal-power-scotland>. [Accessed 15 March 2020].
- [27] F. MacDonald, “Goodbye to Cockerzie power station, a cathedral to coal,” *The Guardian*, 24 September 2015. [Online]. Available: <https://www.theguardian.com/uk-news/scotland-blog/2015/sep/24/goodbye-to-cockerzie-power-station-a-cathedral-to-coal>. [Accessed 15 March 2020].

- [28] J. Ambrose, “UK firm announces plans for first 'liquid to gas' cryogenic battery,” *The Guardian*, 21 October 2019. [Online]. Available: <https://www.theguardian.com/environment/2019/oct/21/uk-firm-highview-power-announces-plans-for-first-liquid-to-gas-cryogenic-battery>. [Accessed 18 March 2020].
- [29] Surf 'N' Turf, “Controllable Clean Energy,” Surf 'N' Turf, [Online]. Available: <http://www.surfturf.org.uk/page/introduction>. [Accessed 16 March 2020].
- [30] R. Norris, “New research shows massive growth in energy storage projects,” *RenewableUK*, 02 December 2019. [Online]. Available: <https://www.renewableuk.com/news/479977/New-research-shows-massive-growth-in-energy-storage-projects.htm>. [Accessed 27 March 2020].
- [31] OFGEM, “Renewables Obligation Certificates (ROCs),” [Online]. Available: <https://www.ofgem.gov.uk/environmental-programmes/ro/about-ro>. [Accessed 14 March 2020].
- [32] OFGEM, “About the FIT scheme,” [Online]. Available: <https://www.ofgem.gov.uk/environmental-programmes/fit/about-fit-scheme>. [Accessed 15 March 2020].
- [33] GOV.UK, “Solar PV cost data,” 30 May 2019. [Online]. Available: <https://www.gov.uk/government/statistics/solar-pv-cost-data>. [Accessed 15 March 2020].
- [34] Department for Business, Energy & Industrial Strategy (BEIS), “Electricity Generation Costs,” UK Government, 2016.
- [35] U.S. Energy Information Authority , “Levelized Cost and Levelized Avoided Cost of New Generation Resources in the Annual Energy Outlook 2020,” February 2020. [Online]. Available: https://www.eia.gov/outlooks/aeo/pdf/electricity_generation.pdf. [Accessed 15 March 2020].
- [36] Fraunhofer Institute for Solar Energy Systems ISE, “Levelized Cost of Electricity - Rene,” March 2018. [Online]. Available: <https://www.ise.fraunhofer.de/content/dam/ise/en/documents/publications/stud>

ies/EN2018_Fraunhofer-ISE_LCOE_Renewable_Energy_Technologies.pdf.
[Accessed 15 March 2020].

- [37] Committee on Climate Change, “Reducing UK emissions - Progress Report to Parliament,” Committee on Climate Change, 2018.
- [38] The Scottish Government, “Scottish Energy Strategy: The future of energy in Scotland,” Edinburgh, 2017.
- [39] The Scottish Government, “2020 Routemap for Renewable Energy in Scotland,” The Scottish Government, Edinburgh, 2011.
- [40] Scottish Government, “Scotland to become a net-zero society,” Scottish Government, 25 September 2019. [Online]. Available: <https://www.gov.scot/news/scotland-to-become-a-net-zero-society/>. [Accessed 26 September 2019].
- [41] P. F. Alberto Carrillo Pineda, “Towards a Science-Based Approach to Climate Neutrality in the Corporate Sector (draft),” September 2019. [Online]. Available: <https://sciencebasedtargets.org/wp-content/uploads/2019/10/Towards-a-science-based-approach-to-climate-neutrality-in-the-corporate-sector-Draft-for-comments.pdf>. [Accessed 1 June 2020].
- [42] SP Energy Networks, “SP Distribution Heat Map,” SP Energy Networks, January 2018. [Online]. Available: https://www.spenergynetworks.co.uk/pages/sp_distribution_heat_maps.aspx.
- [43] DNV-GL, “Energy Transition Outlook : Power Supply and Use - A global and regional forecast to 2050,” DNV-GL, 2019.
- [44] National Grid PLC, “History of electricity transmission in Britain,” National Grid PLC, [Online]. Available: <https://www.nationalgrid.com/group/about-us/our-history/history-electricity-transmission-britain>. [Accessed September 2019].
- [45] Ernst & Young, “Unlocking the Potential of Smart Grid,” Ernst & Young, 2014.

- [46] South Asia Regional Initiative for Energy Integration, “HVDC Protection System,” December 2011. [Online]. Available: https://sari-energy.org/oldsite/PageFiles/What_We_Do/activities/HVDC_Training/Materials/1JNL100020-843 - PDF - Rev. 00.pdf. [Accessed 16 March 2020].
- [47] National Grid, “Protection & Control for HVDC Systems (TS3.24.90 (RES) - Issue 1,” National Grid ESO, 2014.
- [48] A. Lantero, “The War of the Currents: AC vs. DC Power,” Department of Energy, 18 November 2014. [Online]. Available: <https://www.energy.gov/articles/war-currents-ac-vs-dc-power>.
- [49] P. Fairley, “DC Versus AC: The Second War of Currents Has Already Begun,” *IEEE Power and Energy Magazine*, vol. 10, no. 6, pp. 101-103, 2012.
- [50] L. O. Barthold, D. A. Woodford and M. Salimi, “DC Is Where We Started: Is It Also Where We're Going?,” *IEEE Power and Energy Magazine*, vol. 14, no. 2, pp. 112-110, 2016.
- [51] USB Implementers Forum, “USB Charger (USB Power Delivery),” [Online]. Available: <https://www.usb.org/usb-charger-pd>. [Accessed 09 April 2020].
- [52] Scottish Government, “Statistics on the number of electric vehicles in Scotland: FOI release,” 6 February 2019. [Online]. Available: <https://www.gov.scot/publications/foi-19-00181/>. [Accessed 11 April 2020].
- [53] Newmotion, “AC Charging vs DC Charging,” [Online]. Available: https://newmotion.com/en_GB/ac-charging-vs-dc-charging/. [Accessed 10 April 2020].
- [54] Department for Business, Energy & Industrial Strategy (BEIS), “Electricity Generation Cost Report,” November 2016. [Online]. Available: https://assets.publishing.service.gov.uk/government/uploads/system/uploads/attachment_data/file/566567/BEIS_Electricity_Generation_Cost_Report.pdf. [Accessed 15 May 2019].
- [55] Steven W. Blume, *Electric Power System Basics*, Hoboken, New Jersey: John Wiley & Sons, Inc, 2016.

- [56] SP Energy Networks, "Long Term Development Statement," 2016.
- [57] SSEN, "Long Term Development Statement," 2016.
- [58] UK Power Networks, "Long Term Development Statement - London Power Networks," 2013.
- [59] IEEE Std 551-2006, "IEEE Recommended Practice for Calculating Short-Circuit Currents in Industrial and Commercial Power Systems," IEEE, New York, NY, USA, 2006.
- [60] DCODE, "The Distribution Code of licensed DNOs of Great Britain - Issue 29," February 2018.
- [61] SP Energy Networks, "Equipment Ratings," December 2013. [Online]. Available: <https://www.spenergynetworks.co.uk/userfiles/file/ESDD-02-007.pdf>. [Accessed 1 March 2020].
- [62] Scottish & Southern Electricity Networks, "Supporting a Smarter Electricity System," 10 November 2017. [Online]. Available: <https://www.ssen.co.uk/SmarterElectricity/Report/>. [Accessed 27 March 2020].
- [63] J. Song-Manguelle, M. H. Todorovic, S. Chi, S. K. Gunturi and R. Datta, "Power Transfer Capability of HVAC Cables for Subsea Transmission and Distribution Systems," *IEEE Transactions on Industry Applications*, vol. 50, no. 4, pp. 2382 - 2391, 2014.
- [64] "Proposed terms and definitions for flexible AC transmission system (FACTS)," *IEEE Transactions on Power Delivery*, vol. 12, no. 4, pp. 1848 - 1853, 1997.
- [65] X.-P. Zhang, C. Rehtanz and B. Pal, *Flexible AC Transmission Systems: Modelling and Control*, Springer-Verlag Berlin Heidelberg, 2012.
- [66] Mohan, Undeland and Robbins, *Power Electronics - Converters Applications and Designs*, John Wiley & Sons, Inc, 2003.
- [67] ABB, "HVDC - Economic and environmental advantages," [Online]. Available: <https://new.abb.com/systems/hvdc/why-hvdc/economic-and-environmental-advantages>. [Accessed 15 March 2020].

- [68] Scottish and Southern Electricity Networks (SSEN), “Beauly - Denny,” SSEN - Transmission, December 2016. [Online]. Available: <https://www.ssen-transmission.co.uk/projects/beauly-denny/>. [Accessed May 2019].
- [69] Scottish and Southern Electricity Networks (SSEN), “Caithness - Moray,” SSEN Transmission, Jan 2019. [Online]. Available: <https://www.ssen-transmission.co.uk/projects/caithness-moray/>. [Accessed May 2019].
- [70] “Western Link,” [Online]. Available: <http://www.westernhvdclink.co.uk/>. [Accessed May 2019].
- [71] R. Matulka, “The History of the Electric Car,” Department of Energy, 15 September 2014. [Online]. Available: <https://www.energy.gov/articles/history-electric-car>. [Accessed 25 September 2019].
- [72] Crompton Electriccars Ltd., F Range Battery Electric Road Vehicle, Gwent, Wales: Hawker Siddeley Crompton Electriccars, 1960s.
- [73] F. Nyberg and R. Pollard, “Network Rail - A Guide to Overhead Electrification (132787-ALB-GUN-EOH-000001) Rev. 10,” Alan Baxter & Associates LLP, London, UK, 2015.
- [74] G. Weinstein and T. J. Blalock, “Relocating the 50th Street Substation,” IEEE Power & Energy Magazine, July/August 2014. [Online]. Available: <http://magazine.ieee-pes.org/july-august-2014/history-14/>. [Accessed 08 May 2018].
- [75] K. H. Sueker, Power Electronics Design: A Practitioner's Guide, Elsevier Science, 2011.
- [76] Siemens, “Selected HVDC references (HVDC Classic),” 2017. [Online]. Available: <https://assets.new.siemens.com/siemens/assets/public.1525354813.405e0dab4b449fef20f123882700d4f496426149.emts-b10025-00-7600-ws-hvdc-classic144dpi.pdf>. [Accessed June 2019].

- [77] A. S. C. Leavy, W. A. Bukhsh and K. R. Bell, "Optimal Operation of the Western Link Embedded HVDC Connection," in *Power Systems Computation Conference (PSCC)*, Dublin, Ireland, 2018.
- [78] Siemens Mobility, "DC traction power supply system," [Online]. Available: <https://new.siemens.com/global/en/products/mobility/rail-solutions/rail-electrification/dc-traction-power-supply.html>. [Accessed June 2019].
- [79] D. Jovcic and K. Ahmed, *High-Voltage Direct-Current Transmission*, Aberdeen, Scotland: John Wiley & Sons, 2015.
- [80] M. Grady, "Understanding Power System Harmonics," April 2012. [Online]. Available: https://web.ecs.baylor.edu/faculty/grady/Understanding_Power_System_Harmonics_Grady_April_2012.pdf. [Accessed 10 April 2020].
- [81] WG B4.67, "AC Side Harmonics and Appropriate Harmonic Limits for VSC HVDC (Ref: 754)," CIGRE, Paris, France, 2019.
- [82] R. L. Sellick and M. Åkerberg, "Comparison of HVDC Light (VSC) and HVDC Classic (LCC) site aspects, for a 500MW 400kV HVDC transmission scheme," in *10th IET International Conference on AC and DC Power Transmission (ACDC 2012)*, Birmingham, UK, 2012.
- [83] National Grid, "Interconnexion France-Angleterre," [Online]. Available: <http://www.ifa1interconnector.com/>. [Accessed June 2019].
- [84] National Grid ESO, "Interconnector between France and England: Methodology Statement for Determination of System-to-System Flow," April 2019. [Online]. Available: <https://www.nationalgrideso.com/document/89616/download>. [Accessed June 2019].
- [85] P. Rodriguez and K. Rouzbehi, "Multi-terminal DC grids: challenges and prospects," *Journal of Modern Power Systems and Clean Energy*, vol. 5, no. 4, pp. 515 - 523, 2017.
- [86] J. Burr, S. Finney and C. Booth, "Comparison of Different Technologies for Improving Commutation Failure Immunity Index for LCC HVDC in Weak AC

- Systems,” in *11th IET International Conference on AC and DC Power Transmission*, Birmingham, 2015.
- [87] Y. Xue, X.-P. Zhang and C. Yang, “Elimination of Commutation Failures of LCC HVDC System with Controllable Capacitors,” *IEEE Transactions on Power Systems*, vol. 31, no. 4, pp. 3289 - 3299, 2016.
- [88] PROMOTioN - Progress on Meshed HVDC Offshore Transmission Networks, “D5.1 HVDC Network Fault Analysis,” 03 October 2016. [Online]. Available: https://www.promotion-offshore.net/fileadmin/PDFs/D5.1_PROMOTioN_Deliverable_5.1_HVDC_Network_Fault_Analysis.pdf. [Accessed 12 March 2020].
- [89] C.-C. Liu, S. McArthur and S.-J. Lee, *Smart Grid Handbook 3*, Wiley-Blackwell, 2016.
- [90] R. Tumilty, “Caithness – Moray : HVDC System Integration (SSEN),” March 2019. [Online]. Available: <http://www.hvdccentre.com/wp-content/uploads/2019/03/03-Ryan-Tumilty-Detailed-Design-and-Engineering-CM280319.pdf>. [Accessed May 2019].
- [91] J. Khazaei, P. Idowu, A. Asrari, A. Shafaye and L. Piyasinghe, “Review of HVDC control in weak AC grids,” *Electric Power Systems Research*, vol. 162, pp. 194-206, 2018.
- [92] National Grid ESO, “Black Start,” National Grid plc., 22 January 2019. [Online]. Available: <https://www.nationalgrideso.com/balancing-services/system-security-services/black-start>. [Accessed 06 August 2019].
- [93] ABB, “HVDC Light Reference List,” 28 May 2020. [Online]. Available: <https://new.abb.com/systems/hvdc/hvdc-light>. [Accessed 01 June 2020].
- [94] A. Beddard and M. Barnes, “Modelling of MMC-HVDC Systems – An Overview,” in *12th Deep Sea Offshore Wind R&D Conference, EERA DeepWind'2015*, Trondheim, Norway, 2015.

- [95] Power Systems Group (Mitsubishi Electric), “HVDC Solutions,” Mitsubishi Electric, [Online]. Available: <http://psg.mitsubishielectric.co.uk/products/hvdc-facts/hvdc-solutions/>. [Accessed July 2019].
- [96] R. Simpson, A. Plumpton, M. Varley, C. Tonner, P. Taylor and X. Dai, “Press-pack IGBTs for HVDC and FACTs,” *CSEE Journal of Power and Energy Systems*, vol. 3, no. 3, pp. 302 - 310, 2017.
- [97] I. Cowan, “Introduction to HVDC in GB,” The National HVDC Centre, Cumbernauld, Glasgow, 2018.
- [98] ABB, “HVDC Classic (LCC),” ABB, [Online]. Available: <https://new.abb.com/systems/hvdc/hvdc-classic>. [Accessed May 2019].
- [99] ABB, “HVDC Light (VSC),” [Online]. Available: <https://new.abb.com/systems/hvdc/hvdc-light>. [Accessed May 2019].
- [100] R. Marquardt, “Modular Multilevel Converter: An universal concept for HVDC-Networks and extended DC-Bus-applications,” in *International Power Electronics Conference - ECCE ASIA*, Sapporo, Japan, 2010.
- [101] ABB, “BorWin1,” 2015. [Online]. Available: <https://new.abb.com/systems/hvdc/references/borwin1>. [Accessed 01 March 2020].
- [102] ABB, “Why HVDC?,” ABB, [Online]. Available: <https://new.abb.com/systems/hvdc/why-hvdc>. [Accessed 04 June 2019].
- [103] ABB, “The Gotland HVDC link,” ABB, June 2019. [Online]. Available: <https://new.abb.com/systems/hvdc/references/the-gotland-hvdc-link>.
- [104] ABB, “Gotland HVDC Light,” ABB - HVDC - References, [Online]. Available: <https://new.abb.com/systems/hvdc/references/gotland-hvdc-light>. [Accessed 07 May 2019].
- [105] J. Ambrose, “Energy firms face inquiry over £1.3bn green power cable,” *The Guardian*, 28 January 2020. [Online]. Available: <https://www.theguardian.com/business/2020/jan/28/energy-firms-power-cable-national-grid-scottish-power>. [Accessed 19 April 2020].

- [106] OFGEM, “Ofgem opens investigation into National Grid and Scottish Power Transmission over delivery and ongoing operation of the Western HVDC subsea cable,” 28 January 2020. [Online]. Available: <https://www.ofgem.gov.uk/publications-and-updates/ofgem-opens-investigation-national-grid-and-scottish-power-transmission-over-delivery-and-ongoing-operation-western-hvdc-subsea-cable>. [Accessed 18 April 2020].
- [107] ABB, “Introducing HVDC,” 2014. [Online]. Available: https://library.e.abb.com/public/3fe366da840542bbb4359d814925947a/POW0078_rev1.pdf. [Accessed 21 March 2020].
- [108] SP Energy Networks, “Thieves 'Risking Lives' in Livingston After Substation Targeted,” 03 May 2019. [Online]. Available: https://www.spenergynetworks.co.uk/news/pages/thieves_risking_lives_in_livingston_after_substation_targeted.aspx. [Accessed 27 June 2019].
- [109] Scottish and Southern Electricity Networks, “Example of Storm Damage 2018/2019,” 20 September 2018. [Online]. Available: <https://www.facebook.com/ssencommunity/photos/a.143865235752548/1211754328963628/?type=3&theater>. [Accessed 06 March 2019].
- [110] UtilityTraining, “Excavation Safety - Underground Electric Cable Damage,” 13 March 2013. [Online]. Available: <https://youtu.be/UJQ-A9CsK2I>. [Accessed 12 April 2020].
- [111] ENTSOE - Regional Group Nordic, “Nordic Grid Disturbance Statistics 2012,” ENTSOE, Brussels, 2013.
- [112] J. Taft, “Fault Intelligence: Distribution Grid Fault Detection and Classification (PNNL-27602),” Pacific Northwest National Laboratory, Richland, Washington, USA, 2017.
- [113] BS 7671:2018, “Requirements for Electrical Installations. IET Wiring Regulations,” BSI, 2018.
- [114] S. K. Lau and S. K. Ho, “Open-circuit fault detection in distribution overhead power supply network,” *Journal of International Council on Electrical Engineering*, vol. 7, no. 1, p. 269–275, 2017.

- [115] J. L. Blackburn and T. J. Domin, Protective Relaying Principles and Applications 4th Edition, Boca Raton, Florida, USA: CRC Press, 2006.
- [116] J. D. Glover, M. S. Sarma and T. J. Overbye, Power System Analysis and Design, Stamford, CT: Global Engineering, 2012.
- [117] Electricity North West, “Protection for 132kV, 33kV and 11/6.6kV Systems - Issue 5,” March 2015. [Online]. Available: <https://www.enwl.co.uk/globalassets/get-connected/cic/icpsidnos/g81-library/1---design--planning/5-design--planning/epd350---protection-for-132kv-33kv-and-116.6kv-systems.pdf>. [Accessed 21 February 2020].
- [118] Alstom Grid, Network Protection & Automation Guide, Alstom Grid, 2011.
- [119] Bharat Heavy Electricals Limited, Handbook of Switchgears, New York, USA: McGraw-Hill , 2007.
- [120] J. H. Harlow, Electric Power Transformer Engineering Third Edition, Boca Raton, Florida, USA: CRC Press, 2012.
- [121] Schneider Electric, “Indoor Instrument Transformers,” 2012. [Online]. Available: https://download.schneider-electric.com/files?p_enDocType=Catalog&p_File_Name=AMTED300031EN%28web%29.pdf&p_Doc_Ref=AMTED300031EN. [Accessed 4 March 2020].
- [122] IEEE Power Engineering Society, “IEEE Standard for Relays and Systems Associated with Electric Power Apparatus (IEEE Std C37.90-2005),” IEEE, New York, USA, 2006.
- [123] S. H. Horowitz and A. G. Phadke, “Power System Relaying - Third Edition,” Baldock, John Wiley & Sons Ltd, 2008.
- [124] Western Power Distribution, “Low Frequency Demand Disconnection,” June 2018. [Online]. Available: <https://www.westernpower.co.uk/downloads/4093>. [Accessed 17 April 2020].
- [125] National Grid ESO, “Interim Report into the Low Frequency Demand Disconnection (LFDD) following Generator Trips and Frequency Excursion on 9 Aug 2019,” 16 August 2019. [Online]. Available:

- https://www.ofgem.gov.uk/system/files/docs/2019/08/incident_report_lfdd_-_summary_-_final.pdf. [Accessed 17 April 2020].
- [126] National Grid ESO, “Technical Report on the events of 9 August 2019,” 6 September 2019. [Online]. Available: <https://www.nationalgrideso.com/document/152346/download>. [Accessed 28 May 2020].
- [127] R. C. Dorf, *Systems, Controls, Embedded Systems, Energy, and Machines*, Boca Raton, Florida, USA: CRC Press, 2006.
- [128] C. Booth, K. Bell and Z. Melhem, “Protection of Transmission and Distribution (T&D) Networks,” in *Electricity Transmission, Distribution and Storage Systems*, Woodhead Publishing Limited, 2013, pp. 75-107.
- [129] GE Grid Solutions, “Reason RT431 - GPS Precision-Time Clock (RT431-TM-EN-HWB-8v7),” [Online]. Available: <https://www.gegridsolutions.com/products/manuals/RT431-TM-EN-HWB-8v7.pdf>. [Accessed 1 May 2020].
- [130] R. Bansal, *Power System Protection in Smart Grid Environment*, CRC Press, 2019.
- [131] Alstom Grid, “Technical Manual - MiCOM P543-P546,” Alstom Grid, Stafford, UK, 2011.
- [132] P. M. Anderson, *Power System Protection*, Wiley-IEEE Press, 1998.
- [133] GE Power Management, “Distance Relays Fundamentals,” GE MULTILIN, Ontario, 2002.
- [134] A. Dyśko, Writer, *Power System Design, Operation & Protection - Distance Relay Comparators*. [Performance]. University of Strathclyde, 2015.
- [135] J. K. Jr, “Introduction To Symmetrical Components,” 2003. [Online]. Available: https://ocw.mit.edu/courses/electrical-engineering-and-computer-science/6-061-introduction-to-electric-power-systems-spring-2011/readings/MIT6_061S11_ch4.pdf. [Accessed 27 April 2020].

- [136] GEC Measurements, "MicroMho - Static Distance Protection Relay," The General Electric Company p.l.c. England, Stafford, 1984.
- [137] A. Dyško, Writer, *Power System Design, Operation & Protection - Distance protection schemes*. [Performance]. University of Strathclyde, 2015.
- [138] Valence - Electrical Training Services, "Direct Transfer Trip and Direct Under-Reaching Transfer Trip Schemes," 2019. [Online]. Available: <https://relaytraining.com/direct-transfer-trip-direct-reaching-transfer-trip-schemes-video/>. [Accessed 23 March 2020].
- [139] Valence - Electrical Training Services, "Understanding Permissive Over-Reaching Transfer Trip (POTT) Communication Assisted Trip Schemes," 2019. [Online]. Available: <https://relaytraining.com/understanding-permissive-over-reaching-transfer-trip-pott-communication-assisted-trip-schemes-video/>. [Accessed 23 March 2020].
- [140] Valence - Electrical Training Services, "Understanding Permissive Under-Reaching Transfer Trip (PUTT) Communication Assisted Trip Schemes," 2019. [Online]. Available: <https://relaytraining.com/understanding-putt-communication-assisted-trip-schemes-video/>. [Accessed 23 March 2020].
- [141] B. Hussain, S. M. Sharkh, S. Hussain and M. A. Abusara, "An Adaptive Relaying Scheme for Fuse Saving in Distribution Networks With Distributed Generation," *IEEE Transactions on Power Delivery*, vol. 28, no. 2, pp. 669 - 677, 2013 .
- [142] A. Hassall, A. Forsyth, J. Wright, A. Wixon, M. Stockton, P. Newman, D. Johnson, D. Stearn and N. Pavaiya, "Neutral voltage displacement (NVD) protection applied to condenser bushings (capacitor cones)," in *11th IET International Conference on Developments in Power Systems Protection (DPSP 2012)*, Birmingham, UK, 2012.
- [143] A. Dyško, "Advanced Power System Analysis and Protection - Distributed Generator Protection (Lecture Notes)," University of Strathclyde, Glasgow, 2015.

- [144] S. Mirsaedi, X. Dong, S. Shi and D. Tzelepis, "Challenges, advances and future directions in protection of hybrid AC/DC microgrids," *IET Renewable Power Generation*, vol. 11, no. 12, pp. 1495 - 1502, 2017.
- [145] R. Li, C. Booth, A. Dyško, A. Roscoe, H. Urdal and J. Zhu, "Protection challenges in future converter dominated power systems," in *International Conference on Renewable Power Generation (RPG 2015)*, Beijing, China, 2015.
- [146] D. Larruskain, V. Valverde, E. Torres, G. Buigues and M. Santos, "Protection Systems for Multi-Terminal HVDC Grids," in *International Conference on Renewable Energies and Power Quality (ICREPQ'18)*, Salamanca, Spain, 2018.
- [147] S. Fletcher, P. Norman, S. Galloway and G. Burt, "Fault detection and location in DC systems from initial di/dt measurement," in *Euro Tech Con*, Manchester, UK, 2012.
- [148] G. Adam, K. Ahmed, S. Finney and B. Williams, "AC fault ride-through capability of a VSC-HVDC transmission systems," in *IEEE Energy Conversion Congress and Exposition*, Atlanta, GA, USA, 2010.
- [149] P. D. Judge, M. M. C. Merlin, T. C. Green, D. R. Trainer and K. Vershinin, "Thyristor-Bypassed Submodule Power-Groups for Achieving High-Efficiency, DC Fault Tolerant Multilevel VSCs," *IEEE Transactions on Power Delivery*, vol. 33, no. 1, pp. 349 - 359, 2017.
- [150] F. P. Page, *Analysis in Circuit Breaker Performance Requirements for High-Voltage DC Networks*, 2016.
- [151] J. Yang, J. E. Fletcher and J. O'Reilly, "Short-Circuit and Ground Fault Analyses and Location in VSC-Based DC Network Cables," *IEEE Transactions on Industrial Electronics*, vol. 59, no. 10, pp. 3827 - 3837, 2012.
- [152] S. Ademi, D. Tzelepis, A. Dyško, S. Subramanian and H. Ha, "Fault Current Characterisation in VSC-based HVDC Systems," in *13th International Conference on Development in Power System Protection (DPSP)*, Edinburgh, Scotland, 2016.

- [153] R. Smeets and N. Belda, "HVDC Fault Current Interruption Technology," in *5th International Conference on Electric Power Equipment – Switching Technology*, Kitakyushu, Japan, 2019.
- [154] G. Li, *Analysis and Protection of HVDC Systems Subject to AC and DC Faults*, Cardiff, Wales: Cardiff University, 2017.
- [155] A. Mokhberdorani, A. Carvalho, H. Leite and N. Silva, "A review on HVDC circuit breakers," in *3rd Renewable Power Generation Conference (RPG 2014)*, Naples, Italy, 2014.
- [156] J. Häfner and B. Jacobson, "Proactive Hybrid HVDC Breakers - A key innovation for reliable HVDC grids," in *Cigre Symposia - The Electric Power System of the Future - Integrating Supergrids and Microgrids*, Bologna, Italy, 2011.
- [157] R. Li, L. Xu and D. Guo, "Accelerated switching function model of hybrid MMCs for HVDC system simulation," *IET Power Electronics*, vol. 10, no. 5, pp. 2199 - 2207, 2017.
- [158] G. Tang, Z. Xu and Y. Zhou, "Impacts of Three MMC-HVDC Configurations on AC System Stability Under DC Line Faults," *IEEE Transactions on Power Systems*, vol. 29, no. 6, pp. 3030 - 3040, 2014.
- [159] I. A. Gowaid, "A Low-Loss Hybrid Bypass for DC Fault Protection of Modular Multilevel Converters," *IEEE Transactions on Power Delivery*, vol. 32, no. 2, pp. 599-608, 2017.
- [160] D. V. Hertem, M. Ghandhari, J. B. Curis and A. M. O. Despuys, "Protection requirements for a multi-terminal meshed DC grid," in *CIGRE Bologna Symposium*, Bologna, Italy, 2011.
- [161] M. Wang, M. Abedrabbo, W. Leterme, D. V. Hertem, C. Spallarossa, S. Oukaili, I. Grammatikos and K. Kuroda, "A Review on AC and DC Protection Equipment and Technologies: Towards Multivendor Solution," in *CIGRÉ 2017 Colloquium (Study Committees A3, B4 & D1)*, Winnipeg, Canada, 2017.

- [162] T. An, G. Tang and W. Wang, "Research and application on multi-terminal and DC grids based on VSC-HVDC technology in China," *IET High Voltage*, vol. 2, no. 1, pp. 1-10, 2017.
- [163] ABB, "ABB's Hybrid HVDC Breaker," 4 April 2013. [Online]. Available: <https://youtu.be/Uir-BPoTN88>.
- [164] B. Li, J. He, Y. Li and B. Li, "A review of the protection for the multiterminal VSC-HVDC grid," *Protection and Control of Modern Power Systems*, vol. 4, 2019.
- [165] S. LeBlond, R. Bertho, D. Coury and J.C.M. Vieira, "Design of protection schemes for multi-terminal HVDC systems," *Renewable and Sustainable Energy Reviews*, vol. 56, pp. 965-974, 2016.
- [166] O. Cwikowski, J. Sau-Bassols, B. Chang, E. Prieto-Araujo, M. Barnes, O. Gomis-Bellmunt and R. Shuttleworth, "Integrated HVDC Circuit Breakers With Current Flow Control Capability," *IEEE Transactions on Power Delivery*, vol. 33, no. 1, pp. 371 - 380, 2018.
- [167] P. D. Judge, G. Chaffey, M. M. C. Merlin, P. R. Clemow and T. C. Green, "Dimensioning and Modulation Index Selection for the Hybrid Modular Multilevel Converter," *IEEE Transactions on Power Electronics*, vol. 33, no. 5, pp. 3837 - 3851, 2018.
- [168] N. A. Belda, C. Plet, C. Spallarosa and F. Page, "Fault Stress Analysis of HVDC Circuit Breakers (D5.3 PROMOTION)," European Union - Horizon 2020, 2016.
- [169] K. Jennett, F. Coffele and C. Booth, "Comprehensive and quantitative analysis of protection problems associated with increasing penetration of inverter-interfaced DG," in *11th IET International Conference on Developments in Power Systems Protection (DPSP 2012)*, Birmingham, UK, 2012.
- [170] V. Telukunta, J. Pradhan, A. Agrawal, M. Singh and S. G. Srivani, "Protection challenges under bulk penetration of renewable energy resources in power systems: A review," *CSEE Journal of Power and Energy Systems*, vol. 3, no. 4, pp. 365 - 379, 2017.

- [171] F. Coffele, C. Booth, A. Dyško and G. Burt, “Quantitative analysis of network protection blinding for systems incorporating distributed generation,” *IET Generation, Transmission & Distribution*, vol. 6, no. 12, pp. 1218 - 1224, 2012.
- [172] A. Dyško, G. Burt, S. Galloway, C. Booth and J. McDonald, “UK distribution system protection issues,” *IET Generation, Transmission & Distribution*, vol. 1, no. 4, pp. 679 - 687, 2007.
- [173] International Electrotechnical Commission (IEC), “LVDC: Electricity for the 21st century,” International Electrotechnical Commission, Geneva, Switzerland, 2017.
- [174] Intel Corporation, “Desktop Platform Form Factors Power Supply - Design Guide - Revision 2(336521-002),” June 2018. [Online]. Available: <https://www.intel.com/content/dam/www/public/us/en/documents/guides/power-supply-design-guide-june.pdf>. [Accessed 24 April 2019].
- [175] R. W. D. Doncker, “Power electronic technologies for flexible DC distribution grids,” in *International Power Electronics Conference*, Hiroshima, Japan, 2014.
- [176] R. W. D. Doncker, “The War of Currents,” in *International Conference on DC Microgrids*, Nuremberg, 2017.
- [177] R. Fu, D. Feldman and R. Margolis, “U.S. Solar Photovoltaic System Cost Benchmark: Q1 2018,” November 2018. [Online]. Available: <https://www.nrel.gov/docs/fy19osti/72399.pdf>. [Accessed 2 March 2020].
- [178] D. Feldman, M. Zwerling and R. Margolis, “Solar Industry Update - Q2/Q3 2019,” 12 November 2019. [Online]. Available: <https://www.nrel.gov/docs/fy20osti/75484.pdf>. [Accessed 2 March 202].
- [179] International Standard, “IEC Standard Voltages,” IEC, 2009.
- [180] T. Keim and A. Bindra, “Recent Advances in HVDC and UHVDC Transmission,” *IEEE Power Electronics Magazine*, vol. 4, no. 4, pp. 12-17, 2017.
- [181] A. Giannakis and D. Pefitsis, “MVDC Distribution Grids and Potential Applications: Future Trends and Protection Challenges,” in *20th European*

Conference on Power Electronics and Applications (EPE'18 ECCE Europe), Riga, Latvia, 2018.

- [182] F. Mura and R. W. D. Doncker, "Design Aspects of a Medium-Voltage Direct Current (MVDC) Grid for a University Campus," in *8th International Conference on Power Electronics - ECCE Asia*, Korea, 2011.
- [183] Siemens, "MVDC Plus," 2017. [Online]. Available: siemens.com/mvdc.
- [184] RXHK, "Smart VSC-HVDC Transmission," [Online]. Available: <https://www.rxhk.co.uk/solutions/smart-vsc-hvdc-transmission/smart-vsc-mvdc-transmission/>. [Accessed 17 June 2017].
- [185] SP Energy Networks, "Angle-DC - Year One Project Summary," 2016. [Online]. Available: https://www.spenergynetworks.co.uk/userfiles/file/SPEN_Angle_DC_V3.pdf. [Accessed 19 March 2020].
- [186] TNEI, "MVDC Technology Study –Market Opportunities and Economic Impact (9639–01–R0)," 16 February 2015. [Online]. Available: <http://www.evaluationsonline.org.uk/evaluations/Documents.do?action=download&id=737&ui=basic>. [Accessed 24 May 2016].
- [187] Siemens AG, "SINAMICS," 2019. [Online]. Available: <https://new.siemens.com/global/en/products/drives/sinamics/medium-voltage-converters.html>. [Accessed 4 November 2019].
- [188] SP Energy Networks, "Angle-DC 2015 Electricity Network Innovation Competition," 2015. [Online]. Available: https://www.ofgem.gov.uk/sites/default/files/docs/angle_submission.pdf. [Accessed March 2017].
- [189] Western Power Distribution, "Network Equilibrium," 2015-2019. [Online]. Available: <https://www.westernpower.co.uk/projects/network-equilibrium>. [Accessed 12 October 2018].
- [190] The Alaska Center for Energy and Power, "Small-Scale High Voltage Direct Current," University of Alaska Fairbanks, Fairbanks, 2013.

- [191] Western Power Distribution, "DC Share - Electricity NIC Initial Screening Submission 2019," 30 April 2019. [Online]. Available: <https://www.ofgem.gov.uk/publications-and-updates/electricity-nic-initial-screening-submission-2019-dc-share-wpd>.
- [192] GE, "GE Supports Power Grids of the Future with Europe's First MVDC Link," GE Power Conversion, 16 May 2017. [Online]. Available: <https://www.gepowerconversion.com/press-releases/ge-supports-power-grids-future-europe%E2%80%99s-first-mvdc-link>. [Accessed July 2018].
- [193] R. M. Cuzner and V. Singh, "Future Shipboard MVdc System Protection Requirements and Solid-State Protective Device Topological Tradeoffs," *IEEE Journal of Emerging and Selected Topics in Power Electronics*, vol. 5, no. 1, pp. 244-259, 2017.
- [194] J. Fabre, P. Ladoux, E. Solano, G. Gateaul and J.-M. Blaquière, "MVDC Three-Wire Supply Systems for Electric Railways: Design and Test of a Full SiC Multilevel Chopper," *IEEE Transactions on Industry Applications*, vol. 53, no. 6, pp. 5820-5830, 2017.
- [195] C. Yuan, M. A. Haj-ahmed and M. S. Illindala, "Protection Strategies for Medium-Voltage Direct-Current Microgrid at a Remote Area Mine Site," *IEEE Transactions on Industry Applications*, vol. 51, no. 4, pp. 2846-2853, 2015.
- [196] C. Cleary and S. Hay, "DC Array Refresh Study," TNEI Services Ltd, Manchester, UK, 2018.
- [197] W. Chen, A. Q. Huang, C. Li, G. Wang and W. Gu, "Analysis and Comparison of Medium Voltage High Power DC/DC Converters for Offshore Wind Energy Systems," *IEEE Transactions on Power Electronics*, vol. 28, no. 4, pp. 2014-2023, 2013.
- [198] B. Wu and F. DeWinter, "Voltage stress on induction motors in medium-voltage (2300-6900-V) PWM GTO CSI drives," *IEEE Transactions on Power Electronics*, vol. 12, no. 2, pp. 213 - 220, 1997.

- [199] A. Wallace, M. Boger and E. Wiedenbrug, "Medium- and high-voltage, low-speed drives using low-voltage IGBT converters," in *IEEE International Symposium on Industrial Electronics*, Dubrovnik, Croatia, 1995.
- [200] J. Bredthauer and N. Struck, "Starting of large medium voltage motors: design, protection, and safety aspects," *IEEE Transactions on Industry Applications*, vol. 31, no. 5, pp. 1167 - 1176, 1995.
- [201] "IEEE Guide for AC Motor Protection (C37.96-2000)," IEEE, 2000.
- [202] J. v. Bloh and R. W. D. Doncker, "Control strategies for multilevel voltage source converters for medium-voltage DC transmission systems," in *26th Annual Conference of the IEEE Industrial Electronics Society (IECON 2000)*, Nagoya, Japan, Japan, 2000.
- [203] J. v. Bloh, O. F. Kashani and R. W. D. Doncker, "Optimization of multilevel voltage source converters for medium-voltage DC transmission systems," in *IEEE International Symposium on Industrial Electronics (ISIE'2000)*, Cholula, Puebla, Mexico, Mexico, 2000.
- [204] H.-E. Schmidt and M. S. Wieck, "Medium voltage land connection for marine vessels". US Patent US8026629B2, 27 January 2006.
- [205] R. Hartig, H. S. Horn and K. Tigges, "Method for supplying the electrical on-board power network of ships with external energy". US Patent Patent US7919881B2, 05 April 2011.
- [206] J. Flottemesch and M. Rother, "Optimized energy exchange in primary distribution networks with DC links," in *IEEE International Conference on Electric Utility Deregulation, Restructuring and Power Technologies*, Hong Kong, China, 2004.
- [207] K. Ueharaa and H. Ikeda, "Recent and future situation of Japan's T&D system," *Journal of International Council on Electrical Engineering*, vol. 6, no. 1, p. 231–234, 2016.

- [208] T. Ohkami, T. Fujimoto, H. Ito et al., “Development of 300 MW frequency converter,” in *International Power Electronics Conference - ECCE ASIA*, Sapporo, Japan, 2010.
- [209] A. Sannino, G. Demetriades, L. Hultqvist and O. Norén, “System and apparatus for power transfer to vessels”. World Intellectual Property Organization Patent WO2010066888A2, 17 June 2001.
- [210] T. J. McCoy, “Electric Ships Past, Present, and Future [Technology Leaders],” *IEEE Electrification Magazine*, vol. 3, no. 2, pp. 4 - 11, June 2015.
- [211] M. O. Faruque, V. Dinavahi, M. Sloderbeck and M. Steurer, “Geographically distributed thermo-electric co-simulation of all-electric ship,” in *IEEE Electric Ship Technologies Symposium*, Baltimore, Maryland, USA, 2009.
- [212] J. S. Thongam, M. Tarbouchi, A. F. Okou, D. Bouchard and R. Beguenane, “All-electric ships—A review of the present state of the art,” in *Eighth International Conference and Exhibition on Ecological Vehicles and Renewable Energies (EVER)*, Monte Carlo, Monaco, 2013.
- [213] IEEE Recommended Practice for 1 kV to 35 kV Medium-Voltage DC Power Systems on Ships (1709-2010), IEEE, 2010.
- [214] G. Sulligoi, A. Tassarolo, V. Benucci, M. Baret, A. Rebora and A. Taffone, “Modeling, Simulation, and Experimental Validation of a Generation System for Medium-Voltage DC Integrated Power Systems,” *IEEE Transactions on Industry Applications*, vol. 46, no. 4, pp. 1304 - 1310, 2010.
- [215] H. Li, W. Li, M. Luo, A. Monti and F. Ponci, “Design of Smart MVDC Power Grid Protection,” *IEEE Transactions on Instrumentation and Measurement*, vol. 60, no. 9, pp. 3035 - 3046, 2011.
- [216] Y. Lian, G. P. Adam, D. Holliday and S. J. Finney, “Medium-voltage DC/DC converter for offshore wind collection grid,” *IET Renewable Power Generation*, vol. 10, no. 5, pp. 651 - 660, 2016.
- [217] P. K. Steimer and O. Apeldoorn, “Medium voltage power conversion technology for efficient windpark power collection grids,” in *The 2nd*

International Symposium on Power Electronics for Distributed Generation Systems, Hefei, China, 2010.

- [218] J. Robinson, D. Jovcic and G. Joos, "Analysis and Design of an Offshore Wind Farm Using a MV DC Grid," *IEEE Transactions on Power Delivery*, vol. 25, no. 4, pp. 2164 - 2173, 2010.
- [219] G. F. Reed, B. M. Grainger, M. J. Korytowski and E. J. Taylor, "Modeling, analysis, and validation of a preliminary design for a 20 kV medium voltage DC substation," in *IEEE EnergyTech*, Cleveland, OH, USA, 2011.
- [220] G. L. Kusic, G. F. Reed, J. Svensson and Z. Wang, "A case for medium voltage DC for distribution circuit applications," in *IEEE/PES Power Systems Conference and Exposition*, Phoenix, AZ, USA, 2011.
- [221] R. W. D. Doncker, C. Meyer, R. U. Lenke and F. Mura, "Power Electronics for Future Utility Applications," in *7th International Conference on Power Electronics and Drive Systems*, Bangkok, Thailand, 2007.
- [222] M. Monadi, C. Gavriluta, A. Luna, J. I. Candela and P. Rodriguez, "Centralized Protection Strategy for Medium Voltage DC Microgrids," *IEEE Transactions on Power Delivery*, vol. 32, no. 1, pp. 430 - 440, 2017.
- [223] L. Zhang, Y. Chen, C. Shen, W. Tang and J. Liang, "Releasing more capacity for EV integration by DC medium voltage distribution lines," *IET Power Electronics*, vol. 10, no. 15, pp. 2116 - 2123, 2017.
- [224] A. Aithal and J. Wu, "Operation and performance of a medium-voltage DC link," *CIREN - Open Access Proceedings Journal*, vol. 2017, no. 1, pp. 1355 - 1358, 2017.
- [225] L. Michi, E. Carlini, T. B. Scirocco, G. Bruno, L. Caciolli, M. Cortese, G. Ramundo, M. Okuda and T. Murao, "MON.ITA HVDC Link AC & DC Protection System," in *AEIT HVDC International Conference (AEIT HVDC)*, Florence, Italy, Italy, 2019.

- [226] M. M. Alam, H. D. Leite, J. Liang and A. Carvalho, "Effects of VSC based HVDC system on distance protection of transmission lines," *International Journal of Electrical Power & Energy Systems*, vol. 92, pp. 245-260, 2017.
- [227] C. C. Teixeira and H. Leite, "The influence of a VSC based HVDC link on distance protection relay assessed by CAPE software," in *IEEE Manchester PowerTech*, Manchester, UK, 2017.
- [228] S. Tale, M. Mohan and K. P. Vittal, "Performance analysis of distance relay in an AC grid with VSC-HVDC connection," in *International Conference on Intelligent Computing, Instrumentation and Control Technologies (ICICT)*, Kannur, India, 2017.
- [229] L. He and C.-C. Liu, "Effects of HVDC connection for offshore wind turbines on AC grid protection," in *IEEE Power & Energy Society General Meeting*, Vancouver, BC, Canada, 2013.
- [230] C. Long, J. Wu, K. Smith, A. Moon, R. Bryans and J. Yu, "MVDC link in a 33 kV distribution network," *CIGRE - Open Access Proceedings Journal*, no. 1, pp. 1308 - 1312, 2017.
- [231] J. Yu, K. Smith, M. Urizarbarrena, M. Bebbington, N. Macleod and A. Moon, "Initial designs for ANGLE-DC project: challenges converting existing AC cable and overhead line to DC operation," *CIGRE - Open Access Proceedings Journal*, vol. 2017, no. 1, pp. 2374 - 2378, 2017.
- [232] F. Xu, Z. Xu, H. Zheng, G. Tang and Y. Xue, "A Tripole HVDC System Based on Modular Multilevel Converters," *IEEE Transactions on Power Delivery*, vol. 29, no. 4, pp. 1683 - 1691, 2014.
- [233] P. Salonen, T. Kaipia, P. Nuutinen, P. Peltoniemi and J. Partanen, "An LVDC Distribution System Concept," in *Nordic Workshop on Power and Industrial Electronics*, Helsinki, 2008.
- [234] L. Zhang, J. Liang, W. Tang, G. Li, Y. Cai and W. Sheng, "Converting AC Distribution Lines to DC to Increase Transfer Capacities and DG Penetration," *IEEE Transactions on Smart Grid*, vol. 10, no. 2, pp. 477 - 1487, 2019.

- [235] SP Energy Networks, “NIC Project Medium Voltage Direct Current Link Technical Specification,” 2017.
- [236] GE Power Conversion, “MV7000,” GE, 2017. [Online]. Available: <https://www.gepowerconversion.com/product-solutions/medium-voltage-drives/mv7000>. [Accessed 22 May 2017].
- [237] Horizon 2020, “Technology readiness levels (TRL) - General Annexes,” 2014-2015. [Online]. Available: https://ec.europa.eu/research/participants/data/ref/h2020/wp/2014_2015/annexes/h2020-wp1415-annex-g-trl_en.pdf. [Accessed October 2019].
- [238] J. Weber, R. Costello and J. Ringwood, “WEC Technology Performance Levels (TPL) - Metric for Successful Development of Economic WEC Technology,” in *Tenth European Wave and Tidal Energy Conference*, Aalborg, Denmark, 2013.
- [239] R. Bryans, M. Bebbington, J. Yu, K. Smith, J. Knott and A. Moon, “Real time control of a distribution connected MVDC link (ANGLE-DC),” in *13th IET International Conference on AC and DC Power Transmission (ACDC 2017)*, Manchester, UK, 2017.
- [240] Western Power Distribution, “Low Carbon Networks Fund submission from Western Power Distribution – Network Equilibrium,” 24 November 2014. [Online]. Available: <https://www.westernpower.co.uk/downloads/2677>. [Accessed 18 January 2019].
- [241] Western Power Distribution, “Detailed Design of the FPL Method (SDRC-3),” 22 March 2016. [Online]. Available: <https://www.westernpower.co.uk/downloads/2506>. [Accessed 02 March 2020].
- [242] M. Buschendorf, J. Weber and S. Bernet, “Comparison of IGCT and IGBT for the use in the modular multilevel converter for HVDC applications,” in *International Multi-Conference on Systems, Signals & Devices*, Chemnitz, Germany, 2012.
- [243] Western Power Distribution, “Network Equilibrium - Closedown Report,” 16 August 2019. [Online]. Available:

- <https://www.westernpower.co.uk/downloads/51982>. [Accessed 15 October 2019].
- [244] Western Power Distribution, “FPL Development and Improvement Report,” August 2019. [Online]. Available: <https://www.westernpower.co.uk/downloads/51712>. [Accessed September 2019].
- [245] Western Power Distribution, “Trialling and Demonstrating the FPL Method,” October 2018. [Online]. Available: <https://www.westernpower.co.uk/downloads/11843>. [Accessed May 2019].
- [246] J. King, J. Berry and N. Murdoch, “Steady-state modelling for the integration of a bi-directional AC–DC–AC flexible power link,” *CIREN - Open Access Proceedings Journal*, vol. 2017, no. 1, pp. 445-449, 2017.
- [247] S. C. E. Jupe, S. Hoda, J. E. King, D. A. Dale and J. Berry, “Controlling a 33 kV flexible power link in GB's distribution network,” in *15th IET International Conference on AC and DC Power Transmission (ACDC 2019)*, Coventry, UK, 2019.
- [248] J. Berry, N. Murdoch and D. Hardman, “Design and integration of an MVDC system on a GB 33kV network,” in *15th IET International Conference on AC and DC Power Transmission (ACDC 2019)*, Coventry, UK, 2019.
- [249] F. Mura and R. W. D. Doncker, “Preparation of a Medium-Voltage DC Grid Medium-Voltage DC Grid,” Aachen, 2012.
- [250] M. Stieneker, J. Butz, S. Rabiee, H. Stagge and R. W. D. Doncker, “Medium-Voltage DC Research Grid Aachen,” in *International ETG Congress*, Bonn, Germany, 2015.
- [251] S. Taraborrelli, *Bidirectional Dual Active Bridge Converter Using a Tap Changer for Extended Voltage Ranges*, Aachen, Germany: RWTH University Aachen, 2017.
- [252] N. Soltan, *High-Power Medium-Voltage DC-DC Converters: Design, Control and Demonstration*, Aachen, Germany: RWTH Aachen University, 2017.

- [253] Flexible Elektrische Netze FEN GmbH, “FEN Research Campus Celebrates the Launch of the MVDC Grid on Campus Melaten,” 19 November 2019. [Online]. Available: <https://fenaachen.net/en/blog/2019/11/22/fen-launch-mvdc-grid/>. [Accessed 27 November 2019].
- [254] Western Power Distribution, “DC Share,” April 2019. [Online]. Available: https://www.ofgem.gov.uk/system/files/docs/2019/04/electricity_nic_isp_-_dc_share_ricardo_wpd_enwl_issue_1.2.pdf. [Accessed September 2019].
- [255] T. Xu, M. W. Donoghue and C. C. Davidson, “IGBT overcurrent turn-off tests for the MMC-based VSC valves,” in *15th European Conference on Power Electronics and Applications (EPE)*, Lille, France, 2013.
- [256] S. Carullo and C. Nwankpa, “Analysis of measurement delay errors in an Ethernet based communication infrastructure for power systems,” in *IEEE International Symposium on Circuits and Systems*, Phoenix-Scottsdale, AZ, USA, 2002.
- [257] C.-K. Kim, V. K. Sood, G.-S. Jang, S.-J. Lim and S.-J. Lee, *HVDC Transmission: Power Conversion Applications in Power Systems*, Singapore: Wiley-IEEE Press, 2009.
- [258] A. Egea-Alvarez, A. Junyent-Ferré and O. Gomis-Bellmunt, “Active and reactive power control of grid connected distributed generation systems,” in *Modeling and Control of Sustainable Power Systems*, Berlin, Springer, 2012, pp. 47-81.
- [259] DCODE, “The Distribution Code of Licensed DNOs of Great Britain - Issue 44,” March 2020.
- [260] D. Tzelepis, S. Ademi, D. Vozikis, A. Dyško, S. Subramanian and H. Ha, “Impact of VSC converter topology on fault characteristics in HVDC transmission systems,” in *IET International Conference on Power Electronics, Machines and Drives (PEMD 2016)*, Glasgow, UK, 2016.
- [261] R. Li and L. Xu, “Review of DC fault protection for HVDC grids,” *WIREs Energy and Environment*, vol. 7, no. 2, 2017.

- [262] N. Yousefpoor, S. Kim and S. Bhattacharya, "Control of voltage source converter based multi-terminal DC grid under DC fault operating condition," in *IEEE Energy Conversion Congress and Exposition (ECCE)*, Pittsburgh, PA, USA, 2014.
- [263] B. Jiang and Y. Gong, "Arm Overcurrent Analysis and Calculation of MMC-HVDC System with DC-link Pole-to-Pole Fault," *Electric Power Components and Systems*, vol. 46, no. 2, pp. 177-186, 2018.
- [264] W. Leterme and D. V. Hertem., "Classification of fault clearing strategies for HVDC grids," in *CIGRE Symposium*, Lund, 2015.
- [265] A. Dyśko, J. R. McDonald, G. M. Burt, J. Goody and B. Gwyn, "Integrated Modelling Environment: A Platform for Dynamic Protection Modelling and Advanced Functionality," IEEE, New Orleans, LA, USA, 1999.
- [266] L. Hunter, C. Booth, A. J. Ferre and S. Finney, "MVDC for enhanced utility scale distribution power delivery and control," in *52nd International Universities Power Engineering Conference (UPEC)*, Heraklion, 2017.
- [267] S. D'Arco, J. A. Suul and J. Beerten, "Configuration and model order selection of frequency-dependent π -models for representing dc-cables in small-signal eigenvalue analysis of HVDC transmission systems," *IEEE Journal of Emerging and Selected Topics in Power Electronics*, pp. 1-1, 2020.
- [268] T. Joseph, J. Liang, G. Li, A. Moon, K. Smith and J. Yu, "Dynamic control of MVDC link embedded in distribution network: — Case study on ANGLE-DC," in *IEEE Conference on Energy Internet and Energy System Integration (EI2)*, Beijing, China, 2017.
- [269] B. Ravindranath and M. Chander, *Power System Protection and Switchgear*, New Delhi: New Age International Limited, 2005.
- [270] M. Wang, W. Leterme, G. Chaffey, J. Beerten and D. V. Hertem, "Pole Rebalancing Methods for Pole-to-Ground Faults in Symmetrical Monopolar HVDC Grids," *IEEE Transactions on Power Delivery*, vol. 34, no. 1, pp. 188 - 197, 2019.

- [271] Beama, “Guide to Low Voltage Circuit-Breakers Standards,” BEAMA, London, UK, 2015.
- [272] FLUKE, “Fluke 434/435 Three Phase Power Quality Analyzer - Users Manual (Rev. 3),” December 2008. [Online]. Available: http://assets.fluke.com/manuals/434_435_umeng0300.pdf.
- [273] P. Cook, “Harmonised Colours and Alphanumeric Marketing,” *IEE Wiring Matters*, pp. 4-6, Spring 2004.
- [274] Vishay Semiconductors, “Three Phase Bridge Rectifier, 25 A, 35 A - Vishay VS-26MT60,” 15 January 2019. [Online]. Available: <https://docs.rs-online.com/ea0/A700000006404577.pdf>. [Accessed 18 June 2019].
- [275] FLUKE , “i1000s - AC Current Probe for Oscilloscopes - User Manual,” June 2000. [Online]. Available: https://dam-assets.fluke.com/s3fs-public/i1000s__umeng0300.pdf. [Accessed August 2019].
- [276] Raspberry Pi Foundation, “Raspberry Pi 4 Tech Specs,” 2019. [Online]. Available: <https://www.raspberrypi.org/products/raspberry-pi-4-model-b/specifications/>. [Accessed 18 November 2019].
- [277] R. Adapa, L. Barthold and D. Woodford, “Technical and economic incentives for AC to DC line conversion (B2_203_2010),” CIGRE, Paris, France, 2010.
- [278] P. Fairley, “Germany jump-starts the supergrid,” *IEEE Spectrum* , pp. 36 - 41, May 2013.
- [279] Regional Group Nordic, “Nordic and Baltic HVDC Utilisation and Unavailability Statistics 2017,” ENTSOE (European Network of Transmission System Operators for Electricity), Brussels, Belgium, 2018.
- [280] The Engineering Council, “Engineering Recommendation P2/6 - Electricity Distribution Network Planning,” London, 2006.
- [281] The Engineering Council, “Engineering Recommendation P2/8 - Planning limits for voltage fluctuations,” London, 1989.

- [282] R. Fiorotti, J. F. Fardin, L. F. Encarnaç o and C. B. Donadel, "A methodology to determine the firm capacity of distributed generation units," in *IEEE PES Innovative Smart Grid Technologies Latin America (ISGT LATAM)*, Montevideo, Uruguay, 2016.
- [283] M. Bebbington, "Flexible Connections and Principles Of Access Policy (ESDD-01-009 Issue No.1)," SP Energy Networks, 2017.
- [284] J. M. Bloemink and T. C. Green, "Increasing distributed generation penetration using soft normally-open points," in *Power and Energy Society General Meeting, IEEE*, Providence, RI, USA, 2010.
- [285] National Grid, "Electricity Ten Year Statement," 2017.
- [286] A. Elserougi, A. M. Massoud, A. S. Abdel-Khalik and S. Ahmed, "Three-wire bipolar HVDC line using an existing single-circuit HV AC line for integrating renewable energy sources in multiterminal DC networks," *IET Renewable Power Generation*, vol. 10, no. 3, p. 370, 2015.